Inaugural dissertation

for

obtaining the doctoral degree

of the

Combined Faculty of Mathematics, Engineering, and Natural Sciences

of the

Ruprecht - Karls - University

Heidelberg

Presented by

M.Sc. Wiebke Leemhuis

born in: Solingen, Germany

Oral examination: 24th of June 2025

The impact of serine acetyltransferases and their product *O*-acetylserine on the sulfur deficiency response in *Arabidopsis thaliana*

Referees:

Prof. Dr. Rüdiger Hell

Prof. Dr. Thomas Greb

Abstract

Plants assimilate sulfur by the assimilatory sulfate reduction pathway. The final step of this pathway is the incorporation of sulfide into the carbon backbone *O*-acetylserine (OAS) by *O*-acetylserine(thiol)lyases (OAS-TL), resulting in cysteine. OAS production is performed by three major isoforms of the serine acetyltransferases (SERAT), which form cysteine synthase complexes (CSC) with the OAS-TL. During sulfur deficiency, sulfide levels decrease, OAS levels increase, and the CSCs dissociate. Furthermore, the genes encoding two additional isoforms of SERAT subgroup three are upregulated with unknown functions. This work investigates the potential involvement of these factors in the sulfur deficiency response.

Previous studies suggested that the cytosolic CSC (cCSC), composed of SERAT1;1 and OAS-TLA, senses sulfur deficiency and controls the transcriptional response toward this stress in the model plant *Arabidopsis thaliana*. Although transcriptional delays observed in loss-of-cCSC mutants during earlier studies were not confirmed under the here applied experimental conditions, transcriptome analyses with newly generated *oastlA* and *serat1;1* mutants using CRISPR/Cas9 indicate a possible involvement of the cCSC in balancing primary energy metabolism with immune responses under control condition.

A previous study suggested the interaction of SERAT3s with SERAT1;1 *in planta,* especially in response to sulfur deficiency. The interaction of recombinant purified SERAT3;2 with SERAT1;1 was verified *in vitro* and resulted in the formation of hetero-hexamers with reduced OAS-TL A binding capacity. The *in vivo* analysis of a SERAT3;2-mCherry fusion protein verified its predominantly cytosolic localization and uncovered an unexpected localization in the nucleus, indicating independent functions of SERAT3;2, since SERAT1;1 is exclusively localized in the cytosol. The SERAT3;2 minimal native promoter composed of 460 bps upstream of the start codon was found to contain a SURE core motive in the 5' UTR of the mRNA and was shown to induce the SERAT3;2-mCherry expression under sulfur deficiency and in a cell type specific manner. While the double mutant *serat3;1s3;2* (*serat3;1* x *serat3;2*) did not display any visible phenotype, mRNA sequencing of leaves from *serat3;1s3;2* uncovered activation of the OAS gene cluster, mimicking a pre-induced sulfur deficiency response in control condition and over-induced response when cultured with limited sulfur supply. My findings demonstrate a generally repressive function of SERAT group three in regulating sulfur deficiency-related genes.

Furthermore, I analyzed the impact of CSCs in different subcellular compartments on Arabidopsis developmental plasticity under sulfate limitation. OAS was identified as a key signal for long-term adaptation to sulfur deficiency, promoting an increased root-to-shoot FW ratio. OAS functioned independently of CSCs or its function as cysteine precursor because cysteine or glutathione could not complement the OAS-limiting phenotype in the triple knockout mutant *serat tko*, lacking all three major *SERAT* isoforms. Glutathione was shown to be crucial for the maintenance of primary root length and root FW in sulfur deficiency. The sulfur-specific transcription factor SLIM1 was found to be involved in the signaling response, probably working downstream of OAS.

In conclusion, these findings highlight the diverse functions of the SERAT protein family in primary sulfur metabolism. While SERAT isoforms of groups one and two generate OAS as a cysteine precursor in non-stress conditions, OAS accumulation in sulfur deficiency is a central signal initiating long-term physiological adaptation. SERATs of group three play a modulating role as transcriptional repressors on sulfur deficiency-induced genes, fine-tuning the response.

Zusammenfassung

Pflanzen assimilieren Schwefel über den assimilatorischen Sulfatreduktionsweg. Dabei ist der letzte Schritt der Einbau von Sulfid in das Kohlenstoffgrundgerüst von O-Acetylserin (OAS) via *O*-Acetylserin(thiol)lyasen (OAS-TL), wodurch Cystein entsteht. Die OAS-Produktion wird durch drei Haupt-Isoformen der Serin-Acetyltransferasen (SERAT) betrieben, die mit den OAS-TL Cystein-Synthase-Komplexe (CSC) bilden. Bei Schwefelmangel sinkt der Sulfidgehalt, der OAS-Gehalt steigt, und die CSCs dissoziieren. Außerdem werden die Gene der beiden zusätzlichen Isoformen der SERAT-Untergruppe drei mit unbekannten Funktionen hochreguliert. In dieser Arbeit wird die mögliche Beteiligung dieser Faktoren an der Reaktion auf Schwefelmangel untersucht.

Frühere Studien mittel T-DNA Mutanten legen nahe, dass der zytosolische CSC (cCSC), bestehend aus SERAT1;1 und OAS-TLA, Schwefelmangel wahrnimmt und die transkriptionelle Reaktion auf diesen Stress in der Modellpflanze *Arabidopsis thaliana* kontrolliert. Obwohl die in früher beobachteten Transkriptionsverzögerungen bei Verlust von cCSC-Mutanten unter den hier angewandten experimentellen Bedingungen nicht bestätigt werden konnten, deuten die Transkriptomanalysen von neu via CRISPR/Cas9 erzeugten *oastlA* und *serat1;1* Mutanten auf eine mögliche Beteiligung des cCSC in dem Ausbalancieren von Primärenergiestoffwechsels mit Immunreaktionen unter Kontrollbedingungen hin.

Eine frühere Studie deutet auf die Interaktion von SERAT3s mit SERAT1;1 *in planta* hin, insbesondere als Reaktion auf Schwefelmangel. Die Interaktion von rekombinantem, aufgereinigtem SERAT3;2 mit SERAT1;1 wurde *in vitro* verifiziert und führte zur Bildung von Hetero-Hexameren mit reduzierter OAS-TL A-Bindungskapazität. Die *in vivo*-Lokalisierung von SERAT3;2-mCherry verifizierte die bisherige zytosolische Lokalisierung und deckte eine unerwartete Lokalisierung im Zellkern auf, was eine zusätzlich unabhängige Funktion von SERAT3;2 impliziert, da SERAT1;1 ausschließlich im Zytosol lokalisiert ist. Der minimale native SERAT3;2-Promotor, der aus den 460 Basenpaaren aufwärts des Startcodons besteht, enthält ein SURE-Kernmotiv in der 5'-UTR der mRNA und induzierte nachweislich die SERAT3;2-mCherry-Expression schwefelmangel- und zelltypspezifisch. Während die *serat3;1s3;2*-Doppel-Mutante (*serat3;1* x *serat3;2*) keinen sichtbaren Phänotyp aufwies, deckte die mRNA-Sequenzierung von Blättern aus *serat3;1s3;2* eine Aktivierung des OAS-Genclusters auf, die eine vorinduzierte Schwefelmangelreaktion unter Kontrollbedingungen und eine überinduzierte Reaktion bei begrenzter Schwefelzufuhr nachahmte. Meine Ergebnisse zeigen eine allgemein repressive Funktion der SERAT-Gruppe drei bei der Regulierung von Schwefelmangel-bezogenen Genen.

Darüber hinaus habe ich die Auswirkungen von CSCs in verschiedenen subzellulären Kompartimenten auf die Entwicklungsplastizität von Arabidopsis bei Sulfatmangel analysiert. Dabei wurde OAS als Schlüsselsignal für die langfristige Anpassung an Schwefelmangel identifiziert, welche zu einem erhöhten Wurzel-zu-Spross Frischgewichtsverhältnis führt. OAS funktionierte unabhängig von CSCs oder seiner Funktion als Cysteinvorläufer, da Cystein oder Glutathion den Phänotyp in der Triplemutante der SERAT-Hauptisoformen *serat tko* nicht ausgleichen konnten. Glutathion erwies sich dabei für die Aufrechterhaltung der primären Wurzellänge und der Wurzel-FW bei Schwefelmangel als entscheidend. Darüber hinaus wurde festgestellt, dass der Transkriptionsfaktor SLIM1 an der Signalreaktion beteiligt ist und wahrscheinlich in der Signalkette hinter OAS wirkt.

Zusammengefasst unterstreichen die Ergebnisse die vielfältigen Funktionen der SERAT-Proteinfamilie im primären Schwefelstoffwechsel. Während die SERAT-Isoformen der Gruppen eins und zwei unter Normalbedingungen OAS als Cysteinvorläufer erzeugen, ist die OAS-Akkumulation bei Schwefelmangel ein zentrales Signal, das die langfristige physiologische Anpassung einleitet. SERATs der Gruppe drei spielen eine modulierende Rolle als transkriptionelle Repressoren auf Schwefelmangel-induzierte Gene und sorgen für eine Feinabstimmung der Reaktion.

Table of content

1. Introduction

1.1 Relevance of sulfur for plants and humans

Sulfur (S) is a crucial macronutrient for plants, ranking fourth behind nitrogen (N), phosphorus (P), and potassium (K) (Alway, 1940). It is notable for its distinctive redox characteristics, making it indispensable for catalytic and electrochemical processes (Leustek *et al.*, 2000; Leustek and Saito, 1999). In plants, key metabolites relying on sulfur include the proteinaceous amino acids methionine and cysteine, vitamins such as biotin and thiamine, phytochelatins, coenzyme A, and S-adenosyl-methionine (Li *et al.*, 2020; Nakai and Maruyama-Nakashita, 2020; Scherer *et al.*, 2008). Being part of iron–sulfur cluster-containing proteins further highlights the importance of sulfur in fundamental biological processes such as electron transport in photosynthesis and respiration (Couturier *et al.*, 2013). Cysteine, as constituent of proteins, facilitates proper folding and enzymatic regulation through disulfide bond formation (Åslund and Beckwith, 1999). It generally serves as the primary source of reduced sulfur in plants, making it crucial for various abiotic and biotic stress responses. The downstream metabolite glutathione, for example, protects against oxidative damage and contributes to redox homeostasis (Meyer and Rausch, 2008). Other sulfur-containing secondary metabolites, such as glucosinolates, play a significant role in plant defense against herbivores and pathogens (Bednarek, 2012). Because animals and humans lack the necessary enzymes to synthesize cysteine and methionine from inorganic sulfur sources, they rely on plant food sources to meet the nutritional needs for sulfur-containing amino acids (Finkelstein, 1990). With decreasing sulfur levels in soil, sulfur deficiency has become an increasingly limiting factor in agriculture (Feinberg *et al.*, 2021). Since overusing sulfur-based fertilizers poses new environmental risks (Hinckley *et al.*, 2020), understanding and improving plants' sulfur use efficiency is necessary to facilitate sustainable food security (Sharma *et al.*, 2024).

1.2 Assimilation and reduction of sulfate

The primary sulfur source for plants is inorganic sulfate (Leustek, 2002). Sulfate transporters (SULTR)s take up sulfate from the soil and translocate it from roots to the shoots into the plastids of photosynthetically active tissue where the sulfate reduction takes place (Hawkesford and De Kok, 2006a; Takahashi, 2019). SULTRs can be grouped into high ($K_M^{sulfate}$ 1–10 µM) and low ($K_M^{sulfate}$ 0.1–1µM) affinity proton/cotransporters. Sulfate uptake from the environment is facilitated by the high-affinity sulfate transporters, SULTR1;1 and SULTR1;2, which are located at the plasma membrane of cells located in the root epidermis, cortex, and in root hairs (Takahashi *et al.*, 2000; Yoshimoto *et al.*, 2002). Expression profiles and K_M values suggest SULTR1;2 to be the main contributor in sulfate uptake, while SULTR1;1 sustains sulfate uptake during sulfur starvation stress (Shibagaki *et al.*, 2002; Takahashi *et al.*, 2000; Vidmar *et al.*, 2000; Yoshimoto *et al.*, 2002). The translocation from roots to shoots is promoted by the low-affinity sulfate transporters SULTR2;1 and SULTR2;2 (Kataoka *et al.*, 2004a; Takahashi *et al.*, 2000). SULTR3;5 co-localizes with SULTR2;1 to enhance transport capacity, especially under sulfur deficiency (Kataoka *et al.*, 2004a). The primary function of SULTR3 family proteins is the sulfate import into the chloroplast (Chen *et al.*, 2019). SULTR4;1 and SULTR4;2 are localized to the tonoplast and release sulfate from vacuoles, especially in response to sulfur deficiency (Kataoka *et al.*, 2004b). In the plastids, the first step of sulfate reduction is the activation to adenosine 5'-phosphosulfate (APS) by ATP sulfurylase (ATPS) (EC: 2.7.7.4). ATPS1-3 are localized in the plastids, while ATPS4 is expressed in

the cytosol (Hatzfeld *et al*., 2000a; Leustek *et al*., 1994; Logan *et al*., 1996; Murillo and Leustek, 1995; Rotte and Leustek, 2000). Part of the APS pool is further activated by APS kinases (APK) (EC: 2.7.1.25) to 3'-phosphoadenosine 5'-phosphosulfate (PAPS), which is used in downstream sulfation reactions necessary to generate secondary sulfur-containing metabolites like glucosinolates, phytosulfokines or flavonoids (Lee and Leustek, 1998; Lillig *et al*., 2001; Mugford *et al*., 2009b). The bulk of APS is further reduced to sulfite by three plastid-localized APS reductases (APR) (EC: 1.8.99.2), with APR2 being the major isoform (Leustek *et al*., 2000; Loudet *et al*., 2007; Rotte and Leustek, 2000). Sulfite is reduced by sulfite reductase (SiR) (EC: 1.8.7.9) to sulfide (Takahashi *et al*., 2011). Interestingly, SiR is the only enzyme of the reduction pathway with no additional homologs in Arabidopsis (Bork *et al*., 1998; Leustek, 2002). Knock-downs of this gene create a bottleneck in the sulfur reduction pathway and lead to growth retarded phenotypes (Khan *et al*., 2010). Sulfate assimilation is predominantly executed in the shoots; however, the roots are also capable of reducing sulfate, as they possess all the necessary enzymes (Hawkesford and De Kok, 2006b; Lappartient *et al*., 1999; Leustek *et al*., 2000).

1.3 Cysteine biosynthesis

In Arabidopsis, the final step of sulfur assimilation is cysteine biosynthesis from the precursors sulfide and the non-proteogenic amino acid *O*-acetylserine (OAS). First, OAS is synthesized by serine acetyltransferases (SERAT, SAT; EC 2.3.1.30) by transferring an acetyl-moiety from Coenzyme A to serine (Hell *et al*., 2002). Secondly, sulfide is condensed with OAS in a *β*-replacement reaction carried out by *O*-acetylserine(thiol)lyases (OAS-TL, Bsas, EC 2.5.1.47) (Wirtz and Hell, 2006). While sulfide is predominantly produced in plastids, cysteine biosynthesis occurs in all subcellular compartments capable of translation. This is facilitated by specific isoforms of SERAT and OAS-TL localizing to the cytosol, mitochondria, and plastids (Hell *et al*., 2002; Lunn *et al*., 1990; Ruffet *et al*., 1995). Loss of diverse SERAT or OAS-TL isoforms in mutants suggests that OAS, sulfide, and cysteine are exchanged between subcellular compartments (Heeg *et al*., 2008; Wirtz *et al*., 2012, Watanabe *et al*. 2008b). In sulfur-sufficient conditions, SERATs associate with OAS-TL to form the cysteine synthase complex (CSC), and OAS production is the rate-limiting step in cysteine biosynthesis (Wirtz *et al*., 2001; Wirtz and Droux, 2005; Wirtz and Hell, 2006).

1.4 OAS-TL protein family

Nine OAS-TL-like genes exist in Arabidopsis, which are ubiquitously expressed with varying abundance in different cell types during development from seedling to silique (Wirtz *et al*., 2010b). The three main isoforms, OAS-TL A (Bsas1;1, AT4G14880), OAS-TL B (Bsas2;1, AT2G43750), and OAS-TL C (Bsas2;2, AT3G59760) localize to the cytosol and nucleus, plastids, and mitochondria (Barroso *et al*., 1995; Haberland, 2017; Hesse and Hoefgen, 1998; Jost *et al*., 2000b). Based on T-DNA mutant analyses, the loss of these three main isoforms is lethal (Birke, 2012; Birke *et al*., 2013). Of those three, OAS-TL A is the most expressed isoform (Watanabe *et al*., 2008a) and exhibits the highest catalytic activity *in vitro* (Jost *et al*., 2000a). In *oastlA* mutant, OAS-TL activity is reduced by 44-50% in the shoot and 75% in the root (Heeg *et al*., 2008; Watanabe *et al*., 2008a). The additional loss of OAS-LT B in the *oastlAB* mutant reduces the total activity to 5% (Heeg *et al*., 2008 (Heeg *et al*., 2008). Although *oastlA* exhibited 20% lower cysteine and 10% lowered glutathione steady-state levels accompanied by a significantly reduced flux compared to WT, the *oastlA* mutant showed no phenotype different from WT in non-stress conditions (Heeg *et al*., 2008; Watanabe *et al*., 2008a). However, the *oastlA* mutant is sensitive to cadmium application

(Dominguez-Solis *et al*., 2001) and overexpression of *OAS-TL A* is reported to enhance resistance to cadmium (Dominguez-Solis *et al*., 2004).

Other cysteine-producing OAS-TL family members are OAS-TL D1 (Bsas4;1, AT3G04940) and OAS-TL D2 (Bsas4;2, AT5G28020). Like OAS-TL A, they localize to the cytosol but display low expression and catalytic activity. Both isoforms can interact with SERATs, but their biological function remains unknown (Heeg *et al*., 2008; Rabeh and Cook, 2004; Yamaguchi *et al*., 2000). Members of this protein family with other function are the β-cyanoalanine synthase CYSC1 (Bsas3;1, AT3G61440) (EC: 4.4.1.9) (Hatzfeld *et al*., 2000b), the cysteine desulfhydrase DES1 (Bsas4;3, AT5G28030) (Alvarez *et al*., 2010) and S-sulfocysteine synthase CS26 (Bsas5;1, AT3G03630) (EC: 4.4.1.15)(Bermudez *et al*., 2010). The last member, *oasA2* (Bsas1;2, At3g22460), is a pseudogene that is still transcribed but not functionally translated (Jost *et al*., 2000b).

1.5 SERAT protein family

The SERAT protein family consists of five members, which can be subdivided into three groups based on sequence homology: SERAT1;1 (SAT5, AT5G56760), SERAT2;1 (SAT1, AT1G55920), SERAT2;2 (SAT3, AT3G13110), SERAT3;1 (SAT2, AT2G17640), SERAT3;2 (SAT4, AT4G35640) (Initiative, 2000). While according to T-DNA mutant analyses the loss of all five SERAT genes is lethal, the viability of quadruple mutants demonstrates that all isoforms are functional in producing OAS (Watanabe *et al*., 2008b). Isoforms of groups one and two are considered the main OAS-producing isoforms since their K_M values for serine and acetyl-CoA are magnitudes lower than compared to the isoforms of group three (Kawashima *et al*., 2005; Noji *et al*., 1998). They localize to the plastids (SERAT2;1), mitochondria (SERAT2;2), and the cytosol (SERAT1;1) and are broadly expressed in all tissues and developmental stages (Noji *et al*., 1998; Watanabe *et al*., 2008b). Via their conserved C-terminal end, they interact with OAS-TL, promoting the catalytic activity of SERAT (Wirtz and Hell, 2006). Of those three, only SERAT1;1 is feedback inhibited by cysteine (Noji *et al*., 1998). SERAT2;2 is the main contributor to OAS generation, since *serat2;2* is the only *SERAT* single mutant with significantly reduced SERAT activity in leaves (21%) and roots (50%) (Haas *et al*., 2008; Watanabe *et al*., 2008b). In agreement, the lack of all other four SERATs in the quadruple mutant (*Q2;2*) possessing only active SERAT2;2 caused no decrease in the SERAT activity in the shoots (Watanabe *et al*., 2008b). Corroborating this, a SERAT quadruple mutant containing only active SERAT1;1 (*Q1;1*) or SERAT2;1 (*Q2;1*) exhibited strongly diminished SERAT activity of only 9% and 13% in the shoot, respectively. The SERAT activity in the root was also strongly reduced to 27% in *Q1;1* and 5% in *Q2;1*, but resulted only in a small growth-redated phenotype for *Q2;1* (Watanabe *et al*., 2008b).

The SERAT group three isoforms were characterized as having magnitudes of lower catalytic activity *in vitro* and minor expression compared to the main isoforms (Kawashima *et al*., 2005). Interestingly, only SERAT3;2 is feedback-inhibited by cysteine, suggesting specialized functions for both SERAT3 isoforms (Noji *et al*., 1998). *SERAT* quadruple mutants containing only SERAT3;1 (*Q3;1*) or SERAT3;2 (*Q3;2*) exhibited a total SERAT activity of only 5% and 2% WT in the shoots, and 0.1 and 0.4% WT in roots, respectively (Watanabe *et al*., 2008b). Since the mutants were viable but strongly growth retarded, the SERAT3s are hypothesized to have different functions than providing OAS (Watanabe *et al*., 2008b). Although they localize to the cytosol, they are unable to form CSCs because of their elongated C-terminus, which lacks the conserved motif for interacting with OAS-TL (Birke, 2012; Kawashima *et al*., 2005; Watanabe *et al*., 2008b). Unlike the main *SERAT* isoform genes, *SERAT*s of group three are induced by sulfur deficiency and cadmium

treatment (Kawashima *et al*., 2005). Especially *SERAT3;2* is strongly induced to 40-45-fold upregulation after 96 h in both roots and shoots, while *SERAT3;1* is induced only 2-fold in roots after 96 h of sulfur deficiency (Kawashima *et al*., 2005). Interestingly, both SERAT3 proteins were found in pulldowns of STREP-SERAT1;1 from leaves and roots (Haberland, 2017). Thereby, SERAT3;1 protein was found interacting with SERAT1;1 20 times more often than SERAT3;2 in the control condition. Reflecting the transcriptional dynamics of *SERAT3;1* and *SERAT3;2*, SERAT3;1 protein interaction with SERAT1;1 increased two-fold after 72 h sulfur deficiency, while SERAT3;2 interaction increased 40-fold (Haberland, 2017). The interaction of SERAT1;1 and SERAT3;1 in the cytosol was confirmed via bi-fluorescence complementation (BiFC) in Arabidopsis protoplast, leading to the hypothesis that SERAT3 might regulate the cytosolic CSC (Haberland, 2017).

1.6 The role of CSCs in *Arabidopsis thaliana*

In Arabidopsis, the three cysteine synthase complexes (CSC) are constituted by SERAT1;1 and OAS-TL A in the cytosol, SERAT2;1 and OAS-TL B in the plastids, and SERAT2;2 and OAS-TL C in the mitochondria (Heeg *et al*., 2008; Watanabe *et al*., 2008a; Watanabe *et al*., 2008b). The SERATs form hexamers from two trimers assembling via their N-termini (Wirtz and Hell, 2006). One OAS-TL dimer is bound on each side of the hexamer, resulting in a 1:2 ratio of SERAT hexamer and OAS-TL dimers (Wirtz *et al*., 2010a). To facilitate the interaction, the C-terminus of SERAT binds via its conserved amino acid sequence ending on isoleucine into the active center of OAS-TL (Feldman-Salit *et al*., 2012; Francois *et al*., 2006; Kumaran and Jez, 2007). While this interaction promotes SERAT activity, OAS-TL is rendered inactive, and the cysteine biosynthesis is catalyzed by an excess of free unbound OAS-TL dimers (Droux *et al*., 1998; Feldman-Salit *et al*., 2012; Huang *et al*., 2005). Because of this, the CSC is not a substrate-channeling complex. In sulfur deficiency, sulfide levels decline due to reduced flux in the sulfur assimilation pathway. The free OAS-TLs lack sulfide to produce cysteine, and OAS accumulates until it outcompetes the C-terminus from the catalytic center of bound OAS-TL in the CSC, leading to complex dissociation and reduced SERAT activity (Wirtz and Hell, 2006). *In planta*, a resupply with sulfide promotes CSC formation by converting OAS to cysteine via OAS-TL, but *in vitro* experiments also demonstrated an additional direct stabilizing effect of sulfide on the CSC formation via an unknown mechanism (Wirtz and Hell, 2006). With these properties, the CSCs can sense sulfide availability and maintain sulfur homeostasis accordingly (Hell and Wirtz, 2008; Wirtz and Hell, 2006).

1.7 Glutathione biosynthesis

The tripeptide glutathione is synthesized in two steps from cysteine, glutamate, and glycine. First, glutamate-cysteine ligase (GSH1, GCL, GCS, EC 6.3.2.2, AT4G23100) forms a peptide bond between the α-amino group of cysteine and the γ-carboxyl group of glutamate (May and Leaver, 1994). The generated γ-glutamylcysteine (γ-EC) is linked to glycine in an α-peptide bond by glutathione synthetase (GSH2, EC 6.3.2.3, AT5G27380) (Rawlins *et al*., 1995). While GSH1 is exclusively located in the plastids, GSH2 has a dual localization in the plastids and cytosol (Wachter *et al*., 2005). Both enzymes are encoded by single copy genes in Arabidopsis, and the rate-limiting step in glutathione biosynthesis is γ-EC production by GSH1 (Rausch *et al*., 2007). The primary sulfur metabolism leading to glutathione biosynthesis is summarized in Figure 1. Next to various roles in cellular protection and redox homeostasis (Meyer *et al*., 2020), glutathione serves as a storage and transport form of reduced sulfur (Kopriva and Rennenberg, 2004). As a precursor of phytochelatins, glutathione is involved in heavy metal tolerance (Cobbett and Goldsbrough, 2002), explaining the cadmium-sensitive phenotype of *cad2-1* mutant (Howden et

al., 1995). In the *cad2-1* mutant, GSH1 activity is reduced to 40%, resulting in 55-70% lower glutathione steady-state levels and accumulation of cysteine (Cobbett *et al.*, 1998; Parisy *et al.*, 2007). Glutathione has additional functions in biotic defense (Parisy *et al.*, 2007) and in developmental processes, such as promoting flowering (Ogawa *et al.*, 2004). In root development, glutathione is especially important as it participates in the regulation of cell division in root apical meristems (Sánchez-Fernández *et al.*, 1997), in root tip regeneration (Lee *et al.*, 2025), and in the early stages of lateral root branching elicited by H_2 (Liu *et al.*, 2021).

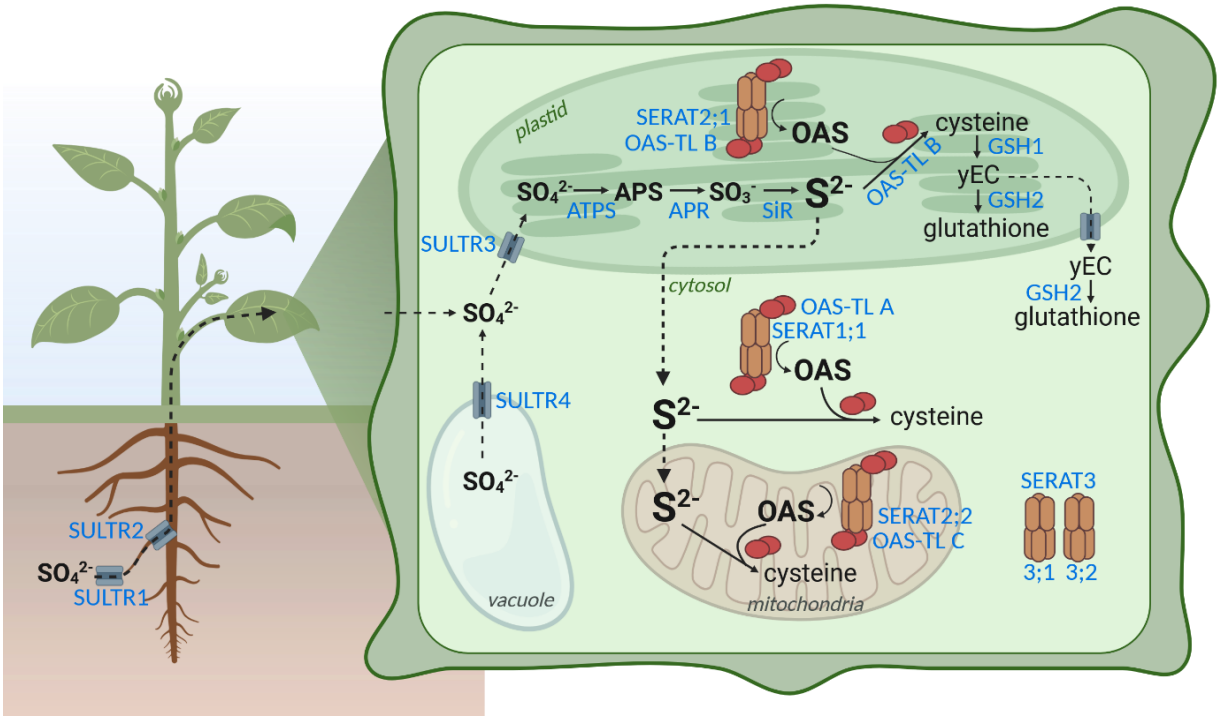

Figure 1: Schematic overview of primary sulfur metabolism. Sulfur assimilation begins with the uptake of sulfate (SO_4^{2-}) from the environment via sulfate transporters (SULTRs) of group one. SULTR2s promote sulfate translocation to the shoots, and SULTR3s import sulfate into the chloroplast. SULTR4s facilitate sulfate efflux from the vacuole, in which sulfate is stored. In the plastid, sulfate is activated by ATP sulfurylase (ATPS) to adenosine 5'-phosphosulfate (APS), which is reduced to sulfite (SO_3^-) by APS reductase (APR). Sulfite reductase (SiR) reduces sulfite to sulfide (SO_4^{2-}), which can diffuse to the cytosol and mitochondria. Sulfide is incorporated into *O*-acetylserine (OAS) to form cysteine by unbound *O*-acetylserine(thiol)lyases (OAS-TL) dimers in the plastid, cytosol, and mitochondria. OAS is produced by serine acetyltransferases (SERAT) associated in the cysteine synthase complex with inactive OAS-TL dimers. SERAT group three isoforms are also located in the cytosol but are unable to form a complex with OAS-TL A. In the plastid, cysteine is used to create γ-glutamylcysteine (γEC) via γ-glutamate-cysteine ligase (GSH1). γEC can be transported to the cytosol and is metabolized to glutathione by glutathione synthetase (GSH2). Metabolite names are in black, and protein names are in blue. Dashed arrows indicate transport routes, and filled arrows show enzymatic reactions. This figure was generated with Biorender (2.1.6).

1.8 The transcriptional response of plants to sulfur deficiency

The sulfur assimilatory reduction pathway is first a demand-driven process. It gets activated in response to sulfur-demanding stresses like sulfur deficiency, heavy metal stress, or pathogen attack (Lee and Leustek, 1999; Nocito *et al.*, 2006; Nocito *et al.*, 2007; Rausch and Wachter, 2005). If, however, sufficient sulfur is available, the pathway is repressed since intermediates like sulfite and sulfide are toxic to the cell (Davidian and Kopriva, 2010; Lappartient and Touraine, 1996; Vauclare *et al.*, 2002; Westerman *et al.*, 2001). The regulation is achieved on transcriptional, post-translational, and metabolic levels (Davidian and Kopriva, 2010; Takahashi *et al.*, 2011). Next to the upregulation of genes from the assimilatory sulfate reduction pathway, genes involved in pathogen defense, cell wall biosynthesis, abiotic stress response, respiration and

photosynthesis, proteasome, flavonoid and glucosinolate biosynthesis change their expression in response to sulfur deficiency (Hirai *et al*., 2003; Maruyama-Nakashita *et al*., 2003; Nikiforova *et al*., 2003; Nikiforova *et al*., 2005). In contrast to nitrogen and phosphorus metabolism, even less is known about the mechanism of sulfate sensing leading to the induction of the transcriptional sulfur deficiency response (Ristova and Kopriva, 2022). A possible candidate for sensing sulfate demand is SULTR1;2, which was hypothesized to be a sulfate transceptor since sulfur deficiency marker genes were induced in *sultr1;2* mutants in high sulfate supply (Koralewska *et al*., 2009; Zhang *et al*., 2014). However, the knowledge about the molecular mechanism remains fragmented (Zheng *et al*., 2014).

The most responsive genes with respect to magnitude and dynamics reacting to sulfate limitation are *SULTR1;1*, *1;2*, *2;1*, *4;2, APR3* (AT4G21990), *SDI1* (*sulfur deficiency induced 1*, *MS5-1*, AT5G48850), *SDI2* (*sulfur deficiency induced 2*, *MS5-2*, AT1G04770), *LSU1* and *LSU2* (*low sulfur induced 1* and 2, AT3G49580, AT5G24660), *BGLU28* (*β-Glucosidase 28*, AT2G44460), *MSA1* (*MORE SULPHUR ACCUMULATION 1*, *Serinehydroxymethyltransferase 7*, *SHM7*, AT1G36370) and *GGCT2;1* (*γ-Glutamyl-Cyclotransferase 2;1*, GGCT2;1-*like*, AT5G26220) (Hirai *et al*., 2003; Howarth *et al*., 2009; Hubberten *et al*., 2012b; Maruyama-Nakashita *et al*., 2003; Nikiforova *et al*., 2003; Nikiforova *et al*., 2005).

Plants react to increasing demand for sulfur by increasing the sulfate uptake rate, especially via upregulation of *SULTR1;1* and *SULTR1;2* (Takahashi *et al*., 2011; Takahashi *et al*., 1997; Yoshimoto *et al*., 2002). Sulfate translocation from roots to shoot is enhanced through upregulation of *SULTR2;1* und *SULTR2;2* as well as remobilization of stored sulfate via induction of *SULTR4;1* and *SULTR4;2* (Kataoka *et al*., 2004b; Takahashi *et al*., 2000)(1.2.). APR upregulation is critical to increase flux through the assimilatory sulfate reduction pathway (Davidian and Kopriva, 2010; Vauclare *et al*., 2002).

The induction of *SDI1* is the fastest and strongest response to sulfate limitation, and it is involved in utilizing stored sulfate, as the *sdi1* mutant exhibits higher internal sulfate levels compared to the WT (Howarth *et al*., 2009). SDI1 and SDI2 repress genes of glucosinolate biosynthesis (Aarabi *et al*., 2016) and sulfur-rich 2S seed storage proteins in Arabidopsis seeds (Aarabi *et al*., 2021), thereby channeling stored sulfate from secondary metabolites into primary metabolism.

The four LSU proteins have a supportive role in fine-tuning the sulfate reduction pathway since the quadruple mutant shows signs of sulfur deficiency in the control condition and accumulates sulfate (Piotrowska *et al*., 2024). They interact with ATPS1 and ATPS3, as well as all three isoforms of APR, and SiR. LSU1 furthermore enhanced the enzymatic activity of SiR *in vitro* (Piotrowska *et al*., 2024).

BGLU28, together with *BGLU30* (AT3G60140), is required for sulfur deficiency-induced glucosinolate catabolism and contributes to sustained plant growth under sulfur deficiency by recycling sulfate from secondary metabolism (Zhang *et al*., 2020). This is especially important in adult leaves and reproductive organs to sustain reproduction in sulfur-limited conditions (Zhang *et al*., 2023).

The nuclear-localized MSA1 is required for SAM biosynthesis and epigenetic maintenance of sulfur homeostasis via DNA methylation of sulfur deficiency marker genes (Huang *et al*., 2016). The *msa1-1* mutant shows a strong sulfur deficiency response in the control condition, resulting

in upregulated *SULTR1;1* and *SULTR1;2* and accumulation of sulfate and primary sulfur metabolites (Huang *et al*., 2016).

GGCT2;1 is one of three isoforms that degrade glutathione into 5-oxoproline and Cys-Gly *in vitro* and complement the glutathione degradation-defective yeast mutant (Kumar *et al*., 2015; Paulose *et al*., 2013). The upregulated expression of *GGCT2;1* under sulfur deficiency is involved in the regulation of root architecture by controlling glutathione homeostasis in the root tip (Joshi *et al*., 2019).

1.8.1 Transcription factors and regulatory elements involved in sulfur deficiency signaling

The sulfur-responsive element (SURE) is a 16-base *cis*-acting element located 2.7 kb upstream of translational start in the *SULTR1;1* promotor that is essential for the induction of SULTR1;1 upon sulfur deficiency (Maruyama-Nakashita *et al*., 2005). This element was also identified in the promoter region of 14 other sulfate deficiency responsive genes among those are the sulfur deficiency marker genes *APR3*, *SDI1*, *LSU1, LSU2*, *MSA1, GGCT2;1, BGLU28, SULTR2;1, SULTR4;2* (Maruyama-Nakashita *et al*., 2005; Maruyama-Nakashita *et al*., 2015). Since the second high-affinity sulfate transporter, *SULTR1;2*, has no SURE element in the promoter (Maruyama-Nakashita *et al*., 2005), the transcriptional regulation must depend on a different regulatory mechanism (Rouached *et al*., 2008). Although the core region of the SURE element GAGAC is found in the auxin response factor (ARF) binding sequence (GAGACA) (Lanctot and Nemhauser, 2020), the SURE is not activated by the synthetic auxin compound naphthalene acetic acid (NAA) (Maruyama-Nakashita *et al*., 2005).

The SULFUR LIMITATION1 (SLIM1, ETHYLENE-INSENSITIVE3-LIKE3 (EIL3), AT1G73730) was shown to bind the SURE element (Rakpenthai *et al*., 2022) but does not rely on it exclusively as many of its target genes in sulfur deficiency lack the SURE element in their promoter, like *SULTR1;2*, *ATPS4* or *APR2* (Maruyama-Nakashita *et al*., 2006). SLIM1 is a homolog of *ETHYLENE-INSENSITIVE3 (EIN3)* and can form homo- and heterodimers with EIN3 but does not regulate ethylene responses (Maruyama-Nakashita *et al*., 2006; Wawrzyńska and Sirko, 2016). Also, none of the additional five genes encoding EIL family proteins (EIN3, EIL1, EIL2, EIL4, and EIL5) (Guo and Ecker, 2004) were able to complement the *slim1* mutation and restore the upregulation of the sulfur deficiency marker genes (Maruyama-Nakashita *et al*., 2006). Nonetheless, EIL1 seems to support the function of SLIM1, since the sulfate uptake rate or glucosinolate catabolism is even less stimulated in sulfur deficiency in the *slim1eil1* double mutant compared to the single mutants (Dietzen *et al*., 2020). Also, EIN3 seems to have an inhibitory effect on SLIM1 as heterodimerization of EIN3/SLIM1 impairs the DNA binding of SLIM1 to the UP9-binding element (UPE)-Box (Wawrzyńska and Sirko, 2016).

The UPE-Box is a 20 bp sequence containing two TEBS motifs (*tobacco ethylene-insensitive 3-like binding*) and is found in several sulfur deficiency-induced genes, including the LSU family and OAS cluster genes (Lewandowska *et al*., 2010; Wawrzynska *et al*., 2010). The OAS cluster is a group of six genes whose expression correlates with OAS steady-state levels: *APR3*, *SDI1*, *SDI2*, *MSA1*, *GGCT2;1*, and *LSU1* (Hubberten *et al*., 2012a). They seem to function as signal multiplicators having their own influence on the sulfur deficiency responsive genes (Ristova and Kopriva, 2022). Notably, SLIM1 does not control all sulfur deficiency genes, since the *APR* genes are still upregulated in the *slim1* mutant in sulfur deficiency (Maruyama-Nakashita *et al*., 2006).

Important for the regulation of *APR1* (AT4G04610) und *APR2* (AT1G62180) genes is the transcription factor HY5 (ELONGATED HYPOCOTYL 5, AT5G11260), which binds to the promoter region of these isoforms but not *APR3* (Lee *et al*., 2011). In the *hy5* mutant, OAS treatment results in less pronounced upregulation of *APR1* and *2* compared to WT (Lee *et al*., 2011). Other transcription factors positively influencing the transcription of *APR*, *ATPS* and *SiR* are the six MYBs (MYB28, MYB29, MYB76, MYB51, MYB34, MYB122) which regulate glucosinolate biosynthesis in response to biotic stress rather than sulfur deficiency (Hirai *et al*., 2007; Koprivova and Kopriva, 2014; Malitsky *et al*., 2008; Mugford *et al*., 2009a; Yatusevich *et al*., 2010).

1.8.2 Post-transcriptional and metabolic regulation of the sulfur deficiency response

Among the genes upregulated by SLIM1 in sulfur deficiency, the microRNA-395 (miR395) (AT1G26973, AT1G26975, AT1G26985, AT1G69792, AT1G69795, AT1G69797) was found to be critical for translocation of sulfate to the shoots and maintaining sulfur homeostasis by regulating *SULTR2;1*, *ATPS1* (AT3G22890), *ATPS3* (AT4G14680) and *ATPS4* post-transcriptionally (Jones-Rhoades and Bartel, 2004; Kawashima *et al*., 2009; Liang *et al*., 2010). Interestingly, miR395 has different effects on target mRNA levels, since ATPS4 is the only isoform with reduced transcript levels upon miR395 induction (Kawashima *et al*., 2009; Liang *et al*., 2010). The transcript level of *ATPS1* and *ATPS3* are not affected (Hirai *et al*., 2003; Jones-Rhoades and Bartel, 2004; Kawashima *et al*., 2009), probably due to a compensatory mechanism of elevated transcription and mRNA degradation (Kawashima *et al*., 2011). Although *SULTR2;1* is a target of miR395, its overall transcript level increases in sulfur deficiency. The reason for this could be the differential spatial expression pattern of *miR395* transcripts in the vascular system which does not overlap with the expression pattern reported for *SULTR2;1* mRNA (Kawashima *et al*., 2009). Next to miR395, the miR157b, miR159b, miR396, miR775, and miR864 are upregulated and miR319a and miR398c downregulated in the shoot in sulfur deficiency, whereas in the root miR395 is the only induced miRNA (Dietzen *et al*., 2020). This indicates complex and distinct regulatory roles of miRNAs in the shoots and roots during sulfur deficiency (Ristova and Kopriva, 2022).

Other modes of post-transcriptional regulation were found via redox control of APR and APK activity (Jez *et al*., 2016). While oxidizing conditions promote APR activity, APK activity is reduced without changing transcript amounts (Bick *et al*., 2001; Kopriva and Koprivova, 2004). In sulfur deficiency, a more oxidizing environment due to decreased glutathione levels could therefore result in favoring the sulfate reduction pathway via APR over APK, resulting in a prioritization of primary sulfur metabolism over secondary metabolism (Jez *et al*., 2016). GSH1 activity itself is also promoted in oxidizing environments to replenish glutathione pools (Jez *et al*., 2004). Crucial for this are redox-sensitive disulfide bridges (Bick *et al*., 2001; Jez *et al*., 2016; Kopriva and Koprivova, 2004). Next to the role of glutathione on APR activity via redox homeostasis (Kopriva and Koprivova, 2004), glutathione and cysteine also have a negative influence on SURE-dependent expression (Maruyama-Nakashita *et al*., 2005). For example, glutathione and cysteine inhibit sulfate uptake rate via transcriptional repression of *SULTR1;1* and *SULTR1;2* (Maruyama-Nakashita *et al*., 2004a). However, no correlation was shown between the internal glutathione steady-state level and the transcript level of the sulfate transporter (Rouached *et al*., 2008).

The complete function of OAS as a signal molecule is not fully understood and is discussed controversially (Apodiakou and Hoefgen, 2023; Hirai *et al*., 2003; Hopkins *et al*., 2005). While cysteine and glutathione levels decline in sulfur deficiency, OAS accumulates (Wirtz *et al*., 2004) and induces *SULTR1;1* and *SULTR1;2* transcription (Hirai *et al*., 2003; Maruyama-Nakashita *et al*.,

2004b; Saito, 2000). OAS treatment was shown to trigger the sulfur deficiency response, characterized by enhanced sulfate uptake and a higher reduction rate, even in sulfur-sufficient conditions, by inducing the transcription of associated genes (Hirai *et al*., 2003; Neuenschwander *et al*., 1991). Other studies have shown that the increase in transcript levels in sulfur deficiency precedes the increase in OAS levels (Hopkins *et al*., 2005).

Another signaling molecule is sulfide in form of HS^- and S^{2-} found to be involved in abiotic stress responses like drought, salinity, hypoxia, as well as developmental processes such as seed germination, root development, and autophagy, as well as hormone signaling (Gotor *et al*., 2019). S^{2-} can be used to alter a thiolate group (–SH) into a persulfide group (–SSH). If cysteine residues of proteins are persulfidated, this posttranslational modification can influence protein stability, localization, and function (Gotor *et al*., 2019). Persulfidation was found to play a role in nitrogen starvation response (Jurado-Flores *et al*., 2021) and might also be important in sulfur deficiency.

Indications for additional modulation mechanisms were identified for SULTR1;1 and SULTR1;2, which accumulate at the plasma membrane in the root epidermis in response to sulfur deficiency, without changes in transcript levels (Yoshimoto *et al*., 2007). Furthermore, the transport activity of SULTR1;2 is dependent on the phosphorylation of its C-terminal STAS domain (sulfate transporter and anti-sigma factor antagonist domain) (Rouached *et al*., 2005; Shibagaki and Grossman, 2004, 2006). *In vitro* experiments identified the STAS domain as an interaction for OAS-TL A, resulting in decreased transporter activity but increased OAS-TL activity and is thought to play a function in high sulfate conditions (Shibagaki and Grossman, 2010).

1.8.3 Evidence for transcriptional functions of the cCSC in signaling early sulfur starvation

The dynamic complex formation of CSC senses sulfide and OAS supply and regulates SEARAT activity accordingly (Droux *et al*., 1998; Hell and Hillebrand, 2001; Wirtz *et al*., 2010a). It is suggested that all CSCs operate this way in the cytosol, mitochondria, and plastids (Wirtz and Hell, 2006). While de novo sulfide synthesis is exclusively localized in plastids, OAS production predominantly occurs in mitochondria (Haas *et al*., 2008). Since all metabolites exchange between compartments, the cytosolic CSC is well supplied with both precursors and is considered the primary contributor to cysteine production (Haas *et al*., 2008; Heeg *et al*., 2008; Watanabe *et al*., 2008a; Watanabe *et al*., 2008b). Additionally, the cCSC shares subcellular localization with SERAT group three isoforms, which were identified as interaction partners of SERAT1;1 and may regulate the cCSC in sulfur deficiency (Haberland, 2017). Its cytosolic localization positions it near the nucleus, where OAS-TL A can freely enter, though its function there remains unknown (Haberland, 2017). The first indications for a signaling function of the cCSC were found in feeding experiments with $^{35}SO_4^{2-}$ applied to T-DNA knock-out mutants. Haas (2010) found a delayed sulfate uptake rate in roots of cCSC mutants *oastlA* and *serat1;1* but not in the other *oastl* or *serat* single mutants in 6 h of sulfur deficiency. After 24 h of sulfur deficiency, the sulfate uptake rate was increased to WT level in all CSC mutants, indicating that the cytosolic CSC is responsible for sensing the onset of sulfur deficiency. This was further supported by the investigation of the double mutant *A1;1* (*oastlA* x *serat1;1*) and the *SERAT* quadruple mutant *Q1;1*, which is left with only the cCSC. While the double mutant also showed a delayed increase in sulfate uptake rate, with no further worsening of the effect, the cCSC alone was sufficient for a WT-like increase in sulfate uptake in *Q1;1* under sulfur deficiency (Haas, 2010). Speiser (2014) verified this finding and linked the delayed sulfate uptake rate to a delayed increase in the

transcript of the *SULT1;1* transporter in the cCSC mutants. To further investigate the transcriptional influence of the cCSC, Speiser (2014) performed a comparative transcriptome analysis of *oastlA* and *serat1;1* with the Affymetrix ATH1 array. Interestingly, in the control condition, *oastlA* and *serat1;1* showed 841 and 320 differentially regulated genes, respectively, compared to WT, of which ~ 90% were coregulated in both mutants (Speiser, 2014). In 6 h sulfur deficiency, WT showed 129 changes in gene expression, while *oastlA* and *serat1;1* exhibited much higher numbers of 608 and 419 affected transgenes, respectively, indicating major misregulation in the mutants in sulfur deficiency. Co-regulated genes in *oastlA* and *serat1;1* mutants were attributed to the loss of CSC formation. The excess of transcriptional changes in *oastlA* compared to *serat1;1* indicates possible additional transcriptional functions of OAS-TL A compared to SERAT1;1 (Speiser, 2014), which might be explained by the additional nuclear localization of OAS-TL A compared to SERAT1;1 (Haberland, 2017). Among the Co-regulated genes, five gene clusters were identified (Speiser, 2014). The first gene cluster contained genes upregulated by the cCSC in response to sulfur deficiency. Candidates are *SDI1* (AT5G48850), *GGCT2;1* (AT5G26220), and *SULTR1;1* (AT4G08620), which were induced in WT in sulfur deficiency but unchanged in the two cCSC mutants. Gene cluster II contained genes that were adjusted in the WT during sulfur deficiency, but in the cCSC mutants, these changes were constitutive and did not require further regulation in sulfur deficiency. Members of this group are *GAT* (AT1G15040), *SEN1* (AT4G35770) and *ANACO029* (AT1G69490). The third gene cluster contained genes that were constitutively pre-induced in the cCSC mutants and further altered during sulfur deficiency. Members are iron-regulated transporter 1 (*IRT1*; AT4G19690) and both nicotianamine synthase genes *NAS2* (AT5G56080) and *NAS1* (AT5G04950). Gene cluster IV comprised genes that remain unresponsive to short-term sulfate deficiency in WT roots but exhibit altered expression in untreated *oastlA* and *serat1;1* mutant with no further adjustments upon sulfate deprivation. So were genes especially connected to jasmonic acid response and signaling. Gene cluster V summarized genes whose expression levels were only changed in the cCSC mutants upon short-term sulfate deficiency like *MYB83* (AT1G79180), *DIN10* (AT5G20250), or *APT5* (AT5G11160) (Speiser, 2014). Next to that, all marker genes of sulfur deficiency were found to be affected in the *oastlA* and *serat1;1* mutant in short-term sulfur deficiency, highlighting the cCSC role in sensing sulfur status and also possibly in starting the signaling cascade (Haberland, 2017; Speiser, 2014).

1.9 Physiological adaptation to long-term sulfur deficiency

As sessile organisms, plants must cope with various abiotic stresses on-site, often leading to morphological adaptations in the overall plant body architecture in long-term exposure. In case of nutrient starvation, especially the root system adapts accordingly to the type of nutrient and depends on the concentration or severity of the deficiency (Gruber *et al*., 2013). There are different and contradictory morphological changes reported in response to sulfur deficiency: While Kutz *et al*. (2002) observed lateral root initiation to be increased by sulfur deficiency especially closer to the root tip, Dan *et al*. (2006) could show inhibited lateral root formation and elongation in sulfur deficiency, and Gruber *et al*. (2013) did not see changes in root architecture at all. The use of different Columbia ecotypes, solid or liquid growth media, and varying concentrations and definitions of sulfur deficiency may explain the differences. Despite using different growth conditions, sulfur deficiency was accompanied by a substantial reduction in shoot FW while the root FW was maintained or only slightly decreased compared to the control condition (Gruber *et al*., 2013; Kutz *et al*., 2002). The observed increase in the root-to-shoot dry or fresh weight ratio is a readout for sulfur deficiency stress, but it is also observed in nitrogen or phosphorus starvation

or water limitation (Ericsson, 1995). Investing all resources in the root allows the plant to forage deeper soil areas for more nutrients or water, respectively (Ericsson, 1995). The molecular and physiological adaptations to sulfur deficiency are summarized in Figure 2.

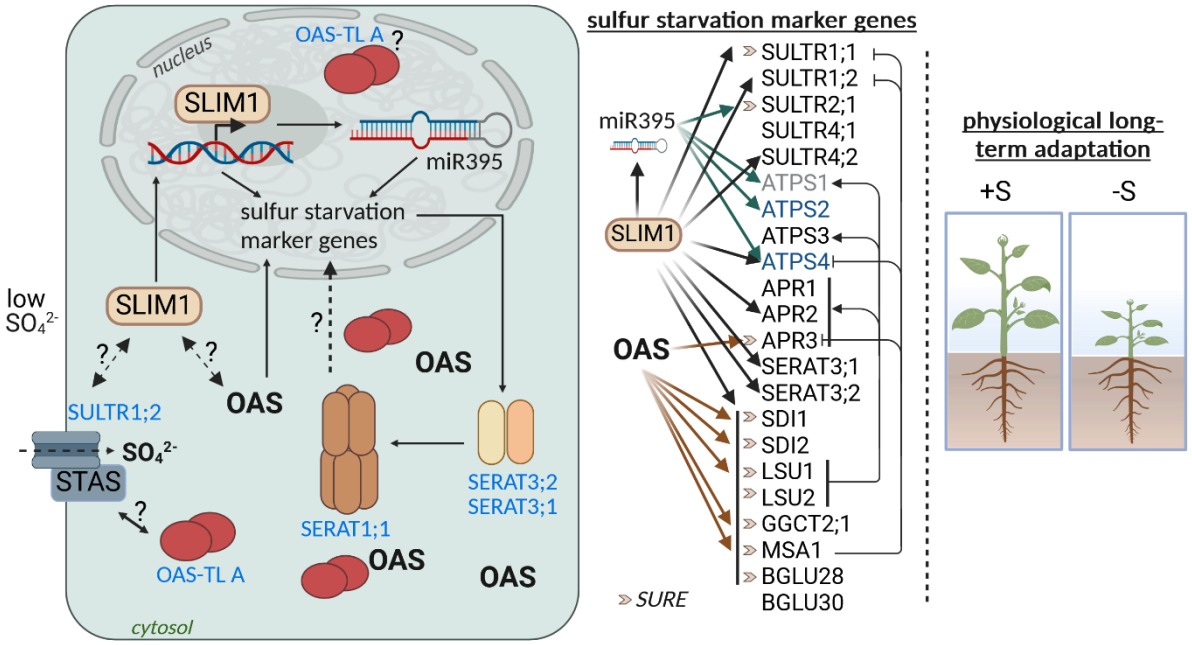

Figure 2: Summary of sulfur deficiency adaptations. SULTR1;2 is hypothesized to function as a transceptor of sulfate and interacts with OAS-TLA via the STAS domain. The function of OAS-TL A dual localization to the cytosol and nucleus independent of the sulfur status remains unsolved. Sulfur deficiency causes OAS accumulation, leading to the dissociation of the cytosolic CSC. The latter was hypothesized to influence the upregulation of sulfur deficiency marker genes. OAS itself has a transcriptional influence via the upregulation of OAS-cluster genes. The transcription factor SLIM1 induces the expression of sulfur deficiency marker genes. A connection between OAS and SLIM1 is hypothesized. Among the sulfur deficiency marker genes, the SERAT group three isoforms are induced and found to interact with SERAT1;1, which has an unknown function. Among the SLIM1-induced genes is miR395 fine-tuning transcription. A set of important sulfur deficiency marker genes and known connections between OAS, SLIM1 and miR395 are listed. Interestingly, the sulfur deficiency marker genes also exhibit regulating effects on each other. In long-term sulfur deficiency, plants prioritize root growth over shoot growth, resulting in an increased root-to-shoot FW ratio.

1.10 Aim of the study

Understanding how plants sense the sulfur status and adapt to sulfur deficiency is crucial for improving plants' sulfur demand and use efficiency to facilitate sustainable food security (Sharma *et al.*, 2024). Cysteine biosynthesis is the last step of the assimilatory sulfate reduction pathway, integrating sulfide availability with carbon-nitrogen metabolism. When sulfide becomes limiting in sulfur deficiency, OAS accumulates, and the CSCs dissociate. This study investigates the impact of SERATs and their product OAS on the sulfur deficiency response in three approaches:

1. The potential role of the SERAT1;1 and OAS-TL A as part of the cCSC in sensing the early onset of sulfur deficiency is investigated. Therefore, newly generated Crispr/Cas9 based single mutants *oastlA* and *serat1;1* will be subjected to mRNA sequencing to verify the transcriptional changes observed by Speiser (2014) and identify new genes and other regulatory RNAs that were not previously measurable with the Affymetrix array.

2. The function of the sulfur deficiency-induced SERAT3s is elucidated using *in silico*, *in vitro,* and *in vivo* studies. First, gene expression analysis from available single-cell databases should be

collected and compared to *in vivo* localization of the full-length SERAT3;2 protein, as previously only the first 100 amino acids were used to determine SERAT3s localization (Kawashima 2015). In transgenic *E. coli*, the protein-protein interaction between SERAT3;2 and SERAT1;1, as identified by Haberland (2017), should be verified and characterized. Furthermore, the double mutant *serat3;1s3;2* should be analyzed regarding a long-term sulfur deficiency phenotype and subjected to metabolite analysis of OAS, sulfide, cysteine, and glutathione. Lastly, transcriptome analysis of *serat3;1s3;2* in sulfur deficiency compared to WT should be performed to investigate a possible transcriptional role of SERAT group three.

3. The molecular signals sulfide, OAS, and CSC dissociation are investigated for an involvement in triggering the sulfur deficiency response, resulting in an increased root-to-shoot FW ratio. Therefore, mutants deficient in these factors should be analyzed for phenotypes in long-term sulfur deficiency.

2. Materials and methods

Devices, chemicals, or consumables not listed are standard laboratory equipment obtained from Eppendorf (Hamburg), AppliChem (Karlsruhe), Merck (Darmstadt), or Sigma-Aldrich (Steinheim).

2.1 Technical equipment and materials

2.1.1 Technical equipment

Autoclave Sanoclav Sanoklav (Bad Uberkingen-Hausen)

ÄKTAexplorer GE (Healthcare GmbH, Freiburg)

Binocular microscope MZFLIII (Leica, Wetzlar)

Camera DSC-RX100 M3 (Sony Deutschland, Cologne)

Centrifuge 5417R (Eppendorf, Hamburg)

CentrifugeMikro200R (Hettich Zentrifugen, Tuttlingen)

Centrifuge Rotanta 460R (Hettich Zentrifugen, Tuttlingen)

Centrifuge Sorvall LYNX 6000 (Thermo Fisher Scientific, Waltham)

Centrifuge Sorvall RC5C, Rotor SCA-1500 (DuPont, Bad Homburg)

Classic Western Blot system Trans-Blot (BioRad, Feldkirchen)

Climate chamber Percival CU-3GL14 (CLF Laborgerate GmbG, Emersacker)

Climate chamber ThermoTEC (ThermoTEC, Weilburg)

Concentrator Plus (Eppendorf, Hamburg)

Confocal microscope Leica Stellaris 8 (Leica, Wetzlar)

DM IRB epifluorescence microscope (Leica, Wetzlar)

DNA gel chamber 40-1214 (PeqLab, Erlangen)

Electrophoresis chamber PerfectBlue Twin ExW (PeqLab, Erlangen)

Electrophoresis chamber Mini Preotean III (Bio-Rad, Feldkirchen)

Electrophoresis chamber Mini Preotean Tetra (Bio-Rad, Feldkirchen)

ElectroporatorMicroPulser (BioRad, München)

ElgaPurelab Classic (VWS Marlow, Bucks)

FastPrepTM Homogenizer (MP Biomedicals, Graffenstaden)

FP-920 fluorescence detector (Jasco, Gros-Umstadt)

Gas burner gasprofi (WLD-Tec GmbH, Arenshausen)

Gel Jet Imager 2000 (Intas, Göttingen)

Heatblock HBT-2 132 (Labor Consult HLC, Bovenden)

Heater (80°C) B6120 (Heraus Instruments, Hanau)

HLC Block Thermostat HTMR 133 (Haep Labor Consult HLC, Bovenden)

Horizontal shaker KS 260 Basic (IKA Werke, Staufen)

Horizontal shaker Belly Dancer (Stovall, Greensboro)

Ice machine (Ziegra Eis Maschinenen, Isernhangen)

ICS-5000+ DC Dionex (Thermo Scientific,Walldorf)

ImageQuant LAS 4000 (GE Healthcare GmbH, Freiburg)

Incubators (28 °C / 37 °C) (Heraeus Instruments, Hanau)

Laminar flow hood Lamin Air 2448/HB 2472 (Heraeus Instruments, Osterode)

Magnetic stirrer MR 3001 (Heidolph Instruments, Schwabach)

Mastercycler Gradient 5531 (Eppendorf, Hamburg)

Mastercycler Personal 5332 (Eppendorf, Hamburg)

Multitron incubator (Inforst HT, Switzerland)

NanoDrop ND-2000 (Peqlab, Erlangen)

Orbital shaker Rotamax 120 (Heidolph Instruments, Schwabach)

PCR cycler VeritiProÒ with Gradient (Applied Biosystems, Waltham)

Peristaltic pump (Behr Labor-Technik, Düsseldorf)

pH meter inoLabTM (Thermo Fisvher Scientific, Walldorf)

Photometer Kontron UVIKON 923 (Secoman, Kandsberg)

Plate reader Fluostar Omega (BMG, Offenburg)

Power supply Power Pac 1000 (BioRad, Feldkirchen)

Precision balance AUW120D (Shimadzu, Griesheim)

Precision balance CY323C (Waagen Friedrichs, Heidelberg)

PURELAB Classic water purification system ELGA (LabWater, Celle)

RT PCR cycler Rotor-Gene 6000 (Qiagen, Hilden)

Spectral photometer Ultraspec III (Pharmacia, Freiburg)

Stereomicroscope Leica MZ FLIII (Leica, Bensheim)

Table Centrifuge 5415 C (Eppendorf, Hamburg)

Ultra-low temperature freezer C660-86 (New Brunswick Scientific, Nurtingen)

Ultrasonic homogeniser UW70 (Bandelin Electronics, Berlin)

Uvikon Spectrophometer (Kontron / S&T, Augsburg)

Vortex 444-1372 (VWR International, Darmstadt)

HiLoad 16/600 Superdex 75 prep grade (GE Healthcare GmbH, Freiburg)

W600 controller (Waters, Milford)

W600E pump (Waters, Milford)

W717 plus autosampler (Waters, Milford)

2.1.2 Consumables

1.5, 2.0 ml microcentrifuge tubes (Eppendorf, Hamburg)

6-, 12- and 96-well plates (Greiner Bio-One, Frickenhausen)

Cover glasses (Menzel, Braunschweig)

Chelating High Performance Column (1 ml) (GE Healthcare, München)

Immobilon®-P PVDF transfer membrane 0.45 µM (Merck Millipore, Darmstadt)

MagStrep "type3" Strep-Tactin® beads (Iba Lifesciences, Göttingen)

Microscope slides (VWR, Darmstadt)

PCR SingleCap 8er-SoftStrips 0.2 ml (Biozym Scientific GmbH, Oldendorf)

Petri dishes (round, 94 x 16 mm) (Greiner Bio-One, Frickenhausen)

Petri dishes (square, 120 x 120 x 17 mm) (Greiner Bio-One, Frickenhausen)

Rotilabo syringe filter (0.22, 0.45 µm) (Roth, Karlsruhe)

Rotor-GeneR Style 4-Strip Tubes and Caps 0.1 mL (Starlab, Hamburg)

Semi-micro cuvettes (10 x 4 x 45mm) (Sarstedt, Nümbrecht)

Single-use syringe Luer-Look (1, 10 ml) (BD Biosciences, Heidelberg)

Strep-Tactin XT Superflow (1 ml) (IBA Lifesciences, Göttingen)

Strep-Tactin Superflow Plus Cartridge (1 ml) (Qiagen, Hilden)

Whatman paper (Cytiva, Freiburg)

2.1.3 Chemicals

1 Kb Plus DNA Ladder GeneRuler TM (New England Biolabs, Beverly)

1 Kb Plus DNA Ladder (New England Biolabs, Beverly)

1 Kb DNA Ladder (New England Biolabs, Beverly)

10X rCutSMART®/NEBBuffer 3.1 (New England Biolabs, Beverly)

6X Gel Loading Dye Purple (New England Biolabs, Beverly)

2-log-DNA-Marker (New England Biolabs, Beverly)

β-mercaptoethanol (Merck, Darmstadt)

AccQ−Tag™ (Waters, Milford)

Acetic acid (Fluka Biochemika, Fuchs)

Acetonitrile (Sigma-Aldrich, Steinheim)

Acetosyringone (Sigma-Aldrich, Steinheim)

Acrylamid (Roth, Karlsruhe)

Agar (Fluka Biochemika, Fuchs)

Agarose (UltraPure™) (Thermo Fisher Scientific, Waltham)

Albumin fraction V (BSA) (Roth, Karlsruhe)

Ammoniumpersulfate (APS) (Serva, Heidelberg)

Ampicillin (Roth, Karlsruhe)

Bacto™ Tryptone (BD Biosciences, Heidelberg)

Bacto™ Yeast Extract (BD Biosciences, Heidelberg)

BCIP (5-Brom-4-chlor-3-indoxylphosphat) (Sigma-Aldrich, Steinheim)

Beef extract powder (Sigma Aldrich, Steinheim)

Bis-acrylamid (AppliChem, Darmstadt)

Bis-Tris (Sigma Aldrich, Steinheim)

BlueStar Prestained Protein Marker (Nippon Genetics, Duren)

Boric acid (Merck, Darmstadt)

Bromophenol blue (Kallies Feinchemie, Sebnitz)

$CaCl_2$ (AppliChem, Darmstadt)

$Ca(NO_3)_2$ (Fluka Biochemika, Fuchs)

Carbenicillin (Duchefa, Haarlem)

Citric acid (AppliChem, Darmstadt)

$CoCl_2$ (Duchefa, Haarlem)

cOmplete protease inhibitor cocktail (Roche, Mannheim)

Coomassie Blue-250 (Merck, Darmstadt)

$CuCl_2$ (Roth, Karlsruhe)

$CuSO_4$ (Merck, Darmstadt)

Deoxynucleotide Solution Mix (New England Biolabs, Beverly)

Desthiobiotin (Sigma-Aldrich, Steinheim)

Dimethylformamide (DMF) (Sigma-Aldrich, Steinheim)

Dimethyl sulfoxide (DMSO) (Roth, Karlsruhe)

Dithiothreitol (DTT) (AppliChem, Darmstadt)

Ethanol (Merck, Darmstadt)

Ethidiumbromide (Sigma-Aldrich, Steinheim)

Ethylenediaminetetraacetic acid (EDTA) (Roth, Karlsruhe)

Fe-EDTA (Duchefa, Haarlem)

Gentamicin (Duchefa, Haarlem)

Glucose (Merck, Darmstadt)

Glufosinate ammonium (Basta) (Bayer, Leverkusen)

Glycerine (Merck, Darmstadt)

H_3BO_3 (Merck, Darmstadt)

HABA (4‘hydroxyazobenzene-2-carboxylic acid) (Sigma-Aldrich, Steinheim)

HCl (Sigma-Aldrich, Steinheim)

Hepes (Roth, Karlsruhe)

Hygromycin (Sigma-Aldrich, Steinheim)

Imidazole (Sigma-Aldrich, Steinheim)

IPTG (Sigma-Aldrich, Steinheim)

Isopropanol (Roth, Karlsruhe)

Kanamycin (Duchefa, Haarlem)

KCl (Merck, Darmstadt)

KH_2PO_4 (Merck, Darmstadt)

KNO_3 (Roth, Karlsruhe)

KOH (Sigma-Aldrich, Steinheim)

Lithiumdodecyl sulfate (AppliChem, Darmstadt)

MES (AppliChem, Darmstadt)

Methanol (Fisher Scientific, Schwerte)

$MgCl_2$ (AppliChem, Darmstadt)

$MgSO_4$ (Merck, Darmstadt)

$MnCl_2$ (AppliChem, Darmstadt)

Monobromobimane (MBB) (Sigma-Aldrich, Steinheim)

Na_2MoO_4 (AppliChem, Darmstadt)

NaCl (AppliChem, Darmstadt)

NaOH (AppliChem, Darmstadt)

$(NH_4)_6Mo_7O_{24}$ (AppliChem, Darmstadt)

Nitrotetrazoliumblue (NBT) (Roche,Mannheim)

Phenol Riedel-de Haen, Seelze

Phenol red (Sigma Aldrich, Steinheim)

Phenylmethanesulfonylfluoride (PMSF) (Serva, Heidelberg)

Polyethylene glycol (PEG) 6000 (Roth, Karlsruhe)

Quick CoomassieR Stain (Serva, Heidelberg)

Rifampicin (Duchefa, Haarlem)

RotiphoreseR Gel 30 (Roth, Karlsruhe)

RotiR-Quant Bradford reagent (Roth, Karlsruhe)

Silvett (Sigma-Aldrich, Steinheim)

Sodium citrate (Riedel-de Haen, Seelze)

Sodium dodecyl sulfate (SDS) (Fluka Biochemika, Seelze)

Sodium hypochlorite (Fluka Biochemika, Seelze)

Spectinomycin (Sigma-Aldrich, Steinheim)

Streptomycin (AppliChem, Darmstadt)

Sucrose (Roth, Karlsruhe)

TCEP (Sigma-Aldrich, Steinheim)

TEMED (Roth, Karlsruhe)

Trishydroxymethylaminomethane (Tris) (Roth, Karlsruhe)

Triton X-100 (Sigma-Aldrich, Steinheim)

Tween 20 (Sigma-Aldrich, Steinheim)

WesternBright ECL HRP substrate (Advansta, San Jose)

$ZnCl_2$ (Merck, Darmstadt)

$ZnSO_4$ (Riedel-de Haen, Seelze)

2.1.4 Buffer and solutions

1/2 Hoagland medium	(2.5 mM $Ca(NO_3)_2$, 0.5 mM $MgSO_4$ (+S) or 0.5 mM $MgCl_2$ + 1 µM $MgSO_4$ (-S), 2.5 mM KNO_3, 0.5 mM KH_2PO_4, 4 µM Fe-EDTA, 25 µM H_2BO_3, 2.25 µM $MnCl_2$, 1.9 µM $ZnCl_2$, 0.15 µM $CuCl_2$, 0.05 µM $(NH_4)6Mo_7O_{24}$; pH 5.8 (+ 0.8% UltraPure™ agarose for solid medium))
1x blotting buffer	(1.44% (w/v) glycine, 0.5% (w/v) Tris, 0.1% (w/v) SDS, 20% (v/v) methanol)
1x SDS running buffer	(25 mM Tris, 192 mM glycine, 0.1% (w/v) SDS; pH 8.3)
1x TAE buffer	(90 mM Tris, 90 mM H_3BO_3, 0.5 mM EDTA)
1x TBS-T buffer	(20 mM Tris, 137 mM NaCl, 0.1% Tween 20; pH 7.6)
5x Lammli buffer	(10% (w/v) SDS, 20% (v/v) glycerine, 100 mM Tris pH 7; 0.1% (w/v) bromophenol blue; 25% (v/v)-mercaptoethanol)
AP buffer	(100 mM Tris, 100 mM NaCl, 5 mM $MgCl_2$; pH 8.8)
Amido black staining	(0.1% amido black, 45% ethanol, 10% acetic acid)
BCIP working solution	(16.5% (w/v) 5-bromo-4-chloro-3-indolyl-phosphate in 100% DMF)
Buffer B	(50 mM Tris pH 8.0, 250 mM NaCl, 20 mM imidazole)
Buffer BXT	(100 mM Tris pH 8.0, 150 mM NaCl, 1 mM EDTA, 2.5 mM desthiobiotin)

Buffer E	(50 mM Tris pH 8.0, 250 mM NaCl, 400 mM imidazole)
BufferW	(50 mM Tris pH 8.0, 250 mM NaCl, 80 mM imidazole)
Coomassie staining	(50% (v/v) ethanol, 1% (v/v) acetic acid, 0.1% (w/v) Coomassie; Brilliant Blue G-250)
Floral dip solution	(50 g/l Saccharose, 200 µl/l Silvett)
Edwards buffer	(0.2 M Tris, 250 mM NaCl, 25 mM EDTA, 0.5% (w/v) SDS; pH 7.5)
LB medium	(1% (w/v) Bacto™ Tryptone, 0.5% (w/v) Bacto™Yeast Extract, 1% (w/v) NaCl (+ 1.5% agar for solid medium))
NBT working solution	(16.5% (w/v) nitrotetrazolium blue in 70% (v/v) DMF)
NuPAGE buffer	(106 mM Tris pH 8.5, 141 mM Tris, 2% (w/v) lithium dodecyl sulfate, 0.51 mM EDTA; 10% (v/v) glycerine, 0.22 mM Coomassie Blue G-250, 0.166 mM Phenol Red; pH 8.0, freshly added 50 mM DTT)
Protein extraction buffer	(50 mM Hepes, 10 mM KCl, 1 mM EDTA; 10% (v/v) glycerine; pH 7.4, freshly added 10 mM DTT and 0.5 mM PMSF)
Resolving gel buffer	(1.5 M Tris, 0.4% (w/v) SDS; pH 8.8)
SEC buffer	(20 mM Tris; 100 mM NaCl; pH 7.5)
Stacking gel buffer	(0.5 M Tris, 0.4% (w/v) SDS; pH 6.8)
YEB medium	(5 g/l Bacto™ Tryptone, 1 g/l Bacto™ Yeast Extract, 5 g/l Beef extract powder, 5 g/l Saccharose (+ 1.5% agar for solid medium))

2.1.5 Enzymes and kits

CloneJET PCR Cloning Kit (Thermo Fisher Scientific, Waltham)

Fast Gene Scriptase II cDNA Synthesis Kit (Nippon Genetics, Düren)

FastGeneR TAQ ReadyMix (NIPPON Genetics, Düren)

Fast Gene Scriptase II cDNA Synthesis Kit (Nippon Genetics, Duren)

FastGene TAQ Ready Mix (Nippon Genetics, Duren)

High and low molecular-weight filtration calibration kit (GE Healthcare, Chicago)

NucleoSpin Gel and PCR Clean-up Kit (Machery-Nagel, Duren)

NucleoSpin Plasmid Kit (Machery-Nagel, Duren)

PCRBIO HiFi polymerase and buffer (PCR Biosystems, London)

Phusion High-Fidelity DNA polymerase (New England Biolabs, Beverly)

qPCRBIO SyGreen Mix Lo-ROX (PCR Biosystems, London)

Restriction enzymes (New England Biolabs, Beverly)

SuperSignal West Extended Duration Substrate (Thermo Scientific, Walldorf)

T4 DNA Ligase and Buffer (New England Biolabs, Beverly)

RNase A, DNase and protease-free (Thermo Fischer Scientific, Waltham)

Roboclon RNA Extraction Kit (Roboclon, Berlin)

RotiÒQuant (Carl Roth, Karlsruhe)

Western Blocking Reagent (Roche, Mannheim)

2.1.6 Software

EndNote X2 (Thomson Reuters, New York)

Fiji (Schindelin *et al.*, 2012)

Geneious (Biomatters, Auckland)

GraphPad Prism (Dotmatics, Boston)

ImageQuant TL 8.1 (GE Healthcare, Munchen)

Millenium32Waters (Waters, Milford)

MS Office 365 (Microsoft, Redmond)

NanoDrop ND-2000 (Peqlab, Erlangen)

Rotor-Gene Q Series Software (Qiagen, Hilden)

Web-based tools

AlphaFold (https://alphafold.ebi.ac.uk/)

Arabidopsis root single-cell atlas (https://phytozome-next.jgi.doe.gov/tools/scrna/)

Arabidopsis shoot single-cell atlas (http://wanglab.sippe.ac.cn/shootatlas/)

BioRender (biorender.com)

ChopChop (https://chopchop.cbu.uib.no/)

KEGG database (https://www.genome.jp/kegg/pathway.html)

Klepikova Arabidopsis Atlas eFP browser (https://bar.utoronto.ca)

Phylogenes (https://phylogenes.arabidopsis.org/tree/PTHR42811)

SUBA5 (https://suba.live/)

targetDesign (http://skl.scau.edu.cn/targetdesign/)

The Arabidopsis Information Resource (TAIR) (arabidopsis.org)

UniProt (https://www.uniprot.org/)

KI-based tools

Elicit (https://elicit.com) was used in literature search

Deepl (https://www.deepl.com) was used for English German translations

Grammarly (https://app.grammarly.com/) for proofreading English grammar

2.2 Microbiological methods

2.2.1 Bacterial strains

Chemo-competent *E. coli* XL1 Blue strain and *E. coli* DB3.1 were used for cloning and vector generation. Chemo-competent *E. coli* BL21 (DE3) was used for protein expression for *in vitro* studies. *A. tumefaciens* strain GV3101 was used for transient expression and transformation of *A. thaliana*.

E. coli XL1-blue (Stratagene)	*recA1 endA1 gyrA96 thi-1 hsdR17 supE44 relA1 lac* [*F' proAB+ lacI^{q}ZΔM15 Tn10* (Tet^r)]
E. coli DB3.1 (Invitrogen)	*F-gyrA462 endA1 glnV44 (sr1-recA) mcrB mrr hsdS20(rB-, mB-) ara14 galK2 lacY1 proA2 rpsL20(Smr) xyl5 leu mtl1*
E. coli BL21 (DE3) (Stratagene)	*F–ompT galdcm lon hsdSB(rB-, mB-) [malB+]K-12(λS)*
A. tumefaciens GV3101 (Goldbio)	*C58, pMP90, pTiC58δT-DNA, Gent^r, Rif^r*

Table 1: List of transgenic bacteria used in this work. ID states the group's internal GMO reference number. All bacteria belong to the *E. coli* BL21 (DE3) strain. Plasmids are listed in 2.4.1.

ID	Plasmids carried	Resistance	generated by
1879	pET3d STREP-SERAT3;2 pET28a HIS-SERAT1;1	*Amp^r*, *Kan^r*	this work
1881	pET3d STREP-SERAT3;2ΔC pET 28a HIS-SERAT1;1	*Amp^r*, *Kan^r*	this work
1894	pET32a OAS-TL A	*Amp^r*	Dr. Shengkai Sun

2.2.2 Bacteria growth condition

All *E. coli* strains (2.2.1) were grown in LB medium (2.1.4) and for *A. tumefaciens* YEB medium (4.1.4) was used either in liquid culture or solid plates containing the appropriate antibiotics for selection (ampicillin: 100 µg/ml, gentamycin 30 µg/ml, kanamycin 50 µg/ml, rifampicin 20 µg/ml, streptomycin 100/µg ml, spectinomycin 100 µg/ml). *E. coli* were incubated at 37 °C for 16 h, whereas *A. tumefaciens* were grown for 24 - 48 h at 28 °C.

2.2.3 Generation of chemo-competent *E. coli*

Chemically competent *E. coli* XL1-Blue cells (2.2.1) were added to 10 ml liquid LB medium (2.1.4) without antibiotics and cultivated at 37 °C and 120 rpm overnight. Next, 500 ml LB medium was inoculated with the overnight culture and incubated at 37 °C and 120 rpm until OD_{600} reached 0.5-1. The cell suspension was incubated on ice for 20 min and centrifuged at 3,500 g for 10 min at 4 °C. Next, the pellet was resuspended in 100 ml pre-cooled LB medium supplemented with 10% (w/v) PEG, 5% (v/v) DMSO and 50 mM $MgCl_2$ at pH 6.5. Finally, the cells were aliquoted in 1.5 mL microcentrifuge tubes to each 100 µl. The aliquots were frozen in liquid nitrogen and stored at -80 °C.

2.2.4 Preparation of chemo-competent *A. tumefaciens*

An *A. tumefaciens* GV3101 (2.2.1) stock culture was prepared by adding chemically competent cells to 5 ml liquid YEB medium (2.1.4) supplemented with gentamycin and rifampicin (2.2.2) and cultivation for two days at 28 °C and 120 rpm. The stock culture was added to 250 ml YEB medium containing gentamycin and rifampicin and incubated at 28 °C and 120 rpm overnight until OD_{600} reached 0.5 - 1. Cells were incubated on ice for 20 min, followed by centrifugation at 3,500 g for 10 min at 4 °C. The pellet was washed with 50 ml pre-cooled sterile 20 mM $CaCl_2$ solution and centrifuged at 3,000 g for 10 min at 4 °C. Finally, the cells were resuspended in 10 ml pre-cooled 20 mM $CaCl_2$ solution and aliquoted to 1.5 ml microcentrifuge tubes to each 200 µl. The aliquots were frozen in liquid nitrogen and stored at -80 °C.

2.2.5 Heat shock transformation of *E. coli*

Chemo-competent XL1 Blue or BL21 (DE3) (2.2.3) were thawed on ice and mixed with 5-10 µl vector DNA. The mixture was incubated on ice for 30 min - 1 h. Bacteria were heat-shocked in a heater at 42 °C for 45 s and directly resuspended in 1 ml LB medium (2.1.2) without antibiotics, followed by 1 h incubation at 37 °C and 120 rpm. The cells were plated on solid LB media containing the appropriate antibiotics and incubated overnight at 37 °C. Positive transformants showed single colonies.

2.2.6 Heat shock transformation of *A. tumefaciens*

Chemo-competent GV3101 (2.2.4) were thawed on ice and mixed with 1 µg of the vector DNA. The mixture was inverted twice, incubated on ice for 10 min, and frozen in liquid nitrogen. Next, bacteria were heat-shocked in a heater at 37 °C for 5 min. 1 ml YEB medium (2.1.2) without antibiotics was added, and the bacteria were incubated at 28 °C and 120 rpm for 3 h. The cells were plated on solid YEB media containing the appropriate antibiotics and incubated for two nights at 28 °C. Positive transformants showed single colonies.

2.2.7 Preparation of glycerol stocks

500 µl of fresh overnight bacterial culture was mixed with 500 µl sterile 50% glycerol (v/v), snap-frozen in liquid nitrogen, and stored at -80 °C until further usage.

2.3 Methods of plant work

2.3.1 Plant material

This work investigates *Arabidopsis thaliana* ecotype Columbia-0 (Col-0), stated as wild type (WT). Table 2 lists further used mutants of the Col-0 background.

Table 2: List of transgenic plant lines used in this work. ID states the group's internal GMO reference number. All mutants belong to the Col-0 ecotype. KO= knock out, KD= knock down.

ID	Name	Affected gene	Description (Reference)
13	*oastlA*	AT4G14880	T-DNA insertion, KO (SP1960; Heeg *et al.*, 2008)
18	*serat2;1*	AT1G55920	T-DNA insertion, KO (SALK_099019; Watanabe *et al.*, 2008b)
25	*serat1;1*	AT5G56760	T-DNA insertion, KO (SALK_050213; Watanabe *et al.*, 2008b)

426	*sir1-1*	AT5G04590	T-DNA insertion, KD (GK-550A09; Khan *et al.*, 2010)
873	*serat3;1s3;2*	AT2G17640 AT4G35640	T-DNA insertion, double KO (SALK_030011; SALK_030223; Watanabe *et al.*, 2008b)
877	*serat tko*	AT5G56760 AT1G55920 AT3G13110	T-DNA insertions, triple KO (SALK_050213; SALK_099019; Kazuza_KG752; Watanabe *et al.*, 2008b)
880	*Q2;2*	AT5G56760 AT1G55920 AT2G17640 AT4G35640	T-DNA insertions, quadruple KO (Watanabe et *al*, 2008b)
881	*Q2;1*	AT5G56760 AT3G13110 AT2G17640 AT4G35640	T-DNA insertions, quadruple KO (Watanabe et *al*, 2008b)
918	*Q1;1*	AT1G55920 AT3G13110 AT2G17640 AT4G35640	T-DNA insertions, quadruple KO (Watanabe et *al*, 2008b)
1120	*slim1-1*	AT1G73730	Missense point mutation (Maruyama-Nakashita *et al.*, 2006)
1202	*cad2-1*	AT4G23100	6 bp deletion, KD (Howden et al., 1995)
1190	*sir1cad2*	AT4G23100 AT5G04590	Double KD (GK-550A09; Speiser 2014)
1210	*A1;1*	AT4G14880 AT5G56760	T-DNA insertions, double KO (SP1960; SALK_050213; Haas, 2010; Speiser, 2014)
1421	*serat2;2*	AT3G13110	T-DNA insertion, KO (Kazuza_KG752; Watanabe *et al.*, 2008b)
2066	*serat1;1;s3;1s3;2*	AT5G56760 AT2G17640 AT4G35640	T-DNA insertion, triple KO (crossed in this work, SALK_050213; SALK_030011; SALK_030223; Watanabe *et al.*, 2008b)
2221	*A1;1_cr#1*	AT5G56760 AT4G14880	1 bps insertion in each locus, double KO (this work, candidate line #2)
2222	*A1;1_cr#2*	AT5G56760 AT4G14880	2 bps deletion in AT4G14880, 45 bps gap spanning intron/exon in AT5G56760, double KO (this work)
2223	*A1;1_cr#3-1*	AT5G56760 AT4G14880	1 bps insertion in AT5G56760, 1 bps insertion and 7 bps deletion in AT4G14880, double KO (this work)
2224	*oastlA_cr#1*	AT4G14880	1 bps insertion, KO (this work)
2225	*serat1;1_cr#1*	AT5G56760	1 bps insertion, KO (this work)

2226	*serat1;1_cr#2*	AT5G56760	2 bps deletion, KO (this work)
2227	*oastlA_cr#2*	AT4G14880	45 bps gap spanning intron/exon, KO (this work)
2232	*prS3;2::SERAT3;2-mCherry*	AT4G35640	Col-0 expressing SERAT3;2-mCherry with minimal native promoter
2231	*prUbi::SERAT3;2-mCherry*	AT4G35640	Col-0 over-expressing SERAT3;2-mCherry with *Ubiquitin* promoter

2.3.2 Plant cultivation on soil and propagation

A. thaliana seeds (2.3.1) were sown on humid soil (Tonsubstrat from Okohum, Herbertingen supplemented with 10% (v/v) vermiculite and 2% (v/v) quartz sand) and stratified for one to two days at 4 °C in darkness. After two weeks in the growth chamber under short-day conditions (8.5 h day/15.5 h night, 50-60% relative humidity, 90 – 130 µmol $m^{-2}s^{-1}$ light intensity, and 22 °C during the light periods and 18 °C in the dark), individual seedlings were pricked out to fresh pots with fresh humid soil. Plants were watered regularly two to three times a week over a period of six to nine weeks until harvest. To induce flowering, plants were moved to long-day conditions (16 h day/8 h night, 50-60% relative humidity, 90 – 130 µmol $m^{-2}s^{-1}$ light intensity, and 22 °C during the light periods and 18 °C in the dark). Inflorescence stems were bound to wooden sticks and covered with plastic or paper bags to collect seeds. The watering was stopped when leaves started to senescence. After the plants turned completely dry, seeds were harvested using a sieve and stored in a dry and dark place.

2.3.3 Seed sterilization

Before starting seed work, a round filter paper was sterilized with 70% ethanol at the sterile bench. *A. thaliana* seeds (2.3.1) were transferred in a 1.5 ml Eppendorf tube and incubated for 2 min with 6% sodium hypochlorite. After brief centrifugation, the seeds were taken to the sterile bench, and the solution was exchanged for 70% (v/v) ethanol. After 5 min incubation, the seeds were washed thrice with sterile ddH_2O and placed on the sterile filter paper to dry.

2.3.4 Plant cultivation on sterile Petri dishes

To prepare solid medium plates, ½ Hoagland medium (2.1.4) was complemented with 0.8% UltraPure™ Agarose and autoclaved. 50 ml of hand-warm medium was poured into a squared Petri dish and let solidify. To generate sulfur deficiency media plates, the amount of sulfate was reduced to 1 µM or 0 µM as indicated by replacing $MgSO_4^{2-}$ with $MgCl_2$. For feeding experiments with sucrose, glutathione, or cysteine, sterilized stock concentrations of the chemicals were added to autoclaved hand-warm 0 µM sulfate ½ Hoagland medium before pouring it into the Petri dish. Sterilized seeds were sown on the plates using an autoclaved toothpick. The WT was always sown next to a mutant to increase comparability. The plates were sealed with surgical tape and stratified for two days at 4 °C before placing them vertically in a Percival incubator with short day conditions (8 h day/16 h night, 50-60% relative humidity, 90 – 130 µmol $m^{-2}s^{-1}$ light intensity, and 22 °C during the light periods and 18 °C in the dark).

2.3.5 OAS and NAS feeding

Long-term feeding of *O*-acetylserine (OAS) can only be performed by applying OAS regularly from fresh stocks, since OAS is naturally unstable and converts to *N*-acetylserine (NAS) quickly in neutral to alkaline conditions. Therefore, a 20 mM OAS stock solution (pH = 2.43) was aliquoted

to each 500 µl and directly frozen at -20 °C. To generate NAS, the pH of half of the OAS stock was adjusted to > 9.8 using 5 M KOH and incubated at room temperature for 12 hours to promote the conversion to NAS. After incubation, the solution was set to pH 2.43 with HCl, aliquoted to 500 µl, and frozen at -20 °C. Surface sterilized WT and mutant seeds (2.3.3) were sawn on ½ Hoagland +S (500 µM sulfate) and -S (1 µM sulfate) plates (2.3.4). The first treatment was applied after five days of growth in short-day conditions. For this, the plates were taken to the sterile bench and opened. 5 - 15 ml of 100 µM OAS and NAS solutions were freshly prepared by diluting the aliquoted 20 mM stocks in 100 mM MES pH 5.8 buffer. The solutions were filtered through a 0.22 µM sterile filter and directly dropped on top of the roots. As the mock control, +S and –S control plates were treated with sterile 100 mM MES pH 5.8 in the same way without adding OAS or NAS. The plates were left open to dry for 20 to 30 min at the sterile bench and placed back in short-day condition after sealing with surgical tape. The treatment was repeated three times a week for a total of nine treatments. Then, the average root length was measured with a ruler, and the pooled shoot FWs and root FWs were measured with a fine scale. Each data point is generated from one pooled plate.

2.3.6 Grafting of *A. thaliana*

To perform the grafting of different *A. thaliana* genotypes (2.3.1), seedlings were grown on plates containing sterile ½ Hoagland medium in short-day conditions (2.3.4). After nine days of growth, always two seedlings of similar size were transferred to fresh ½ Hoagland plates containing 1% sucrose, 1.4% UltraPure™ agarose, and 40 µg/ml ampicillin to inhibit bacteria growth. Seedlings were cut midway through the hypocotyls using a sterile scalpel. The shoots were switched using sterile forceps and placed in direct contact with the root's cutting site. Hence the small size of Arabidopsis, a binocular was used for precise positioning. This procedure was performed in the laminar flow cabinet. After twelve seedling pairs were generated, the plate was sealed and placed back in short-day condition. Plantlets were inspected for adventitious root formation on the scion seven days after grafting. Those roots were removed by cutting them with a sterile scissor. Successfully grafted plants were transferred to fresh ½ Hoagland medium with 500 µM sulfate or 1 µM sulfate and maintained for four weeks in the same growth conditions. Each week, adventitious roots on the scion were removed. At the end of the fourth week, the shoot and root were cut and weighed separately with a fine scale. The root-to-shoot FW ratio was calculated for each graft.

2.3.7 Plant cultivation in hydroponic system

The culture of *A. thaliana* in hydroponics is adapted from Tocquin *et al*. (2003). To create the pre-cultures, the lids and bottoms of 0.5 ml Eppendorf tubes were cut off and stacked in empty 1 ml tip boxes. After autoclaving, the tubes were filled with hand-warm ½ Hoagland 0.8% UltraPure™ agarose (2.1.4) by adding one drop in each 0.5 ml tube. When the agar cooled and thereby sealed the hole in the bottom, the remaining tube was filled with agar until a hump was generated on top. With a sterile toothpick, three surface sterilized seeds (2.3.3) are placed on each hump. It is especially important to gently push the seed into the surface of the agar so the roots will develop inside rather than on top of the agar. Then, the tube box is filled with sterile ½ Hoagland medium (~ 650 ml) via an autoclaved funnel and sealed with surgical tape. The seeds are stratified in the boxes for 2 - 3 days at 4 °C in the dark before transfer to the Percival growth chamber with short-day conditions (8 h day/16 h night; day temperature: 22 °C; night temperature: 18 °C; light intensity: 90-120 $\mu molm^{-2}s^{-1}$; relative humidity: 50-60%). After two weeks of growth, the seedling's

roots have grown through the 0.5 ml tubes and can be transferred to 6 l pots filled with ½ Hoagland liquid medium. For each 6 l box there is one holding plate with 18 holes fitting 18 tubes. To ensure that only one seedling was growing per tube, additional germinated seedlings were removed by gently pulling them out of the agar. The space in each 6 l pot was divided among the chosen genotypes to ensure similar growth conditions. The pots were placed in the Waiss growth cabinets with short-day conditions (8.5 h day/15.5 h night; day temperature: 22 °C; night temperature: 18 °C; relative humidity: 50-60%; light intensity: 90-120 $\mu molm^{-2}s^{-1}$). The medium was exchanged weekly to ensure a consistent nutrient supply until the plants reached a total age of seven to eight weeks. In the case of the application of a treatment, the normal medium was exchanged one last time 24 hours before the start. The roots were quickly washed when transferring the plants to the treatment medium by dipping them in ddH_2O. On the day of harvest, the shoots of individual plants were cut, weighed, and wrapped in aluminum foil before freezing in liquid nitrogen. The roots were quickly dried in a paper towel without much pressure before weighing and freezing in 5 ml Eppendorf tubes. The root-to-shoot ratio was calculated from the FWs for each individual.

2.3.8 Crossing of *A. thaliana*

To induce flowering, seven-week-old soil-grown *A. thaliana* plants (2.3.1) were transferred from short-day to long-day conditions (2.3.2). With 10x magnification of a binocular microscope, the unripe anthers of developmentally advanced buds of the mother plants were carefully removed without damaging the stigma to prevent self-fertilization. By taking a fully developed bud from the father plant with ripe anthers, the pollen of the father plant was carefully distributed on top of the stigma of the emasculated mother buds. Additionally, all unused flowers, already formed siliques, and new apical meristems were removed from the mother plant to enhance the energy and nutrient distribution into the buds used for crossing. Furthermore, all successfully cross-pollinated flowers were covered in little translucent plastic bags to protect the stigma from further unwanted pollination and to prevent any loss of seeds after the siliques were successfully generated and matured. Seeds were harvested when siliques appeared dark brown, and after 24 h of drying, the harvested seeds were ready to be sown again. The naming of the crossed lines indicates the crossing direction, as the mother plant is always listed first, followed by the male plant line name.

2.3.9 Stable transformation of *A. thaliana*

A. thaliana (2.3.1) was transformed using the floral dip transformation protocol by Clough and Bent (1998). For this, a 250 ml overnight culture of *A. tumefaciens* containing the desired T-DNA construct was grown to an OD_{600} = 0.8 – 1.2 in YEB medium with all necessary antibiotics (2.2.2). The bacteria were harvested by centrifugation at 5000 x g for 15 min. In addition to the protocol, the bacteria pellet was once washed with 200 ml cold H_2O to remove traces of antibiotics. The pellet was resuspended in 200 ml transformation medium (4.1.4) to an OD_{600} of 1. Flowering *A. thaliana* plants were dipped into the bacteria-containing transformation medium three times by thoroughly covering all flowers. Then, the plants were wrapped in cling film to keep the humidity and placed horizontally on a closed tray in darkness for 24 h. The plants were allowed to recover for one week before repeating the procedure. They were kept in long-day conditions until the siliques became ripe (2.3.2). Harvested seeds were sown on soil, and after two weeks, they were sprayed with 200 µM/ml Basta to select for the T-DNA insertions. Surviving plants were pricked out and further grown for genotypic analysis.

2.3.10 Measurement of root-to-shoot FW ratio

A. thaliana seedlings (2.3.1) were grown on solid media plates (2.3.4) or in the hydroponic system (2.3.7). On the day of harvest, plants were cut at the hypocotyl to separate shoot from root. Shoots and roots from plants growing on solid media plates were pooled for each genotype and weighed with the precision balance AUW120D (Shimadzu, Griesheim). The average root or shoot FW was calculated by dividing the weight of the FW pool by the number of used individuals. Seedlings that failed to develop true leaves were not used in the analysis. Shoots and roots from plants growing in the hydroponic system were weighed individually with the precision balance CY323C (Waagen Friedrichs, Heidelberg). The root-to-shoot FW ratio was calculated by dividing root FW by shoot FW.

2.3.11 Measurement of average primary root length

The primary root length of seedlings grown on sterile media plates (2.3.4) was measured with a ruler. Therefore, individual seedlings were taken from the plate using forceps and laid on top of the ruler. The root length was noted, and the average was calculated.

2.3.12 Rosette diameter measurement

To assess the rosette diameter, pictures of rosettes were analyzed with FIJI (1.4.6). First a scale was set, then a circle was drawn around the rosette of each plant and the area (A) was measured. The diameter (d) was calculated according to:

$$d = 2 * \sqrt{\frac{A}{\pi}}$$

2.3.13 Transient transformation of *N. benthamiana*

Infiltration of *N. benthamiana* leaves was performed according to Sparkes *et al*. (2006). 200 ml *A. tumefaciens* (2.2.1) overnight culture was generated using YFB medium (2.1.4) supplemented with the necessary antibiotics (2.2.2). The bacteria were harvested by centrifugation at 5,000 g at RT for 10 min. The supernatant was removed, and the bacteria were washed twice with ddH_2O to remove traces of antibiotics by repeating the centrifugation. Afterward, the bacteria were resuspended in 7 - 10 ml ddH_2O to an OD_{600} of 1. Five weeks old *N. benthamiana* were placed in 100% humidity for at least one hour to open the stomata. The abaxial side of the leaves was infiltrated with the bacteria solution by applying pressure carefully on a 1 ml syringe. Infiltrated leaves were marked with tape, and the plants were placed in long-day conditions (Waiss) to recover. After two days the expression was analyzed by Confocal Laser Scanning Microscopy (CLSM) (2.3.15).

2.3.14 DAPI staining

To visualize the nucleus of seedlings and plant tissue in microscopy, the fluorophore DAPI (4',6-diamidino-2-phenylindole) was used. It is membrane permeable, binds strongly to adenine-thymine-rich DNA, and incorporates into double-stranded nucleic acids. For staining, whole seedlings grown on solid media plates (2.3.4) or pieces of transient transformed *N. benthamiana* leaves (2.3.13) were transferred to six-well plates containing 5 µM DAPI dissolved in ddH_2O and incubated for 2 - 3 min. After 5 min destaining in ddH_2O, the plant tissues were used for microscopy. The used excitation wavelength was 405 nm, and the detector was set to the range of 420 - 495 nm.

2.3.15 Confocal Laser Scanning Microscopy (CLSM)

Transient and stable transformed plants containing fluorescent proteins were analyzed with CLSM (Leica Stellaris 8), HC PL APO CS2 20x / 0.75 DRY objective, and LAS X 4.5.0.25531 software. The used excitation and emission wavelength were for mCherry: $\lambda_{ex}\backslash\lambda_{em}$ = 587 nm\595 nm - 630 nm for autofluorescence of chloroplast: $\lambda_{ex}\backslash\lambda_{em}$ = 653 nm\ 659 nm - 753 nm. A bright field image was generated using the white light laser. The images were processed using the software Fiji ImageJ. The mCherry, autofluorescence, and bright field channels were split, and false colors were assigned to each channel (red - mCherry, green - autofluorescence, grey - bright field). If necessary, contrast and brightness were carefully adjusted. In addition, a merged picture of all three channels was created.

2.4 Molecular biology methods

2.4.1 Plasmid listing

Table 3: List of plasmids used in this work.

ID	Name	Resistance	Generated by
402	pET28a HIS-SERAT1;1	*Kan*^{r}	Dr. Corinna Heeg
1878	pET3d STREP-SERAT3;2	*Amp*^{r}	this work
1880	pET3d STREP-SERAT3;2ΔC	*Amp*^{r}	this work
1894	pET32a OAS-TL A	*Amp*^{r}	Dr. Shengkai Sun
2120	pDGE332 (M1) OAS-TL A target 1	*Amp*^{r}	this work
2121	pDGE333 (M2) OAS-TL A target 2	*Amp*^{r}	this work
2122	pDGE335 (M3) SERAT1;1 target 1	*Amp*^{r}	this work
2123	pDGE337 (M4) SERAT1;1 target 2	*Amp*^{r}	this work
2124	pDGE347 A1;1_cr	*Spec*^{R}, *Basta*^{R}	this work
2231	prUbi::SERAT3;2-mCherry	*Basta*^{R}	Diana Gabler
2232	prSERAT3;2::SERAT3;2-mCherry	*Basta*^{R}	Diana Gabler

2.4.2 Isolation of plasmid DNA from *E. coli*

Plasmid DNA was extracted from 5 ml overnight cultures (2.2.2) using the mini kit NucleoSpin® Plasmids following the kit's protocol (2.1.5). DNA was stored at -20 °C for short-term or -80 °C for long-term storage.

2.4.3 Extraction of genomic DNA from plant tissue

To extract genomic DNA from plant tissue, the protocol of Edwards *et al*. (1991) was used. Therefore, plants (2.3.1) were grown for at least three weeks on soil until enough biomass was produced so that harvesting of one leave would not kill the plants (2.3.2). The leaf material was placed in an Eppendorf tube and frozen in liquid nitrogen to store at -80 °C if gDNA extraction was not performed subsequently. The plant material was ground directly in the Eppendorf tube with a plastic mortar and resuspended in 400 µl Edward's buffer (2.1.4). Each sample was vortexed for 10 s and centrifuged at 14,000 x g for 5 min. 300 µl of supernatant was mixed with 300 µl of 100% isopropanol in a new microcentrifuge tube by inverting the tube several times. After incubation for 2 min at RT, samples were centrifuged at 14,000 g for 10 min to precipitate the DNA. The supernatant was removed, and the pellet was washed with 70% (v/v) ethanol and centrifuged for 2 min at 14,000 g. The supernatant was discarded, and the gDNA was air-dried for 30 min. The

dried pellet was resolved in 50 µl ddH_2O. gDNA was either directly used or stored at 4 °C for up to two weeks.

2.4.4 Isolation of total RNA from plant tissue

Total RNA was isolated from 50 – 100 mg of plant tissue using the Roboklon Universal RNA Kit (Roboklon, Berlin) (2.1.5), following the manufacturer's protocol. RNA was eluted in 50 µl of RNase-free water and stored at 4 °C for short-term usage or -80 °C for long-term storage.

2.4.5 cDNA synthesis

The fast Gene Scriptase II cDNA kit (Nippon Genetics) (2.1.5) was used to generate cDNA from 1 µg of total RNA (2.4.4) following the manufacturer's protocol. cDNA was stored at -20 °C for short-term usage or -80 °C for long-term storage.

2.4.6 Primer design and listing

Primers for cloning, genotyping, and qRT-PCR were designed with melting temperatures of 55 - 65 °C using the Geneious software application (2.1.6) and were purchased from Sigma-Aldrich (Steinheim) (Table 4). Lyophilized primers were resuspended in ddH_2O to a stock concentration of 100 µM and stored at -20 °C.

Table 4: List of primers.

Cloning primers		
ID	**Sequence (5' to 3')**	**Description**
5355	AACACCATGGGTTGGTCTCATCCTCAGTTCG AGAAGGCTTGTATAAACGGCGAGAATCG	Strep_S3-2_f
5356	AACAGGATCCTTAATGTCTCCTTTCCCTGCAAC	S3;2_BamHI_r
5420	ACAAGGATCCTTAAACAAACCCGATGAGTTTT GCTGG	S3;2dC_BamHI_r
5651	AACAGAAGACATATTGCACATCTTTAGCAATTC TCGGTTTAAGTCTTCTTGT	OAS-TLA _target_1_forward
5652	ACAAGAAGACTTAAACCGAGAATTGCTAAAGA TGTGCAATATGTCTTCTGTT	OAS-TLA_target_1_reverse
5653	AACAGAAGACATATTGCAAGTGGAAACACTGG AGTTGTTTAAGTCTTCTTGT	OAS-TLA _target_2_forward
5654	ACAAGAAGACTTAAACAACTCCAGTGTTTCCA CTTGCAATATGTCTTCTGTT	OAS-TLA _target__2_reverse
5655	AACAGAAGACATATTGAGCGTCAGCAGCGAT ATCTGGTTTAAGTCTTCTTGT	SERAT1;1_target_1_forward
5656	ACAAGAAGACTTAAACCAGATATCGCTGCTG ACGCTCAATATGTCTTCTGTT	SERAT1;1_target_1_reverse
5657	AACAGAAGACATATTGGAACAGATCGTATAAA AGTGGTTTAAGTCTTCTTGT	SERAT1;1_target_2_forward
5658	ACAAGAAGACTTAAACCACTTTTATACGATCT GTTCCAATATGTCTTCTGTT	SERAT1;1_target_2_reverse
Genotyping primers		
ID	**Sequence (5' to 3')**	**Description**
302	CTCACAAGATTCAAGGGATAGGA	OAS-TLA_WT_region_f

653	GTCATGGCTTCCGCTTCTTTC	OAS-TLA_WT_region_r
1225	GAACATCGGTCTCAATGCAAAAGGGGAAC	OAS-TLA_T-DNA_r
1401	ATTTTGCCGATTTCGGAAC	T-DNA_region for SERAT1;1, SERAT3;1, and SERAT3;2
1639	GGATGCTTTTGAGCACTTTTG	SERAT1;1_WT_region_f
1640	TGCGCCTAATTCAAATTCAAC	SERAT1;1_WT_region_r
2217	CTCCTGCTGAAAGTGATGGTC	SERAT3;1_WT_region_r
2218	CTTTTGGTTGAGTCTTGCTGG	SERAT3;1_WT_region_f
2219	GATCATGGAACTGGTGTGGTC	SERAT3;2_WT_region_f
2220	TTCCAGGCTAAGCATGCTTAG	SERAT3;2_WT_region_r
5728	GGATTGGTGCTCATACATCTG	OAS-TLA_CRISPR_targets_f
5729	CCTTTCATGCCCTTAGCTG	OAS-TLA_CRISPR_targets_r
5730	GCACCAGGTGGACTATC	SERAT1;1_CRISPR_targets_f
5731	CAACAAAGCCAAATCATGATC	SERAT1;1_CRISPR_targets_r

qRT-PCR primers

ID	Sequence (5' to 3')	Description
1841	GCCATCACAATCGCTCTCCAA	SULTR1;1_forward
1842	TTGCCAATTCCACCCATGC	SULTR1;1_reverse
2457	GATGAGGCACCAACTGTTCTTCGTG	TIP41_forward
2458	CTGACTGATGGAGCTCGGGTCG	TIP41_reverse
2611	GTGTTTAATCGCGGCTCTTC	IRT1_forward
2612	GTTAAGCCCATTTGGCGATA	IRT1_reverse
3014	GTGGAGACACTCCTTATGTCAGAGC	SDI1_forward
3015	CTCTGTCTCCAGTGTTGATGGC	SDI1_reverse
3024	CCGGAGCTATTTGCTGGGGTG	GGCT2;1_forward
3025	GTCGTATTCACACTCTCTTCGTTCC	GGCT2;1_reverse
3026	CCGACTAGAGCCATCAACGTACC	SEN1_forward
3027	GACATTTGACCGCTCTCACAACC	SEN1_reverse
3028	CGATCTCATCGTCTCCTCCGGTG	GAT_forward
3029	CGCAGAGGAGGACACCATGAATAG	GAT_reverse
3034	CGACCCATGGCAATTACCCG	ANAC029_forward
3035	GCCCGGTTTGGTCTGACTCC	ANAC029_reverse
3038	CCTCCCCAACACAACGTTCC	NAS2_forward
3039	GGTCTAACCCCTCCTTAGCG	NAS2_reverse
3040	GTCCGATGCCTCTCACATCCATC	NAS1_forward
3041	GAAGCGAGTGTGTTTGCGTGTG	NAS1_reverse
4167	GCTCATCTTCTTCGCTTTCTG	DIN10_forward
4168	GCGACGCTGCTTCGCTTC	DIN10_reverse

2.4.7 Polymerase chain reaction (PCR)

PCR is used to amplify DNA fragments specified by primers (2.4.6) to genotype plants or bacterial colonies and generate DNA fragments for cloning. The FastGene® TAQ Ready Mix PCR Kit (2.1.5) was used for genotyping with the following mix: 2 µl gDNA (2.4.3) or one bacterial colony (2.2.5; 2.2.6), 1 µl each primer (10 µM), 10 µl FastGene® TAQ ReadyMix PCR, and 6 µl ddH_2O. The PCR reaction was performed using the PCR program according to Table 5. The PCRBIO HiFi Polymerase

kit (2.1.5) was used to amplify DNA fragments for cloning, sequencing, and other applications that required downstream restriction enzyme reactions. For one PCR reaction, 1 µl template (2.4.2) or cDNA (2.4.5), 10 µl 5x PCRBIO HiFi buffer, 2 µl each 10 µM primer, 0.5 µl PCRBIO HiFi Polymerase, and 34.5 µl sterile ddH_2O were mixed to a total volume of 50 µl. The PCR reaction was performed using the PCR program according to Table 6.

Table 5: PCR cycle program for FastGene® TAQ Ready Mix PCR Kit.

Cycle	Step	Temperature	Time
1	Initial denaturation	95 °C	3 min
35	Denaturation	95 °C	30 sec
35	Annealing	55-65 °C	30 sec
35	Extension	72 °C	1 min/kb
1	Final extension	72 °C	5 min
1	Hold	12 °C	Infinite

Table 6: PCR cycle program for PCRBIO HiFi Polymerase kit.

Cycle	Step	Temperature	Time
1	Initial denaturation	95 °C	30 sec
35	Denaturation	95 °C	15 sec
35	Annealing	55-65 °C	15 sec
35	Extension	72 °C	30 sec/kb
1	Final extension	72 °C	2 min
1	Hold	12 °C	Infinite

2.4.8 Quantitative real-time polymerase chain reaction (qRT-PCR)

Quantitative real-time PCR (qRT-PCR) was performed to analyze gene expression levels. For this, cDNA (2.4.5) was diluted 1:2 with 20 µl DNAse free water to a total volume of 40 µl. One qRT-PCR reaction mix contained 2 µl of cDNA, 0.5 µl primer mix (5 µM each), 3.75 µl ddH_2O, and 6.25 µl qPCRBIO SyGreen Mix Lo-ROX (PCR Biosystems, London) (2.1.5). The used primers are listed in 2.4.6 (Table 4) and the PCR reaction was carried out following the manufacturer's instructions. All samples were measured in duplicates. One WT sample was used to prepare the standard curve (1:1, 1:10, and 1:100). The expression of the genes of interest was normalized to the housekeeping gene *TIP41* (*AT4G34270*). Measured Ct values were then normalized to the mean of the Ct values of WT samples, if not stated otherwise.

2.4.9 Agarose gel electrophoresis

DNA molecules with sizes > 600 bps, like PCR products (2.4.7) or digested plasmids (2.4.11), were separated by agarose gel electrophoresis using gels containing 0.8% agar and ~ 0.5 µg/ml Ethidium bromide. The agarose concentration in the gel was increased to 2% to separate smaller DNA fragments. The samples were mixed with 6x loading dye (New England Biolabs, Beverly), loaded on the gel next to 1 kb plus DNA ladder (New England Biolabs, Beverly), and run in TAE buffer (2.1.4) at 110 V for 30 min. The DNA fragments were visualized with UV light and digitalized using an Intas Science Imaging device (INTAS, Göttingen).

2.4.10 DNA extraction from agarose gels

DNA was purified from agarose gels (2.4.9) using NucleoSpin® Gel and PCR Clean-up kit (Macherey and Nagel) (2.1.5) according to the manufacturer's protocol. Finally, extracted DNA fragments were eluted in 20 µl ddH_2O.

2.4.11 DNA digestion using restriction enzymes

Since restriction enzymes (New England Biolabs, Beverly) cut specific DNA sequences, they are used in conventional restriction enzyme cloning of new plasmids (2.4.12) or in verifying existing plasmids. Therefore, DNA was incubated with different restriction enzymes according to the plasmids-specific restriction enzyme recognition sites predicted by the Geneious software application (2.1.6). One digestion reaction contained DNA with a total mass of 1 µg, 2 µl of CutSmart® buffer, 1 µl per restriction enzyme, and a total volume of 20 µl. The mix was incubated at 37 °C for at least 2 h before analyzing using gel electrophoresis (2.4.9).

2.4.12 Restriction enzyme cloning

To generate new plasmids, digested (2.4.11) and purified (2.4.10) vector backbone and PCR insert (2.4.7) were mixed in a molar ratio of 1:3 and incubated in 2 µl 10x T4 DNA ligase buffer and 1 µl T4 DNA ligase (New England Biolabs, Beverly) in a volume of 20 µl. The reaction was incubated for 30 min RT or overnight at 16 °C, followed by inactivation of the enzyme at 65 °C for 10 min. 10 µl of the reaction mix was used to transform *E. coli* (2.2.5). Selected colonies were used to generate overnight cultures (2.2.2) from which the plasmids were purified (2.4.2). The correct assembly was checked with test digestion (2.4.11) and sequencing (2.4.14).

2.4.13 Cloning of CRISPR/Cas9 vectors

To generate CRISPR/Cas9 plant transformation vectors, the cloning system by Stuttmann *et al*. (2021) was used. Two targets in each *OAS-TL A* and *SERAT1;1* locus were chosen using the internet tools ChopChop and targetDesign (2.1.6), resulting in primers 5651 – 5658 (2.4.6). For each target, the forward and reverse primers were hybridized by mixing the primers at 10 µM and heating at 98 °C for 5 min, followed by cooling down at RT. The hybridized primers were diluted 1:200 to 50 fmol/µl and kept on ice. To load the hybridized primers into sgRNA shuttle vectors, the reaction mix of 1 µl hybridized primers (50 fmol/µl), 1 µl shuttle vector (M1-M4) (60 ng/µl), 1 µl T4 Ligase buffer, 1 µl CutSmart® buffer, 0.3 µl BpsI, and 0.3 µl T4 Ligase in a total volume of 10 µl, was incubated according to the GreenGate® reaction cycle (Table 7). The reaction mix was used to transform chemo-competent XL1 blue (2.2.5) and bacteria were selected with Ampicillin. Plasmids were purified from a 5 ml overnight culture (2.2.2), and the successful ligation was verified by sequencing (2.4.14). The primers 5651 and 5652 were thereby cloned into M1 as pDGE332 (M1) OAS-TL A target 1 (2120). 5653 and 5654 were cloned into M2 generating pDGE333 (M2) OAS-TL A target 2 (2121). 5655 and 5656 were cloned into M3 as pDGE335 (M3) SERAT1;1 target 1 (2123) and 5657 and 5658 were cloned into M4E as pDGE337 (M4) SERAT1;1 target 2 (2123). The successfully generated shuttle vectors M1, M2, M3, and M4E were diluted to 40 ng/µl. The four sgRNA targets were cloned into the pDGE347 recipient vector in a reaction mix containing 1 µl of each shuttle vector, 1 µl of pDGE347 destination vector (300 ng/µl), 2 µl of CutSmart®, 2 µl T4 Ligase Buffer, 1 µl BpsI and 1 µl T4 Ligase filled to 20 µl with ddH_2O. The reaction was carried out following the GreenGate® cycle program (Table 7), transformed into XL1 blue (2.2.5), and

selected with Spectinomycin. The successful assembly of pDGE347 A1;1_cr (2124) (Supplemental Figure 4) was verified by test digestion (2.4.12) and sequencing (2.4.14).

Table 7: GreenGate® reaction cycle program according to Lampropoulos *et al.* (2013).

Cycle	Step	Temperature [°C]	Duration [min]
30	Restriction	37	2
30	Ligation	16	2
1	Final ligation	16	2
1	Inactivation T4 Ligase	50	5
1	Inactivation BsaI	80	5

2.4.14 Sequencing

Eurofins Genomics (Ebersberg) performed the sequencing of newly generated DNA vectors (2.4.12, 2.4.13) or PCR products (2.4.7). Samples were prepared according to Eurofins instructions and sequencing results were analyzed using the software application Geneious (Biomatters, Auckland) (2.1.6).

2.4.15 mRNAseq analysis

Total RNA (2.4.4) was sent to BGI TECH SOLUTIONS (Hongkong) or Novogene GmbH (München) for transcriptome analysis following the companies' instructions. After RNA quality control, the mRNA library preparation was performed with poly A enrichment. Novogene used NovaSeq X Plus Series (PE150bp) with 6 Gb of raw data per sample as the Sequencing Platform & Strategy. BGI used DNBseq as the sequencing platform with the same read length of PE150bp and also 6 Gb of Clean data output per sample. The raw data was sent to the NGS Core Facility, Medical Faculty Mannheim, University of Heidelberg, for bioinformatic analysis. RNA-seq data processing was performed with R (version 3.6.3) and bioconductor (version 3.9) in Rstudio (version 1.1.463). Quality control of clean sequencing reads was performed using FastQC (Babraham Bioinformatics). Low-quality reads were removed using trim galore (version 0.6.4). The resulting reads were aligned to the arabidopsis genome version TAIR10 and counted using kallisto version 0.46.1 (Bray *et al.*, 2016). The count data was transformed to log2-counts per million (logCPM) using the voom-function from the limma package (Ritchie *et al.*, 2015). Differential expression analysis was performed using the limma package in R. A false positive rate of α= 0.05 with FDR correction was taken as the level of significance. Volcano plots and heatmaps were created using ggplot2 package (version 2.2.1) and the complexHeatmap package (version 2.0.0) (Gu *et al.*, 2016). For enrichment analysis, we used the fgsea (Korotkevich *et al.*, 2021), the enrichmentbrowser (Geistlinger *et al.*, 2016), and the Enrichr packages (Chen *et al.*, 2013). The pathway analysis was made with fgsea package (Korotkevich *et al.*, 2021) and the enrichmentbrowser package (Geistlinger *et al.*, 2016) in R using the pathway information from KEGG database (2.1.6).

2.5 Protein biochemical methods

2.5.1 Expression of recombinant proteins in *E. coli*

E. coli BL21 (DE3) cells carrying protein expression vectors were cultured in 10 ml LB medium (2.1.4) containing the appropriate antibiotics at 37 °C and 180 rpm for 16 hours (2.2.2). The overnight culture was used to inoculate an Erlenmeyer flask filled with 300 ml of the same medium. The bacteria were grown at 37 °C and 180 rpm until OD_{600} reached 0.6 - 0.8. For the

induction of protein expression, IPTG was added to the flask to a final concentration of 1 mM. After 4 hours at 37 °C and 180 rpm, the bacteria were harvested by centrifugation at RT and 10,000 rpm for 10 min. The bacterial pellet was frozen in liquid nitrogen and stored at -80 °C until further usage.

2.5.2 His-tagged recombinant proteins from *E. coli*

A bacteria pellet containing His-tagged proteins (2.5.1) was resuspended in 10 - 30 ml Buffer B (2.1.4), depending on the size of the pellet. PMSF was added to 1 mM working concentration, and cells were sonicated using Sonopuls GM70 sonicator (Bandelin) on ice twice at 60% activity for 10 min. Afterward, cells were centrifuged at 20,000 g and 4 °C for 10 min. The supernatant, further named crude extract (CE), was filtered with a 0.45 µM sterile filter. 500 µl CE was taken as input control. The HiTrap® Chelating High-Performance Column (GE Healthcare) was connected to a peristaltic pump (Behr Labor-Technik), and the flow rate was calibrated to 1 ml/min. The column was washed with ddH_2O for 5 min and loaded with 50 mM $NiCl_2$ for 5 min. Afterward, the column was equilibrated with Buffer B (2.1.4) for 10 min. The CE was circulated for at least 1 h or until the total CE volume had passed three times through the column. 500 µl of flow-through (FT) was collected after 2 min as column loading control. Subsequently, the column was washed with buffer W (2.1.4) for at least 30 min. The last 500 µl of flow through were collected as washing control (W). The proteins were eluted from the column by applying buffer E (2.1.4), and the flow-through was collected in 500 µl fractions between minute 1 and minute 4 (E_1 - E_4). The protein concentration was measured (4.5.5), and CE, FT, W, and E with the highest concentration were denatured (2.5.8) and stored at -20 °C until further use. For size exclusion chromatography (SEC) (2.5.5), the two to three highest elution fractions were combined and either directly loaded onto the SEC or stored at 4 °C. The Ni^{2+} ions bound to the column were removed by applying 10 mM EDTA for 5 min. The column was washed with 10 min ddH_2O and sealed with parafilm for storage at 4 °C.

2.5.3 Extraction of StrepII®-tagged recombinant proteins from *E. coli*

A bacteria pellet containing STREPII®-tagged proteins was resuspended in 10 - 30 ml Strep buffer (2.1.4) containing 1 mM PMSF. The cells were sonicated with the Sonopuls GM70 sonicator (Bandelin) on ice twice at 60% activity for 10 min and centrifuged at 20,000 g at 4 °C for 10 min. The supernatant is further termed crude extract (CE) and was filtered with a 0.45 µM sterile filter. 500 µl were kept in ice as loading control. The Strep-Tactin® Superflow® high capacity FPLC column (Iba Lifescience) or Streptactin® superflow Plus cartridge (Roth) was connected to a peristaltic pump (Behr Labor-Technik) and equilibrated in Strep buffer for 10 min. The flow rate was set to 1 ml/min, and the CE was circulated for at least 1 h or until CE volume had passed through the column at least three times. After 2 min, 500 µl of the flow through (FT) was collected as a column loading control. Subsequently, the column was washed with Strep buffer for at least 30 min, after which 500 µl of the flow through was collected as a washing control (W). For purification of Strep-SERAT3;2 expressed together with His-*SERAT1;1* bacterial O-acetylserine(thio)lyase (CysK) was eluted with 10 mM OAS dissolved in Strep buffer for 5 min. The elution fractions were collected starting from minute 1 min to minute 4 in 500 µl volumes ($E_{1OAS}E_{4OAS}$). Afterward, washing was performed with Strep buffer for 10 min. The final elution was performed with 10 mM desthiobiotin dissolved in Strep buffer, and the E fractions were collected from minute 1 to 4 in 500 µl units (E_{1dest} – E_{4dest}). The protein concentration was measured (2.5.8), and CE, FT, W, and E with the highest concentration were denatured (2.5.9) and stored at -20 °C

until further use. For size exclusion chromatography (SEC) (2.5.5) the two to three highest E fractions were combined and either directly loaded onto the SEC or stored at 4 °C. The column was regenerated with 1 mM HABA solved in Strep buffer for 10 min. Afterward, the column was washed with Strep buffer until the column turned colorless. The column was sealed with parafilm and stored at 4 °C.

2.5.4 Extraction of StrepII®-tagged recombinant proteins from *A. thaliana*

For purification of StrepII®-tagged proteins from plant tissue, 3 to 10 g of ground leaf material was mixed in at least 1.5x Strep buffer (2.1.4) supplemented with 10 mM dithiothreitol (DTT), 1mM phenylmethylsulfonylfluorid (PMSF) and 1x cOmplete EDTA-free Protease inhibitor (Roche). The mixture was centrifuged at 20,000 g at 4 °C for 10 min. The supernatant was taken off and further referred to as crude extract (CE). It was filtered with a 0.45 µM sterile filter, and 500 µl was set aside as input control. The Strep-Tactin® Superflow® high capacity FPLC column (Iba Lifescience) was connected to a peristaltic pump (Behr Labor-Technik), and the flow rate was calibrated to 1 ml/min. Before the CE was applied, the column was equilibrated with Strep buffer for 10 min. The CE was circulated for at least one hour or until the CE volume had passed through the column at least thrice. After 2 min, 500 µl of flow-through (FT) was kept as column loading control. Subsequently, the column was washed with Strep buffer for at least 30 min, and the last 500 µl were collected as washing control (W). Finally, proteins were eluted with 5 ml of 10 mM desthiobiotin dissolved in Strep buffer into a 15 ml concentration tube (Vivaspin 2, 5000 MWCO, Sartoris). The elution was concentrated to 200 µl by centrifugating at 6,000 g at 4 °C for 12 min (Swing bucket Centrifuge Rotanta 460R, Hettich Zentrifugen). Afterward, the protein concentration was measured (2.5.8), and proteins were denatured (2.5.9) and stored at -20 °C until further use. The column was regenerated in 1 mM HABA dissolved in Strep buffer for 10 min. Afterward, the column was washed with Strep buffer until the column turned colorless. The column was sealed with parafilm and stored at 4 °C.

2.5.5 Size exclusion chromatography (SEC)

Size exclusion chromatography (SEC) was applied to determine the molecular weight and quaternary structure of protein complexes. Therefore, Superdex200 HiLoadTM 16/60 prep grade (GE Healthcare) was connected to the Pharmacia FPLCTM system (GE Healthcare). Before use, the column was washed and equilibrated in SEC buffer (2.1.4) with a flow rate of 1 ml/min. Calibration was performed with a high- and low-molecular-weight filtration calibration kit (GE Healthcare) (2.1.5) according to the manufacturer's instructions. 0.5 mg - 3 mg protein solution was loaded into the input valve with a 1 ml syringe. The run was performed with a flow rate of 1 ml/min. After the void volume had passed the column, 5 ml flow-through fractions were collected from minute 45 up to minute 75. The proteins were separated by size and detected by UV absorbance at 280 nm. The run was finished after 120 min once the conductance curve displayed a peak. Afterward, the column was washed with 20% ethanol and sealed with parafilm for storage.

2.5.6 Isolation of total proteins with NuPAGE buffer

Frozen plant material was ground with a pestle and mortar or a precooled drill. 100 mg of plant material was topped with 800 µl of NuPAGE buffer (2.1.4) in a 1:8 w/v ratio. After being vortexed on ice for 5 min, the samples were centrifuged at 14,000 g at 4 °C for 15 min. The supernatant was transferred to a fresh tube, and the proteins were denatured by boiling at 95 °C for 10 min.

Bacterial pellets were topped with NuPAGE buffer in a 1:8 w/v ratio and directly boiled at 95 °C for 10 min, followed by centrifugation. The supernatants were directly used for the SDS page or stored at -20 °C.

2.5.7 Extraction of total soluble proteins from plant tissue

Soluble proteins were extracted from 50 - 100 mg of frozen plant tissues ground with a pestle and mortar or a pre-cooled drill. 250 - 350 µl of protein extraction buffer (2.1.4) was added to the material and the mixture was vortexed for 15 min, followed by centrifugation at maximum speed at 4 °C for 10 min. The supernatant was transferred to a new tube, and the centrifugation was repeated until the supernatant was clear. Extracted proteins were kept on ice for subsequent use or stored at -20 °C.

2.5.8 Quantification of protein concentration according to Bradford

Bradford's (1976) protocol was used to quantify protein concentration. Protein extracts (2.5.2, 2.5.3, 2.5.4, 2.5.7) were diluted 1:10 or 1:5 to stay in range with the BSA standard curve of 0, 0.1, 0.2, and 0.4 µg/µl. All samples were measured in duplicates. Therefore, 10 µl samples were placed in a U-bottom 96 well plate (Greiner Bio-One) and topped with 250 µl 1x Roti®Quant (Roth). The absorption was measured at 595 nm using a FLUOStar Optima Microplate Reader (BMG Labtech). The protein concentration was determined for all samples after calculating the standard curve with the software application FLUOstar Optima 1.30 (BMG Labtech).

2.5.9 Protein denaturation

Protein concentrations of samples from the same experiment were equalized by diluting according to their concentration (2.5.8) using their isolation buffer. For denaturation, the protein samples were mixed with 5x SDS protein loading buffer (2.1.4) in a 1:5 (v/v) ratio, vortexed, and boiled at 95 °C for 10 min.

2.5.10 SDS-polyacrylamide gel electrophoresis (SDS-PAGE)

Mini-PROTEAN II-System (Bio-Rad) or PerfectBlue Twin ExW S-System (Peqlab) systems were used in SDS-Polyacrylamide gel electrophoresis (SDS-PAGE) to separate proteins according to their molecular weight. Every gel consists of a 12.5% Polyacrylamide resolving gel which is topped by a 7.5% stacking gel. The recipe for two resolving gels for both systems is displayed in Table 8.

Table 8: Recipe for Polyacrylamide gels used in SDS-PAGE. The recipes for resolving and stacking gel buffers can be found in 2.1.4.

Gel type (System)	ddH_2O [ml]	Buffer [ml]	Rotigel 30 [ml]	10% APS [µl]	TEMED [µl]
2x Resolving gel 12.5% (Mini-Protean II-System)	4.5	3.3 (Resolving)	5.55	90	16
2x Stacking gel 7.5% (Mini-Protean II-System)	2.61	0.72 (Stacking)	1.13	45	9
2x Resolving gel 12.5% (PerfectBlue Twin ExW S-System)	13.5	9.9 (Resolving)	16.65	270	48
2x Stacking gel 7.5% (PerfectBlue Twin ExW S-System)	7.83	2.16 (Stacking)	3.39	90	18

Depending on the gel system and protein concentration, 10 - 25 µl denatured protein samples were loaded on the gel. 5 µl of BlueStar Prestained Protein Marker (NIPPON Genetics) was used as the protein molecular size reference. The PAGE was performed in 1x SDS running buffer (2.1.4) at 80 V for the first 20 min, followed by 200 V for 1 h. Afterward, the gels were stained with Coomassie staining solution (2.5.11) or used for Western blotting (2.5.12).

2.5.11 Visualization of proteins by Coomassie Brilliant Blue staining

To visualize the size-separated proteins from SDS-PAGE (2.1.10), the gels were incubated in Coomassie staining solution (2.1.4) on a horizontal shaker for at least 30 min. The staining solution was recovered for reuse and the gels were washed with ddH_2O until the background of the gel was clear again. The gels were visualized with ImageQuant LAS 400 (GE Healthcare).

2.5.12 Western blotting

Gels with size-separated proteins from SDS-PAGE (2.5.10) were subjected to Western blotting to prepare for the immunological detection (2.5.11) of target genes. Therefore, the gel was transferred to a Methanol-activated PVDF membrane (Immobilon-P TransferMembrane, 0.45 µm; Millipore). Mini Trans-Blot Cell systems (Bio-Rad) were used to transfer proteins from gels of the Mini-Protean II-System (Bio-Rad) (2.5.10), and blotting was performed in 1x blotting buffer (2.1.4) at 360 mA for 1.15 h at 4 °C or 60 mA for 16 h at 4 °C. To transfer proteins from the gels of the PerfectBlue Twin ExW S-System (Peglab) (2.5.10), Trans-Blot Cell systems (Bio-Rad) were used in 1x blotting buffer (2.1.4) with 200 mA for 16 h at 4 °C.

2.5.13 Immunological detection of proteins

To detect proteins of interest, the blotted membranes (2.5.12) were incubated with specific antibodies after unspecific epitopes of the membrane were blocked. The blocking was performed by incubation in 5% BSA (w/v) in TBS-T (2.1.4) on a horizontal shaker at RT for 1.5 h and the list of used antibodies can be found in Table 9. The blocking solution was recovered, and the membranes were washed three times for 5 min with 1x TBS-T followed by incubation with the primary antibody for 1.5 h. The three washing steps with 1x TBS-T for each 5 min were repeated before the secondary antibody was applied for 1 h. Finally, the membrane was washed three times for each 5 min in 1x TBS-T and developed with WesternBright™ Chemiluminescence Substrate (Biozym) following the manufacturer's instructions. The chemiluminescence signal was measured with the ImageQuant LAS 400 (GE Healthcare). Subsequently, the membrane was stained with an amido black solution as a loading control (2.5.14).

Table 9: List of used antibodies, their dilutions, and manufacturers.

antibody	type	dilution	manufacturer
mouse-anti-6xHis	primary	1: 3,000	Thermofischer (MA1-21315)
anti-Streptactin HRP conjugate	primary	1: 25,000	IBA (2-1502-001)
anti-ACTIN	primary	1: 10,000	Agrisera (AS13 2640)
rabbit-anti-SERAT1;1	primary	1: 5,000	unpublished
rabbit-anti-OAS-TL A	primary	1: 5,000	Heeg *et al.* (2008)
anti-mouse-HRP	secondary	1: 4,000	Agrisera (AS10 1033)
anti-rabbit-HRP	secondary	1: 25,000	Agrisera (AS09 602)

2.5.14 Visualization of proteins by amido black staining

Developed membranes (2.5.13) were stained with amido black solution for 5 min and washed with ddH_2O until the background was clear again. The stained membranes were imaged with ImageQuant LAS 400 (GE Healthcare).

2.5.15 Determination of signal intensity

After the detection of developed (2.1.13) or stained membranes (2.1.14) or stained gels (2.5.11) with ImageQuant LAS 4000 (GE Healthcare), the signal intensities of the protein bands were determined with the software application FIJI (2.1.6) using the Analyze>>Gels option.

2.6 Metabolomics

2.6.1 Metabolite extraction from plant tissue

Ground plant material was weighed, and metabolites were extracted using HCl. Shoot material was ground using a pre-chilled mortar, and root material was processed with a pre-chilled drill. The samples were kept frozen during processing. Around 100 mg per ground shoot material and around 50 mg per ground root material were weighed in 2 ml Eppendorf tubes. The precise weights were recorded for normalizing metabolite concentrations. 1 ml of 0.1 M HCl was added to the shoot samples, while 0.5 ml of 0.1 M HCl was added to the root samples. All samples were kept on ice for 5 minutes while vortexing every 2 min. Afterward, the samples were centrifuged at 15,000 g at 4°C for 5 min. The supernatant was transferred to new tubes, and the centrifugation step was repeated. The clear supernatant was stored in a fresh tube at -80 °C or directly used for derivatization.

2.6.2 Derivatization of OAS

For OAS derivatization, 30 µl of 0.8 M borate buffer was preloaded into 1.5 ml Eppendorf tubes. 50 µl of plant extract (2.6.1) was added to each tube and mixed thoroughly. Immediately, 20 µl of AccQ-Tag™ (0.3 mg/ml acetonitrile) was pipetted into the mixture, followed by additional mixing. The samples were incubated at RT for 1 min, then heated at 55 °C for exactly 10 min. After incubation, the samples were centrifuged at maximum speed for 15 min, and the supernatant was transferred into UPLC vials. For OAS standards, 30 µl borate buffer, 10 µl of OAS standard (10, 50, and 100 µM), and 40 µl ddH_2O were used to mix with 20 µl of AccQ-Tag™. The final OAS concentrations in the derivatization volumes were 1, 5, and 10 pmol/µl. To create a blank, 50 µl ddH_2O was mixed with 30 µl borate buffer and 20 µl of AccQ-Tag™.

2.6.3 Derivatization of thiols

For thiol derivatization, 25 µl of plant extract (2.6.1) was mixed with 270 µl of the reduction buffer containing 190 µl ddH_2O, 20 µl 1 M Tris pH 8.3, 10 µl 10 mM DTT, and 25 µl 0.08 M NaOH. The samples were vortexed, briefly centrifuged, and incubated in the dark for 20 min at RT. Subsequently, 25 µl of 10 mM monobromobimane (Mbb) was added, and the samples were vortexed and briefly spun down. After an additional 15 min incubation at RT in the dark, 705 µl of 5% acetic acid was added and mixed. The samples were centrifuged at maximum speed at 4 °C for 45 min, and the supernatant was transferred into UPLC vials. To prepare the standards, 230 µl of ddH_2O was mixed with 20 µl Tris and 10 µl DTT. Instead of adding plant extract, 10 µl of standard solution (1, 5, and 10 µM) containing equal concentrations of Cys, γ-EC, Cys-Gly, and glutathione was added. The final concentration after derivatization was 0.1, 0.5, and 1 pmol/µl. To create a

blank, 240 µl of ddH_2O was mixed with 20 µl of Tris and 10 µl of DTT. The remaining steps of the standard derivatization process were performed as described for the plant extracts samples.

2.6.4 Derivatization of sulfide

To derivatize sulfide, 50 mg of ground sample was mixed with 500 µl extraction buffer containing 20 mM Tris pH = 8.5, 100 mM NaCl, 1 mM EDTA and freshly added 1 mM TCEP. The samples were vortexed for 2 min for homogenization followed by centrifugation at 20,000 g at 4 °C for 5 min. The supernatant was transferred to a new tube, and the centrifugation step was repeated. 40 µl of clear supernatant was added to 30 µl of 100 mM borate buffer (pH = 9.5) and 20 µl of 20 mM monobromobimane (Mbb). The samples were briefly mixed and spun down before incubation at 25 °C in dark for 60 min. Afterward, 10 µl of 3.7% HCl was added to decrease pH to 1. The samples were centrifuged at 20,000 g at 4 °C for 45 min and the supernatant (100 µl) was transferred to UPLC vials for analysis. To create standards, 10 µl of sulfide solved in ddH_2O (100 µM, 50 µM, 10 µM or 0 µM for blank) was added to 30 µl of 100 mM borate pH 9.5, 30 µl ddH_2O and 20 µl of 20 mM Mbb. The mix was incubated at 25 °C in the dark for 60 min. After adding 10 µl of 3.7% HCl, the standards were centrifuged at 20,000 g at 4 °C for 45 min and supernatant transferred to UPLC vials.

2.6.5 UPLC measurement

Ultra-performance liquid chromatography (UPLC) was performed to separate metabolites and quantify steady-state levels of targeted metabolites using ACQUITY UPLC H-class with Sample Manager FTN, Quaternary Solvent Manager, and FLR detector from Waters.

The ACQUITY BEH C18 column was installed and kept at 42 °C for measuring OAS. Mobile phase A consisted of 140 mM sodium acetate with 7 mM triethanolamine (pH 6.3) and mobile phase B consisted of 100% acetonitrile. The run started after the flow rate was slowly increased to 0.45 ml/min and performed according to Table 10. OAS was detected at Ex/Em=250/395 nm and gain: 20.

Table 10: UPLC run settings for OAS measurement. As Mobile phase A 140 mM sodium acetate, 7 mM triethanolamine, pH 6.3 was used. Mobile phase B consisted of 100% acetonitrile.

Step	Time [min]	Initial flow rate	Mobile phase A	Mobile phase B
1	0-1	0.45	92%	8%
2	1-7	0.45	91%	9%
3	7-7.3	0.45	85%	15%
4	7.3-12.21	0.45	82%	18%
5	12.21-13.09	0.45	59%	41%
6	13.09-15.09	0.45	20%	80%
7	15.09-17.26	0.45	20%	80%
8	17.26-18.35	0.45	92%	8%
9	18.35-20	0.45	92%	8%

Thiols and sulfide were measured using ACQUITY BEH Shield RP18 column at 42 °C. The mobile phase A consisted of 100 mM potassium acetate buffer (pH 6.5) and mobile phase B was 100% acetonitrile. The run was started after the flow rate was slowly increased to 0.85 ml/min for thiol measurement and to 0.7 ml/min for sulfide measurement and performed according to Table 11 and Table 12. For detection Ex/Em=380/480 nm, gain: 100 was used.

Table 11: UPLC run settings for thiol measurement. Mobile phase A: 100 mM K-acetate buffer, pH 6.5. Mobile phase B: 100% acetonitrile. The transition from step 1 to 2 was linear and from 2 to 3 a direct switch.

Step	Time [min]	Initial flow rate	Mobile phase A	Mobile phase B
1	0-1.19	0.85	97.7%	2.3%
2	1.19-1.65	0.85	30%	70%
3	1.65-2.7	0.85	97.7%	2.3%

Table 12: UPLC run settings for sulfide measurement. Mobile phase A: 100 mM K-acetate buffer, pH 6.5. Mobile phase B: 100% acetonitrile. The transition from step 1 to 2 was linear, the rest direct switches.

Step	Time [min]	Initial flow rate	Mobile phase A	Mobile phase B
1	0-0.1	0.7	80%	20%
2	0.1-5	0.7	60%	40%
3	5-6	0.7	60%	40%
4	6-8	0.7	80%	20%

The steady-state levels of OAS, thiols and sulfide were quantified using the Waters LC control and analysis software Millenium32Waters (2.1.6).

2.7 Statistical analysis

Statistical analyses were conducted using GraphPad Prism 10. Initially, data normality was assessed with the Shapiro-Wilk test, and a Quantile-Quantile plot was used to confirm a Gaussian distribution. Additionally, a homoscedasticity plot was generated to assess equal variances among groups, and a residual plot was created to examine residual distributions. If data were normally distributed and showed equal variances, a two-way analysis of variance (ANOVA) was applied. Group differences were assessed using Tukey's multiple comparison test, with significant differences ($p < 0.05$) marked by different letters. Data that did not meet the normality and equal variance requirements was normalized using log10 transformation. If a new QQ plot, homoscedasticity, and residual plot of the transformed data confirmed normal distribution and equal variances, the two-way ANOVA analysis with Tukey's multiple comparison test ($p < 0.05$) was performed to assess group differences. The y-axis scale of graphs generated with non-transformed data was adjusted to a logarithmic scale.

3. Results

3.1 Understanding the impact of the cCSC on transcription in sulfur deficiency stress

Previous transcriptome analysis using the Affymetrix ATH1 microarray revealed significant transcriptomic alterations in the *oastlA* and *serat1;1* single T-DNA mutants compared to WT upon six hours of sulfur deficiency stress (Speiser, 2014). Notably, one gene cluster exhibited upregulated transcript levels in WT in response to sulfur deficiency while remaining unchanged in the mutants. This cluster included well-established sulfur deficiency marker genes such as *SDI1*, *GGCT2;1*, and *SULTR1;1* indicating a potential role of the cCSC in sulfur deficiency sensing.

3.1.1 Sulfur deficiency-induced *SDI1* upregulated in cCSC mutants contradicts previous findings

To further investigate the role of the cCSC in the transcriptional response to sulfur deficiency using an independent approach, mRNA sequencing was planned with mutant plants lacking either OAS-TL A or SERAT1;1. Therefore, the *oasltA* and *serat1;1* mutants (2.3.1), as previously used by Speiser (2014), were hydroponically grown alongside WT in short-day conditions for seven weeks (2.3.7). On the day of harvest, half of the plants were subjected to sulfur deficiency (0 µM sulfate) for six hours, while the remaining plants served as controls under sulfur-sufficient conditions (500 µM sulfate) (2.3.7). To verify the effectiveness of the treatment, qRT-PCR analysis of the sulfur deficiency marker gene *SDI1* was performed. Root material was harvested and ground in liquid nitrogen, followed by RNA extraction (2.4.4) and cDNA synthesis (2.4.5). qRT-PCR (2.4.8) was then conducted using *SDI1*-specific primers (2.4.6) to confirm transcript induction.

As expected, the WT exhibited a significant upregulation of *SDI1* transcripts in response to sulfur deficiency (Figure 3).The single mutants *oastlA* and *serat1;1*, which were previously reported to lack this transcriptional response, instead displayed WT-like *SDI1* induction. After double checking the mutants for the correct T-DNA insertions (Supplemental Figure 1), the experiment was repeated twice, incorporating the *A1;1* double mutant (2.3.1), which was also previously reported to be insensitive to short-term sulfur deficiency stress (Speiser, 2014). While *SDI1* upregulation in *A1;1* was statistically different from WT under sulfur-deficient conditions, comparison to the control condition clearly demonstrated transcriptional induction of *SDI1* in *A1;1* upon sulfur deficiency (Figure 3). These findings contradict previous results reported by Speiser (2014) and warrant further investigation

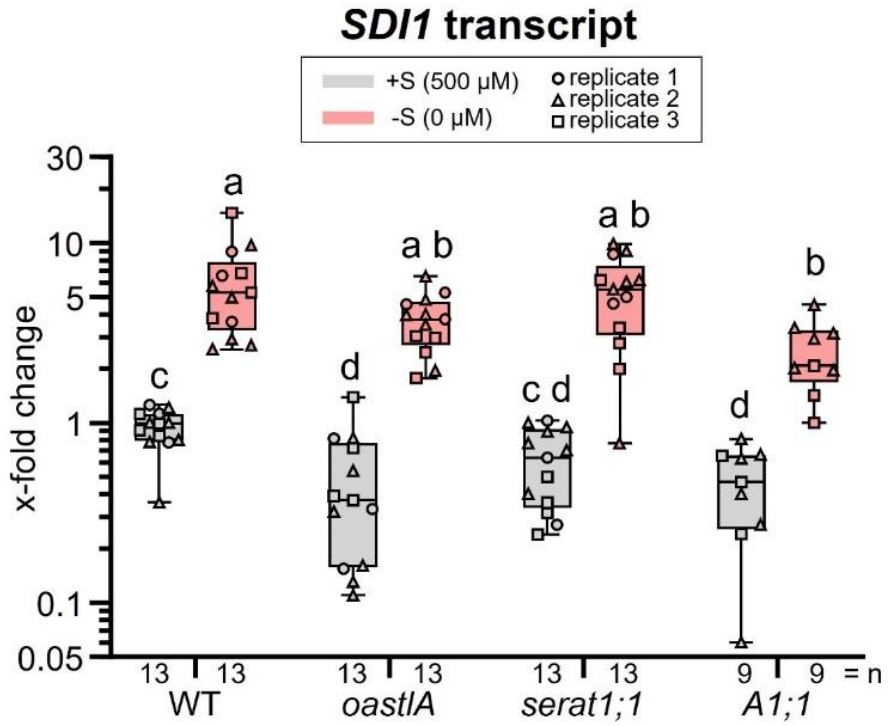

Figure 3: *SDI1* transcript levels in cCSC mutants during short-term sulfur deficiency. WT and the single cCSC mutants *oastlA*, *serat1;1* and the double mutant A1;1 (2.3.1) were grown for seven weeks in liquid +S ½ Hoagland medium (500 µM sulfate) (2.3.7). Before harvest, half of the plants were subjected to sulfur deficiency stress (0 µM sulfate) for 6 h. The root material was snap-frozen, ground, and the RNA extracted (2.4.4). From this mRNA a cDNA library was synthesized (2.4.5) and used for qRT-PCR (2.4.8) with *SDI1*-specific primers (2.4.6). The data is combined from three independent replicates, and each data point indicates an individual plant. The A1;1 mutant was only included in replicates two and three. For statistical analysis (2.7), the ANOVA 2-way with $p < 0.05$ was used after assessing the correct data transformation.

3.1.2 Sulfur deficiency marker gene upregulation in the cCSC mutants is dependent on the duration and severity of sulfur deficiency

Since the cCSC single and double mutants showed upregulation of the SDI1 transcript after six hours of sulfur deficiency (3.1.1), experimental key variables were systematically examined to explain the discrepancy with previous findings by Speiser (2014). As an initial approach, also the transcripts *GGCT2;1* and *SULTR1;1* were analyzed to exclude the possibility that the observed effect on *SDI1* was specifically influenced by the experimental repetitions. Previous studies have indicated that the lack of transcriptional response is time-dependent (Speiser, 2014), as initial genotype-specific differences observed at six hours converged after 24 hours (Speiser, 2014). To rule out the possibility that significant differences in transcript levels were missed due to late sampling, an additional independent experiment was conducted, in which samples were harvested after four hours instead of six hours of sulfur deficiency (Figure 4).

Therefore, WT, *oasltA*, and *serat1;1* mutants (2.3.1) were grown in the hydroponic system for seven weeks in short-day conditions (2.3.7). Half of the plants were exposed to sulfur deficiency (0 µM sulfate) and were either harvested after four or six hours. The remaining plants served as control and stayed in sulfur-sufficient conditions (500 µM sulfate). The root material was snap-frozen, ground and used for RNA extraction (2.4.4). The corresponding cDNA (2.4.5) was used for qRT-PCR (2.4.8) with specific primers for *SDI1*, *GGCT2;1*, and *SULTR1;1* transcripts (2.4.6).

After six hours of sulfur deficiency, the WT exhibited an upregulation of *SDI1*, *GGCT2;1*, and *SULTR1;1* (Figure 4), consistent with previously reported transcriptomic changes under these conditions (Speiser, 2014). This confirms the correct application of sulfur deficiency stress. Contrary to earlier findings, the *oastlA* and *serat1;1* mutants also displayed WT-like transcript upregulation across all three genes, ruling out the possibility that *SDI1* was an isolated exception. Furthermore, after four hours of sulfur deficiency, transcript levels in the mutants and WT were similarly upregulated, indicating that the correct time window for measurement was not missed (Figure 4).

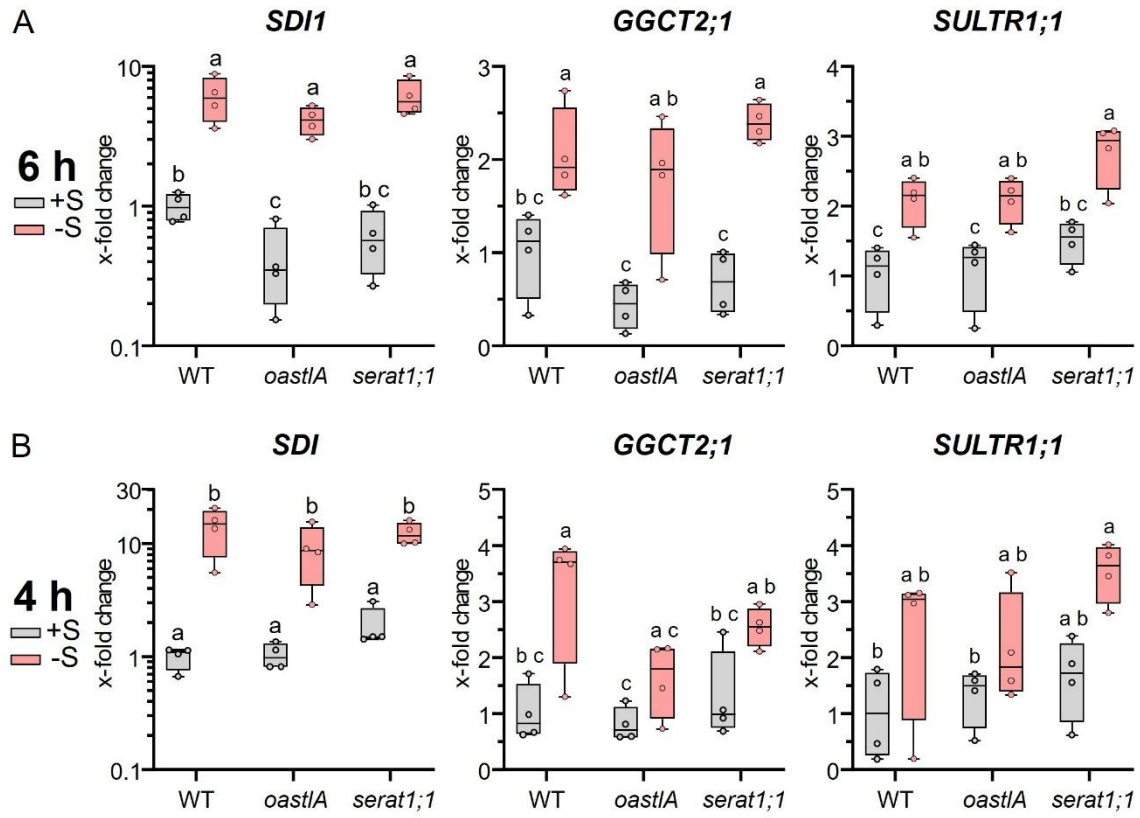

Figure 4: Time-dependent *SDI1*, *GGCT2;1*, and *SULTR1;1* transcript upregulation of single cCSC mutants in sulfur deficiency. The single cCSC mutants, *oastlA* and *serat1;1*, were grown next to WT (2.3.1) for seven weeks in liquid ½ Hoagland medium in +S condition (500 µM sulfate) (2.3.7). Before harvest, two-thirds of the plants were subjected to sulfur deficiency stress (0 µM sulfate) for 4 h (A) or 6 h (B). The root material was snap-frozen, ground and the RNA extracted (2.4.4). The cDNA (2.4.5) was used for qRT-PCR (2.4.8) with gene-specific primers (2.4.6). The data is collected from one independent replicate for each harvesting time and each data point indicates an individual plant. For statistical analysis (2.7), the ANOVA 2-way with $p < 0.05$ was used after assessing the correct data transformation.

Although previous sulfur deficiency experiments (Speiser, 2014) were stated to be conducted in 0 µM sulfate conditions, I hypothesized that the purity of the chemicals used for preparing ½ Hoagland medium (2.1.4) has improved over the past decade, resulting potentially in lower sulfate contamination than in earlier studies. To determine whether plants respond differently to low sulfate levels compared to complete sulfate deprivation, a sulfur deficiency experiment was conducted using 0 µM and 2 µM sulfate (2.1.4).

Therefore, the cCSC mutants *oastlA*, *serat1;1*, and *A1;1* (2.3.1) were grown hydroponically next to WT for seven weeks (2.3.7). Six hours before harvest, the plants were either treated with 0 µM, 2 µM or 500 µM (control) sulfate (2.3.7). To additionally ensure an independent analysis, an

internship student, David Sauer, performed the harvest of plants, RNA extraction (2.4.4), cDNA synthesizis (2.4.5), and qRT-PCR analysis (2.4.8) of *SDI1* and *GGCT2;1* transcripts using gene-specific primers (2.4.6).

After six hours of sulfur deficiency, the cCSC mutants exhibited WT-like *SDI1* transcript upregulation (Figure 5). Thereby, the sulfur deficiency treatment with 0 µM sulfate resulted in a stronger transcriptional increase than using 2 µM sulfate, supporting the hypothesis that the stress response is concentration-dependent. While no significant differences were observed in the *GGCT2;1* transcript across genotypes and treatments, the overall trends aligned with the expectation of higher transcript upregulation under more severe sulfur deficiency conditions (Figure 5).

Summarized, the cCSC mutants exhibited a WT-like regulation of *SDI1*, *GGCT2;1,* and *SULTR1;1* transcript, depending on the duration and severity of sulfur deficiency stress. These results are consistent with the findings from section 3.1.1, yet they do not resolve the underlying reasons for the discrepancies observed in comparison to the findings of Speiser (2014).

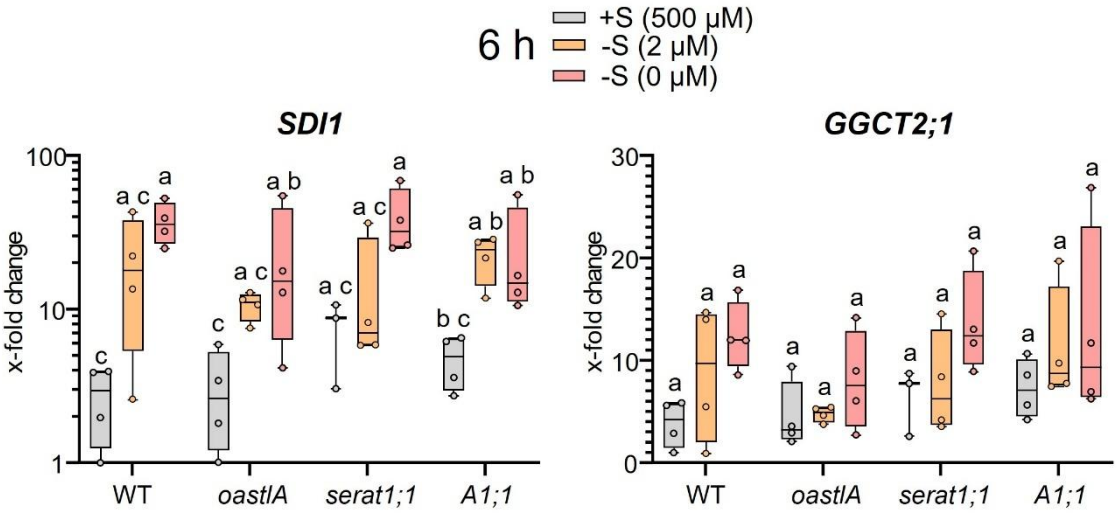

Figure 5: Concentration-dependent *SDI1* and *GGCT2;1* transcript upregulation of cCSC mutants after 6 h of sulfur deficiency stress. WT, *oastlA*, *serat1;1*, and the double mutant A1;1 (2.3.1) were grown for seven weeks in the hydroponic system in +S condition (500 µM sulfate) (2.3.7). Before harvest, a third of the plants were subjected for 6 hours to ½ Hoagland solution containing either 0, 2, or 500 µM sulfate. The root material was harvested, snap-frozen, and ground, and the RNA was extracted by David Sauer (2.4.4). He transcribed the RNA to cDNA (2.4.5) and used it for qRT-PCR (2.4.8) with *SDI1* and *GGCT2;1* specific primers (2.4.6). The transcript levels were normalized to WT control sample one. The whole data is collected from one replicate, and each data point (n=4) indicates a pool of two individual plants. For statistical analysis, the ANOVA 2-way with $p < 0.05$ was used after assessing the correct data transformation (2.7).

3.1.3 cCSC mutants show WT-like transcript level in sulfur-sufficient condition

The transcripts *SDI1*, *GGCT2;1*, and *SULTR1;1* are part of a gene cluster previously shown to be upregulated in WT under sulfur deficiency, but unchanged in the single cCSC mutants (Speiser, 2014). In my experiments, the mutants exhibited a similar transcriptional response to WT with respect to the upregulation of these three genes under sulfur deficiency (3.1.1, 3.1.2). To eliminate the stress treatment application as a possible cause for the discrepancy to the findings of Speiser (2014), I focused on transcriptional differences observed among the genotypes under sulfur-sufficient conditions. Therefore, I selected a set of genes, including *GAT*, *SEN1*, and *ANAC029*, which were previously reported to be approximately 100-fold upregulated in cCSC mutants

compared to WT in control condition (Speiser, 2014). The second gene set, which included *IRT1*, *NAS1*, and *NAS2*, was chosen based on its reported downregulation to approximately 10% of WT levels in the cCSC mutants (Speiser, 2014). Additionally, *DIN10* was chosen as a transcript previously independently upregulated in the cCSC mutants in sulfur-sufficient and deficient conditions (Speiser, 2014).

To investigate these transcripts, WT, *oasltA*, and *serat1;1* (2.3.1) were hydroponically cultured for seven weeks in sulfur-sufficient conditions (2.3.7). Root tissue was snap-frozen in liquid nitrogen, ground, and used for RNA extraction (2.4.4). The synthesized cDNA (2.4.5) was then subjected to qRT-PCR (2.4.8) using specific primers for *GAT*, *SEN1*, *ANAC029*, *IRT1*, *NAS1*, *NAS2*, and *DIN10* (2.4.6). No significant differences in transcript levels were observed when comparing WT with the cCSC mutants (Figure 6), which indicates so far un-recognized, yet fundamental differences between the experimental conditions used in the current study and those previously conducted by Speiser (2014).

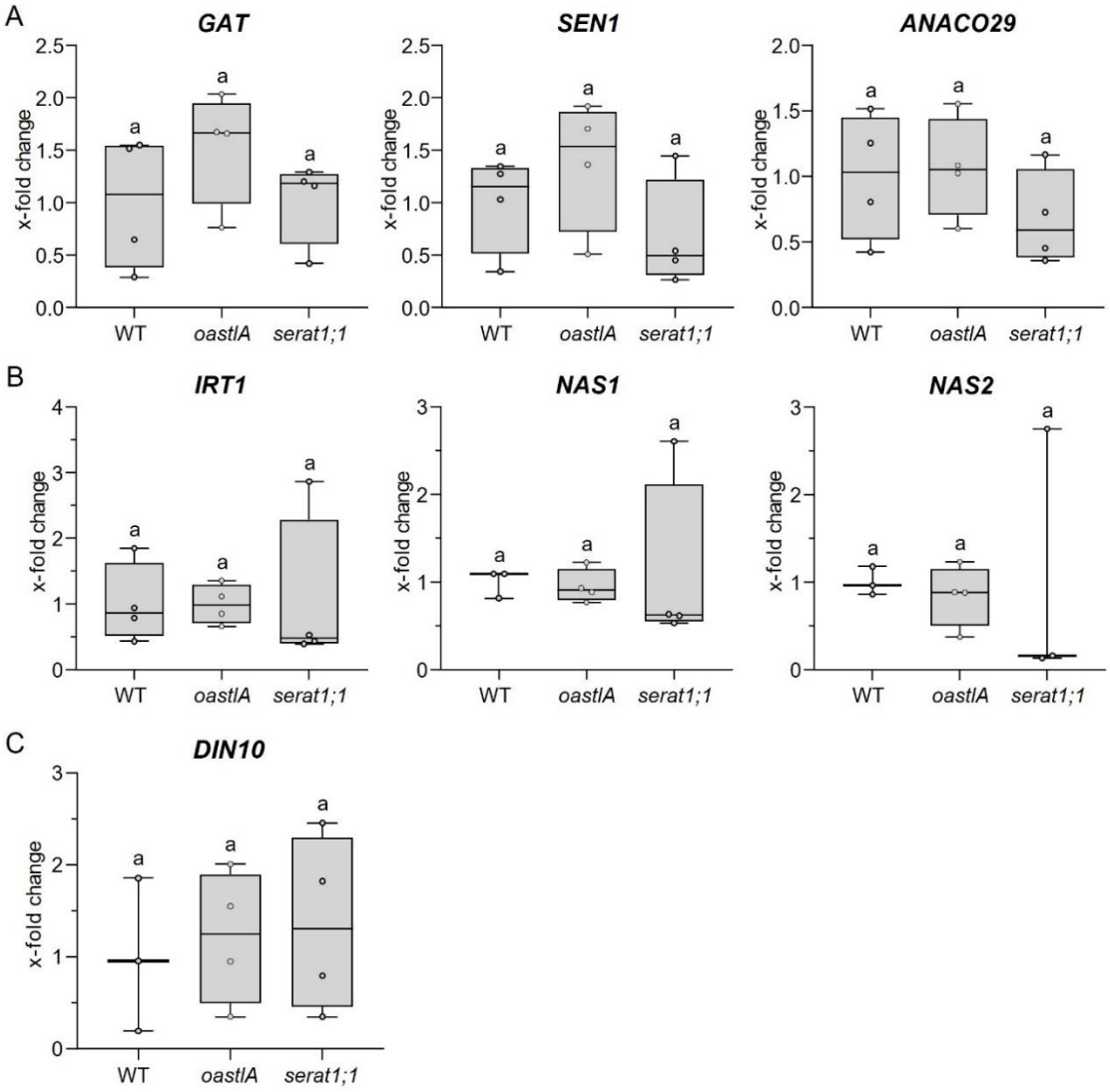

Figure 6: cCSC single mutants show WT-like transcript levels for genes previously reported to differ significantly from WT in sulfur-sufficient conditions. WT and the single cCSC mutants *oastlA* and *serat1;1* (2.3.1) were grown for seven weeks in liquid ½ Hoagland +S (500 µM sulfate) condition (2.3.7). The root material was snap-frozen, ground, and the RNA extracted (2.4.4). The cDNA (2.4.5) was used for qRT-PCR (2.4.8) with gene-specific primers (2.4.6). For statistical analysis, the ANOVA 2-way with $p < 0.05$ was used after assessing the correct data transformation (2.7).

3.1.4 Generation of new *A1;1* mutant lines using CRISPR/Cas9 system

Since the publication of Speiser's data in 2014, the *oasltA* and *serat1;1* T-DNA mutant lines have undergone several generations of propagation. Although the T-DNA insertions responsible for the loss of cCSC remain present in both mutants (Supplemental Figure 1), we cannot rule out the possibility that epigenetic modifications may have led to transcriptome adjustments resembling a WT-like state. To investigate this, I generated new *oasltA* and *serat1;1* mutant lines in the Col-0 ecotype using the multiplex CRISPR/Cas9 editing approach described by Stuttmann *et al*. (2021). This method allows for simultaneous targeting of up to twelve loci. For each locus, I selected two target sites within the *OAS-TL A* and *SERAT1;1* coding sequences (CDS) based on editing efficiency predictions from the CHOPCHOP and targetDesign tools (2.1.6). The sequences and locations of the target sites for the *OAS-TL A* CDS and *SERAT1;1* CDS are illustrated in Figure 7. The predicted off-target sequences for both loci are provided in Supplemental Figure 2 (*OAS-TL A*) and Supplemental Figure 3 (*SERAT1;1*).

All four target sequences were synthesized as primers by Eurofins Genomics (2.4.6) and assembled into the plant transformation vector pDGE347 A1;1_cr (2124) (Supplemental Figure 4) according to the protocol described by Stuttmann *et al*. (2021) (2.4.13) with the assistance of my student Leonie Wood. pDGE347 A1;1_cr (2124) was subsequently introduced into *Agrobacterium tumefaciens* (2.2.6) for *A. thaliana* Col-0 floral dip transformation (2.3.9) resulting in a total of 40 transgenic lines selected based on BASTA resistance (2.3.9). To verify the successful mutagenesis of the *OAS-TL A* and *SERAT1;1* loci, genomic DNA was extracted from four-week-old transformants (2.4.3) by my student Stefan Stojilkovic, followed by PCR amplification (2.4.7) using primer combinations 2728/2729 and 2730/2731 flanking the target sites (2.4.6) (Supplemental Figure 5). The amplification products were analyzed via gel electrophoresis (2.4.9), and positive PCR products were subsequently sequenced (2.4.14) using the forward primers 2728 and 2730 (2.4.6) to confirm target site modifications. Genotyping was stopped after identification of lines #2, #30, #32 and #38 harboring mutations in both *OAS-TL A* and *SERAT1;1*. All 40 transformants were then transferred to long-day conditions for seed propagation (2.3.2). To eliminate potential off-target effects, the *Cas9* transgene was segregated out in the four mutant lines by utilizing the FAST marker, an RFP-tagged seed coat protein integrated into the CRISPR/Cas9 transformation vector (Stuttmann *et al*., 2021) (Supplemental Figure 4). Seed fluorescence was evaluated with a binocular microscope (Leica MZFLIII, Wetzler) equipped with UV excitation (λ_{ex}=340 nm) and an RFP filter (λ_{em}>590 nm) in 10 times magnification (Supplemental Figure 6). Non-fluorescent seeds, indicative of a T-DNA loss, were transferred to freshly prepared soil-containing pots (2.3.2). Segregation analysis revealed that lines #2, #30, and #32 exhibited a Mendelian 3:1 fluorescence pattern, consistent with a single T-DNA insertion, whereas line #38 displayed a 15:1 segregation ratio, indicative of two independent T-DNA insertions.

Figure 7: Indication of the CRISPR/Cas9 target sides in *OAS-TL A* and *SERAT1;1* CDS. This picture was generated with Geneious software application (2.1.6).

Non-fluorescent seeds from mutant candidate lines #2, #30, #32, and #38 were cultivated in short-day conditions for four weeks (2.3.2). Sixteen seedlings per line were genotyped as described before to identify homozygous mutants for both loci.

Candidate line #2 was designated *A1;1_cr#1 (2210)* (2.3.1). This line harbored an adenine insertion at position 1037 bp in the gDNA of the *OAS-TL A* locus, leading to a frameshift and a premature stop codon after 103 amino acids (Figure 8). The *SERAT1;1* locus carried a thymidine insertion at position 230 bp of gDNA, resulting in a premature stop codon after 55 amino acids (Figure 8).

Figure 8: Mutations of *A1;1_cr#1*. The sequence of the gDNA of *OAS-TL A* is visualized at the top as a query sequence. In red, the sgRNA of target two is marked. The genotyping sequence results are stated below the query sequence. In the region of target two, a single base pair addition of A was found, leading to a frameshift resulting in an early stop codon. In the second half, the query sequence of *SERAT1;1* gDNA is visualized, spanning the sgRNA of target one in red. Below, the genotyping sequencing result is stated, showing a single base pair addition of T in the region of the target one, leading to a frameshift and an early stop codon. The image was generated from the software application Geneious (2.1.6).

Candidate line #38, designated *A1;1_cr#2 (2211)* (2.3.1), exhibited a 45-bp deletion in the *OAS-TL A* locus beginning at position 996 bp of gDNA. This deletion spans the splice junction between exon 3 and exon 4 and is likely to disrupt correct splicing (Figure 9). The *SERAT1;1* locus in this line carried a 2-bp deletion starting at position 230 bp of gDNA, generating a premature stop codon after 55 amino acids (Figure 9).

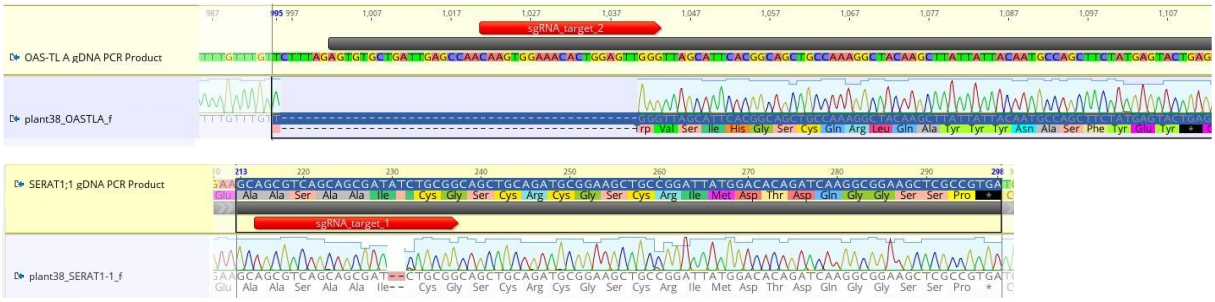

Figure 9: Mutations of *A1;1_cr#2*. At the top, *OAS-TL A*'s gDNA sequence is visualized as a query sequence. In grey, the start of exon four is indicated. In red, the sgRNA of target two is marked. The genotyping sequence result is shown below the query sequence. In the region of target two, a 45 bps gap spans the splicing region of exons three and four, probably leading to splicing errors. In the second half, the query sequence of *SERAT1;1*'s gDNA sequence is visualized, spanning the sgRNA of target one in red. The genotyping sequencing results are stated below and show a 2 bps gap in the region of target one, leading to a frameshift and an early stop codon. The image was made with Geneious software application (2.1.6).

Candidate line #32 was named *A1;1_cr#3 (2212)* (2.3.1) and contained a guanine insertion at position 625 bp in the *OAS-TL A* gDNA, causing a frameshift and a premature stop codon after 103 amino acids (Figure 10). The *SERAT1;1* locus exhibited two different segregating mutant alleles, both of which resulted in a homozygous *A1;1* mutant. The first allele carried a thymidine insertion at position 231 bp of gDNA, introducing a premature stop codon after 55 amino acids. The second allele featured a 7-bp deletion beginning at position 233 bp of gDNA, leading to a premature stop codon after 60 amino acids (Figure 10).

Candidate line #30 displayed a 12-bp in-frame deletion in the *OAS-TL A* locus starting at position 1027 bp of gDNA. As this mutation did not induce a frameshift or an early stop codon, the line was not further analyzed.

Figure 10: Mutations of *A1;1_cr#3*. *OAS-TL A*'s gDNA sequence is shown as a query sequence at the top. In red, the sgRNA of target two is visualized. The genotyping sequence result is stated below the query sequence and shows 1 bp addition in the region of target two, leading to a frameshift and an early stop codon. In the second half, the sequence of *SERAT1;1*'s gDNA is visualized with the sgRNA sequence of target one indicated in red. Below, the genotyping sequencing results show two different alleles segregating in this line. The first allele has a 1 bp addition leading to a frameshift and an early stop codon. The second allele exhibits a 7 bps gap, also leading to a frameshift and an early stop codon. The image was generated using the Geneious software application (2.1.6).

Next, the *A1;1_cr#1–3* plant lines were analyzed to determine whether the introduced mutations resulted in the loss of *OAS-TL A* and *SERAT1;1* protein expression. Therefore, 0.2 g of leaf tissue was collected from eight-week-old soil-grown plants (2.3.2), and total protein was extracted using NuPAGE buffer (2.5.6). Protein separation was performed via SDS-PAGE (2.5.10), followed by Western blotting (2.5.12) and immunological detection (2.5.13). WT Col-0 served as a positive control, while the *A1;1* T-DNA mutant was used as a negative control. To verify equal protein loading, an anti-actin antibody was used (2.5.13), and amido black staining was performed to confirm successful protein transfer onto the membrane (2.5.14). While both antibodies cross-detected also other OAS-TL and SERAT isoforms, the absence of specifically OAS-TL A and SERAT1;1 protein was confirmed in all *A1;1_cr* lines (Figure 11).

To assess whether epigenetic modifications influence transcription in the cCSC mutants, the newly generated *A1;1_cr#1* and *A1;1_cr#2* lines were examined for their *SDI1* and *GGCT2;1* transcript upregulation in response to short-term sulfur deficiency. Therefore, WT, *A1;1_cr#1*, *A1;1_cr#2*, and the *A1;1* T-DNA mutant (2.3.1) were grown in the hydroponic culture for seven weeks (2.3.7). On the day of harvest, images of the rosettes were taken to measure rosette diameters for phenotypic assessment (2.3.12). To induce sulfur deficiency, half of the plants were transferred to a sulfur-depleted medium for six hours, while the remaining plants remained in a sulfur-sufficient control condition (2.3.7). Root tissue was then harvested, snap-frozen, and ground for RNA extraction (2.4.4). Following cDNA synthesis (2.4.5), qRT-PCR analysis (2.4.8) was conducted using *SDI1* and *GGCT2;1*-specific primers (2.4.6).

As previously observed, WT plants exhibited a significant upregulation of *SDI1* after six hours of sulfur deficiency (Figure 12). The *A1;1* T-DNA mutant and the two *A1;1* CRISPR/Cas9 mutants (*A1;1_cr#1* and *A1;1_cr#2*) were similar in rosette diameter (Supplemental Figure 8) or *SDI1* transcript upregulation when compared to WT (Figure 12). While all genotypes displayed an increasing trend in *GGCT2;1* transcript levels in response to sulfur deficiency, this upregulation was not statistically significant compared to control conditions.

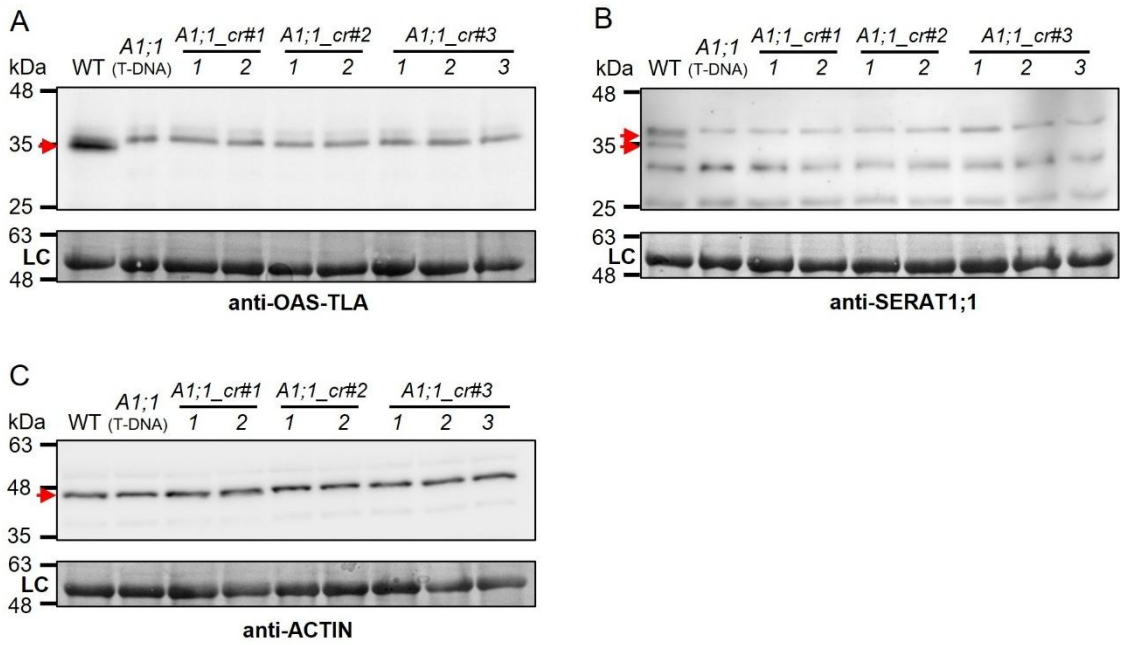

Figure 11: Verification of *A1;1_cr#1-3* mutants on protein level. 0.2 g leaf material of seven weeks old soil-grown WT, *A1;1*, *A1;1_cr#1, A1;1_cr#2*, and *A1;1_cr#3* (2.3.2) was used to extract proteins with the NuPAGE buffer (2.5.6). Two individual plants were tested for each *A1;1_cr#1* and *#2*. The *A1;1_cr#3-1* and *3-2* contained the *serat1;1* allele with the 1 bp addition, while the *A1;1_cr#3-3* contained the *serat1;1* allele with the 7 bp gap. WT served as positive control and *A1;1* T-DNA mutant as negative control. The plant extracts were used for SDS-PAGE (2.5.10) and Western blotting (2.5.12) followed by immunological detection using anti-OAS-TL A and anti-SERAT1;1 antibody (2.5.13). Amido black staining was performed as loading control (LC) (2.5.14). **A:** Detection of OAS-TL A. **B:** Detection of SERAT1;1. **C:** Detection of ACTIN as antibody control. Red arrows indicate the expected size of proteins. All *A1;1* mutants lack the OAS-TL A and SERAT1;1 protein. The uncropped membranes are deposited in Supplemental Figure 7.

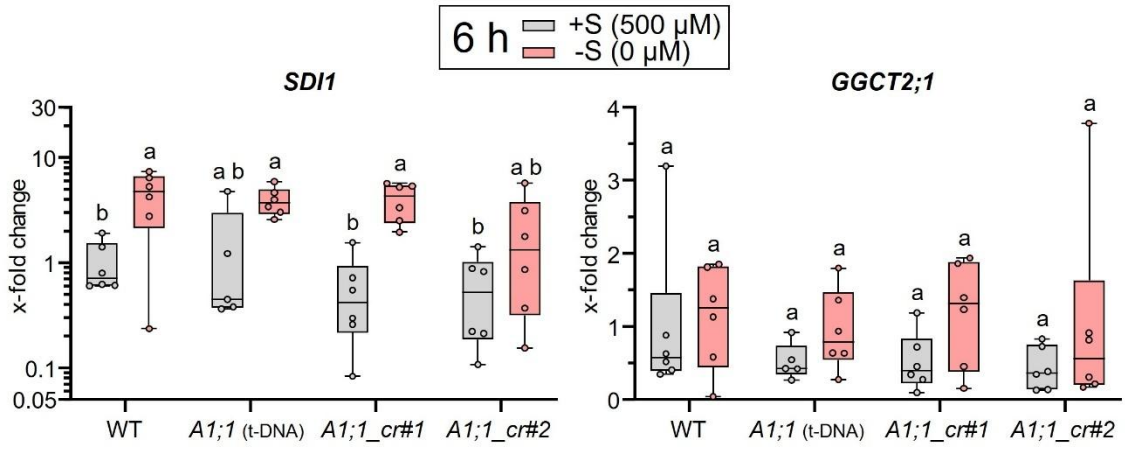

Figure 12: Transcript levels of *A1;1_cr#1* and *#2* in short-term sulfur deficiency are WT-like. The *A1;1_cr#1* and *#2* were grown next to WT and *A1;1* T-DNA mutant in liquid ½ Hoagland medium in sulfur sufficient condition (500 µM sulfate, +S) (2.3.7) for seven weeks. Before harvest, half of the plants were subjected to sulfur deficiency stress (0 µM sulfate, -S) for 6 h. The root material was snap-frozen, ground, and the RNA extracted (2.4.4). The cDNA (2.4.5) was used for qRT-PCR (2.4.8) with *SDI1* and *GGCT2;1* specific primers (2.4.6). The data were obtained from one experiment, and each data point represents an individual plant (n = 6). The 2-way ANOVA with $p < 0.05$ was used for statistical analysis, following assessment of the correct data transformation (2.7).

In conclusion, three new *A1;1_cr* lines were generated using CRISPR/Cas9 genome editing and verified at both the DNA and protein levels. Phenotypic analysis revealed a WT-like phenotype, consistent with observations for the *A1;1* T-DNA mutant. Similarly, *A1;1_cr#1* and *A1;1_cr#2* displayed WT-like *SDI1* and *GGCT2;1* transcript regulation in sulfur deficiency. Since the mutations in the CRISPR/Cas9 lines were newly introduced, epigenetic modifications can be ruled out as an explanation for the divergence between the results of this study and those reported by Speiser (2014). These findings suggest that the transcriptional delay in cCSC mutants compared to WT, as reported by Speiser (2014), is likely influenced by an, so far, unidentified factor. A possible factor could be the set-up of completely new climate chambers compared to Speiser (2014) that occurred shortly before I began my experiments.

3.1.5 Transcriptome analysis of *oastlA_cr#2* and *serat1;1_cr#2*

Previous findings by Speiser (2014) suggested a strong regulatory influence of the cCSC on transcription. However, the present study did not reproduce these observations in the analyzed transcripts under the experimental conditions used here (3.1.1, 3.1.2, 3.1.3). To comprehensively investigate potential transcriptional differences and verify untested observations from Speiser (2014), whole transcriptome analysis via mRNA sequencing (mRNAseq) was pursued.

For this purpose, *A1;1_cr#1* and *A1;1_cr#2* mutant plants were backcrossed with WT Col-0 (2.3.8) to segregate out single *oastlA_cr* and *serat1;1_cr* mutants. Heterozygous offspring were grown on soil and self-fertilized (2.3.2). The subsequent generation was grown for four weeks (2.3.2) before gDNA was extracted (2.4.3) and used for genotyping. PCR amplification (2.4.7) of *OAS-TL A* and *SERAT1;1* target site was performed employing primer pairs 2728/2729 and 2730/2731, respectively (2.4.6). The PCR products were sequenced (2.4.14) using forward primers 2728 and 2730 (2.4.6) to identify homozygous *oastlA_cr* and *serat1;1_cr* mutants. To confirm that the mutations lead to a loss of OAS-TL A and SERAT1;1 protein, total proteins were extracted from 0.2 g of leaf material using NuPAGE buffer (2.5.6) and were subjected to SDS-PAGE (2.5.10), followed by Western blotting (2.5.12) and immunological detection (2.5.13) with anti-OAS-TL A and anti-SERAT1;1 antibody. All analyzed mutant lines displayed protein expression patterns consistent with their genotypes (Figure 13).

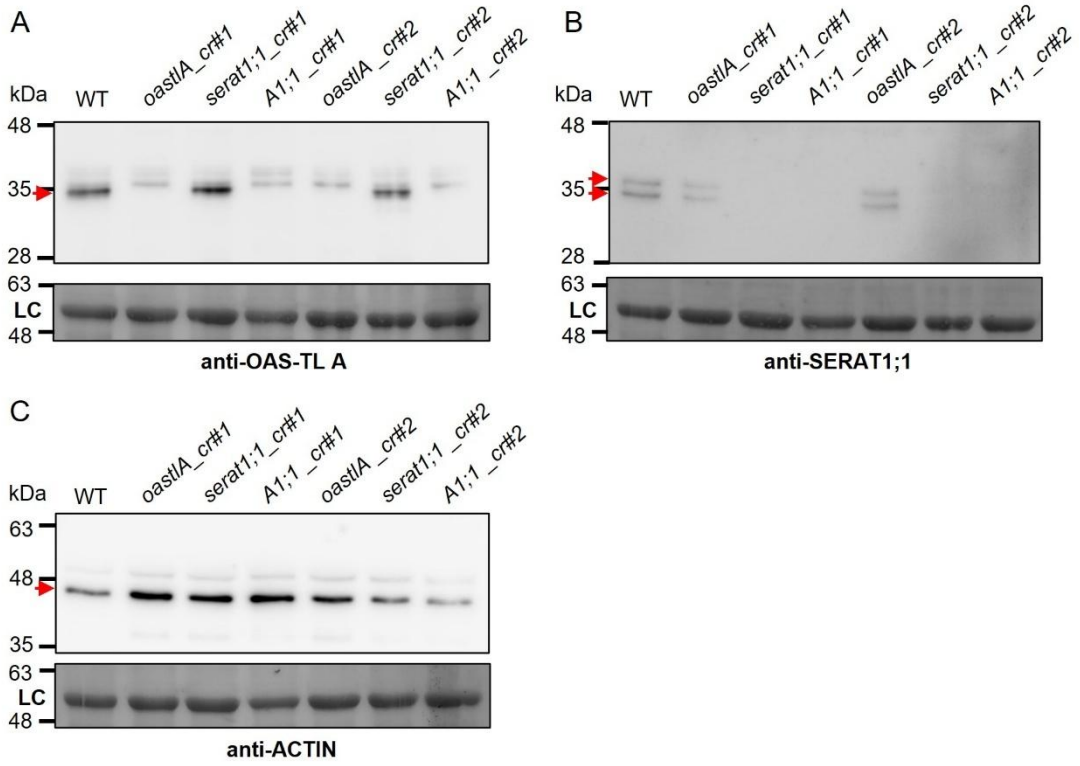

Figure 13: Verification of the newly generated single cCSC mutants on the protein level. 0.2 g leaf material of seven weeks old soil-grown *oastlA_cr#1-#2*, *serat1;1_cr#1-#2* and *A1;1_cr#1-#2* (2.3.2) was used to extract proteins with the NuPage buffer (2.5.6). The plant extracts were used for SDS-Page (2.5.10) and Western blotting (2.5.12) followed by immunological detection (2.5.13) and amido black staining as loading control (LC) (2.5.14). **A:** Anti-OAS-TL A antibody detection. **A:** Anti-SERAT1;1 antibody detection. **A:** Anti-ACTIN antibody detection. All mutants show the expected protein pattern. The uncropped membranes are deposited in Supplemental Figure 9.

To generate material for mRNA-seq, WT, *oastlA_cr#1*, *oastlA_cr#2*, *serat1;1_cr#1*, and *serat1;1_cr#2* plants were cultivated hydroponically in sulfur-sufficient conditions for seven weeks (2.3.7). On the day of harvest, images of the shoot rosettes were captured and analyzed using FIJI software (2.1.6) to quantify rosette diameter (2.3.12). The *oastlA_cr#* and *serat1;1_cr#* mutants exhibited a WT-like phenotype, consistent with previous observations of *oastlA* and *serat1;1* T-DNA insertion mutants (Supplemental Figure 10). Roots and shoots were harvested and snap-frozen in liquid nitrogen. The shoot material from *oastlA_cr#2*, *serat1;1_cr#2*, and WT plants was ground, RNA was extracted (2.4.4), and samples were sent to BGI TECH SOLUTIONS (Hong Kong) for mRNA sequencing (2.4.15). The overall RNA quality was high, with sequencing coverage exceeding 90%. However, principal component analysis (PCA) and the correlation heat map analysis revealed highly similar transcriptomes across genotypes, with a Pearson correlation coefficient of >0.92 (Figure 14). The primary variation in sequencing reads originated from replicate sets rather than genotype differences (Supplemental Figure 11).

As anticipated from PCA and correlation heat map analyses, only a small number of genes were differentially expressed between *oastlA_cr#2* and WT (Figure 15), while *serat1;1_cr#2* showed no significant transcriptional differences compared to WT (Figure 16).

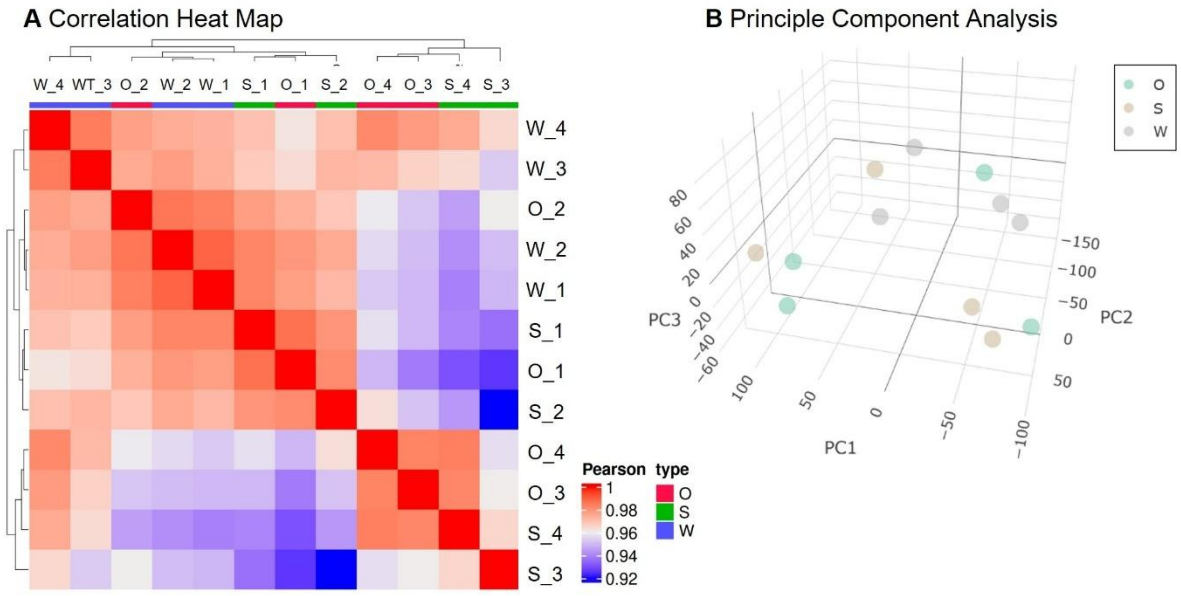

Figure 14: Correlation heat map and principle component analysis. WT, *serat1;1_cr#2* and *oastlA_cr#2* plants (2.3.1) were grown hydroponically in sulfur-sufficient conditions for seven weeks (2.3.7). Shoot material was harvested, snap-frozen and ground for RNA extraction (2.4.4). Total RNA was sequenced by BGI TECH SOLUTIONS (Hong Kong) (2.4.15), and bioinformatic analysis was conducted in collaboration with Dr. Carolina de la Torre from the NGS Core Facility, University of Mannheim (2.4.15). **A:** Correlation heat map**. B:** principle component analysis. W = WT, O = *oastlA_cr#2*, S = *serat1;1_cr#2*.

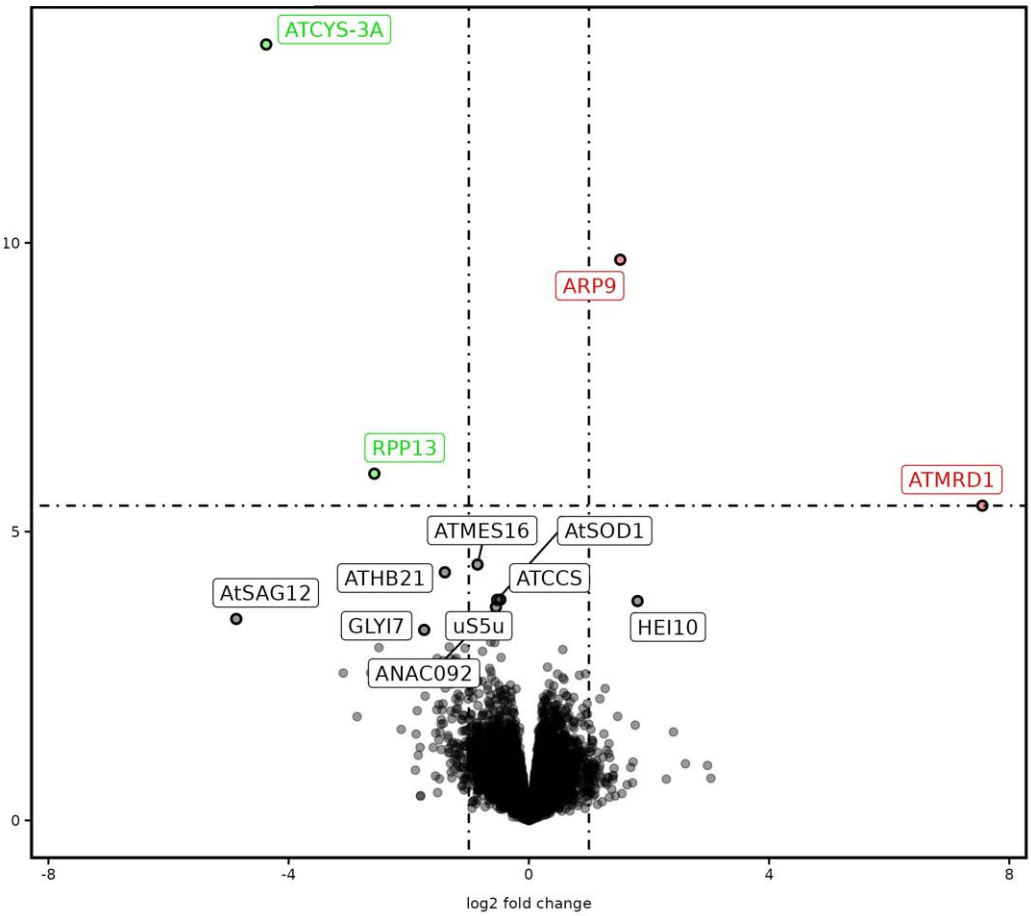

Figure 15: Volcano plots of *oastlA_cr#2* vs. WT. WT, *serat1;1_cr#2* and *oastlA_cr#2* plants (2.3.1) were grown hydroponically in sulfur-sufficient conditions for seven weeks (2.3.7). Shoot material was harvested, snap-frozen and ground for RNA extraction (2.4.4). Total RNA was sequenced by BGI TECH SOLUTIONS (Hong Kong) (2.4.15), and bioinformatic analysis was conducted in collaboration with Dr. Carolina de la Torre from the NGS Core Facility, University of Mannheim (2.4.15).

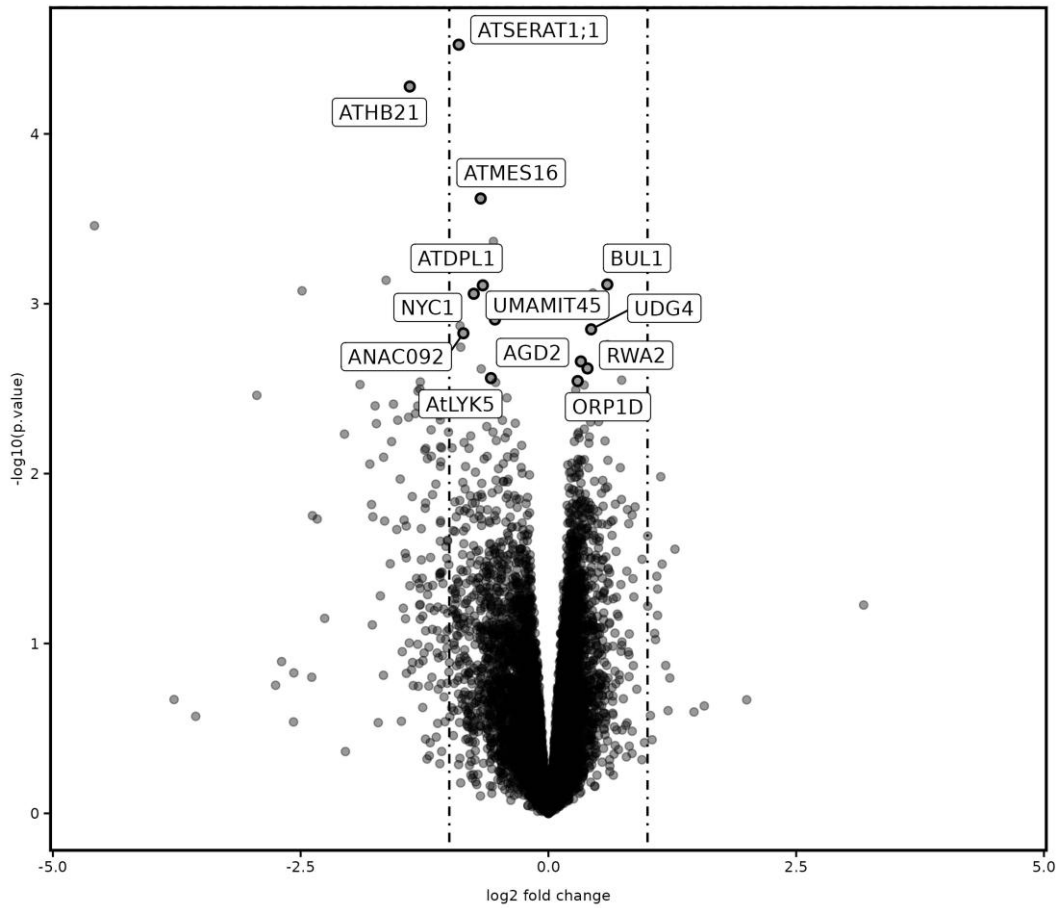

Figure 16: Volcano plots of *serat1;1_cr#2* vs WT. WT and *serat1;1_cr#2* (2.3.1) were grown hydroponically in sulfur-sufficient conditions for seven weeks (2.3.7). Shoot material was harvested, snap-frozen and ground for RNA extraction (2.4.4). Total RNA was sequenced by BGI TECH SOLUTIONS (Hong Kong) (2.4.15), and bioinformatic analysis was conducted in collaboration with Dr. Carolina de la Torre from the NGS Core Facility, University of Mannheim (2.4.15).

In *oastlA_cr#2*, two genes were significantly upregulated, and two were significantly downregulated compared to WT (Table 13). As expected, *OAS-TL A* transcript levels were the lowest, reaching only 4.8% of WT expression. Among the upregulated genes, *ARP9* (*ACTIN-RELATED PROTEIN 9*) showed a 2.87-fold increase. Its function is so far unknown, and bioinformatic predictions using SUBA (2.1.6) suggest that *ARP9* is localized exclusively in the nucleus. The most highly upregulated transcript was *MRDI* (*mto1 RESPONDING DOWN*), which exhibited a 187.5-fold increase relative to WT. This gene was initially identified in the *mto1-1* mutant, which over-accumulates soluble methionine. Its localization is predicted to be primarily cytosolic with a weak nuclear localization (SUBA, 2.1.6). *RPP13* encodes a putative disease-resistance protein and was significantly reduced to 16.8% of WT levels. It is predicted to be exclusively cytosolic localized (SUBA, 2.1.6) and of unknown function.

Table 13: List of significantly differentially expressed genes in *oastlA_cr#2* compared to WT. WT and *oastlA_cr#2* plants were grown hydroponically in sulfur-sufficient conditions for seven weeks (2.3.7). Shoot material was harvested, snap-frozen and ground for RNA extraction (2.4.4). Total RNA was sequenced by BGI TECH SOLUTIONS (Hong Kong) (2.4.15), and bioinformatic analysis was conducted in collaboration with Dr. Carolina de la Torre from the NGS Core Facility, University of Mannheim (2.4.15). Differentially expressed genes in *oastlA_cr#2* are listed with log2 fold change (FC). The p-value is adjusted with the false discovery rate (adj. p-value).

TAIR ID	Symbol	log2FC	adj. p-value
AT4G14880	ATCYS3-3A/OAS-TL A	-4.37	7.15E-10
AT5G43500	ARP9	1.52	1.91E-06
AT1G59218	RPP13	-2.57	6.45E-03
AT1G53480	MRD1	7.55	1.73E-02

Kyoto Encyclopedia of Genes and Genomes (KEGG) pathway analysis identified significant alterations in metabolic pathways associated with *oastlA_cr#2* (Table 14). Matching to *OAS-TL A* function in cysteine biosynthesis, the most negatively affected pathways included 'sulfur metabolism', 'cysteine and methionine metabolism', and 'glucosinolate biosynthesis'. Additional negatively affected pathways included 'phenylpropanoid biosynthesis', 'fatty acid degradation', and '2-oxocarboxylic acid metabolism'. Conversely, positively affected pathways included 'photosynthesis' and 'antenna proteins of photosynthesis', followed by 'ribosome biogenesis'. An increase in 'fatty acid biosynthesis' and 'fatty acid elongation' was observed, correlating with a decrease in 'fatty acid degradation'. Furthermore, 'biosynthesis of nucleotide sugars', 'amino sugar and nucleotide sugar metabolism', and 'DNA replication' were promoted. Additional upregulated pathways included 'phagosome formation', 'homologous recombination', and 'steroid biosynthesis'.

Table 14: KEGG pathway enrichment analysis for *oastlA_cr#2* compared to WT in shoots under sulfur-sufficient growth conditions. WT and *oastlA_cr#2* plants were grown hydroponically in sulfur-sufficient conditions for seven weeks (2.3.7). Shoot material was harvested, snap-frozen and ground for RNA extraction (2.4.4). Total RNA was sequenced by BGI TECH SOLUTIONS (Hong Kong) (2.4.15), and bioinformatic analysis was conducted in collaboration with Dr. Carolina de la Torre from the NGS Core Facility, University of Mannheim (2.4.15). The table lists the KEGG pathway identifier (ID) alongside the pathway description, normalized enrichment score (NES), and false discovery rate (FDR)-adjusted p-value (p.adjust). Negative NES values indicate pathways that are downregulated in *oastlA_cr#2* relative to WT, while positive NES values denote upregulated pathways.

ID	Description of negatively affected pathways	NES	p.adjust
ath00920	Sulfur metabolism	-2.23	0.001
ath00270	Cysteine and methionine metabolism	-2.05	0.002
ath00966	Glucosinolate biosynthesis	-2.02	0.036
ath00940	Phenylpropanoid biosynthesis	-1.96	0.018
ath00071	Fatty acid degradation	-1.88	0.016
ath01210	2-Oxocarboxylic acid metabolism	-1.66	0.028
ID	**Description of positively affected pathways**	**NES**	**p.adjust**
ath00195	Photosynthesis	2.69	0
ath00196	Photosynthesis - antenna proteins	2.61	0
ath03010	Ribosome	2.51	0
ath00062	Fatty acid elongation	2.15	0.003
ath01250	Biosynthesis of nucleotide sugars	2.01	0
ath04145	Phagosome	1.99	0.001
ath03030	DNA replication	1.95	0.008
ath00520	Amino sugar and nucleotide sugar metabolism	1.84	0.001
ath00061	Fatty acid biosynthesis	1.78	0.019
ath03440	Homologous recombination	1.78	0.021
ath00100	Steroid biosynthesis	1.78	0.022

In alignment with KEGG results, the most positively affected biological processes found in gene ontology (GO) enrichment analysis were 'cell cycle', and 'cell cycle process' (Figure 17). Increased cell cycle activity may also contribute to the enhancement of 'cytoskeleton organization', 'microtubule-based processes', and 'microtubule cytoskeleton organization'. Additionally, 'photosynthesis', and specifically the 'light reaction', were enhanced. The most negatively affected GO terms were associated with 'response to salicylic acid', a key plant defense hormone against pathogens, which is likely linked to downregulated pathways of 'response to fungus' and 'defense response to bacterium'.

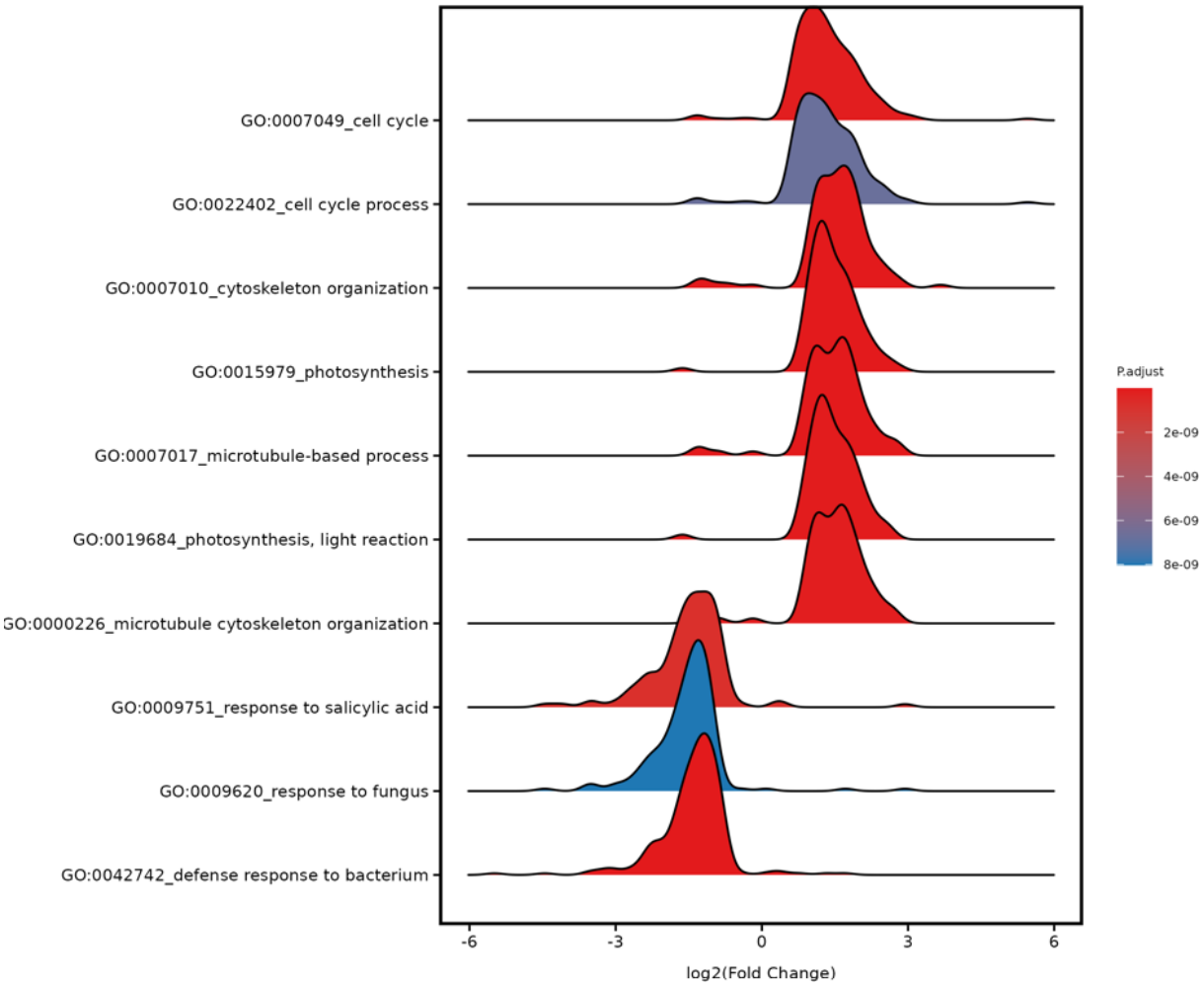

Figure 17: Gene Ontology (GO) enrichment analysis for differentially expressed genes in *oastlA_cr#2* compared to WT in shoots grown in sulfur-sufficient conditions. WT and *oastlA_cr#2* plants were grown hydroponically in sulfur-sufficient conditions for seven weeks (2.3.7), after which shoot material was harvested, snap-frozen, and ground for RNA extraction (2.4.4). Total RNA was sequenced by BGI TECH SOLUTIONS (Hong Kong) (2.4.15), and bioinformatic analysis was conducted in collaboration with Dr. Carolina de la Torre from the NGS Core Facility, University of Mannheim (2.4.15). The x-axis represents the density distribution of log2(Fold Change) values for different GO terms (y-axis). Negative log2(Fold Change) values indicate downregulated biological processes in *serat1;1_cr#2* relative to WT, whereas positive values denote upregulated processes. The color gradient represents the statistical significance of the p-value adjusted with the false discovery rate (p.adjust). Red indicates highly significant enrichment, and blue denotes lower significance.

Taken together, the loss of OAS-TL A results in increased primary metabolism, including enhanced photosynthetic activity and biosynthetic processes, but comes with the cost of decreased defense metabolism compared to WT, affecting salicylic acid signaling and pathogen-related responses.

Although no significantly differentially expressed genes were found in the *serat1;1_cr#2* mutant compared to WT, the KEGG analysis found one pathway negatively and 20 pathways positively affected (Table 15). The most negatively affected pathway was 'autophagy', which is necessary for general recycling and adaptation to stress responses. The second most negatively affected pathway was 'sulfur metabolism' although not statistically significant ($p = 0.06$). Among the most positively affected pathways, 'photosynthesis' and 'antenna proteins for photosynthesis' were found, along with the pathway of 'carbon fixation in photosynthetic organisms' and 'glycolysis/gluconeogenesis'. The upregulated photosynthesis and, therefore, carbon and energy surplus could be a reason for the upregulated biosynthesis of 'nucleotide sugars', 'nucleotide metabolism', and 'amino sugar and nucleotide sugar metabolism', leading possibly to the enhanced 'DNA replication pathway'. This might necessitate equally enhanced pathways of 'mismatch repair' and 'nucleotide excision repair'. Additionally enhanced was the pathway 'ribosome', indicating, together with 'aminoacyl-tRNA biosynthesis', enhanced translation or other ribosome modification. Other pathways positively affected in this mutant were 'histidine metabolism', 'ascorbate and aldarate metabolism', 'fatty acid biosynthesis', 'cutin, suberine and wax biosynthesis', 'biosynthesis of cofactors', 'pyruvate metabolism', 'phosphatidylinositol signaling system' and 'phagosome', supporting the hypothesis of a generally enhanced metabolism.

Table 15: KEGG pathway enrichment analysis for *serat1;1_cr#2* compared to WT in shoots under sulfur-sufficient growth conditions. The table lists the KEGG pathway identifier (ID) alongside the pathway description, normalized enrichment score (NES), and false discovery rate (FDR)-adjusted p-value (p.adjust). Negative NES values indicate pathways that are downregulated in *serat1;1_cr#2* relative to WT, while positive NES values denote upregulated pathways.

ID	Description of negatively affected pathways	NES	p.adjust
ath04136	Autophagy	-2.19	0
ath00920	Sulfur metabolism	-1.58	0.06
ID	**Description of positively affected pathways**	**NES**	**p.adjust**
ath00195	Photosynthesis	2.63	0
ath03010	Ribosome	2.32	0
ath03030	DNA replication	2.24	0
ath00196	Photosynthesis - antenna proteins	2.2	0
ath01250	Biosynthesis of nucleotide sugars	2.18	0
ath00520	Amino sugar and nucleotide sugar metabolism	2.05	0
ath00340	Histidine metabolism	1.83	0.042
ath00053	Ascorbate and aldarate metabolism	1.79	0.014
ath00010	Glycolysis / Gluconeogenesis	1.78	0.009
ath00061	Fatty acid biosynthesis	1.78	0.034
ath00073	Cutin, suberine and wax biosynthesis	1.74	0.046
ath00970	Aminoacyl-tRNA biosynthesis	1.72	0.038
ath03430	Mismatch repair	1.71	0.042
ath01232	Nucleotide metabolism	1.68	0.038
ath01240	Biosynthesis of cofactors	1.64	0.003
ath00620	Pyruvate metabolism	1.63	0.038
ath00710	Carbon fixation in photosynthetic organisms	1.61	0.042
ath04070	Phosphatidylinositol signaling system	1.59	0.043
ath03420	Nucleotide excision repair	1.58	0.043
ath04145	Phagosome	1.57	0.046

The GO analysis of *serat1;1_cr#2* mutant found positive enrichments in processes related to 'photosynthesis' and the 'light response.' The GO term 'cell cycle' was also upregulated, alongside with 'generation of precursor metabolites and energy' and 'microtubule-based processes' (Figure 18). Conversely, the most negatively affected GO terms were related to plant defense, particularly the 'response to salicylic acid,' 'response to fungus,' and 'defense response to bacterium.'

Taken together, the loss of SERAT1;1 led to increased primary metabolism at the expense of defense metabolism, mirroring the effects observed in the *oastlA_cr#2* mutant. Interestingly, both mutants share 7 out of the 10 most significantly affected GO terms ('cell cycle', 'photosynthesis', 'photosynthetic light reactions', 'microtubule-based processes', 'response to salicylic acid', 'response to fungus', and 'defense response to bacterium'). Since OAS-TL A and SERAT1;1 possess different enzymatic functions but form a complex together, the high degree of overlap in their affected GO terms suggests that the observed effects are caused by the absence of the CSC complex rather than the absence of the individual proteins. This finding implies that the CSC complex plays an inhibitory role in primary energy metabolism while promoting defense metabolism in control conditions.

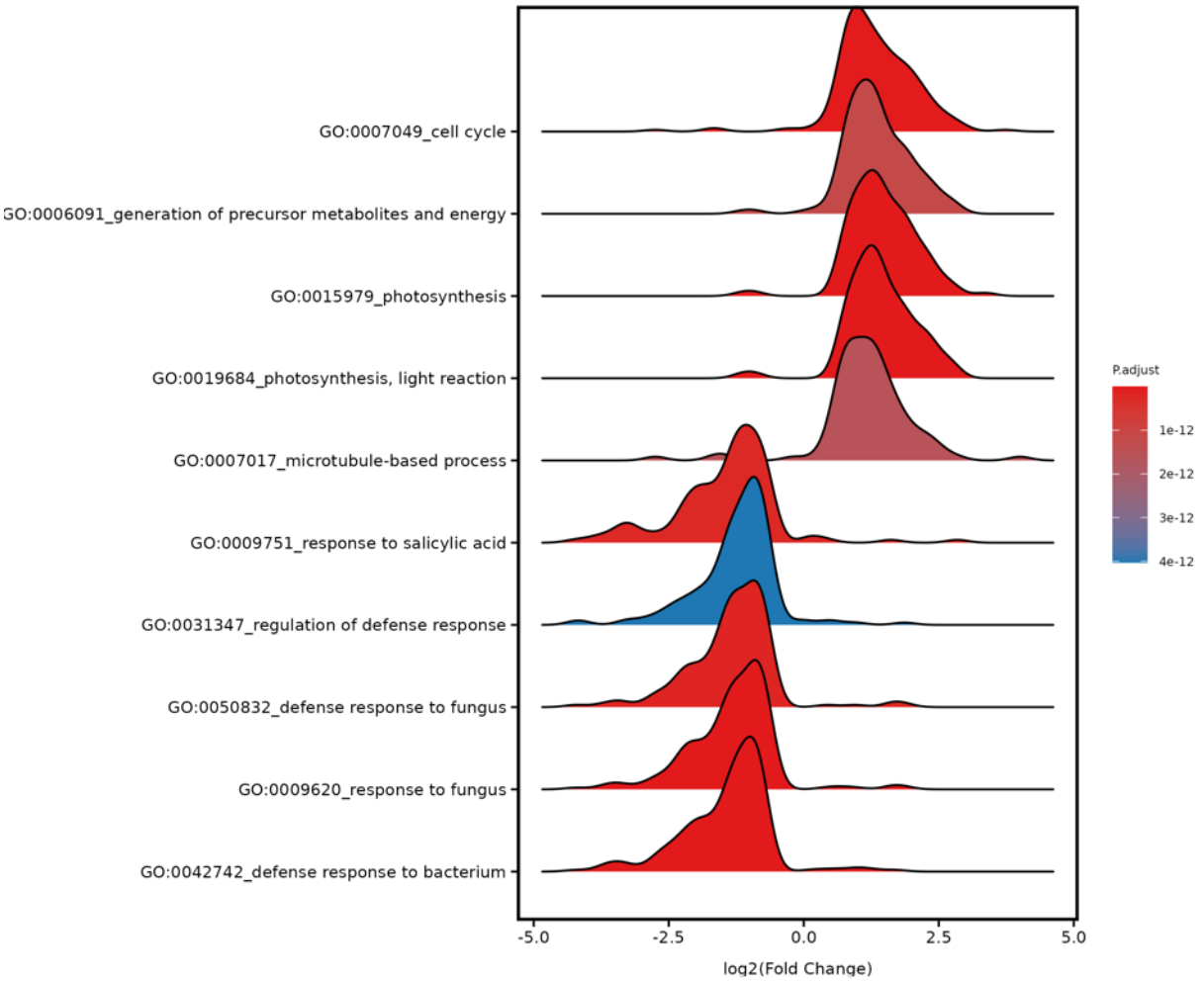

Figure 18: Gene Ontology (GO) enrichment analysis for differentially expressed genes in *serat1;1_cr#2* compared to WT in shoots grown in sulfur-sufficient conditions. WT and *serat1;1_cr#2* plants were grown hydroponically in sulfur-sufficient conditions for seven weeks (2.3.7), after which shoot material was harvested, snap-frozen, and ground for RNA extraction (2.4.4). Total RNA was sequenced by BGI TECH SOLUTIONS (Hong Kong) (2.4.15), and bioinformatic analysis was conducted in collaboration with Dr. Carolina de la Torre from the NGS Core Facility, University of Mannheim (2.4.15). The x-axis represents the density distribution of log2(Fold Change) values for different GO terms (y-axis). Negative log2(Fold Change) values indicate downregulated biological processes in *serat1;1_cr#2* relative to WT, whereas positive values denote upregulated processes. The color gradient represents the statistical significance of the p-value adjusted with the false discovery rate (p.adjust). Red indicates highly significant enrichment, and blue denotes lower significance.

3.2 Investigating the function of SERAT group three isoforms in sulfur deficiency

The SERAT group three isoforms remain largely uncharacterized. Their expression levels and catalytic activities are significantly lower than those of group one and two isoforms (Noji *et al*., 1998). Nevertheless, they are the only SERAT isoforms that are transcriptionally induced under sulfur deficiency (Kawashima *et al*., 2005). Additionally, they were found in protein interaction studies performed on SERAT1;1, especially during sulfur deficiency (Haberland, 2017), indicating a possible involvement of SERAT3 isoforms in the sulfur deficiency response.

3.2.1 SERAT3 are evolutionarily conserved throughout the plant kingdom

To investigate the evolutionary conservation of the SERAT protein family, I used the web-based tool Phylogenes (2.1.6) to generate a phylogenetic tree (Figure 19). Different form bacteria and fungi, plants have undergone a duplication event within the SERAT protein family, leading to the divergence of SERAT group three from the ancestral SERAT isoforms resulting in groups one and two. Since an additional SERAT3 isoform was found next to a SERAT1/2 isoform in the single-celled green alga *Chlamydomonas reinhardtii*, SERAT3 must have an ancient function. This pattern was also observed in early land plants such as *Marchantia polymorpha* and *Selaginella moellendorffii*. In higher vascular plants, an additional duplication event resulted in the distinction of SERAT group one and two isoforms. In *Arabidopsis thaliana*, SERAT group two underwent further duplication, resulting in the two paralogs SERAT2;1 and SERAT2;2. The examination of several common crop species found at least one SERAT3 isoform in *Zea mays* (corn), *Oryza sativa* (rice), *Solanum tuberosum* (potato), and *Manihot esculenta* (cassava). In *Gossypium hirsutum* (cotton), as in *Arabidopsis*, two SERAT3 isoforms were detected. *Triticum aestivum* (wheat) harbors three isoforms, while *Glycine max* (soybean) contains four distinct SERAT3 isoforms. This suggests that the conservation of at least one SERAT3 isoform provides a selective advantage. The expansion of this isoform group in some species may confer to additional functional specialization.

Overall, these findings indicate that the presence of SERAT3 is not a unique occurrence in *Arabidopsis* but rather represents an ancient and highly conserved protein family.

The C-terminus of SERAT group one and two isoforms terminates with the conserved EWSDYV(I)I sequence, which is essential for interaction with OAS-TLs (Francois *et al*., 2006). In contrast, SERAT group three isoforms possess an extended C-terminus that lacks this conserved motif (Liu *et al*., 2022; Tavares *et al*., 2015). Interestingly, within this C-terminal extension, a structural alpha helix was predicted by AlphaFold (2.1.6) (Figure 20) consistently for both *A. thaliana* SERAT3 isoforms, the SERAT3 isoform of *Oryza sativa*, *Marchantia polymorpha*, and *Chlamydomonas reinhardtii*. This alpha-helical domain might pose a conserved characteristic of the SERAT3 subfamily with potential roles in protein stability, localization, or interactions. Nonetheless, its presence and biological significance remain to be verified.

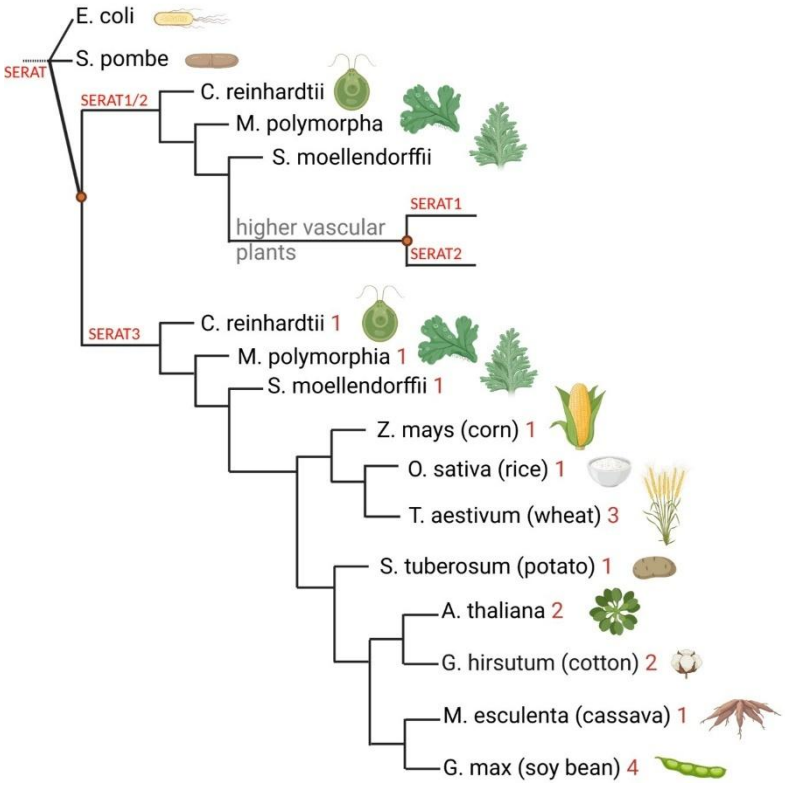

Figure 19: Phylogenetic analysis of SERAT group three protein family. The qualitative phylogenetic tree was made with the protein sequences of selected species with the online tool Phylogene (1.4.6). The annotations and drawings were added with Biorender (1.4.6). The numbers in brown behind the species names indicate the number of distinct SERAT group three isoforms.

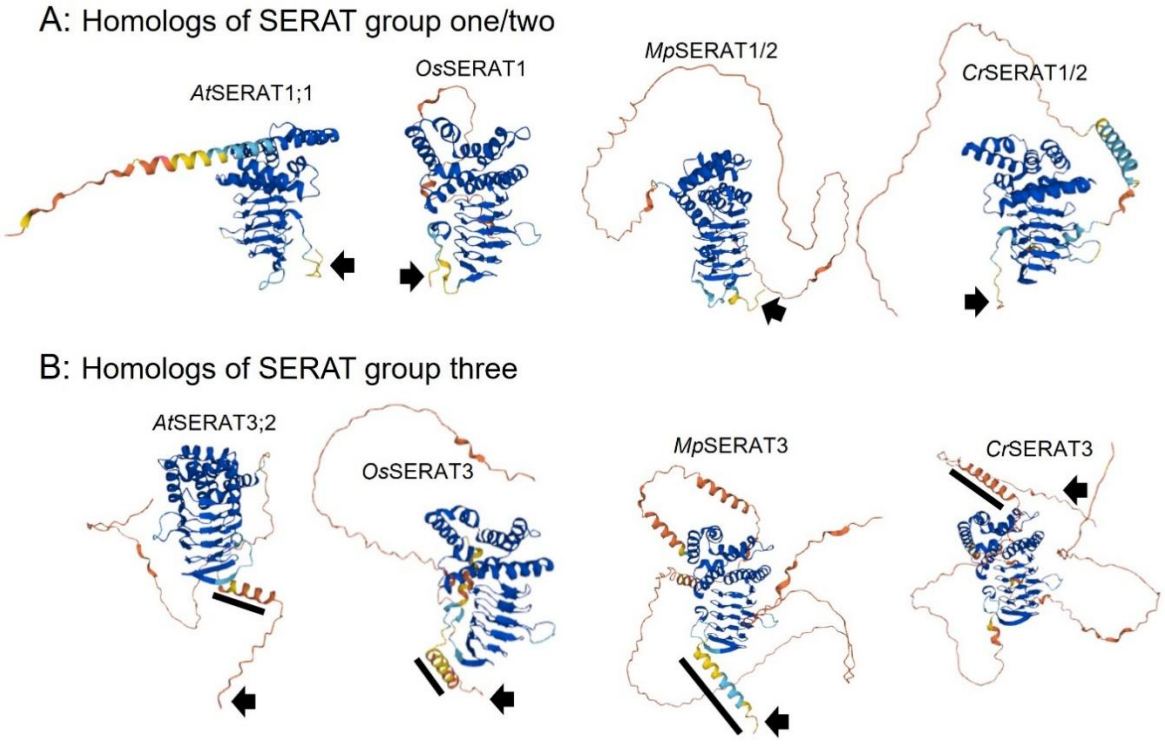

Figure 20: Structural comparison of SERAT isoforms among different plant species. A: Predicted protein structures of SERAT1;1 from *A. thaliana* (Q42538) and *O. sativa* (Q0DGG8) in comparison to SERAT1/2 progenitor isoforms of *M. polymorpha* (A0A2R6WLY8) and *C. reinhardtii* (Q8LPN9). **B:** Predicted protein structures of SERAT3;2 from *A. thaliana* (Q8W2B8) compared to SERAT3 of *O. sativa* (Q10S58), *M. polymorpha* (A0A2R6X8T9), and *C. reinhardtii* (A8JDD3). The black arrows point to the C-terminus, and the black line indicates a predicted alpha helix in the C-terminal domain of SERAT group three. In brackets are the UniProt IDs used for the predictions made by AlphaFold (2.1.6).

3.2.2 Expression analysis of SERAT group three and subcellular localization

Previously, SERAT group three expression was shown to be approximately tenfold lower than SERAT groups one and two and located mainly in the vasculature and junction of lateral roots (Kawashima *et al.*, 2005). However, detailed knowledge regarding the tissue specificity and developmental stage-dependent expression of SERAT3 remains fragmented. Available online expression databases were searched to obtain a more comprehensive overview of SERAT3 expression.

The analysis of the eFP browser as part of the Klepikova Arabidopsis Atlas (2.1.6)(Winter *et al.*, 2007) revealed that *SERAT3;1* is predominantly expressed in mature leaves, whereas *SERAT3;2* was strongest expressed in mature flowers (Figure 21). However, absolute expression levels remained low, with *SERAT3;2* never exceeding a value of 2 and *SERAT3;1* reaching a maximum expression level of 15. Since these expression levels were still an order of magnitude lower than *SERAT1;1*, which displayed an absolute maximum of 100, these findings are consistent with previous observations by Kawashima *et al.* (2005). This expression pattern of *SERAT1;1* being broadly expressed, followed by *SERAT3;1* and *SERAT3;2* at progressively lower levels was similar in the Arabidopsis Atlas for embryo development, the shoot apical meristem, gynoecium, siliques, and seeds (Winter *et al.*, 2007).

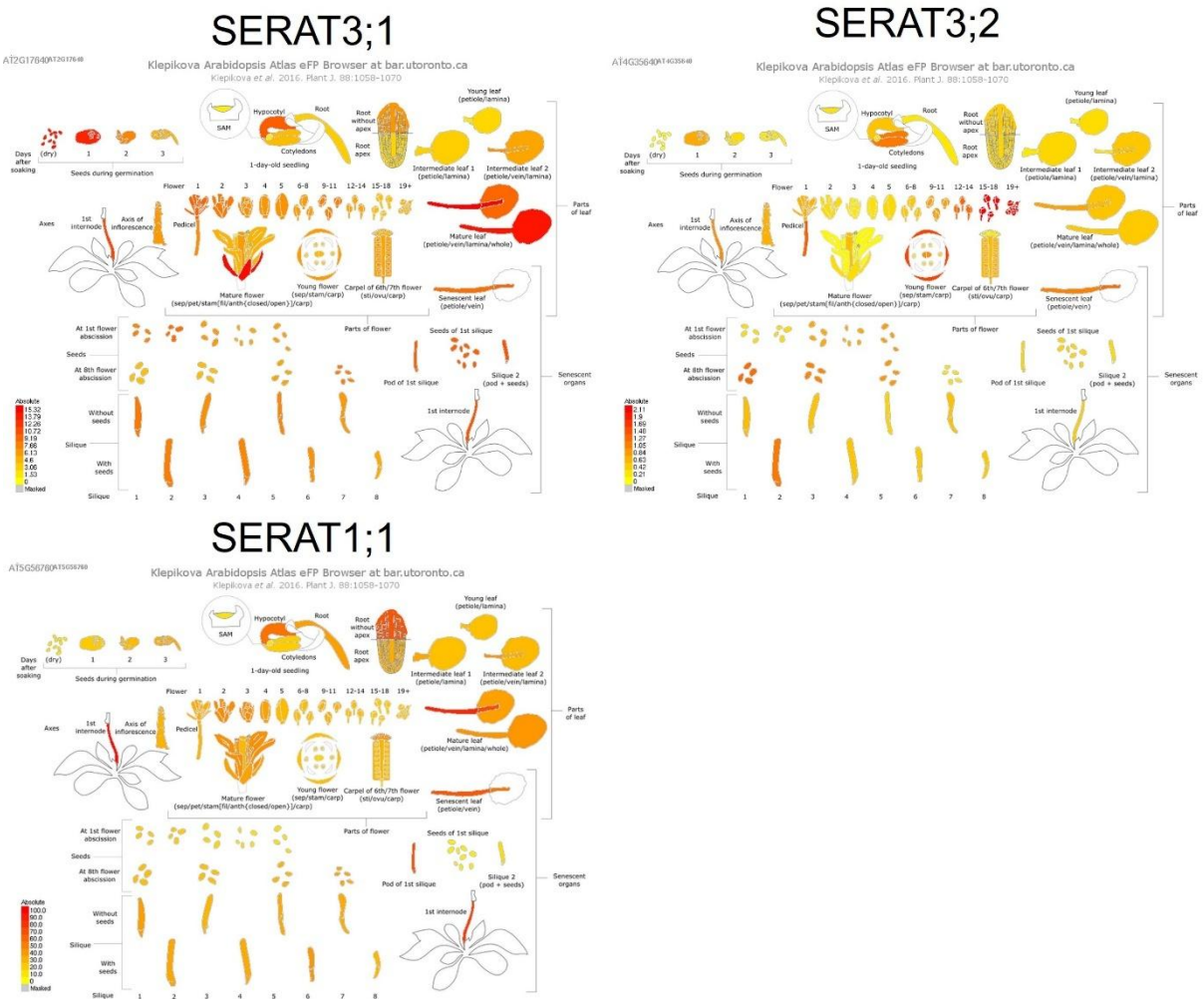

Figure 21: Expression profile of SERAT3;1 and SERAT3;2 in comparison to SERAT1;1 in the shoots. The Klepikova Arabidopsis Atlas eFP browser was used to generate this figure (Winter *et al.*, 2007).

To refine the cell type-specific expression profiles, the Arabidopsis shoot single-cell atlas was examined (2.1.6) (Zhang *et al*., 2021). Unlike the ubiquitously expressed *SERAT1;1*, *SERAT3;1* was found exclusively in vascular tissues. *SERAT3;2* was barely detectable but also localized primarily to the vasculature (Figure 22).

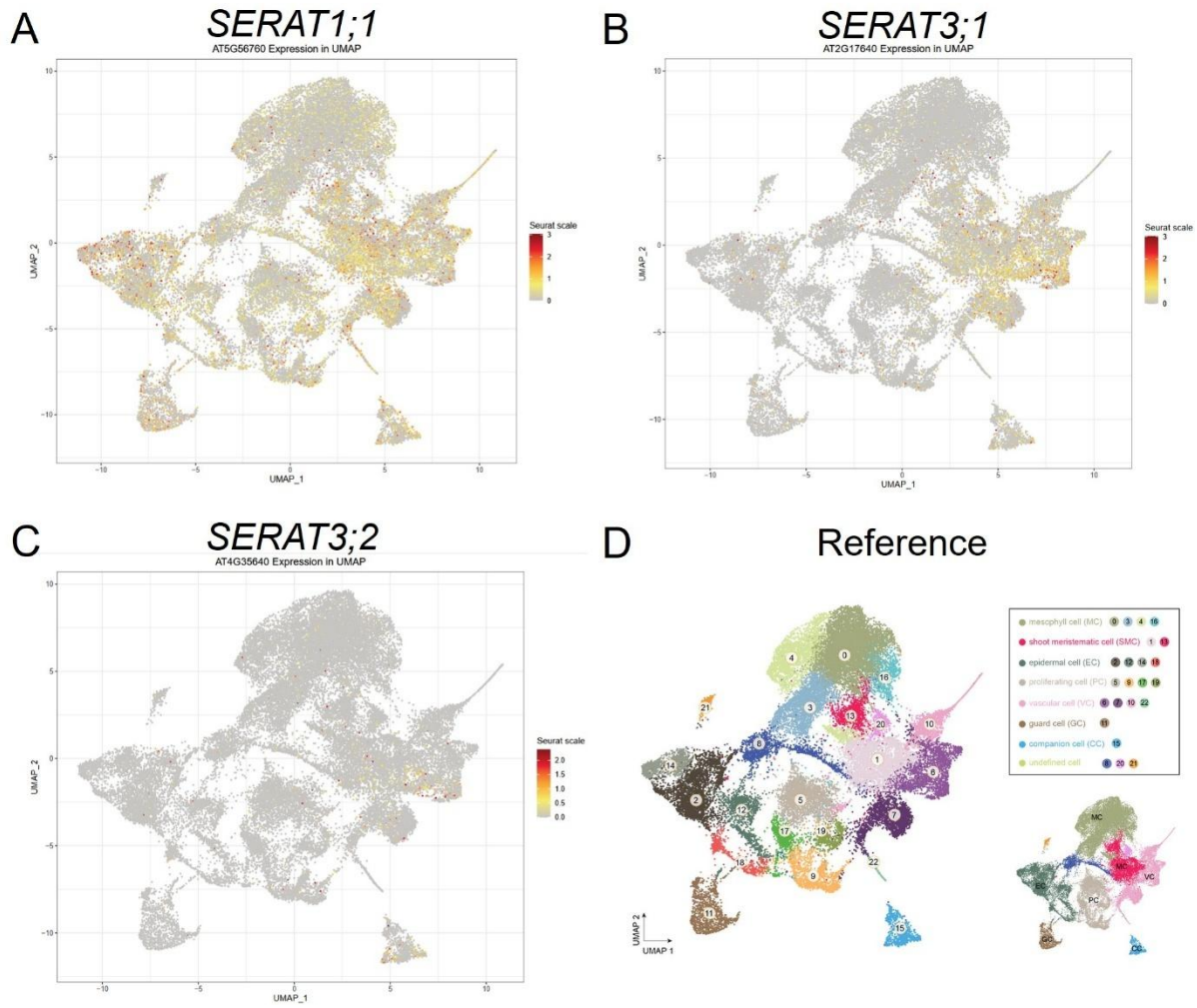

Figure 22: Single-cell expression analysis of SERAT group three in the shoot. Expression analysis of *SERAT1;1* (A), SERAT3;1 (B), and SERAT3;2 (C) with the cell type reference in (D) generated with Arabidopsis shoot single-cell atlas (2.1.6) (Zhang *et al*., 2021).

Using the Arabidopsis root single-cell atlas (1.4.6) (Shahan *et al*., 2022), a similar decreasing strength in expression was observed in the root. While *SERAT1;1* was universally expressed, *SERAT3;1* was mainly found in cells of endodermis, neocortex, stele, and phloem (Figure 23). Again, *SERAT3;2* was more restricted in its expression to endodermis and stele cells, including the pericycle. The magnitudes of expression were one to two magnitudes lower than *SERAT1;1,* matching previous observations by Kawashima *et al.* (2005).

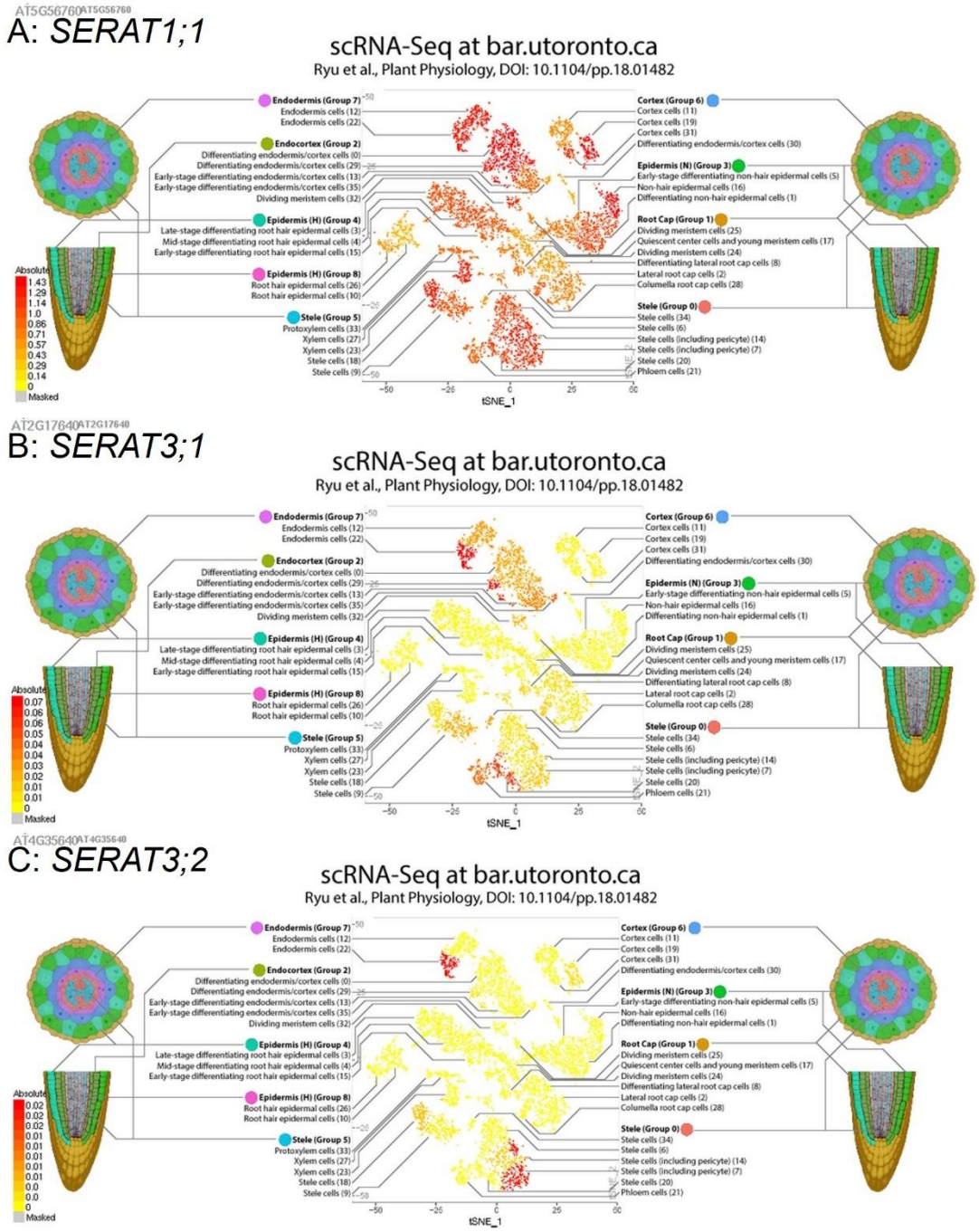

Figure 23: Single-cell expression analysis of SERAT group three in the root. Expression analysis of *SERAT1;1* (A), SERAT3;1 (B), and SERAT3;2 (C) generated with Arabidopsis root single-cell atlas (2.1.6) (Shahan *et al.*, 2022).

Previous studies reported the transcriptional induction of *SERAT* group three genes in response to sulfur deficiency and cadmium stress (Kawashima *et al.*, 2005). While *SERAT3;1* expression was found to increase twofold in root tissue after 96 h of sulfur deprivation, *SERAT3;2* exhibited a 45-fold upregulation under the same conditions (Kawashima *et al.*, 2005). Given its higher sensitivity to sulfur deficiency, *SERAT3;2* was selected for further validation of its transcriptional response.

WT seeds (2.3.1) were surface-sterilized (2.3.3) and germinated on solid ½ Hoagland medium plates (2.3.4). After six days in short-day conditions (2.3.4), the seedlings were divided into two groups and transferred to fresh ½ Hoagland plates containing either sulfur-deficient conditions (0 µM sulfate) or sulfur-sufficient conditions (500 µM sulfate) as a control (2.3.4). Seedlings were

harvested after 12 h, 25 h, 48 h, 72 h and 96 h and used for RNA extraction (2.4.4), followed by cDNA synthesis (2.4.5) and qRT-PCR analysis (2.4.8) using *SERAT3;2*-specific primers (2.4.6).

After 96 h of sulfur deficiency, *SERAT3;2* transcript levels exhibited a 60-fold increase compared to the 0 h control, confirming its strong transcriptional induction in sulfur deficiency (Figure 24).

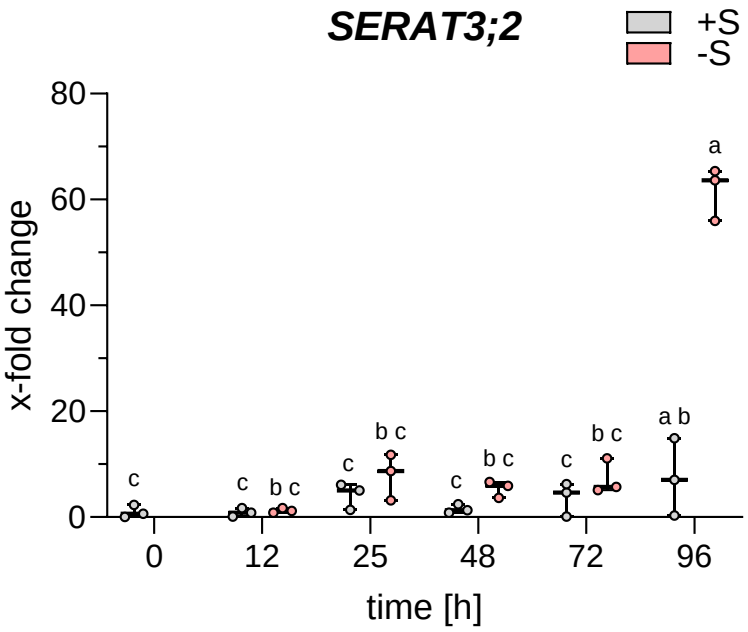

Figure 24: SERAT3;2 transcript upregulation in response to sulfur deficiency in seedlings. WT seeds were surface sterilized (2.3.3) and sown on ½ Hoagland plates containing 500 µM sulfate (+S) (2.3.4). After three weeks, seedlings were transferred to fresh +S media plates or ½ Hoagland plates containing 1 µM sulfate (-S) for inducing sulfur deficiency. Nine seedlings were directly harvested as control plants and pooled into three samples. The remaining seedlings were further grown in short-day conditions (2.3.4). At the indicated time points, seedlings were harvested as described for the control. The seedlings were snap-frozen, ground, and used to extract RNA (2.4.4). cDNA was generated (2.4.5) and qRT-PCR (2.4.8) performed with primers for *SERAT3;2* (2.4.6). The data is collected from one independent replicate and each data point indicates a pool of three plants. For statistical analysis (2.7), the ANOVA 2-way with $p < 0.05$ was used after assessing the correct data transformation.

3.2.3 *In vivo* localization of SERAT3;2-mCherry

Previously, the subcellular localization of SERAT3;1 and SERAT3;2 was determined to be cytosolic (Kawashima *et al*. 2005). This analysis had been performed using the first 100 amino acids with N-terminally fused GFP in transiently transformed Arabidopsis seedlings (Kawashima *et al*. 2005). The promoter activity of both genes was tested using the sequence 2,500 bps upstream of ATG to express GFP in stably transformed Arabidopsis (Kawashima *et al*., 2005). Here, *SERAT3;2* was selected due to its strong transcriptional upregulation under sulfur deficiency, as verified in Figure 24 (3.2.2).

To investigate the subcellular localization of the full-length *SERAT3;2* protein and its spatial and temporal expression pattern *in vivo*, two DNA constructs were generated. These constructs expressed full-length *SERAT3;2* CDS C-terminally fused to mCherry, driven either by the constitutive *Ubiquitin10* promoter (*prUbi::SERAT3;2-mCherry*) or by its minimal native promoter (*prSERAT3;2::SERAT3;2-mCherry*). The minimal native promoter was defined as the 460 bp intergenic region upstream of the *SERAT3;2* start codon, preceding the *ADHII* open reading frame on the complementary strand. Raipuria *et al*. (2017) previously demonstrated that this promoter region exhibits strong activity in flowers in sulfur-sufficient conditions. Its inducibility in sulfur

deficiency had not been tested, but sequence analysis using the TAIR-based seqViewer tool (2.1.6) identified a sulfur-responsive element (SURE) core motif (GAGAC) 227 bp upstream of the start codon as part of the 5' UTR. Under my supervision, a Master student (Diana Gabler), designed primers for the minimal promoter. She successfully cloned the plasmids prUbi::SERAT3;2-mCherry (2231) and prSERAT3;2::SERAT3;2-mCherry (2232) and used them to generate stable transgenic *Arabidopsis* lines (Gabler, 2023). Vector maps are available in Supplemental Figure 12 and Supplemental Figure 13.

To investigate fluorescence signals, seeds of the T2 generation were surface sterilized (2.3.3) and germinated on solid media plates containing either 500 µM sulfate (sulfur-sufficient condition) or 1 µM sulfate (sulfur-deficient condition) (2.3.4). Since the T2 lines were not homozygous, seedlings were treated with 200 µM/ml Basta after one week to select for the T-DNA. After three weeks, seedlings were stained with DAPI (2.3.14) and analyzed using confocal laser scanning microscopy (CLSM) (2.3.15).

Plants expressing *prUbi::SERAT3;2-mCherry* (2231) (2.3.1) exhibited strong mCherry fluorescence in all investigated tissues in both sulfur-sufficient and sulfur-deficient conditions (Figure 25), consistent with the expected ubiquitous activity of the *Ubiquitin10* promoter. The subcellular localization confirmed the previously reported cytosolic localization of *SERAT3;2*. Interestingly, the mCherry signal was also found in the nucleus. The DAPI colocalization corroborated the nuclear localization, highlighting a significant difference between *SERAT3;2* and the strictly cytosolic *SERAT1;1*.

In contrast, plants expressing *prSERAT3;2::SERAT3;2-mCherry* (2232) (2.3.1) exhibited weak fluorescence, with signal detection only in transgenic lines #1 and #21, indicating weaker expression relative to the *Ubiquitin10* promoter. Notably, fluorescence was only observed in plants subjected to sulfur deficiency, confirming that the minimal promoter is sufficient for sulfur-responsive gene expression (Figure 25 B). The expression was restricted to the stele, suggesting both sulfur deficiency-induced regulation and cell type-specific expression. Although the cytosolic localization was confirmed, the weak fluorescence intensity precluded definitive conclusions regarding nuclear localization.

Taken together, these results validate the previously reported cytosolic localization of *SERAT3;2* while also suggesting an additional nuclear localization. Furthermore, the minimal 460 bp promoter was shown to be sufficient for driving *SERAT3;2* expression in stele cells in sulfur deficiency. These transgenic lines improve our understanding of *SERAT3;2* localization and may serve as valuable tools for future investigations into *SERAT3;2* induction dynamics in response to sulfur deficiency.

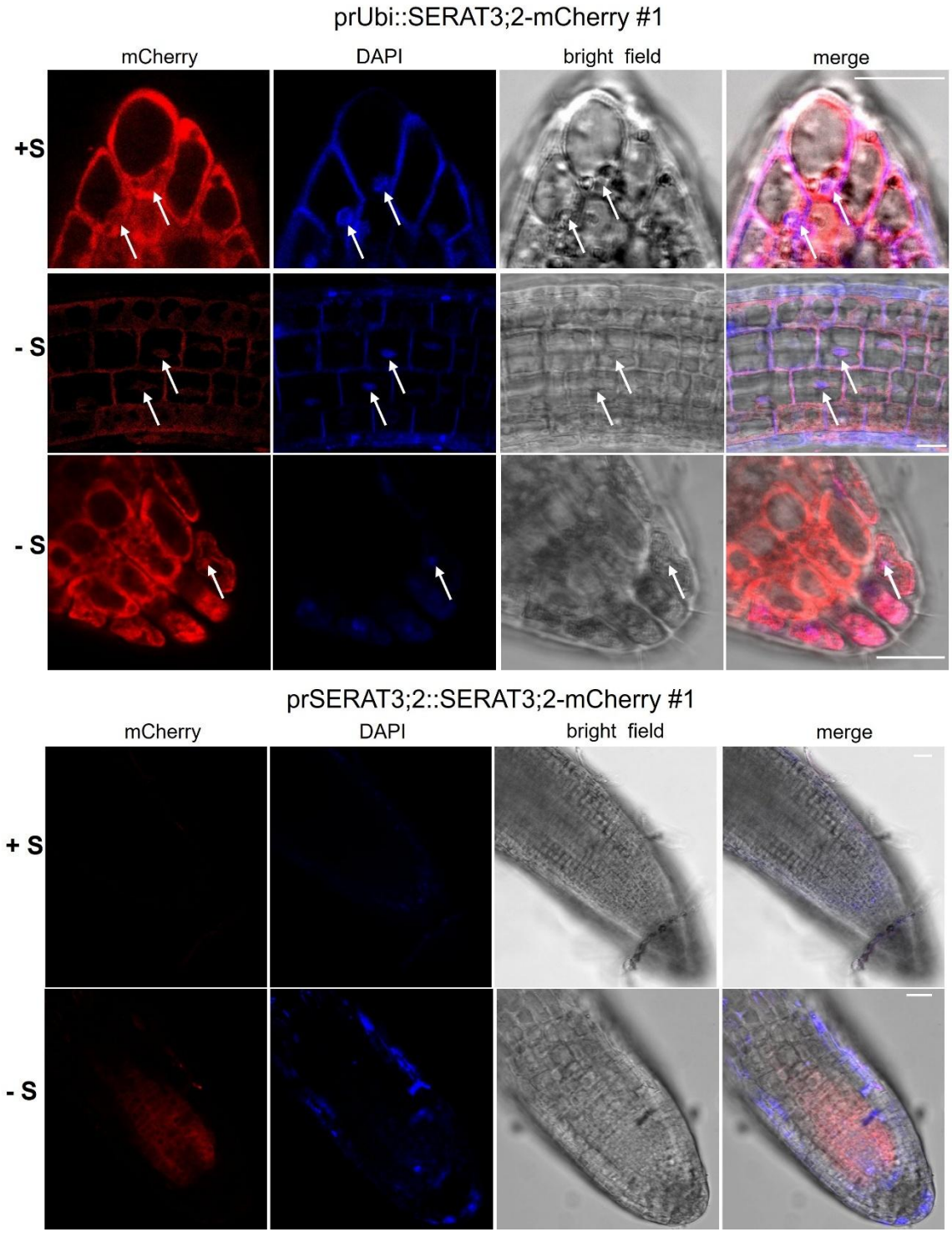

Figure 25: *In vivo* localization of SERAT3;2-mCherry in roots of *A. thaliana*. Seeds of prUbi::SERAT3;2-mCherry (2231) and prSERAT3;2::SERAT3;2-mCherry (2232) (2.3.1) T2 generation were surface sterilized (2.3.4) and grown on sterile media plates in sulfur sufficient (+S, 500 µM sulfate) and deficient condition (-S, 1 µM sulfate) for three weeks (2.3.4). Two weeks before the analysis, the plants were sprayed with Basta (2.3.9). Seedlings were stained with DAPI (2.3.14) and imaged with CLSM (2.3.15). mCherry channel: λ_{ex}= 587 nm. DAPI channel: λ_{ex} = 405 nm. White arrows mark nuclei. Scale bar = 20 µm.

3.2.4 *In vitro* interaction studies of SERAT3;2

Haberland (2017) found both SERAT group three isoforms in Co-IP experiments with SERAT1;1 as bait in Arabidopsis roots and leaves. Thereby, the SERAT3;1 interaction was found in the control condition, and the application of sulfur deficiency doubled the amount of Co-purified SERAT3;1. SERAT3;2 interaction with SERAT1;1 was 20 times lower in the control condition compared to SERAT3;1, but increased 40-fold in response to sulfur deficiency after 72 h. The protein-protein interaction of SERAT3;1 and SERAT1;1 was verified in Split-YFP experiments in Arabidopsis protoplast by Haberland (2017).

To verify the protein-protein interaction between SERAT3;2 and SERAT1;1, I designed *in vitro* Co-IP experiments with purification tags. Therefore, I created NcoI-STREP-SERAT3;2-BamHI PCR product (2.4.7) by using the primers 5355/5356 (2.5.5) and Col-0 cDNA as template (2.4.5). The PCR reaction was size-separated using gel electrophoresis (2.4.9). The DNA fragment with the expected size of 1111 bps was purified from the gel (2.4.10) and digested with BamHI and NcoI (2.4.11). The vector backbone pET3d was digested with the same enzymes and used for restriction enzyme cloning with the PCR insert (2.4.12). The ligation mix was transformed into XL1 blue and selected on ampicillin (2.2.5). Two bacterial colonies were cultured to purify plasmid DNA (2.4.2). The plasmids were test-digested with BamHI and NcoI (2.4.11) and analyzed after gel electrophoresis (2.4.9). Since both plasmids showed the expected bands, both plasmids were sequenced (2.4.14) using the cloning primers 5355 and 5356 (2.5.5). Both plasmids showed the correct sequence and were named pET3d STREP-SERAT3;2 (1878). The vector card is deposited in Supplemental Figure 14. The vector was co-transformed (2.2.5) with pET28a HIS-SERAT1;1 (1879) into *E. coli* BL21 (DE3) (2.2.1) creating BL21 (DE3) pET3d STREP-SERAT3;2 pET28a HIS-SERAT1;1 (1879). Bacteria carrying both plasmids were cultured to induce protein expression (2.5.1). The bacteria were harvested and lysed. The crude extract (CE) was purified with a STREP-tag purification column (2.5.3) or a HIS-tag purification column (2.5.2). The concentration of the purified proteins was determined (2.5.8), and samples were denaturated (2.5.9) for SDS-PAGE (2.5.10). With Western blotting (2.5.12) and immunodetection using antibodies against either HIS- or STREP-tag (2.5.13), the presence of HIS-SERAT1;1 and STREP-SERAT3;2 was visualized.

HIS-SERAT1;1 was detected in the HIS-tag purification slightly above 35 kDa, as expected for HIS-SERAT1;1 (37 kDa) (Figure 26 A). Compared to the crude extract (CE) input control, the flowthrough (FT) fraction contained less protein, confirming the successful retention of HIS-SERAT1;1 in the affinity column. The wash (W) fraction showed minimal protein presence, indicating a clean purification process and ensuring that specific proteins were selectively eluted (E). A second Western blot using an aliquot of the same samples was performed with immunodetection against the STREP-tag, revealing the presence of STREP-SERAT3;2 at the expected size of 40 kDa. This co-purification strongly indicates a protein-protein interaction between SERAT1;1 and SERAT3;2. To further validate this interaction, CE purification was performed using the STREP-tag, and both proteins were detected again, confirming their association (Figure 26 B).

Interestingly, differences in protein recovery ratios were observed depending on the purification method. Amido black staining of membranes and Coomassie staining of SDS-PAGE gels revealed varying proportions of STREP-SERAT3;2 and HIS-SERAT1;1 in the elution fractions. By quantifying the signal intensities (2.5.15) in the Coomassie-stained elution fractions (2.5.11), the STREP-SERAT3;2:HIS-SERAT1;1 ratio was determined to be 1:39 when purified via the HIS-tag and 1:1.5 when purified via the STREP-tag. These results suggest a preferential retention of HIS-SERAT1;1 in

HIS-tag purification, whereas STREP-tag purification leads to a more balanced co-purification of both proteins.

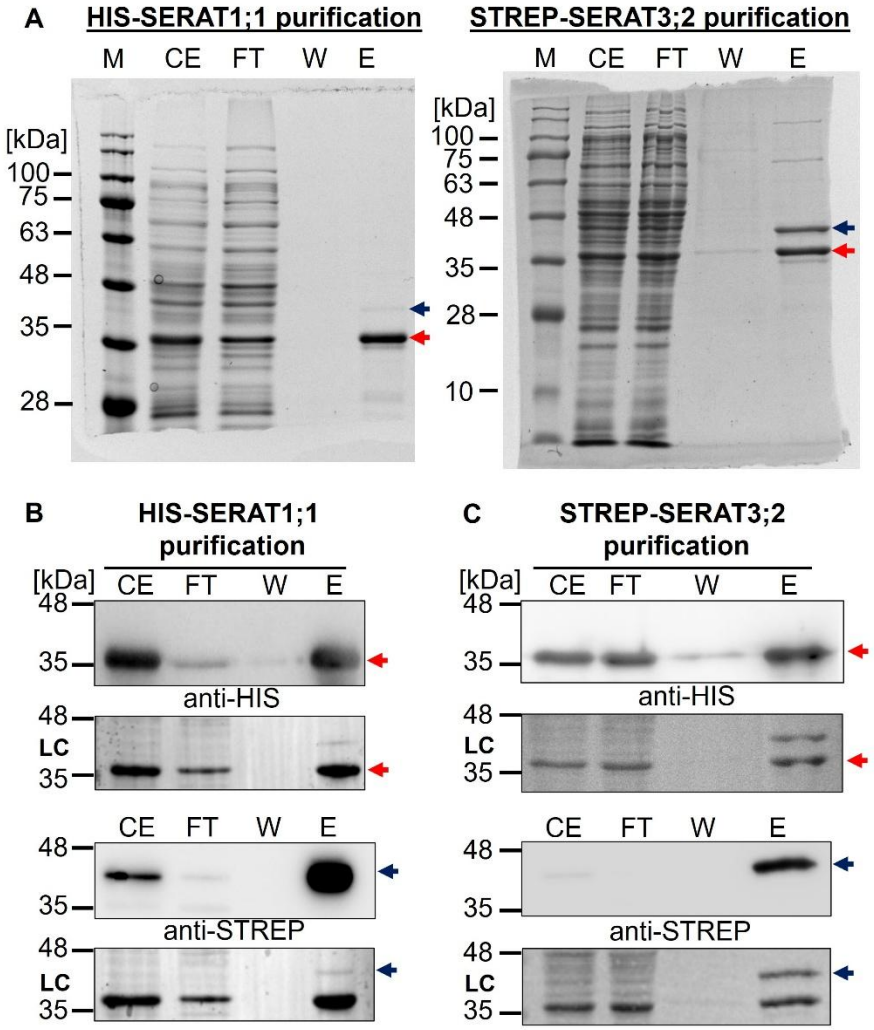

Figure 26: Interaction study of SERAT3;2 and SERAT1;1 *in vitro*. BL21 (DE3) (2.2.1) transformed (2.2.5) with the plasmids pET3d STREP-SERAT3;2 (1878) and pET28a HIS-SERAT1;1 (402) (2.4.1) was cultured to express STREP-SERAT3;2 and HIS-SERAT1;1 (2.5.1). Half of the protein extract was used for purification of HIS-tagged proteins (2.5.2), the other half was used to purify STREP-tagged proteins (2.5.3). The concentration of the purified proteins was determined (2.5.8). After protein denaturation (2.5.9), SDS-PAGE (2.5.10) and Western blotting were performed (2.5.12). The Coomassie staining of the gels to quantify SERAT3;2:SERAT1;1 are shown in **A**. Immunological detection was performed using anti-STREP and anti-HIS antibodies (2.5.13) for HIS-tag purification in **B** and STREP-tag purification in **C**. Amido black-stained membranes served as the loading control (2.5.14). Red and blue arrows indicate the expected height of HIS-SERAT1;1 and STREP-SERAT3;2, respectively. M: marker, CE: crude extract control, FT: flow-through control, W: washing control, E: elution. The uncropped membranes in B and C can be found in Supplemental Figure 15 and Supplemental Figure 16, respectively.

Since both SERAT1;1 and SERAT3;2 have previously been shown to form homo-hexamers when expressed independently *in vitro* (Birke, 2012), I hypothesized that the co-expression results in hetero-hexamers. To test this hypothesis, the quaternary structure of the HIS-SERAT1;1-STREP-SERAT3;2 complex was analyzed using size-exclusion chromatography (SEC) (2.5.5) on the STREP-tag elution fraction, since the ratio analysis revealed a more balanced presence of HIS-SERAT1;1 and STREP-SERAT3;2 than the HIS-tag purified elution fraction.

The detected retention times were 66.33 min, 65.87 min, and 65.40 min, resulting in an estimated molecular weight of 231 ± 38 kDa (Figure 27). This result strongly supports the formation of a hetero-hexamer composed of HIS-SERAT1;1 and STREP-SERAT3;2, as it lies between the expected sizes of the HIS-SERAT1;1 and STREP-SERAT3;2 homo-hexamers of 222 kDa (6 × 37 kDa) and 240 kDa (6 × 40 kDa), respectively. The third replicate, as well as the verification of the presence of both HIS-SERAT1;1 and STREP-SERAT3;2 proteins in the SEC fractions, was performed with the assistance of the Master student, Diana Gabler.

It is well established that SERAT1;1 homo-hexamers interact with OAS-TL A to form the cysteine synthase complex (cCSC) (Wirtz and Hell, 2006), whereas SERAT3;2 homo-hexamers are unable to bind OAS-TL A (Birke, 2012). Since STREP-purified complexes contained significantly more STREP-SERAT3;2 than HIS-tag purified complexes, this was used to investigate how the incorporation of SERAT3;2 into the hetero-hexamer affects SERAT1;1's ability to bind OAS-TL A. To assess this, I compared the OAS-TL A binding capacity of STREP-SERAT3;2/HIS-SERAT1;1 complexes immobilized on a STREP-column to those immobilized on a HIS-column. The relative OAS-TL A binding capacity was then evaluated by comparison of the quantified signal intensities of OAS-TL A antibody in both elution fractions.

Equal amounts of bacterial crude extract containing STREP-SERAT3;2 and HIS-SERAT1;1 (2.2.1, 2.5.1) were loaded onto both STREP and HIS purification columns (2.5.2, 2.5.3). After washing with 50 mM OAS, a bacterial crude extract containing OAS-TL A (*E. coli* BL21 (DE3) pET32 OAS-TL A (1894) was applied (2.2.1, 2.5.1). Following additional washing steps, bound proteins were eluted using the respective STREP- or HIS-tag elution buffers (2.5.2, 2.5.3). After the determination of protein concentrations (2.5.8), the samples were prepared for SDS-PAGE (2.5.10) and Western blotting (2.5.12). Immunological detection (2.5.13) and signal quantification (2.5.15) was used to quantify relative OAS-TL A contents in equally loaded elution fractions.

In two independent experiments, the OAS-TL A signal intensity in the STREP-tag purified samples was reduced to less than 60% compared to HIS-tag purified samples. In one additional repetition, it was reduced to just 6% (Figure 28).

These findings indicate that OAS-TL A binding is impaired as the SERAT3;2 content increases within the hetero-complex. Given that SERAT3;2 interacts with SERAT1;1 in *planta* under sulfur deficiency, this suggests a modulatory role for SERAT3;2 in the cCSC complex during sulfur deficiency stress conditions.

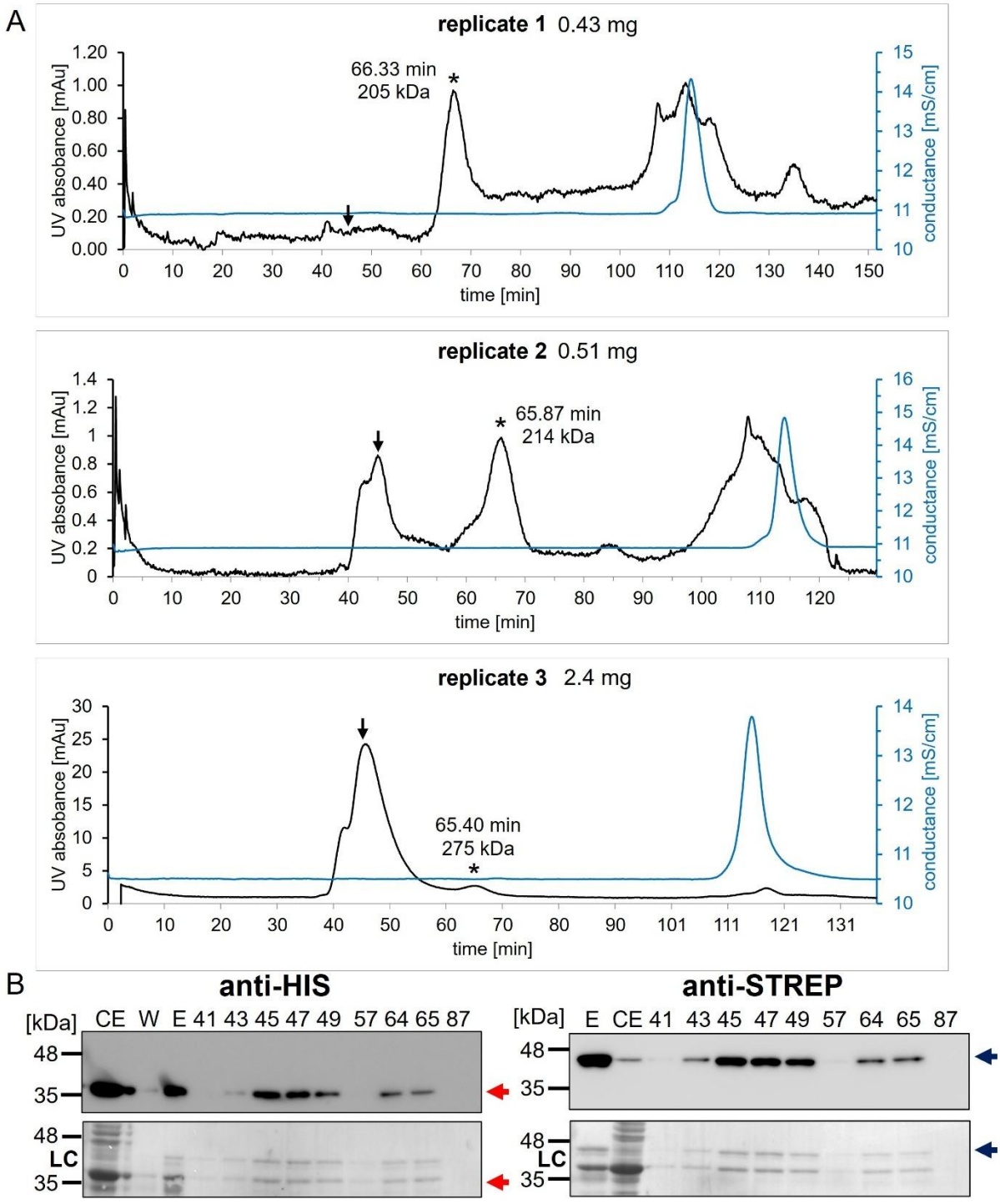

Figure 27: Size exclusion chromatography of STREP-SERAT3;2/HIS-SERAT1;1 hetero-complexes. BL21 (DE3) (2.2.1) transformed (2.2.5) with the plasmids pET3d STREP-SERAT3;2 (1878) and pET28a HIS-SERAT1;1 (402) (2.4.1) was cultured to express STREP-SERAT3;2 and HIS-SERAT1;1 (2.5.1). The protein crude extract was purified using the STREP-tag (2.5.3). The concentration of the purified proteins was determined (2.5.8), and 430 µg, 510 µg and 2.4 mg in 1 ml buffer was applied to SEC replicate 1-3 (2.5.5). **A:** UV absorption vs retention time of the three independent repetitions. The conductance was plotted to mark the end of the run. The loaded protein amount is indicated in mg, and the protein peak of interest is marked with an asterisk. The retention time and the calculated molecular weight are indicated above. The black arrows indicate the dead volume of the column. **B:** With the help of Diana Gabler, the crude extract control (CE), the SEC input control (E), a wash control, and the 1 ml fractions collected in SEC after min 41, 43, 45, 47, 49, 57, 64, 65, and 87 of replicate three were denaturated (2.5.9) and used for SDS-PAGE (2.5.10) and Western blotting (2.5.12). Immunological detection was performed using anti-STREP and anti-HIS antibodies (2.5.13). The membranes were stained with amido block as the loading control (LC) (2.5.14). Red and blue arrows indicate the expected height of HIS-SERAT1;1 and STREP-SERAT3;2, respectively. The uncropped membranes are found in the appendix in Supplemental Figure 17.

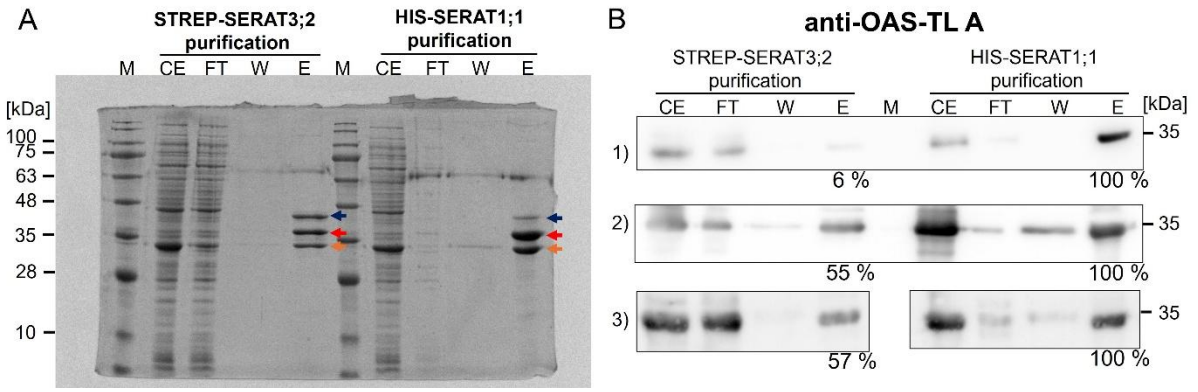

Figure 28: OAS-TLA binding capacity of STREP-SERAT3;2/HIS-SERAT1;1 heterocomplexes *in vitro*. BL21 (DE3) (2.2.1) transformed (2.2.5) with the plasmids pET3d STREP-SERAT3;2 (1878) and pET28a HIS-SERAT1;1 (402) (2.4.1) was cultured to express STREP-SERAT3;2 and HIS-SERAT1;1 (2.5.1). Half of the protein extract was used to purify HIS-tagged proteins (2.5.2), and the other half was used to purify STREP-tagged proteins (2.5.3). After applying the crude extracts, BL21 protein crude extract containing OAS-TL A (1894) was loaded on both columns in equal amounts. The elution was performed with HIS or STREP elution buffers. The concentration of the purified proteins was determined (2.5.8). After protein denaturation (2.5.9), SDS-PAGE (2.5.10) for Coomassie staining (2.5.11) and Western blotting were performed (2.5.12). Immunological detection (2.5.13) and signal quantification (2.5.15) were performed using anti-OAS-TL A antibody (2.5.13). The experiment was repeated three times. **A:** Coomassie control. HIS-SERAT1;1, STREP-SERAT3;2 and OAS-TL A are indicated by red, blue, and orange arrows. **B:** Immunological detection and quantification of OAS-TL A antibody signal in the elution fraction. Since the loading was reversed in replicate three, the membrane was cut to fit the other replicates. The uncut blots can be found in the appendix in Supplemental Figure 18**.** Replicates two and three were performed under my supervision by my Master's student, Diana Gabler, and Bachelor's student, Nicolas Düster, respectively. M: marker, CE: crude extract control, FT: flow-through control, W: washing control, E: elution.

One of the most striking structural differences between SERAT1;1 and SERAT3;2 is the elongated C-terminus of SERAT3;2, which may inhibit SERAT1;1's binding to OAS-TL A through steric hindrance. To determine whether the C-terminus of SERAT3;2 is responsible for the reduced OAS-TL A binding capacity in the heterocomplex with SERAT1;1, I designed a truncated STREP-SERAT3;2ΔC protein lacking the last 44 amino acids and repeated the OAS-TL A binding assay.

To generate STREP-SERAT3;2ΔC, I used primers 5355/5420 (2.4.6) with plasmid 1878 as a template in a PCR reaction (2.4.7) to create the NcoI-STREP-SERAT3;2ΔC-BamHI DNA fragment. Following the same cloning procedures used for pET3d STREP-SERAT3;2, I generated pET3d STREP-SERAT3;2ΔC (1880) (Supplemental Figure 19). This plasmid was then co-transformed (2.2.5) with pET28a HIS-SERAT1;1 (1879) into E. coli BL21 (DE3) (2.2.1), creating BL21 (DE3) pET3d STREP-SERAT3;2ΔC pET28a HIS-SERAT1;1 (1881).

Bacteria carrying both plasmids were cultured to induce protein expression (2.5.1), and the harvested bacteria were lysed. The resulting crude extract (CE) was purified using either a STREP-tag purification column (2.5.3) or a HIS-tag purification column (2.5.2). After washing the columns, equal amounts of OAS-TL A-containing bacterial crude extract (1894, 2.5.3) were loaded onto both columns to assess the binding ability of the heterocomplexes to OAS-TL A.

After protein elution and determination of protein concentration (2.5.8), the protein samples were denatured (2.5.9) and analyzed via SDS-PAGE (2.5.10), followed by Western blotting (2.5.12) and immunological detection (2.5.13) of STREP-SERAT3;2ΔC, HIS-SERAT1;1, and OAS-TL A. The blots were also stained with amido black (2.5.14) as loading controls.

Purification using either STREP- or HIS-tag resulted in the co-purification of STREP-SERAT3;2ΔC and HIS-SERAT1;1 (Figure 29 A and B), indicating that STREP-SERAT3;2ΔC interacts with HIS-

SERAT1;1, as previously observed for full-length STREP-SERAT3;2. The OAS-TL A binding capacity of the heterocomplex purified with the STREP-tag was reduced to 40% compared to the heterocomplex purified via the HIS-tag (Figure 29 C).

This matches the observations with the full-length STREP-SERAT3;2, thereby falsifying the hypothesis that the C-terminus of SERAT3;2 sterically hinders the ability of SERAT1;1 to bind OAS-TL A.

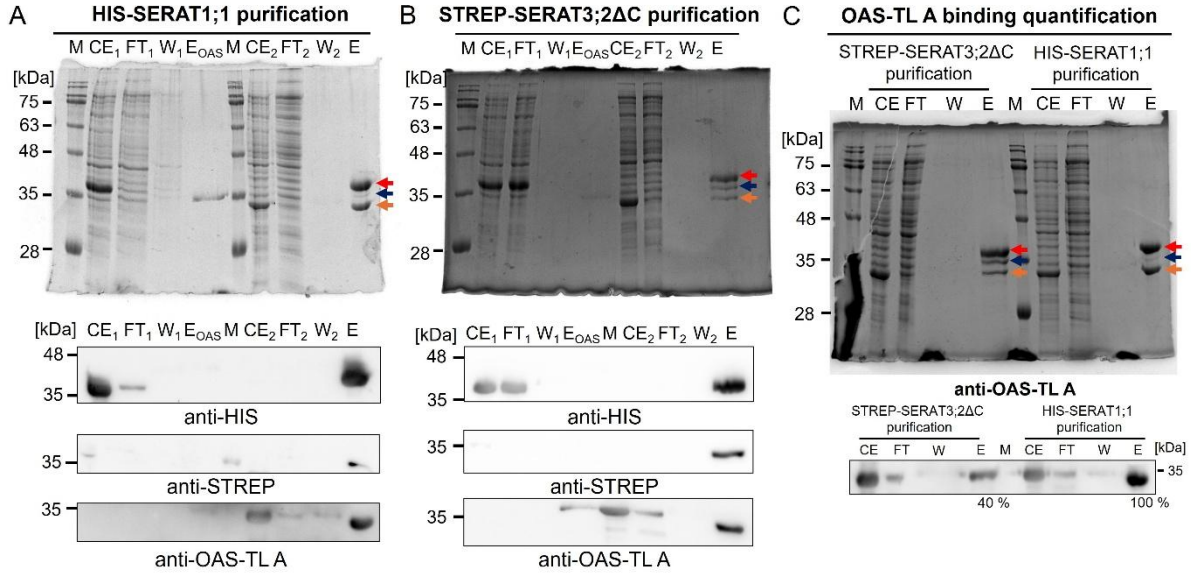

Figure 29: OAS-TLA binding capacity of STREP-SERAT3;2ΔC/HIS-SERAT1;1 heterocomplexes *in vitro*. BL21 (DE3) (2.2.1) transformed (2.2.5) with the plasmids pET3d STREP-SERAT3;2ΔC (1880) and pET28a HIS-SERAT1;1 (402) (2.4.1) was cultured to express STREP-SERAT3;2ΔC and HIS-SERAT1;1 (2.5.1). With the help of my Master's student Diana Gabler, half of the protein extract was used to purify HIS-tagged proteins (2.5.2), and the other half was used to purify STREP-tagged proteins (2.5.3). After applying the crude extracts, BL21 (DE3) (1894) protein crude extract containing OAS-TL A was loaded on both columns in equal amounts. The elution was performed with HIS or STREP elution buffers. The concentration of the purified proteins was determined (2.5.8). After protein denaturation (2.5.9), SDS-PAGE (2.5.10) with Coomassie staining of the gel (2.5.11) or Western blotting (2.5.12) for immunological detection using anti-STREP antibody, anti-HIS-antibody, and anti-OAS-TL A antibody (2.5.13). **A:** Coomassie of the HIS-tag purification with immunological detection of HIS-SERAT1;1, STREP-SERAT3;2ΔC and OAS-TL A. **B:** Coomassie of the STREP-tag purification with immunological detection of HIS-SERAT1;1, STREP-SERAT3;2ΔC and OAS-TL A. **C:** Coomassie of both STREP-tag and HIS-tag purification and immunological detection of OAS-TL A to test binding capacity to the heterocomplexes. HIS-SERAT1;1 in the Coomassie stainings are indicated by red arrow, STREP-SERAT3;2ΔC is marked by blue arrows and OAS-TL A by orange arrows. The uncut blots are deposited in the appendix in Supplemental Figure 20. M: marker, CE_1: crude extract control of 1881, FT_1: flow-through control of 1881, W_{1-2}: washing controls, E_{OAS}: OAS washing elution, CE_2: crude extract control of 1894, FT_2: flow-through control of 1894, W: washing, E: final elution.

3.2.5 Sulfur deficiency phenotype of *serat3;1s3;2*

Sulfur deficiency limits plant growth due to the lack of sulfur-containing amino acids like cysteine. To cope with this nutrient stress, plants developed adaptation strategies. One physiological acclimation strategy to sulfur deficiency is to adjust growth. Limitations of nitrogen, phosphorus or sulfur deficiency affects primarily shoot growth while root growth is maintained (Ericsson, 1995). Investing available resources in the root allows the plant to forage deeper soil areas for more nutrients. This phenotype of developmental plasticity can be quantified by dividing the root FW by the shoot FW, thereby creating the root-to-shoot FW ratio. So far, the phenotype of the single knockout mutants *serat3;1* and *serat3;2* were WT-like in sulfur sufficient condition (Watanabe *et al.*, 2008b). Furthermore, *serat3;2* did not show a phenotype different from WT in sulfur deficiency and cadmium stress (Watanabe *et al.*, 2008b). Since the SERAT group has three

isoforms that might have redundant functions, the double mutant *serat3;1s3;2* was investigated in this work for its phenotype in sulfur deficiency. Since the SERAT group three isoforms were found as interaction partners of SERAT1;1 (Haberland, 2017), I generated a triple mutant *serat1;1s3;1s3;2* to be able to differentiate between the loss of SERAT3s and the loss of all cytosolic SERAT isoforms. Therefore, I crossed *serat1;1* mutant with *serat3;1s3;2* (2.3.8) and genotyped 150 individuals of the T2 generation for homozygous candidates containing the three mutated alleles. After analyzing the genotyping PCR (2.4.7) with gel electrophoresis (2.4.9), plants #23 and #59 were identified as homozygous *serat1;1s3;1s3;2* mutants (Supplemental Figure 21).

To investigate the root-to-shoot FW ratio of *serat3;1s3;2* and *serat1;1s3;1s3;2* mutants in comparison to WT, I sowed surface-sterilized seeds (2.3.1, 2.3.3) on ½ Hoagland solid media plates under sulfur-sufficient (+S, 500 µM sulfate) and sulfur-deficient (-S, 1 µM sulfate) conditions (2.3.4). After four weeks in short-day conditions, I quantified the root-to-shoot FW ratio (2.3.10) and the average primary root length (2.3.11). Interestingly, both mutants, *serat3;1s3;2* and *serat1;1s3;1s3;2*, exhibited a WT-like physiological adaptation to sulfur deficiency (Figure 30).

The root-to-shoot FW ratio in both mutants showed a WT-like increase upon sulfur deficiency (Figure 30 A, E), driven by a reduction in root FW to 50% of control conditions and a pronounced decrease in shoot FW to 20% of control conditions (Figure 30 B, C). Notably, all genotypes maintained a consistent average primary root length between control and sulfur-deficient conditions, suggesting that SERAT groups one and three are not essential for the developmental adaptation response induced by sulfate deficiency (Figure 30 D).

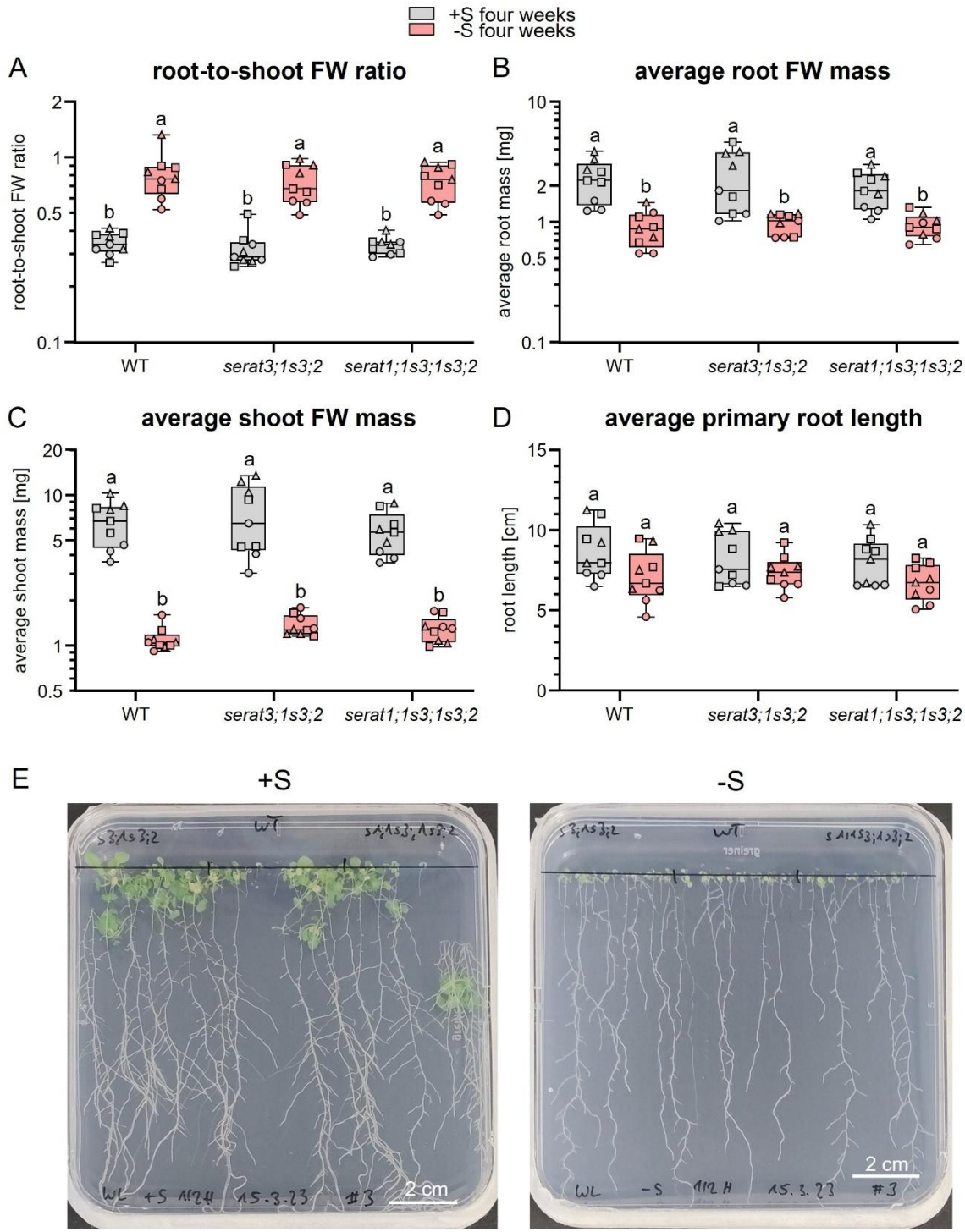

Figure 30: Root-to-shoot FW ratio phenotype of *serat3;1s3;2* and serats1;1*s3;1s3;2* on solid media plates in sulfur deficiency condition. WT, *serat3;1s3;2* and serats1;1*s3;1s3;2* (2.3.1) were grown on solid ½ Hoagland plates containing either 500 µM sulfate (+S control) or 1 µM sulfate (-S)(2.3.4). After four weeks, the phenotype regarding average primary root length (2.3.11) and regarding FWs of roots and shoots was measured (2.3.10). **A:** root-to-shoot FW ratio. **B:** average root FW. **C:** average shoot FW. **D:** average primary root length. **E:** example picture of plant culture plates. Shapes of data points define three independent experimental repetitions. ANOVA two-way with $p < 0.05$ (n = 9 of three independent replicates) was used for statistical analysis after proper data transformation (2.7).

SERAT group three isoforms have magnitudes lower catalytic activity than isoforms of group one and two (Noji *et al.*, 1998). Still, one single isoform can provide sufficient OAS supply for plants survival (Watanabe *et al.*, 2008b). SERAT3;1 was also found to be insensitive to feedback

inhibition by cysteine, and it was previously proposed that the isoforms of group three might provide OAS supply during stress conditions (Kawashima *et al.*, 2005). To investigate the influence of the SERAT group three isoforms on the metabolite steady-state levels of primary sulfur metabolites, *serat3;1s3;2* and *serat1;1s3;1s3;2* were cultured in the hydroponic system together with the WT control and *serat1;1* single mutant (2.3.1, 2.3.7). After four weeks of growing in sulfur-sufficient ½ Hoagland medium (+S, 500 µM sulfate), half of the plants were transferred to sulfur deficiency medium (-S, 1 µM sulfate) and grown for an additional four weeks. On the day of harvest, pictures of three representative plants per genotype and condition were taken (Figure 31). The *serat1;1* mutant showed like *serat3;1s3;2* and *serat1;1s3;1s3;2* a WT-like root-to-shoot FW phenotype in sulfur deficiency and control condition (Figure 32) corroborating the results gained from the solid plates experiments (Figure 30). The root-to-shoot FW ratio increase in the hydroponic culture was less pronounced than observed using the solid media plates, although the same sulfate concentrations were used. Most likely, sulfate uptake by the roots is limited by diffusion when grown on a solidified media compared to liquid media. Being submerged in liquid probably improves nutrient uptake of the roots compared to growing over the surface of the solidified media, explaining the less pronounced sulfur deficiency phenotype in the hydroponic culture.

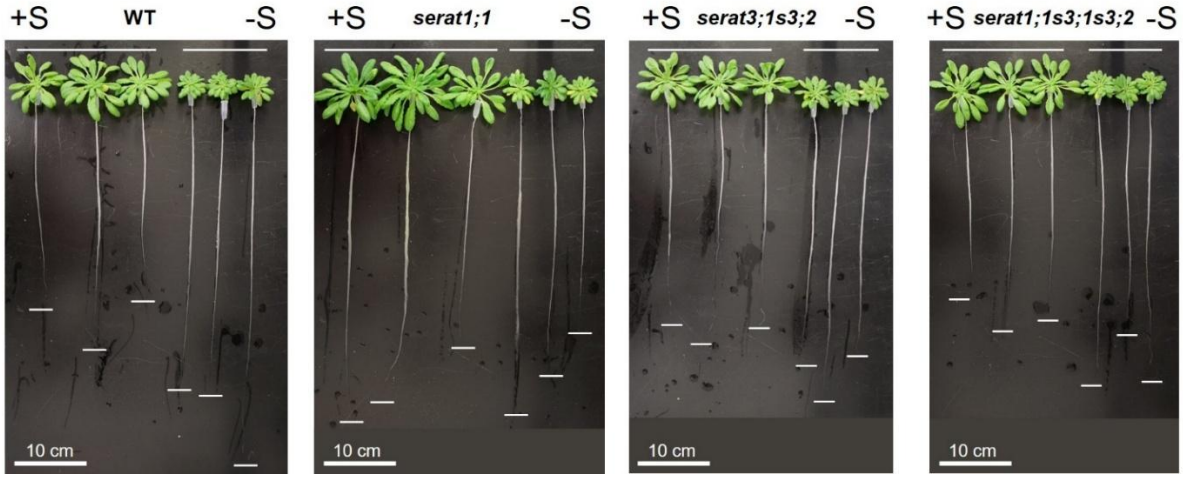

Figure 31: Phenotype of *serat1;1*, *serat3;1s3;2* and *serat1;1s3;1s3;2* grown in sulfur deficiency in the hydroponic system. *serat1;1*, *serat3;1s3;2* and *serat1;1s3;1s3;2* were grown next to WT (2.3.1) for four weeks in liquid ½ Hoagland medium containing 500 µM sulfate (+S) (2.3.7). Half of the plants were transferred to sulfur deficiency medium containing 1 µM sulfate for *an* additional four weeks (-S). The other half remained in the control medium (2.3.7). Three individuals per genotype and treatment are depicted. The white lines indicate root tips. The scale bar is 10 cm.

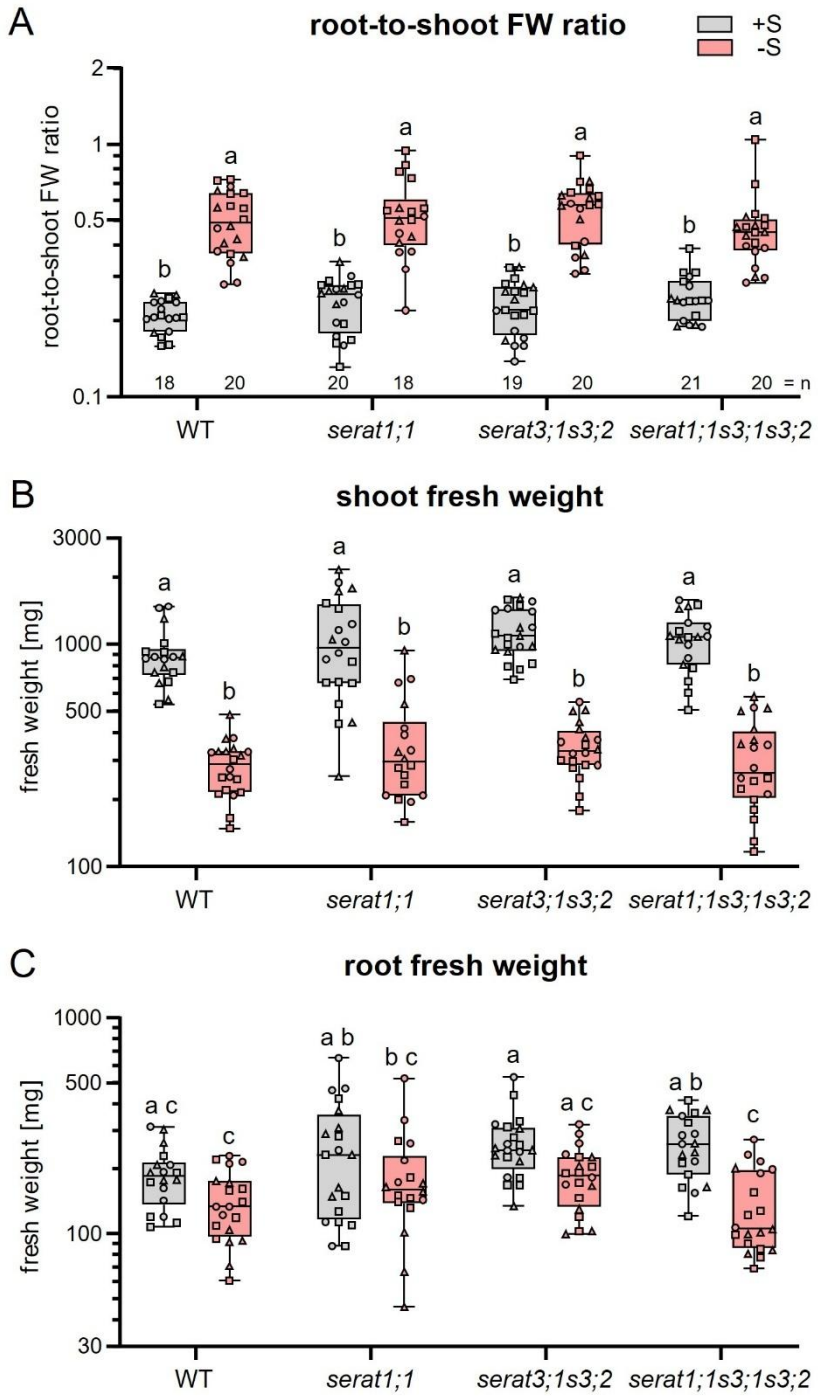

Figure 32: Root-to-shoot FW ratio in *serat1;1*, *serat3;1s3;2* and *serat1;1s3;1s3;2* grown in sulfur deficiency in the hydroponic system. *serat1;1*, *serat3;1s3;2* and *serat1;1s3;1s3;2* were grown next to WT (2.3.1) for four weeks in liquid ½ Hoagland medium containing 500 µM sulfate (+S) (2.3.7). Half of the plants were transferred to sulfur deficiency medium containing 1 µM sulfate for additional four weeks (-S). The other half remained in the control medium (2.3.7). **A:** root-to-shoot FW ratio. **B:** root FWs. **C:** shoot FWs. Different shapes of data points indicate different replicate sets. ANOVA two-way with $p < 0.05$ (n as indicated from three independent replicates) was used for statistical analysis after proper data transformation (2.7).

The harvested shoot and root material was snap-frozen and ground to extract metabolites (2.6.1). Aliquots were used to label OAS (2.6.2), cysteine (2.6.3), glutathione (2.6.3) and sulfide (2.6.4) by a fluorescent dye, followed by separation and quantification by UPLC (2.6.5). As expected for

sulfur deficiency, the WT showed increased OAS steady-state levels in both root and shoot tissue (Figure 34 A and B). While *serat1;1* and *serat3;1s3;2* showed WT-like OAS *steady-state* levels in both sulfur deficiency and control condition in the roots, *serat1;1s3;1s3;2* was affected in OAS accumulation in sulfur deficiency showing an intermediate *steady-state* level between WT control and stress condition. In the shoots, all three mutants showed a trend for higher OAS steady-state levels in sulfur deficiency compared to WT, which was only significant for *serat3;1s3;2*. As expected, sulfur deficiency led to reduced cysteine steady-state levels in WT roots (Figure 33 C), which was also observed for the mutants. In the shoot tissue, the steady-state levels of cysteine were kept constant in all genotypes between control and stress conditions (Figure 33 D). Glutathione steady-state levels were also reduced in sulfur deficiency in all genotypes in both root and shoot tissue (Figure 33 E and F). Due to the smaller FW of roots, the sulfide levels were only determined for the shoots. All genotypes showed a similar significant reduction in sulfide steady-state levels in sulfur deficiency (figure G).

Taken together, only OAS steady-state levels were weakly affected by the loss of all cytosolic SERAT isoforms. The downstream metabolite levels of cysteine and glutathione were unaffected as well as sulfide. This indicates that the cytosolic isoforms might only play a role in modulating OAS levels rather than driving them. Interestingly, the loss of one of the main isoforms, *serat1;1,* did not affect OAS steady-state levels more strongly than the loss of the two SERAT group three isoforms, indicating adaptable compensations of *SERAT2;1* and *SERAT2;2,* keeping OAS steady-state levels constant.

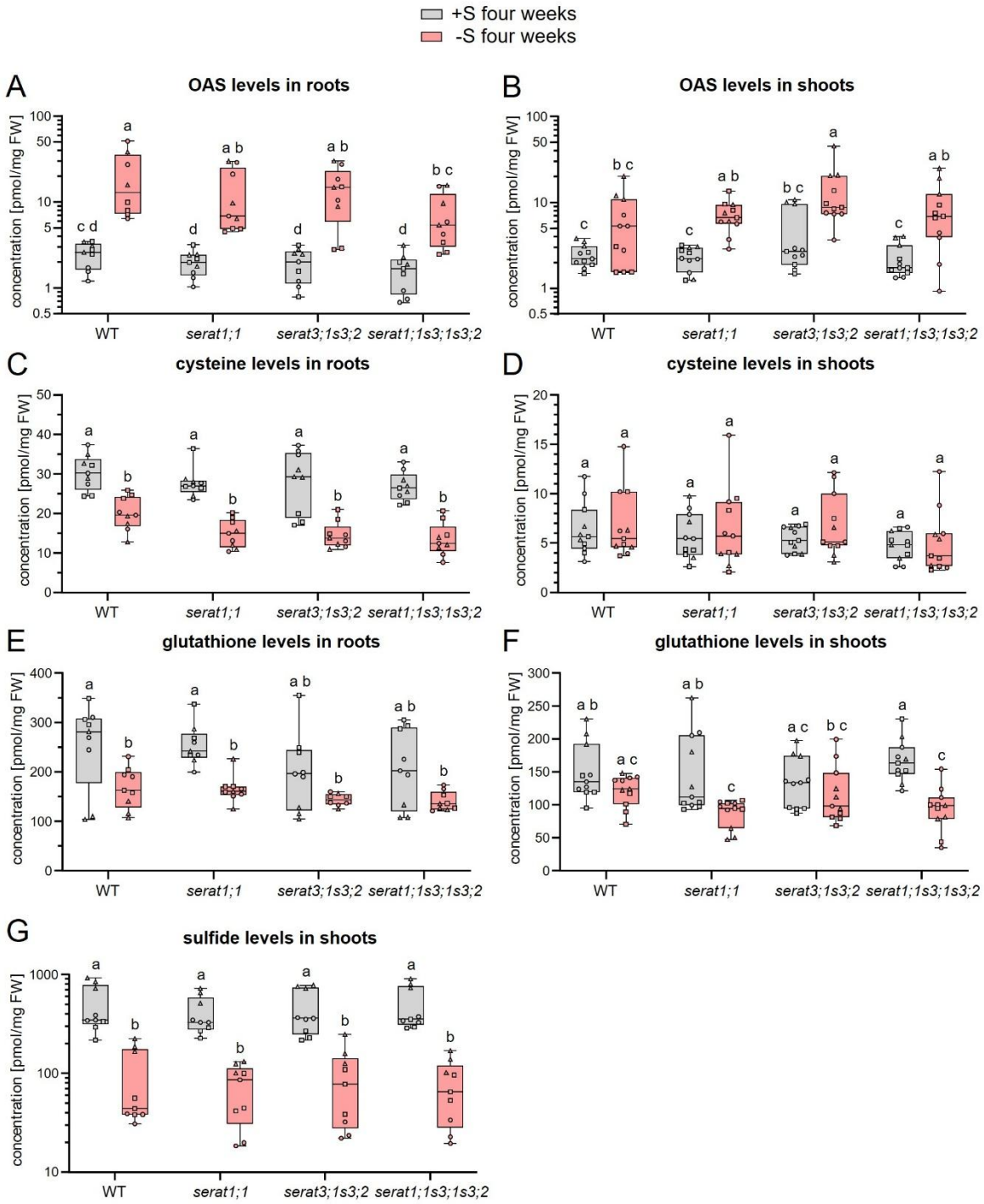

Figure 33: Metabolite steady-state levels of *serat1;1*, *serat3;1s3;2* and *serat1;1s3;1s3;2* grown in sulfur deficiency in the hydroponic system. *serat1;1*, *serat3;1s3;2* and *serat1;1s3;1s3;2* were grown next to WT (2.3.1) for four weeks in liquid ½ Hoagland medium containing 500 µM sulfate (+S) (2.3.7). Half of the plants were transferred to sulfur deficiency medium containing 1 µM sulfate for additional four weeks (-S). The other half remained in the control medium (2.3.7). Harvested material was used to extract metabolites (2.6.1, 2.6.4). After compound labeling (2.6.2, 2.6.3, 2.6.4), quantification was performed after with UPLC (2.6.5). **A:** OAS levels in roots. **B:** OAS levels in shoots. **C:** cysteine levels in roots. **D:** cysteine levels in shoots. **E:** glutathione levels in roots. **F:** glutathione levels in shoots. **G:** sulfide levels in shoots. The shapes of data points indicate different independent repetitions. ANOVA two-way with $p < 0.05$ was used for statistical analysis after proper data transformation (2.7).

3.2.6 Transcriptome analysis of *serat3;1s3;2* compared to WT in control and sulfur deficiency conditions

So far, the function of SERAT group three remains unresolved. These genes are highly conserved across the plant kingdom (3.2.1) and are transcriptionally induced under sulfur deficiency (3.2.2) (Kawashima *et al*., 2005; Watanabe *et al*., 2008b). Upon sulfur deficiency, their protein-protein interactions with SERAT1;1 increase (Haberland, 2017), potentially modulating the binding capacity of OAS-TL A within the cCSC (3.2.4). However, this does not result in a physiological phenotype of *serat3;1s3;2* mutant distinct from WT under sulfur deficiency (3.2.5). Consistent with SERAT3's low catalytic activity (Kawashima *et al*., 2005), its absence did also not impact the steady-state levels of primary sulfur metabolites (3.2.5), further supporting the lack of a physiological phenotype.

Since SERAT group three isoforms are uniquely transcriptionally upregulated upon sulfate deprivation within the SERAT family, I hypothesize a potential regulatory function in sulfur deficiency and conducted mRNA sequencing experiments to investigate this. Therefore, I used WT and *serat3;1s3;2* shoot material from plants grown hydroponically for four weeks in sulfur-sufficient medium, followed by an additional four weeks under sulfur deficiency stress (3.2.5), previously used for phenotype and metabolite analysis in 3.2.5. After RNA extraction (2.4.4), samples were sent for sequencing to Novogene GmbH (2.4.15). The data processing was performed by my collaborator, Dr. Carolina de la Torre (NGS Core Facility, Medical Faculty Mannheim, University of Heidelberg).

The correlation heatmap and principal component analysis illustrate significant transcriptomic differences between *serat3;1s3;2* and WT under control and sulfur-deficient conditions, as each genotype forms distinct clusters (Figure 34). In WT, the transition from control to sulfur-deficient conditions resulted in a distinct shift along the principal component 2, as expected for substantial transcriptional reprogramming in response to sulfur deficiency. Interestingly, *serat3;1s3;2* exhibited also distinct transcriptomic changes upon sulfur deficiency, but the trajectory of change was opposite to that observed in WT. This already indicates transcriptional misregulatation in *serat3;1s3;2* under control and sulfur deficiency conditions.

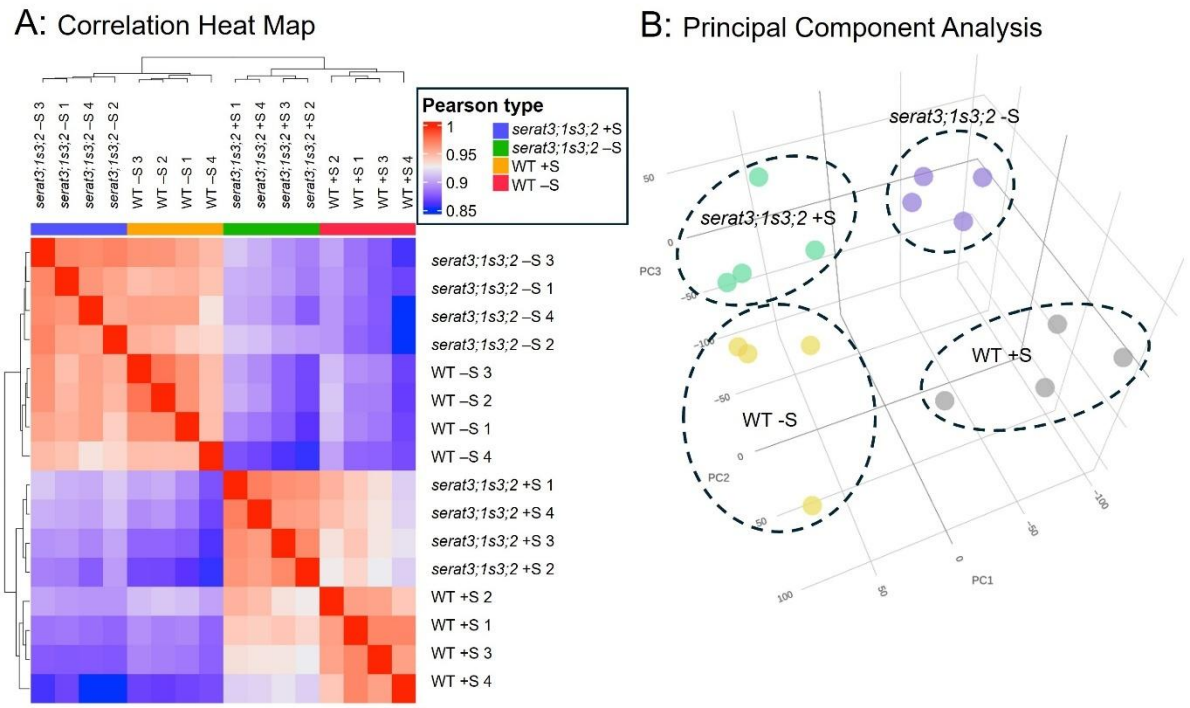

Figure 34: Correlation heat map and principal component analysis of transcriptomic changes in serat3;1s3;2 shoots in control and sulfur deficiency condition. WT and *serat3;1s3;2* (2.3.1) were cultured in liquid ½ Hoagland medium containing 500 µM sulfate (+S) for four weeks (2.3.7). Half of the plants were transferred to a sulfur deficiency medium containing 1 µM sulfate for an additional four weeks (-S). The other half remained in the control medium (2.3.7). Shoot material was harvested and used for RNA extraction (2.4.4). Total RNA was sequenced by Novogene GmbH (München) (2.4.15), and bioinformatic analysis was conducted in collaboration with Dr. Carolina de la Torre from the NGS Core Facility, University of Mannheim (2.4.15). **A:** Correlation heat map. **B:** Principal component analysis.

A total of 2817 genes were found differentially expressed in *serat3;1s3;2* in control conditions, whereas 2664 differentially expressed genes were identified in sulfur deficiency conditions (Figure 35). Among these, 1144 genes were commonly regulated in both conditions, while 1673 genes were uniquely found for the control condition, and 1540 for sulfur deficiency (Figure 36), indicating condition-dependent regulatory roles for SERAT group three. Genes differentially expressed in both conditions exhibited generally a stronger response under control condition and were categorized into three subgroups: (1) genes with higher expression in control condition than in sulfur deficiency, (2) genes with stronger repression in the control condition than in sulfur deficiency, and (3) genes similarly regulated in both conditions. The 10 most up- and downregulated genes for each of the three subgroups are listed in Table 16.

Additionally, genes differentially regulated exclusively in either control condition or sulfur deficiency were further divided into upregulated and downregulated groups. The top 10 most affected genes are listed in Supplemental Table 1 for control condition and Supplemental Table 2 for sulfur deficiency condition.

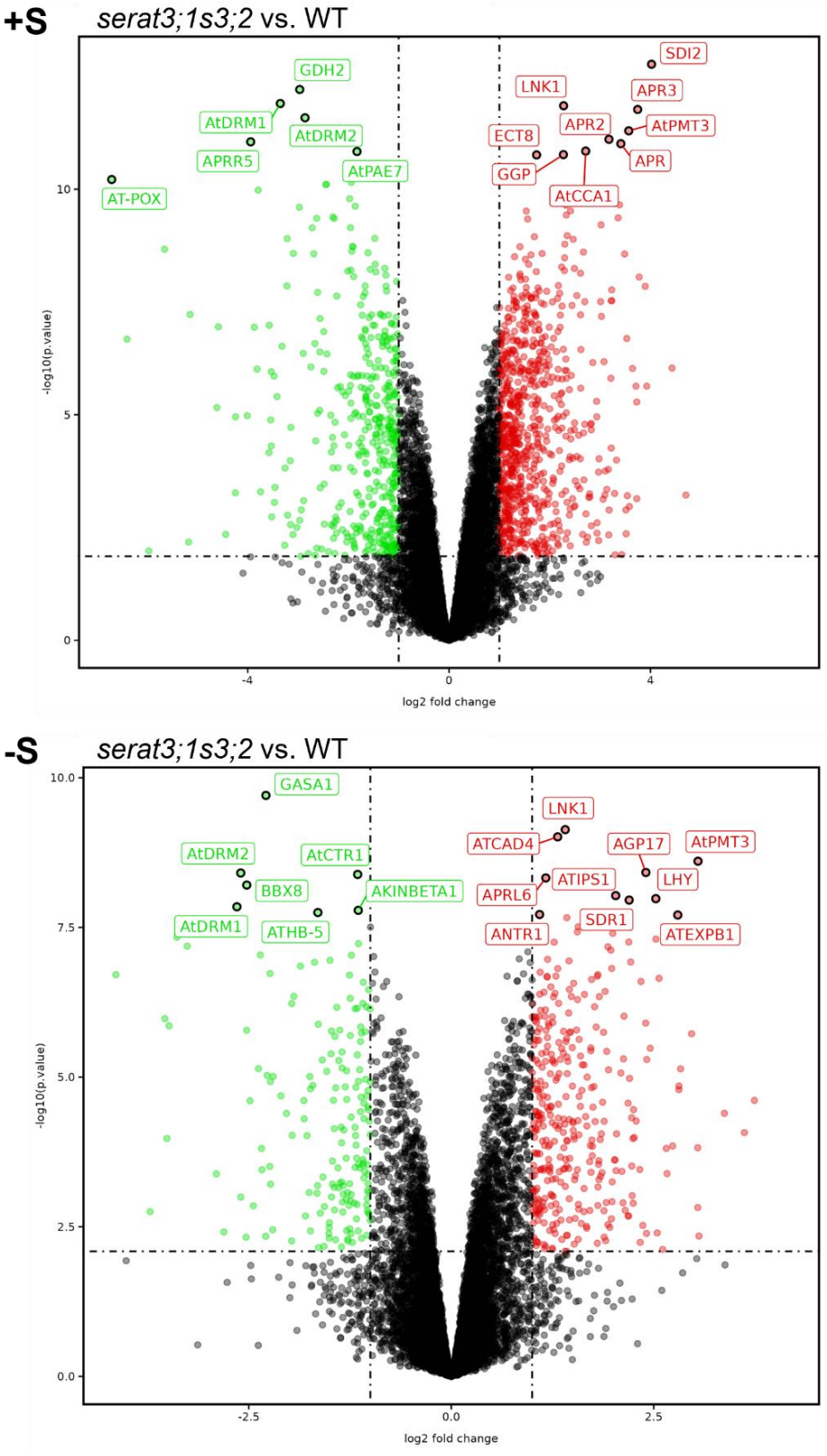

Figure 35: Volcano plot of *serat3;1s3;2* compared to WT in control (+S) and sulfur deficiency (-S). WT and *serat3;1s3;2* (2.3.1) were cultured in liquid ½ Hoagland medium containing 500 µM sulfate (+S) for four weeks (2.3.7). Half of the plants were transferred to a sulfur deficiency medium containing 1 µM sulfate for an additional four weeks (-S). The other half remained in the control medium (2.3.7). Shoot material was harvested and used for RNA extraction (2.4.4). Total RNA was sequenced by Novogene GmbH (München) (2.4.15), and bioinformatic analysis was conducted in collaboration with Dr. Carolina de la Torre from the NGS Core Facility, University of Mannheim (2.4.15).

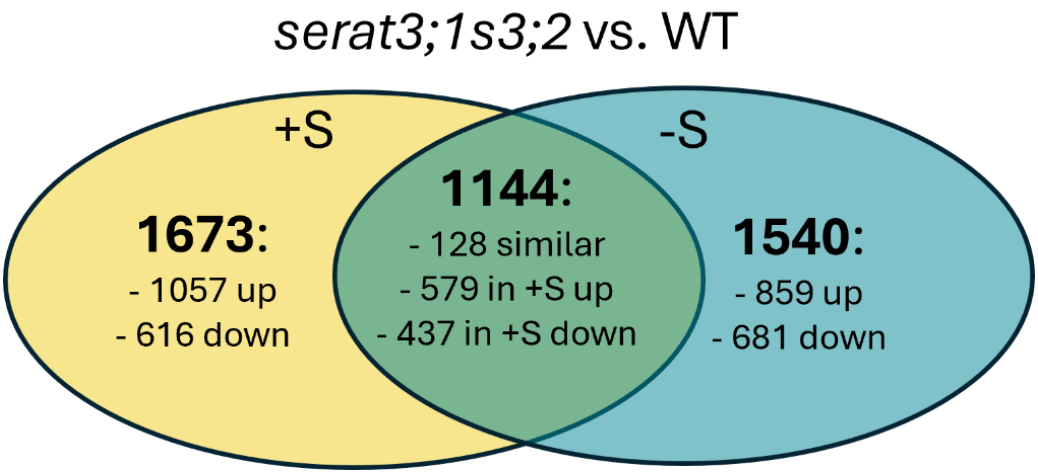

Figure 36: Ven diagram of differentially regulated genes in *serat3;1s3;2* compared to WT in sulfur sufficient and deficient condition. WT and *serat3;1s3;2* (2.3.1) were cultured in liquid ½ Hoagland medium containing 500 µM sulfate (+S) for four weeks (2.3.7). Half of the plants were transferred to a sulfur deficiency medium containing 1 µM sulfate for an additional four weeks (-S). The other half remained in the control medium (2.3.7). Shoot material was harvested, and used for RNA extraction (2.4.4). Total RNA was sequenced by Novogene GmbH (München) (2.4.15), and bioinformatic analysis was conducted in collaboration with Dr. Carolina de la Torre from the NGS Core Facility, University of Mannheim (2.4.15). A total of 2817 genes were differentially regulated in *serat3;1s3;2* under +S conditions, while 2664 genes showed differential expression under -S conditions. Of these, 1144 genes were shared between both conditions, 1673 were unique to +S, and 1540 were specific to -S.The differentially regulated genes shared in both growth conditions were found to generally be stronger affected by +S than by -S . 579 genes were found stronger upregulated in *serat3;1s3;2* in control than sulfur deficiency, while 437 were stronger down regulated in *serat3;1s3;2* than in sulfur deficiency. A set of 128 genes was similarly changed in *serat3;1s3;2* compared to WT in both growth conditions.

Table 16: Differentially expressed genes in *serat3;1s3;2* compared to WT found in both sulfur sufficient and deficient condition. WT and *serat3;1s3;2* (2.3.1) were cultured in liquid ½ Hoagland medium containing 500 µM sulfate (+S) for four weeks (2.3.7). Half of the plants were transferred to a sulfur deficiency medium containing 1 µM sulfate for an additional four weeks (-S). The other half remained in the control medium (2.3.7). Shoot material was harvested, and used for RNA extraction (2.4.4). Total RNA was sequenced by Novogene GmbH (München) (2.4.15), and bioinformatic analysis was conducted in collaboration with Dr. Carolina de la Torre from the NGS Core Facility, University of Mannheim (2.4.15). The table is sorted by the difference in the log2 fold change (FC). The p-value is adjusted with the false discovery rate (adj. p-value).

(1) 10 most over-expressed genes in +S compared to -S					
TAIR ID	**Symbol**	**log2FC +S**	**adj. p-value +S**	**log2FC -S**	**adj. p-value -S**
AT1G04770	SDI2	4.02	3.40E-09	0.96	8.26E-03
AT4G21990	APR3	3.74	5.70E-09	0.82	2.16E-02
AT1G76530	PILS4	4.70	4.86E-03	1.82	7.38E-03
AT2G06995	*lncRNA*	-2.48	2.53E-04	-5.11	1.84E-04
AT5G48850	SDI1	4.43	4.08E-05	1.84	6.75E-03
AT1G65870	DIR21	3.61	1.50E-04	1.11	3.57E-02
AT5G67450	AZF1	3.77	1.81E-06	1.28	3.07E-02
AT3G49570	LSU3	3.93	7.91E-05	1.71	4.58E-03
AT1G62180	APR2	3.17	1.64E-08	1.12	3.00E-04
AT1G36370	MSA1	3.39	1.47E-07	1.34	1.73E-03
(2) 10 most over-repressed genes in +S compared to -S					
TAIR ID	**Symbol**	**log2FC +S**	**adj. p-value +S**	**log2FC -S**	**adj. p-value -S**
AT5G20250	DIN10	-5.65	7.40E-07	-1.82	9.02E-04
AT2G19800	MIOX2	-6.40	1.48E-05	-2.60	1.17E-02
AT3G30775	AT-POX	-6.70	6.11E-08	-3.48	1.60E-04
AT4G21870	*protein coding*	-4.93	1.95E-03	-2.20	2.89E-02
AT5G41080	AtGDPD2	-4.61	1.75E-04	-1.97	3.70E-02
AT5G51550	EXL3	-1.79	6.50E-04	0.82	1.92E-02
AT5G05440	AtPYL5	-3.32	1.85E-05	-0.77	2.93E-02
AT2G40330	PYL6	-4.24	4.47E-03	-1.74	2.86E-02
AT3G57520	AtSIP2	-3.79	8.06E-08	-1.45	1.88E-03
AT1G69760	*protein coding*	-1.37	5.19E-03	0.94	5.32E-03
(3) 10 most significant genes similarly expressed in +S and -S					
TAIR ID	**Symbol**	**log2FC +S**	**adj. p-value +S**	**log2FC -S**	**adj. p-value -S**
AT3G09440	HSP70-3	1.38	2.09E-04	1.43	2.03E-05
AT3G07650	BBX7	-3.22	2.52E-06	-3.26	3.27E-05
AT3G53830	*protein coding*	1.33	1.36E-06	1.35	3.84E-05
AT3G54500	LNK2	0.94	4.88E-06	0.98	4.37E-05
AT1G15950	ATCCR1	0.85	2.37E-05	0.82	6.06E-05
AT5G53120	ATSPDS3	1.53	2.63E-06	1.51	6.12E-05
AT1G64970	G-TMT	1.50	1.75E-05	1.46	7.19E-05
AT4G35300	TMT2	1.12	6.93E-04	1.15	7.58E-05
AT4G22570	APT3	0.99	2.79E-04	0.97	8.15E-05
AT1G72330	ALAAT2	-1.08	2.13E-03	-1.09	9.41E-05

Interestingly, within subgroup three, exhibiting higher expression under sulfur-sufficient condition than sulfur deficiency condition, five out of the six core OAS cluster genes were identified: *SDI1, APR3, MSA1, LSU1,* and *GGCT2;1* (Table 17). The sixth member, *BGLU28*, was not found differentially expressed in *serat3;1s3;2* in either growth condition compared to WT.

Table 17: Differentially regulated core OAS cluster genes according to Hubberten *et al.* (2012a) in *serat3;1s3;2* compared to WT. WT and *serat3;1s3;2* (2.3.1) were cultured in liquid ½ Hoagland medium containing 500 µM sulfate (+S) for four weeks (2.3.7). Half of the plants were transferred to a sulfur deficiency medium containing 1 µM sulfate for an additional four weeks (-S). The other half remained in the control medium (2.3.7). Shoot material was harvested, and used for RNA extraction (2.4.4). Total RNA was sequenced by Novogene GmbH (München) (2.4.15), and bioinformatic analysis was conducted in collaboration with Dr. Carolina de la Torre from the NGS Core Facility, University of Mannheim (2.4.15). The table is sorted by the difference in the log2 fold change (FC). The p-value is adjusted with the false discovery rate (adj. p-value).

TAIR ID	Symbol	log2FC +S	adj. p-value +S	log2FC -S	adj. p-value -S
AT5G48850	SDI1	4.43	4.08E-05	1.84	6.75E-03
AT4G21990	APR3	3.74	5.70-09	0.82	2.16E-02
AT1G36370	MSA1	3.39	1.47E-07	1.34	1.73E-03
AT3G49580	LSU1	3.32	1.25E-03	1.29	7.18E-03
AT5G26220	GGCT2;1	3.21	5.82E-05	1.64	9.44E-03

A similar expression pattern was observed for *SDI2, APR1, APR2, LSU2, LSU3, AtBBE18*, and *AtAvt6C* which were previously categorized within the extended OAS cluster network (Apodiakou and Hoefgen, 2023) (Table 18). *LSU4* was the only member of the OAS cluster network exhibiting a slightly higher expression in *serat3;1s3;2* in sulfur deficiency than control condition. The additional members of the extended OAS cluster network *SULTR4;2, SULTR1;2, PYD4, AT5G40670*, and *NmrA-like* protein were overexpressed only upon sulfur deficiency in *serat3;1s3;2* compared to WT. The two remaining members of the extended OAS cluster network, *AT2G32487* and *SIP1;2*, did not exhibit significant differential expression in *serat3;1s3;2* under either condition. This indicates a general negative modulating function of SERAT three isoforms on OAS associated genes.

Table 18: Differentially regulated genes of the extended OAS cluster network according to Apodiakou and Hoefgen (2023) in *serat3;1s3;2* compared to WT. WT and *serat3;1s3;2* (2.3.1) were cultured in liquid ½ Hoagland medium containing 500 µM sulfate (+S) for four weeks (2.3.7). Half of the plants were transferred to a sulfur deficiency medium containing 1 µM sulfate for an additional four weeks (-S). The other half remained in the control medium (2.3.7). Shoot material was harvested, and used for RNA extraction (2.4.4). Total RNA was sequenced by Novogene GmbH (München) (2.4.15), and bioinformatic analysis was conducted in collaboration with Dr. Carolina de la Torre from the NGS Core Facility, University of Mannheim (2.4.15). The table is sorted by the difference in the log2 fold change (FC). The p-value is adjusted with the false discovery rate (adj. p-value). – indicates non-significant changes in transcript levels in *serat3;1s3;2* compared to WT.

TAIR ID	Symbol/Description	log2FC +S	adj. p-value +S	log2FC -S	adj. p-value -S
AT1G04770	SDI2	4.02	3.40E-09	0.96	8.26E-03
AT3G49570	LSU3	3.93	7.91E-05	1.71	4.58E-03
AT5G24660	LSU2	3.90	2.52E-06	2.13	3.40E-04
AT4G04610	APR1	3.41	1.64E-08	-	-
AT1G62180	APR2	3.17	1.64E-08	1.12	3.00E-04
AT4G20820	AtBBE18	2.69	3.32E-04	2.20	5.24E-04
AT3G56200	AtAvt6C	1.70	1.11E-05	1.06	6.05E-04
AT5G24655	LSU4	1.61	5.06E-03	1.87	9.50E-04
AT3G08860	PYD4	-	-	1.92	2.83E-04
AT1G75280	NmrA-like protein	-	-	1.87	8.40E-04
AT3G12520	SULTR4;2	-	-	1.24	1.08E-03
AT1G78000	SULTR1;2	-	-	0.55	1.60E-02
AT1G77670	Pyridoxal phosphate (PLP) protein	-	-	0.53	1.30E-03
AT5G40670	PQ loop repeat family protein	-	-	0.45	2.10E-03
AT2G32487	hypothetical protein in ABA signaling	-	-	-	-
AT5G18290	SIP1;2	-	-	-	-

Similar to the core OAS cluster genes, *PILS4, DIR21*, and *AZF1* exhibited also stronger overexpression in *serat3;1s3;2* in control condition compared to sulfur deficiency for *serat3;1s3;2* (Table 16). They function in abiotic and biotic stress responses (TAIR).

The most pronounced inverse expression pattern relative to the OAS cluster genes was observed for *DIN10* (Table 16). In *serat3;1s3;2*, *DIN10* was already strongly downregulated in the control condition and remained downregulated in sulfur deficiency, albeit to a lesser extent. Notably, *DIN10* belongs to the most interconnected genes in the sulfate co-expression network and is typically downregulated in WT under sulfur deficiency (Henriquez-Valencia et al., 2018). A similar expression pattern was found for *SEN1, AtRZPF34*, *BAM9* and 30S ribosomal protein of AT5G24490 (Table 19) which also belong to the sulfate co-expression network. Together with *TPS8*, *KFB20*, and the three OAS associate genes *MSA1*, *SULTR4;2*, and *AtAvt6C*, a total of 12 out of the 14 most interconnected genes in the sulfate co-expression network exhibited already pre-induced expression under control condition in *serat3;1s3;2* relative to WT. This indicates that *serat3;1s3;2* exhibits a strong sulfur deficiency response in control condition and an over-amplified response in sulfur deficiency. The only two genes in the sulfate co-expression network that did not exhibit differential expression in *serat3;1s3;2* were *bZIP1* and *TPS11*, suggesting that their regulation occurs independently of SERAT group three.

Additional genes displaying expression patterns similar to *DIN10* and *SEN1* included *MIOX2, AT-PoX, AT4G21870, AtGDPD2, EXL3, PYL5, PYL6*, and *SIP2*, with functions in abiotic stress responses (Table 16).

Table 19: Differentially regulated genes belonging to the 14 most connected genes in the sulfate co-expression network according to Henriquez-Valencia *et al.* (2018). WT and *serat3;1s3;2* (2.3.1) were cultured in liquid ½ Hoagland medium containing 500 µM sulfate (+S) for four weeks (2.3.7). Half of the plants were transferred to a sulfur deficiency medium containing 1 µM sulfate for an additional four weeks (-S). The other half remained in the control medium (2.3.7). Shoot material was harvested, and used for RNA extraction (2.4.4). Total RNA was sequenced by Novogene GmbH (München) (2.4.15), and bioinformatic analysis was conducted in collaboration with Dr. Carolina de la Torre from the NGS Core Facility, University of Mannheim (2.4.15). *MSA1*, *SULTR4;2* and *AtAvt6C* are listed in Table 18. *bZIP1* and *TPS11* were not differentially regulated in *serat3;1s3;2* compared to WT in either condition. The table is sorted by the difference in the log2 fold change (FC). The p-value is adjusted with the false discovery rate (adj. p-value). – indicates non-significant changes in transcript levels in *serat3;1s3;2* compared to WT.

TAIR ID	Symbol	log2FC +S	adj. p-value +S	log2FC -S	adj. p-value -S
AT5G20250	DIN10	-5.65	7.40E-07	-1.82	9.02E-04
AT4G35770	SEN1	-2.90	2.42E-05	-2.23	5.72E-04
AT5G22920	AtRZPF34	-2.69	8.30E-07	-1.36	1.80E-03
AT5G18670	BAM9	-2.49	1.12E-05	-	-
AT5G24490	30 S ribosomal prot	-1.47	1.36E-06	-1.26	1.52E-05
AT1G70290	TPS8	0.69	6.98E-04	0.55	3.94E-03
AT1G80440	KFB20	0.80	2.83E-03	0.73	2.40E-02
AT3G16410	NSP4	-	-	0.84	2.05E-02
AT3G29240	DUF179-3	-	-	1.07	1.74E-04

Among the differentially regulated genes, 420 transcription factors (TF) were identified in *serat3;1s3;2* compared to WT in the control condition and 182 were found in sulfur deficiency. 118 were found differentially regulated in both conditions, 302 exclusively for the control condition and 64 exclusively in sulfur deficiency.

Since *serat3;1s3;2* exhibited induced OAS-cluster associated genes, the list of differentially expressed TF was examined for known regulators of the extended OAS cluster network (Table 20). The five TF *CCA1, LHY, LCL5, NFYB2,* and *HAP5B* were found to be upregulated in both sulfur-sufficient and sulfur-deficient conditions. Additionally, the four transcription factors *HB7, PAP3, HY5,* and *PIF4* were exclusively upregulated in control conditions. In contrast, *EIN3* and *EIL1* were the only TFs exclusively downregulated in *serat3;1s3;2* under sulfur deficiency. Several other TFs known to influence OAS cluster genes, including *SLIM1, MYB67 (AT3G12720), DTAF1 (AT3G45810), ERF115 (AT5G07310), E2Fa (AT2G36010), NRPE1 (AT2G40030), BBM (AT5G17430), MYB3 (AT1G22640), MYB-related (AT3G10580), HB6 (AT2G22430),* and *DTAF (AT5G50360)*, did not exhibit differential expression in *serat3;1s3;2* compared to WT.

Table 20: Differentially regulated TF regulating the extended OAS cluster network according to Apodiakou and Hoefgen (2023) in *serat3;1s3;2* compared to WT. WT and *serat3;1s3;2* (2.3.1) were cultured in liquid ½ Hoagland medium containing 500 µM sulfate (+S) for four weeks (2.3.7). Half of the plants were transferred to a sulfur deficiency medium containing 1 µM sulfate for an additional four weeks (-S). The other half remained in the control medium (2.3.7). Shoot material was harvested and used for RNA extraction (2.4.4). Total RNA was sequenced by Novogene GmbH (München) (2.4.15), and bioinformatic analysis was conducted in collaboration with Dr. Carolina de la Torre from the NGS Core Facility, University of Mannheim (2.4.15). The table is sorted by the difference in the log2 fold change (FC). The p-value is adjusted with the false discovery rate (adj. p-value). – indicates non-significant changes in transcript levels in *serat3;1s3;2* compared to WT.

TAIR ID	Symbol	log2FC +S	adj. p-value +S	log2FC -S	adj. p-value -S
AT2G46830	AtCCA1	2.71	1.95E-08	2.53	2.86E-05
AT1G01060	LHY	2.35	4.47E-07	2.53	1.55E-05
AT3G09600	LCL5	2.08	1.44E-05	1.21	1.16E-03
AT2G46680	HB7	1.76	6.31E-04	-	-
AT5G47640	NF-YB2	1.63	8.43E-07	1.22	4.73E-04
AT1G56170	ATHAP5B	1.57	4.34E-05	2.73	2.97E-03
AT1G09530	PAP3	0.84	4.71E-04	-	-
AT5G11260	HY5	0.80	2.19E-02	-	-
AT2G43010	PIF4	0.56	4.31E-03	-	-
AT3G20770	EIN3	-	-	-0.31	2.07E-02
AT2G27050	EIL1	-	-	-0.39	2.20E-02

The six TF, *MYB75, HYH, BBX16, MYB29, MYC2,* and *MYB28*, which have been previously associated with sulfur deficiency signaling (Fernandez *et al*., 2024), were additionally upregulated in *serat3;1s3;2* compared to WT under sulfur-sufficient conditions (Table 21). Among these, only *MYB75* was also upregulated in sulfur deficiency, indicating again a strong pre-induction of sulfur deficiency response in control condition and a slight over-amplification of the response in sulfur deficiency.

Table 21: Differentially regulated TF in *serat3;1s3;2* compared to WT involved in sulfur deficiency signaling according to Fernandez *et al*. (2024). WT and *serat3;1s3;2* (2.3.1) were cultured in liquid ½ Hoagland medium containing 500 µM sulfate (+S) for four weeks (2.3.7). Half of the plants were transferred to a sulfur deficiency medium containing 1 µM sulfate for an additional four weeks (-S). The other half remained in the control medium (2.3.7). Shoot material was harvested and used for RNA extraction (2.4.4). Total RNA was sequenced by Novogene GmbH (München) (2.4.15), and bioinformatic analysis was conducted in collaboration with Dr. Carolina de la Torre from the NGS Core Facility, University of Mannheim (2.4.15). The table is sorted by the difference in the log2 fold change (FC). The p-value is adjusted with the false discovery rate (adj. p-value). – indicates non-significant changes in transcript levels in *serat3;1s3;2* compared to WT.

TAIR ID	Symbol	log2FC +S	adj. p-value +S	log2FC -S	adj. p-value -S
AT1G56650	MYB75	3.29	4.57E-03	3.37	1.25E-03
AT3G17609	HYH	2.34	6.45E-03	-	-
AT1G73870	BBX16	1.83	4.14E-06	-	-
AT5G07690	MYB29	1.21	3.84E-03	-	-
AT1G32640	MYC2	1.09	2.12E-02	-	-
AT5G61420	MYB28	0.74	1.65E-03	-	-

The top 10 exclusively regulated TFs in control and sulfur deficiency condition are listed in Supplemental Table 3 and Supplemental Table 4, respectively. The most significant commonly misregulated TF in both conditions are listed in Supplemental Table 5.

Additionally, two *miRNAs* were found to be upregulated in the shoot, exclusively under sulfur-sufficient conditions. *MIR841b (AT4G04835)* and *MIR850a (AT4G13493)* exhibited 3.9-fold and 2-fold upregulation, respectively. However, *miR395*, a key regulator of sulfur metabolism, was not differentially expressed in *serat3;1s3;2* compared to WT under either condition.

The loss of the two *SERAT3* isoforms resulted in widespread dysregulation of KEGG pathways. In the control condition, seven pathways were downregulated and 14 were upregulated (Table 22). In sulfur deficiency, seven pathways were downregulated while 32 were upregulated (Table 23). Particularly noteworthy are the upregulated pathways involved in sulfur and glutathione metabolism, which align with the observation that *serat3;1s3;2* exhibits a pre-induced sulfur deficiency response in control conditions and an over-amplified response in sulfur deficiency compared to WT.

Table 22: Affected KEGG pathways in *serat3;1s3;2* compared to WT under control growth conditions in shoots. WT and *serat3;1s3;2* (2.3.1) were cultured in liquid ½ Hoagland medium containing 500 µM sulfate (+S) for four weeks (2.3.7). Half of the plants were transferred to a sulfur deficiency medium containing 1 µM sulfate for an additional four weeks (-S). The other half remained in the control medium (2.3.7). Shoot material was harvested and used for RNA extraction (2.4.4). Total RNA was sequenced by Novogene GmbH (München) (2.4.15), and bioinformatic analysis was conducted in collaboration with Dr. Carolina de la Torre from the NGS Core Facility, University of Mannheim (2.4.15). The pathway identity (ID) and the pathway description are stated with the normalized enrichment score (NES) and the adjusted p-value adjusted to the false discovery rate (p.adjust). Negative NES values indicate negatively affected pathways, and positive NES values indicate positively affected pathways.

ID	Description of negatively affected pathways	NES	p.adjust
ath03010	Ribosome	-2.51	0
ath03008	Ribosome biogenesis in eukaryotes	-1.85	0.008
ath04130	SNARE interactions in vesicular transport	-1.85	0.023
ath00908	Zeatin biosynthesis	-1.76	0.041
ath00640	Propanoate metabolism	-1.71	0.041
ath02010	ABC transporters	-1.6	0.041
ath03040	Spliceosome	-1.52	0.031
ID	**Description of positively affected pathways**	**NES**	**p.adjust**
ath00906	Carotenoid biosynthesis	1.98	0.008
ath00920	Sulfur metabolism	1.95	0.005
ath00710	Carbon fixation in photosynthetic organisms	1.91	0.005
ath00561	Glycerolipid metabolism	1.87	0.006
ath00630	Glyoxylate and dicarboxylate metabolism	1.82	0.006
ath00500	Starch and sucrose metabolism	1.77	0.005
ath00130	Ubiquinone and other terpenoid-quinone biosynthesis	1.76	0.038
ath00480	Glutathione metabolism	1.7	0.017
ath00030	Pentose phosphate pathway	1.68	0.041
ath00010	Glycolysis / Gluconeogenesis	1.63	0.031
ath00564	Glycerophospholipid metabolism	1.57	0.041
ath00620	Pyruvate metabolism	1.57	0.041
ath01200	Carbon metabolism	1.49	0.028
ath01240	Biosynthesis of cofactors	1.44	0.041

Table 23: Affected KEGG pathways in *serat3;1s3;2* compared to WT in sulfur deficiency in shoots. WT and *serat3;1s3;2* (2.3.1) were cultured in liquid ½ Hoagland medium containing 500 µM sulfate (+S) for four weeks (2.3.7). Half of the plants were transferred to a sulfur deficiency medium containing 1 µM sulfate for an additional four weeks (-S). The other half remained in the control medium (2.3.7). Shoot material was harvested and used for RNA extraction (2.4.4). Total RNA was sequenced by Novogene GmbH (München) (2.4.15), and bioinformatic analysis was conducted in collaboration with Dr. Carolina de la Torre from the NGS Core Facility, University of Mannheim (2.4.15). The pathway identity (ID) and the pathway description are stated with the normalized enrichment score (NES) and the adjusted p-value adjusted to the false discovery rate (p.adjust). Negative NES values indicate negatively affected pathways, and positive NES values indicate positively affected pathways.

ID	Description of negatively affected pathways	NES	p.adjust
ath04130	SNARE interactions in vesicular transport	-1.99	0.002
ath00513	Various types of N-glycan biosynthesis	-1.79	0.017
ath04136	Autophagy - other	-1.78	0.017
ath02010	ABC transporters	-1.68	0.021
ath04075	Plant hormone signal transduction	-1.6	0.002
ath04120	Ubiquitin mediated proteolysis	-1.55	0.02
ath04144	Endocytosis	-1.4	0.049
ID	**Description of positively affected pathways**	**NES**	**p.adjust**
ath00630	Glyoxylate and dicarboxylate metabolism	2.17	0
ath00710	Carbon fixation in photosynthetic organisms	2.03	0
ath00592	alpha-Linolenic acid metabolism	2.03	0.002
ath00500	Starch and sucrose metabolism	2.02	0
ath00130	Ubiquinone and other terpenoid-quinone biosynthesis	2	0.002
ath00073	Cutin, suberine and wax biosynthesis	1.95	0.005
ath00940	Phenylpropanoid biosynthesis	1.91	0.004
ath00670	One carbon pool by folate	1.91	0.009
ath00941	Flavonoid biosynthesis	1.89	0.009
ath00053	Ascorbate and aldarate metabolism	1.87	0.009
ath00906	Carotenoid biosynthesis	1.85	0.009
ath00195	Photosynthesis	1.83	0.01
ath01200	Carbon metabolism	1.81	0
ath00480	Glutathione metabolism	1.8	0.005
ath00062	Fatty acid elongation	1.74	0.028
ath00340	Histidine metabolism	1.74	0.032
ath00920	Sulfur metabolism	1.73	0.032
ath00010	Glycolysis / Gluconeogenesis	1.71	0.017
ath00460	Cyanoamino acid metabolism	1.71	0.021
ath00620	Pyruvate metabolism	1.7	0.014
ath00190	Oxidative phosphorylation	1.7	0.017
ath00260	Glycine, serine and threonine metabolism	1.7	0.02
ath00350	Tyrosine metabolism	1.64	0.048
ath00330	Arginine and proline metabolism	1.63	0.048
ath00030	Pentose phosphate pathway	1.61	0.048
ath00380	Tryptophan metabolism	1.6	0.042
ath04146	Peroxisome	1.57	0.032
ath01212	Fatty acid metabolism	1.57	0.048
ath00270	Cysteine and methionine metabolism	1.54	0.032
ath01250	Biosynthesis of nucleotide sugars	1.52	0.048
ath01240	Biosynthesis of cofactors	1.47	0.032
ath01230	Biosynthesis of amino acids	1.43	0.032

Similar to the KEGG pathway analysis, GOs were mainly enriched in *serat3;1s3;2*, corroborating the hypothesis of a repressive function for SERAT3s.

In the control conditions, *serat3;1s3;2* exhibited enriched GOs for the response to both biotic and abiotic stresses. The most strongly induced GO term was 'defense response to bacterium,' which is most likely linked to the concomitant upregulation of 'response to salicylic acid.' Upregulated GO terms related to abiotic stress included 'response to water,' 'response to water deprivation,' and 'response to heat.' In line with the pre-induced sulfur deficiency response observed in *serat3;1s3;2*, the GO category 'sulfur compound metabolic process' was also significantly enriched. Other enhanced GO terms related to 'photosynthesis,' particularly 'photosynthesis, light reaction,' 'generation of precursor metabolites and energy,' and 'secondary metabolic processes,' were upregulated.

In sulfur deficiency, the GO term associated with 'secondary metabolic processes' exhibited the highest enrichment in *serat3;1s3;2* compared to WT. This was accompanied by an enrichment of GO terms linked to 'flavonoid biosynthetic processes' and 'flavonoid metabolic processes,' likely contributing to the observed increase in 'pigment biosynthetic pathways' and 'pigment metabolic processes.' Other enriched GO were 'photosynthesis', 'generation of precursor metabolites and energy,' 'cellular carbohydrate metabolic processes,' 'chloroplast organization,' and 'starch biosynthetic process.'

The transcriptome analysis suggests that *SERAT3s* are involved in inhibiting the sulfur deficiency response but also contribute to inhibiting other stress-related pathways.

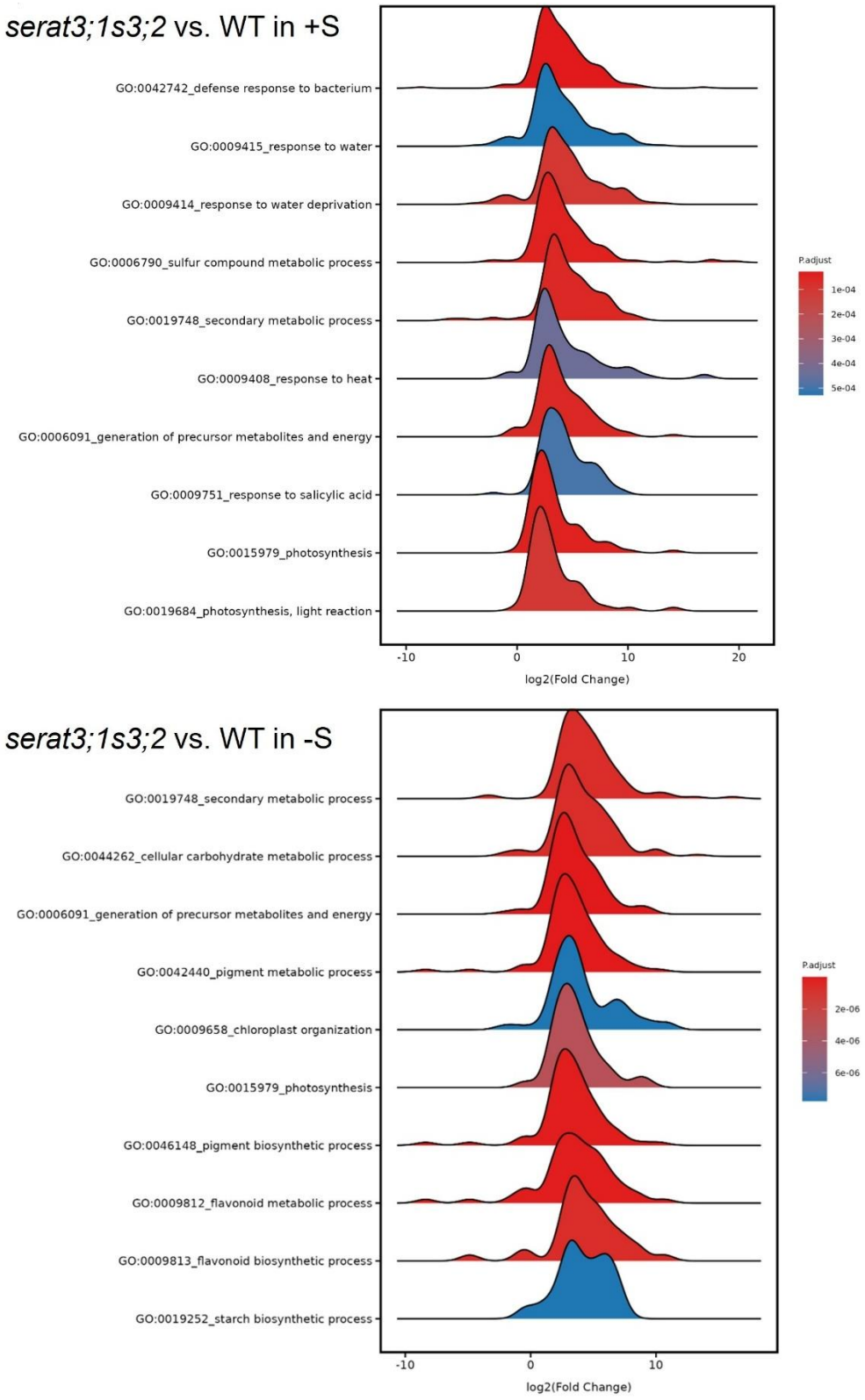

Figure 37: GO enrichment analysis for differentially expressed genes in *serat3;1s3;2* compared to WT in shoots grown. WT and *serat3;1s3;2* (2.3.1) were cultured in liquid ½ Hoagland medium containing 500 µM sulfate (+S) for four weeks (2.3.7). Half of the plants were transferred to a sulfur deficiency medium containing 1 µM sulfate for an additional four weeks (-S). The other half remained in the control medium (2.3.7). Shoot material was harvested, and used for RNA extraction (2.4.4). Total RNA was sequenced by Novogene GmbH (München) (2.4.15), and bioinformatic analysis was conducted in collaboration with Dr. Carolina de la Torre from the NGS Core Facility, University of Mannheim (2.4.15). x-axis represents the density distribution of log2(Fold Change) values for different GO terms (y-axis). The color gradient represents the statistical significance of the p-value adjusted with the false discovery rate (p.adjust).

3.3 Deciphering the molecular signal for the physiological adaptation to long-term sulfur deficiency

3.3.1 Quantification of the WT root-to-shoot FW increase in response to long-term sulfur deficiency on solid media plates

In conditions of sulfate deficiency, plants prioritize root growth over shoot growth to forage for additional sulfate supplies in the soil (Ericsson, 1995). The greater the sulfur deficiency stress condition, the greater the plants must adapt. To investigate the sensitivity of plants to the stress condition and its translation to the physiological level, WT was challenged with distinct concentrations of low sulfate. As readouts of the developmental plasticity, the root-to-shoot FW ratio and the average primary root length were measured.

Therefore, WT seeds (2.3.1) were surface sterilized (2.3.3) and sown on ½ Hoagland plates either containing sufficient sulfate (500 µM) or deficient sulfate concentrations (20 µM, 10 µM, and 1 µM sulfate) (2.3.4). After four weeks in short-day conditions, the average primary root length was measured (2.3.11), and the root-to-shoot FW ratio quantified (2.3.10).

The root-to-shoot FW ratio of WT increased stepwise from 0.4 to 0.6, 0.8, and 1 as the sulfate concentration decreased from 500 µM (control condition) to 20 µM, 10 µM, and 1 µM sulfate, respectively (Figure 38). The distinct increases in the root-to-shoot FW ratio indicate a precise regulation of the resource allocation according to the available sulfate in the growth media. Interestingly, WT growing at 20 µM and 10 µM exhibited a trend for higher root FW compared to the 500 µM sulfate condition as a sulfur-sufficient control, indicating an over-induction of root growth in mild sulfur deficiency (Figure 38). Conversely, the shoot FW demonstrated a strict decreasing trend with decreasing sulfate concentration. At 1 µM sulfate, both the shoot and root FWs were significantly reduced indicating severe sulfur deficiency stress. While the root FW was reduced to half the FW in the control condition, the shoot FW was reduced to a fifth of the control condition (Figure 38). Notably, WT maintained the average primary root length in the concentration range of 500 to 1 µM sulfate, indicating that WT can access equivalent soil depths in sulfur deficiency conditions as in control conditions (Figure 38). Concomitant with the sustained increase in the root-to-shoot FW ratio, it can be deduced that plants must tightly perceive the sulfate availability in the environment and modulate their physiological processes accordingly. A comprehensive understanding of the sensing and signaling mechanism in Arabidopsis would significantly enhance our knowledge of plant resilience to sulfur deficiency.

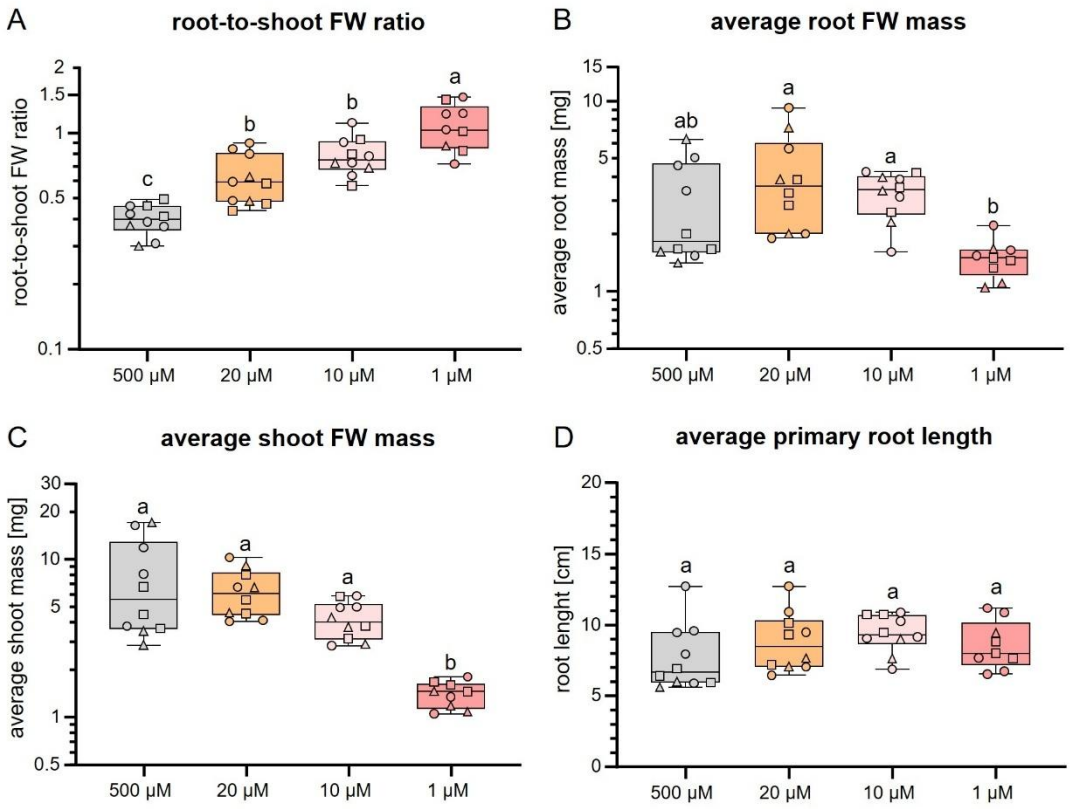

Figure 38: The WT long-term sulfur deficiency phenotype tightly depends on sulfate concentration. WT seeds were surface sterilized (2.3.3) and sown on ½ Hoagland plates with decreasing sulfate concentrations (2.3.4). After four weeks, the root-to-shoot FW ratio (2.3.10) and the primary root length were quantified (2.3.11). **A:** The root-to-shoot FW ratio. **B:** The average root FW. **C:** The average shoot FW. **D:** The average primary root length. Shapes of data points indicate different replicate sets. ANOVA one-way with $p < 0.05$ (n = 9 of three independent replicates) was used for statistical analysis after proper data transformation (2.7). The data was obtained with the help of my Bachelor's student Daniel Szabo.

3.3.2 Mutants affected in primary sulfur metabolism show impairments in adaptation to four weeks of sulfur deficiency on solid media plates

The molecular mechanisms underlying sulfur deficiency sensing remain to be fully elucidated. Given the established role of the CSC as a central regulatory node connecting sulfide availability with carbon-nitrogen metabolism through OAS production (Wirtz and Hell, 2006), I hypothesized a possible involvement of sulfide, OAS, and CSC dissociation in signaling the modulation of developmental plasticity in long-term sulfur deficiency. To explore this hypothesis, I used Arabidopsis mutants deficient in these three factors to analyze their root-to-shoot FW ratio increase and maintenance of primary root length in sulfur deficiency conditions.

The *serat tko* mutant (*serat1;1s2;1s2;2*), which retains only 5 ± 2% SERAT activity in leaves (Dong *et al.*, 2017), was used to assess the impact of OAS. The *sir1-1* mutant, exhibiting only 8 ± 4% of WT sulfite reductase (*SiR*) transcript levels (Khan *et al.*, 2010), was selected to evaluate the role of sulfide. Since Arabidopsis possesses three distinct CSCs localized in the cytosol, plastids, and mitochondria, the single mutants *serat1;1*, *serat2;1*, and *serat2;2,* were included to investigate the contribution of CSC disruption in developmental responses to sulfur deficiency.

First, phenotypes of *serat tko* and *sir1-1* mutants were analyzed in long-term sulfur deprivation conditions. To this end, seeds of WT, *serat tko*, and *sir1-1* (2.3.1) were surface-sterilized (2.3.3) and sown on ½ Hoagland plates containing either sufficient (500 µM) or deficient (1 µM) sulfate

concentrations (2.3.4). After four weeks of growth, the root-to-shoot FW ratio (2.3.10) and average primary root length (2.3.11) were quantified to assess the developmental adaptations of these mutants to sulfur limitation.

While the WT exhibited the expected increase in root-to-shoot FW ratio under sulfur deficiency from 0.4 in control conditions to 1.1 in deficiency (Figure 39 A), the *serat tko* mutant displayed a significantly different response. In control conditions, its root-to-shoot FW ratio of 0.3 was significantly lower than WT and in sulfur deficiency, it failed to significantly increase its root-to-shoot FW ratio. This was driven by *serat tko's* inability to maintain root FW as effectively as WT, and its reduced capacity in downregulating shoot FW (Figure 39 B, C). In contrast, the *sir1-1* mutant exhibited a WT-like root-to-shoot FW ratio in control condition. Upon sulfur deficiency, *sir1-1* exhibited 90% of the WT root-to-shoot FW ratio response. This was driven by a trend for impaired reduction in shoot FW, since *sir1-1* maintained root FW comparable to WT (Figure 39B, C). The previously reported growth retarded phenotypes for both *serat tko* and *sir1;1* (Dong *et al*., 2017) were not reflected in the shoot and root FWs, probably due to the chosen growth period of four weeks, giving not enough time to develop significant differences.

With respect to average primary root length, WT and *sir1-1* exhibited similar growth patterns. In control conditions, both had an average root length of approximately 9 cm, which was only slightly reduced under sulfur deficiency to 8 cm in WT and 7.5 cm in *sir1-1* (Figure 39 D). In contrast, *serat tko* displayed a significantly shorter average primary root length of 5 cm in control conditions compared to WT, which was further reduced in sulfur deficiency to 2.5 cm (Figure 39 D). The observed differences in developmental plasticity are illustrated in Figure 39 E. Its substantial difference to the WT phenotype in response to sulfur deficiency places *serat tko* in the focus of the investigation.

Since *serat tko* lacks all three CSC, the single mutants *serat1;1*, *sert2;1* and *serat2;2* were investigated regarding their involvement in *serat tko's* phenotype. Therefore, seeds of the single mutants *serat1;1*, *serat2;1,* and *serat2;2* (2.3.1) were surface sterilized (2.3.3) and grown next to WT on solid media plates complemented with sufficient (500 µM) or deficient (1 µM) sulfate concentrations (2.3.4) for four weeks to assess their phenotype (2.3.10, 2.3.11). As observed before, the WT showed an increased root-to-shoot FW ratio in sulfur deficiency compared to the control condition driven by a strongly reduced shoot FW and maintained root FW (Figure 40). All three single mutants *serat1;1*, *serat2;1,* and *serat2;2* exhibited WT-like root-to-shoot FW ratios. The shoot and root FWs in both control and sulfur deficiency conditions were also similar to WT, with the only exception for *serat2;1*, which showed generally both higher root and shoot FW than WT in sulfur deficiency. Additionally, all mutants exhibited WT-like average primary root lengths in control and sulfur deficiency conditions (Figure 40), indicating none of the CSC is necessary to adapt to long-term sulfur deficiency.

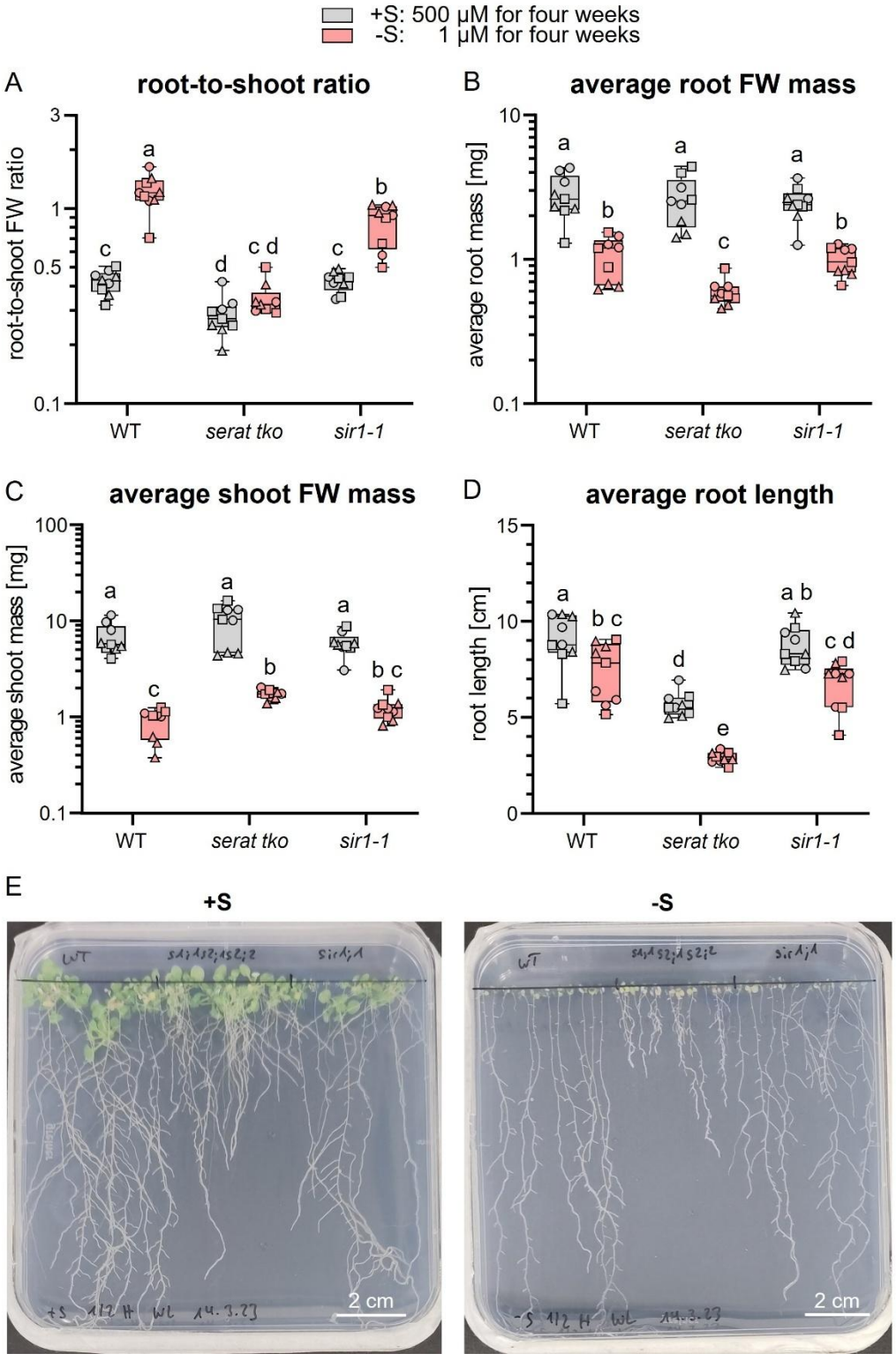

Figure 39: Long-term sulfur deficiency phenotype of *serat tko* and *sir1-1* on solid media plates. WT, *serat tko*, and *sir1-1* seeds (2.3.1) were surface sterilized (2.3.3) and grown on ½ Hoagland plates containing sufficient sulfate (+S, 500 µM) or deficient sulfate concentration (-S, 1 µM) (2.3.4). After four weeks, the root-to-shoot FW ratio (2.3.10) and the average primary root length were measured (2.3.11). **A:** root-to-shoot FW ratio. **B:** root FW. **C:** shoot FW. **D:** average primary root length. **E:** An example image of a +S and -S media plate to visualize the phenotypes. *serat tko* is the triple mutant *s1;1s2;1s2;1*. Shapes of data points define independent experimental repetitions. ANOVA two-way with $p < 0.05$ ($n = 9$ of three independent replicates) was used for statistical analysis after proper data transformation.

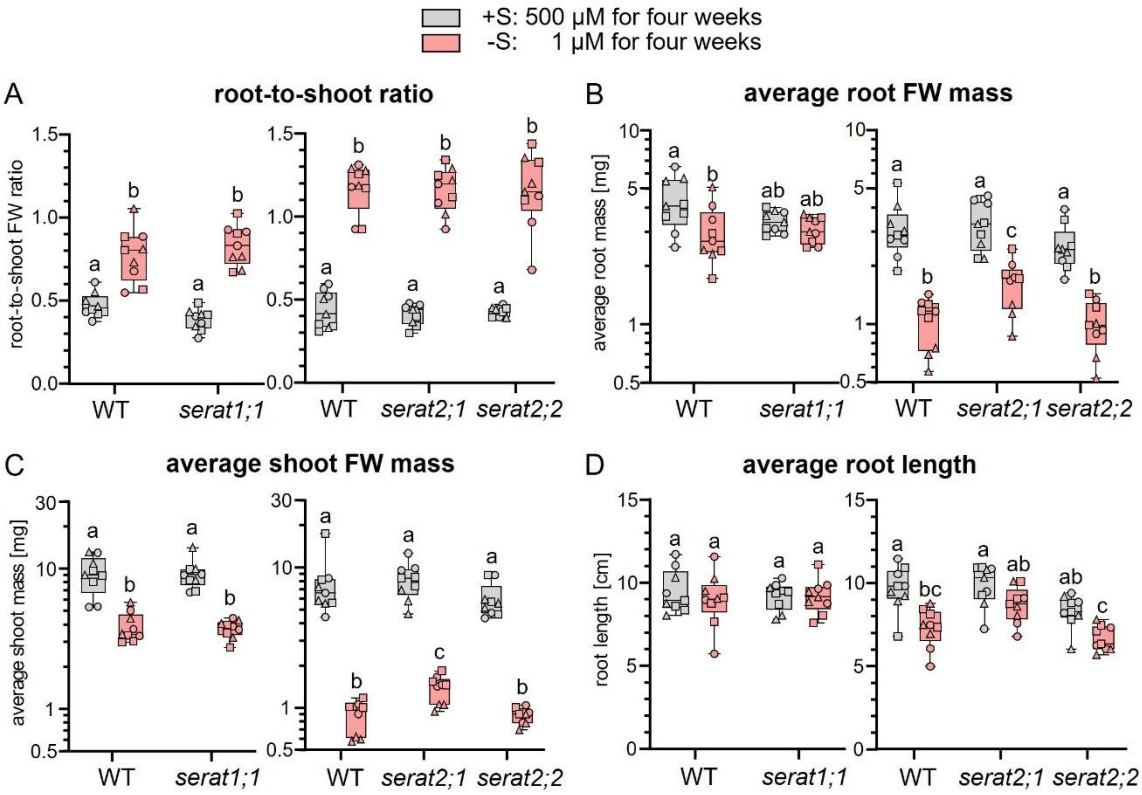

Figure 40: Long-term sulfur deficiency phenotype of *serat1;1*, *serat2;1* and *serat2;2* on solid media plates. WT, *serat1;1*, *serat2;1,* and *serat2;2* (2.3.1) seeds were surface sterilized (2.3.3) and grown on either 500 µM sulfate ½ Hoagland plates (+S control) or 1 µM sulfate ½ Hoagland plates (-S sulfur deficiency) (2.3.4). After four weeks, the phenotype was assessed regarding the root-to-shoot FW ratio (2.3.10) and average primary root length (2.3.11). **A:** root-to-shoot FW ratio. **B:** root FW. **C:** shoot FW. **D:** average primary root length. Shapes of data points define independent experimental repetitions. ANOVA two-way with $p < 0.05$ (n = 9 of three independent replicates) was used for statistical analysis after proper data transformation.

To test if a specific CSC in either the cytosol, the plastids, or the mitochondria is sufficient for a WT-like adaptation to sulfur deficiency, I tested the *SERAT* quadruple mutants *Q1;1*, *Q2;1*, and *Q2;2*, respectively (Watanabe *et al*., 2008b). Therefore, the seeds of *Q1;1*, *Q2;1*, and *Q2;2* (2.3.1) were surface sterilized (2.3.3) and grown next to WT on solid media plates either containing 500 µM sulfate (control) or 1 µM sulfate (sulfur deficiency). After four weeks, the root-to-shoot FW ratio (2.3.10) and average primary root length were quantified (2.3.11).

Unexpectedly, all quadruple mutants were affected in the root-to-shoot FW ratio increase as response to sulfur deficiency (Figure 41 A). While *Q1;1* exhibited 86% of the WT response, *Q2;2* and *Q2;1* demonstrated stronger impairment, with only 38% and 31% of the WT root-to-shoot FW increase, respectively.

A reduction in root FW in sulfur deficiency was a common trend among the quadruple mutants, but it was statistically significant only in *Q2;2* (Figure 41 B). Similarly, all mutants demonstrated a trend for reduced average primary root lengths upon sulfur deficiency, although this was only statistically significant in *Q2;1* and *Q2;2* (Figure 41D). Since shoot FW remained unaffected across all genotypes in both control and sulfur-deficient conditions (Figure 41 C), this indicates that the primary defect was in root growth rather than shoot biomass reduction.

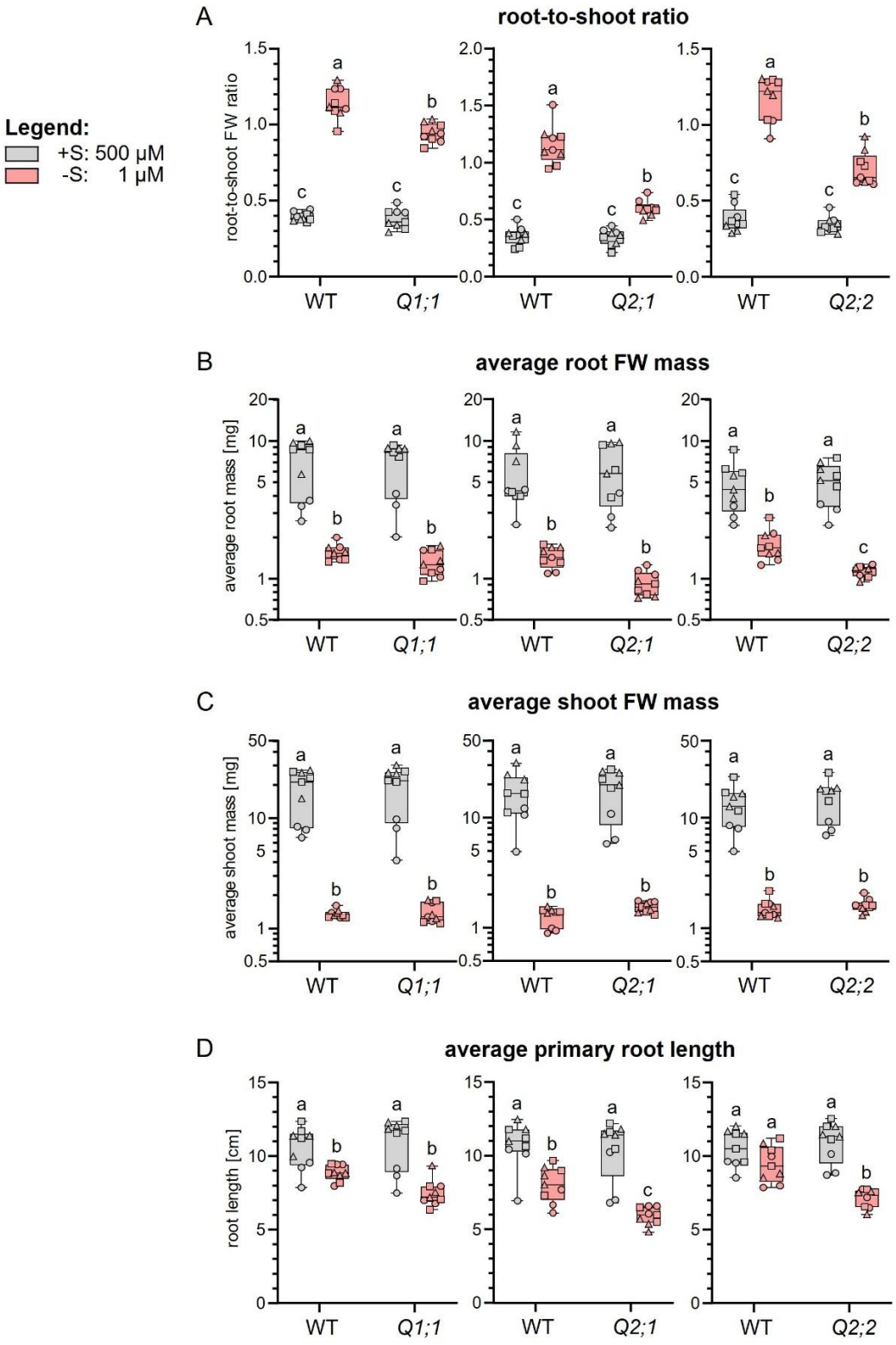

Figure 41: Long-term sulfur deficiency phenotype *Q1;1*, *Q2;1* and *Q2;2* on solid media. WT, *Q1;1*, *Q2;1,* and *Q2;2* (2.3.1) seeds were surface sterilized (2.3.3) and grown on ½ Hoagland plates containing either 500 µM sulfate (+S, control) or 1 µM sulfate (-S, sulfur deficiency) (2.3.4). After four weeks, the phenotype was assessed regarding the root-to-shoot FW ratio (2.3.10) and average primary root length (2.3.11). **A:** root-to-shoot FW ratio. **B:** root FW. **C:** shoot FW. **D:** average primary root length. Shapes of data points define independent experimental repetitions. ANOVA two-way with $p < 0.05$ (n = 9 of three independent replicates) was used for statistical analysis after proper data transformation.

Taken together, the subcellular location of the CSCs did influence their contribution to sulfur deficiency adaptation. Thereby, the cytosolic CSC (*Q1;1*) exhibited the greatest capacity to support a WT-like response, highlighting its pivotal role in this response. However, since the absence of any single CSC is insufficient to fully compensate for the loss of the others, I hypothesized that the product OAS is more important than a specific SERAT isoform for comprehensive adaptation to long-term sulfur deficiency.

3.3.3 Phenotypic and metabolic response of *serat tko* and *sir1-1* to sulfur deficiency stress in the hydroponic system

The *serat tko* and *sir1-1* are both affected in cysteine biosynthesis. While the *serat tko* showed a severe lack of adaptation to long-term sulfur deficiency, the *sir1-1* was only slightly impaired when grown and germinated on solid media plates in sulfur deficiency (3.3.2). To further investigate the different responses of the mutants, they were subjected to an environmental shift from growth in sulfur sufficient to sulfur deficient conditions. Therefore, *serat tko* and *sir1-1* (2.3.1) were grown next to WT in a hydroponic system (2.3.7) in liquid ½ Hoagland medium (500 µM sulfate) for four weeks. Half of the plants were shifted to the sulfur deficiency medium (1 µM sulfate), and the rest remained in the control medium. After an additional four weeks, the plants were harvested, and the root-to-shoot FW ratio was quantified for all individual plants (2.3.7).

All genotypes exhibited a similar root-to-shoot FW ratio of 0.2 in control conditions (Figure 42 A), which was substantially lower than the ratio when grown on a solid medium (0.4) with the same sulfate concentration, likely due to improved sulfate absorption in liquid culture. While both WT and *sir1-1* exhibited a significant increase in the root-to-shoot ratio to 0.5, the *serat tko* plants showed no significant change (Figure 42 A). The ratio difference in WT plants was predominantly driven by a substantial reduction in shoot FW to one-fifth of the control condition, while maintaining root FW (Figure 42 B-D), similar to the observation using solid media (3.3.1, 3.3.2).

Both *sir1-1* and *serat tko* exhibited the expected growth retardation as previously observed in soil-grown plants after eight weeks of growth (Dong *et al.*, 2017). In the control conditions, their shoot FWs were comparable to WT under sulfur deficiency, exhibiting only one-fifth of WT FW. The root FW in both mutants was half that of WT in control. Under sulfur deficiency, *sir1-1* reduced its shoot FW further by half while significantly increasing root FW (Figure 42 B-D), leading to a WT-like root-to-shoot FW ratio increase despite its growth defect. In contrast, *serat tko* showed no significant changes in either shoot or root FW in sulfur deficiency compared to the control condition, explaining its unchanged root-to-shoot FW ratio. Since *sir1-1* exhibited a WT-like response despite its growth retardation, it can be concluded that the absence of adaptation to long-term sulfur deficiency in *serat tko* cannot be solely attributed to limited cysteine biosynthesis.

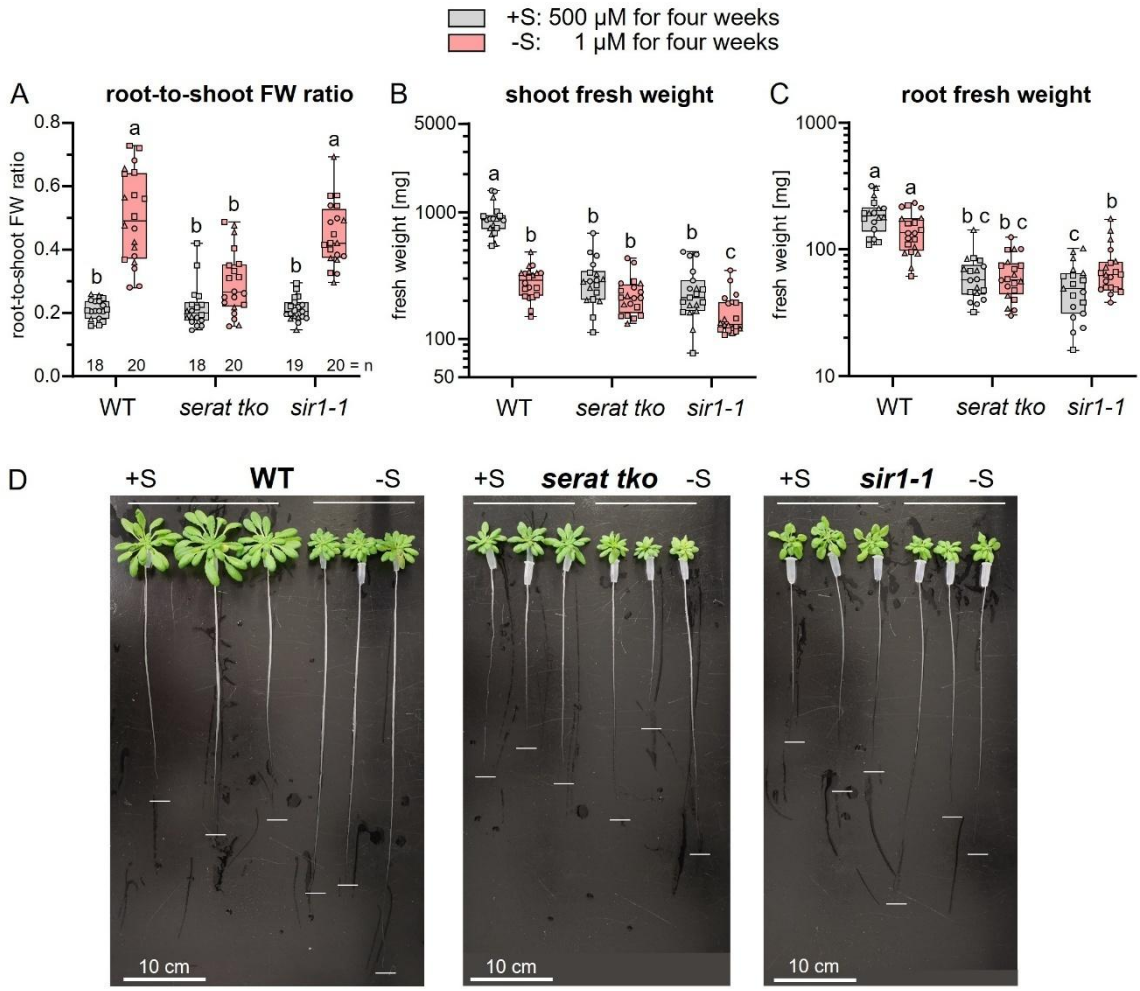

Figure 42: Phenotype of *serat tko* and *sir1-1* after a shift from four weeks control to four weeks sulfur deficiency condition. *serat tko* and *sir1-1* (2.3.1) were grown next to WT in ½ Hoagland medium containing 500 µM sulfate (+S) (2.3.7). Half of the plants were subjected to ½ Hoagland medium containing 1 µM sulfate for four additional weeks (-S), the other half remained in the control medium (2.3.7). Pictures were taken on the day of harvest, and the root-to-shoot FW ratio was determined (2.3.7). **A:** root-to-shoot FW ratio. **B:** root FWs. **C:** shoot FWs. **D:** photographs of example individuals. The data points shapes indicate independent repetitions. ANOVA two-way with $p < 0.05$ was used for statistical analysis after proper data transformation.

To assess the link between phenotypic observations and primary sulfur metabolism, the harvested tissues of WT, *serat tko,* and *sir1-1* mutant were ground and used for metabolite extraction (2.6.1). The extracts were derivatized for OAS (2.6.2), sulfide (2.6.4), cysteine and glutathione (2.6.3), and steady-state levels were quantified via UPLC (2.6.5).

OAS steady-state level increased in WT roots fivefold in sulfur deficiency compared to the control condition (Figure 43 A). The *sir1;1* mutant showed WT-like OAS level and also accumulated fivefold more OAS in sulfur deficiency compared to the control condition. Interestingly, the *serat tko* mutant showed significantly reduced OAS steady-state levels in the control condition compared to WT and *sir1;1*. In sulfur deficiency, the OAS content doubled in *serat tko* roots but did not exceed the levels of the WT control condition. In contrast to the root tissue, the OAS steady-state levels in the shoots were similar among all genotypes and conditions (Figure 43 B).

Cysteine steady-state levels in WT roots were decreased in sulfur deficiency by a third of the control condition (Figure 43 C). Like the OAS steady-state levels, the *serat tko* showed only half of the cysteine concentration of WT roots in the control condition and were further decreased by a

third in sulfur deficiency. In contrast, *sir1-1* roots exhibited 50% higher cysteine steady-state levels than WT in the control condition control, but WT-like levels in sulfur deficiency (Figure 43 C). As observed for the OAS levels, the genotypes exhibited no significant differences in cysteine steady-state levels in the shoots among control and sulfur deficiency conditions. Nonetheless, the *serat tko* and *sir1-1* mutant exhibited both a trend for 50% reduced cysteine steady-state level compared to WT, although not statistically significant.

As observed with the cysteine steady-state levels, the glutathione steady-state levels decreased in WT roots in response to sulfur deficiency by half compared to the control condition (Figure 43 E). The glutathione levels of *serat tko* roots in the control condition were similar to the WT levels in sulfur deficiency and further decreased by a third in sulfur deficiency. In contrast, the glutathione levels in the roots of *sir1-1* were similar to WT in both control and sulfur-deficient conditions (Figure 43 E). Compared to the WT, the glutathione steady-state levels in the shoots of *serat tko* and *sir1;1* were decreased by a third in the control condition. In sulfur deficiency, *serat tko* and *sir1;1* exhibited a trend for further decreased glutathione steady-state levels, although this was not statistically significant (Figure 43 F).

Given the limited root FW of *serat tko* and *sir1-1*, sulfide steady-state levels were only quantified in shoots (Figure 43 G). Thereby, WT and *serat tko* exhibited similar sulfide levels in both control condition, which was similarly decreased in sulfur deficiency. In contrast, *sir1-1* exhibited a 50% reduction in sulfide levels compared to WT in the control condition (Mann-Whitney test, $p = 0.0056$), but WT-like sulfide levels in sulfur deficiency. In the WT roots, the sulfide levels were one order of magnitude lower than in WT shoots in control conditions and were further decreased by an additional magnitude in sulfur deficiency. The substantial difference in sulfide levels between WT shoot and root indicates the predominant role of photosynthetically active tissues for sulfide production.

Taken together, the metabolic analysis corroborated earlier findings of diminished OAS steady-state levels in serat tko and decreased sulfide levels in *sir1-1* under standard conditions, thereby validating the selected genotypes. The WT exhibited the anticipated response to sulfur deficiency with increased OAS levels and diminished thiol and sulfide levels, thus validating the efficacy of the sulfur deficiency treatment. *sir1-1* demonstrated WT-like metabolite trends, which are consistent with its WT-like increase in root-to-shoot FW ratio. In contrast, the *serat tko* roots exhibited no OAS accumulation in sulfur deficiency, exceeding the WT level in the control condition. Also, the thiol levels in roots of *serat tko* in the control condition were already pre-decreased to the WT levels of sulfur deficiency. Therefore, I hypothesize that either the absent OAS accumulation or the pre-decreased thiol levels may underlie the impaired root-to-shoot FW ratio increase in *serat tko* under sulfur deficiency.

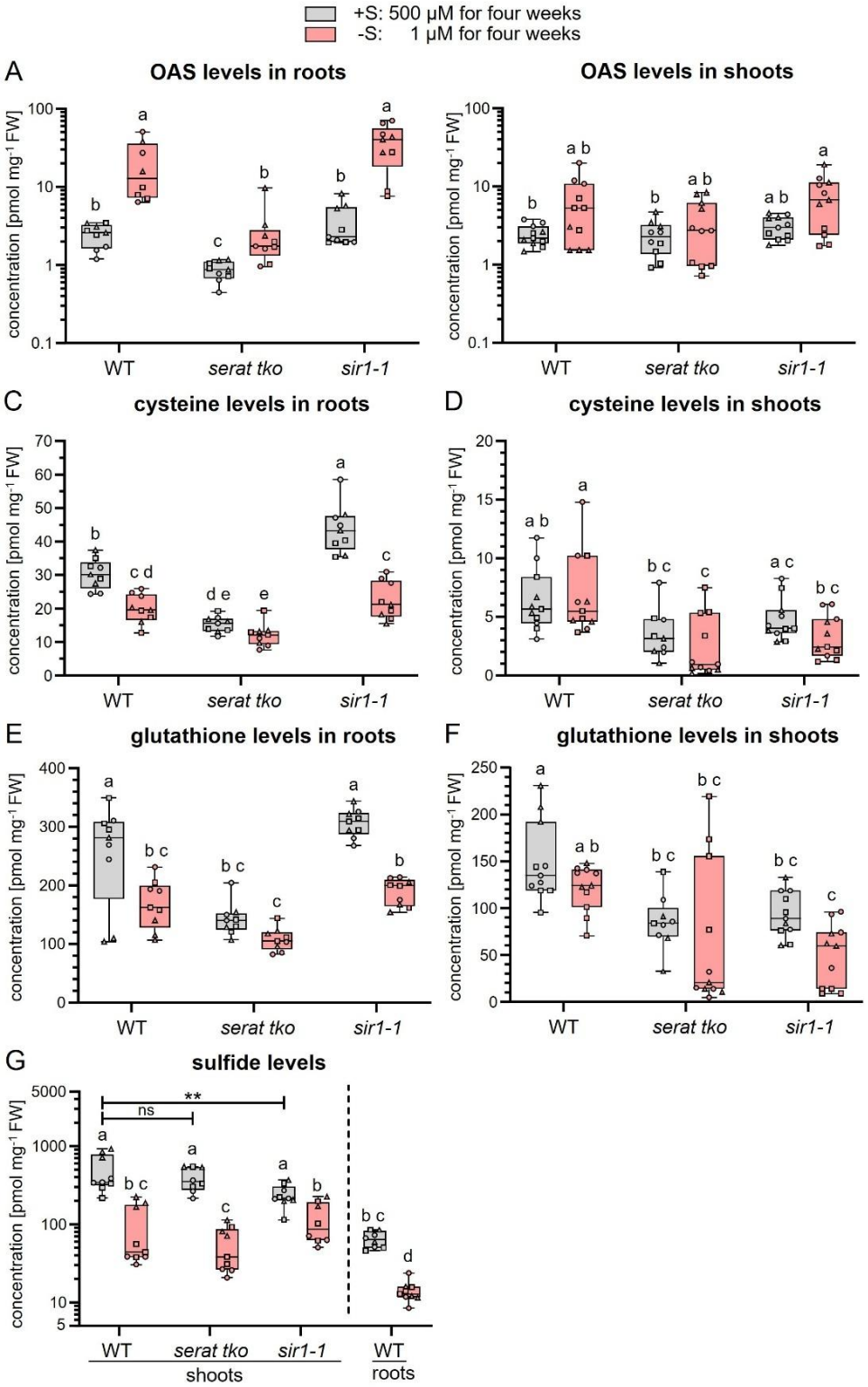

Figure 43: Metabolite steady-state levels of *serat tko* and *sir1-1* after a shift from four weeks control to four weeks sulfur deficiency condition. *serat tko*, *sir1-1*, and WT (2.3.1) were grown in sulfur sufficiency control medium (500 µM sulfate, +S) for four weeks (2.3.7). Half of the plants were subjected to sulfur deficiency medium (1 µM sulfate, -S) for an additional four weeks. The other half remained in the control medium (2.3.7). Harvested material was used to extract metabolites (2.6.1). Quantification was performed after compound labeling (2.6.2, 2.6.3, 2.6.4) and detection with UPLC (2.6.5). **A:** OAS levels in roots. **B:** OAS levels in shoots. **C:** cysteine levels in roots. **D:** cysteine levels in shoots. **E:** glutathione levels in roots. **F:** glutathione levels in shoots. **G:** sulfide levels. Shapes of data points indicate independent replicates. ANOVA two-way with $p < 0.05$ was used for statistical analysis after proper data transformation. For direct comparison of sulfide control levels between WT and *serat tko* or *sir1-1* a two-tailed Mann-Whitney test was performed with $p < 0.05$.

3.3.4 OAS steady-state levels correlate with the root-to-shoot FW ratio increase in response to sulfur deficiency

In contrast to *sir1-1*, *serat tko* exhibited an inability to enhance its root-to-shoot FW ratio in sulfur deficiency conditions, which was accompanied by disrupted OAS and thiol steady-state levels in the root (3.3.3). To elucidate the correlation between this phenotype and primary sulfur metabolism, mutants previously affected in solid media culture (3.3.2) were cultivated hydroponically for metabolite extraction. Therefore, *Q1;1*, *Q2;1*, *Q2;2*, *serat tko*, and *sir1-1* were cultivated with the WT in liquid ½ Hoagland medium containing 500 µM sulfate for a period of two weeks. Thereafter, the plants were transferred to either 1 µM sulfate (-S) or maintained under control conditions (+S) for a duration of six additional weeks (2.3.7). The duration of the sulfur deficiency application was extended compared to 3.3.3 to amplify the phenotypic response.

The WT demonstrated an increase in its root-to-shoot FW ratio from 0.2 (+S) to 0.6 (-S) (Figure 44 A and Figure 45). Notably, despite previous impairments observed when grown on solid media (3.3.2), *Q1;1*, *Q2;2*, and *sir1-1* exhibited a WT-like response in hydroponics, likely attributable to enhanced sulfate uptake in liquid media. The *Q2;1* exhibited the strongest phenotype in the solid media culture and remained affected in the hydroponic culture. Surprisingly, *serat tko* exhibited also a significant yet incomplete root-to-shoot FW ratio increase under sulfur deficiency (3.3.2, 3.3.3).

While *serat tko* and *sir1-1* displayed growth retardation as previously observed in 3.3.3, *Q1;1*, *Q2;1*, and *Q2;2* maintained a WT-like FW in control conditions. In sulfur deficiency, WT, *Q1;1*, and *Q2;2* reduced shoot FW to 10% of control levels while maintaining 90% root FW. *Q2;1* exhibited a comparable reduction in shoot FW, while retaining 85% of the root FW, contributing to its impaired FW ratio increase. *serat tko* and *sir1-1* reduced shoot FW by one-third under sulfur deficiency. However, *serat tko* also exhibited a 30% reduction in root FW, whereas *sir1-1* increased root FW by 40%, explaining their distinct root-to-shoot FW ratio. These findings clearly indicate that the root-to-shoot FW ratio increase in response to sulfur deficiency occurs independently of plant size.

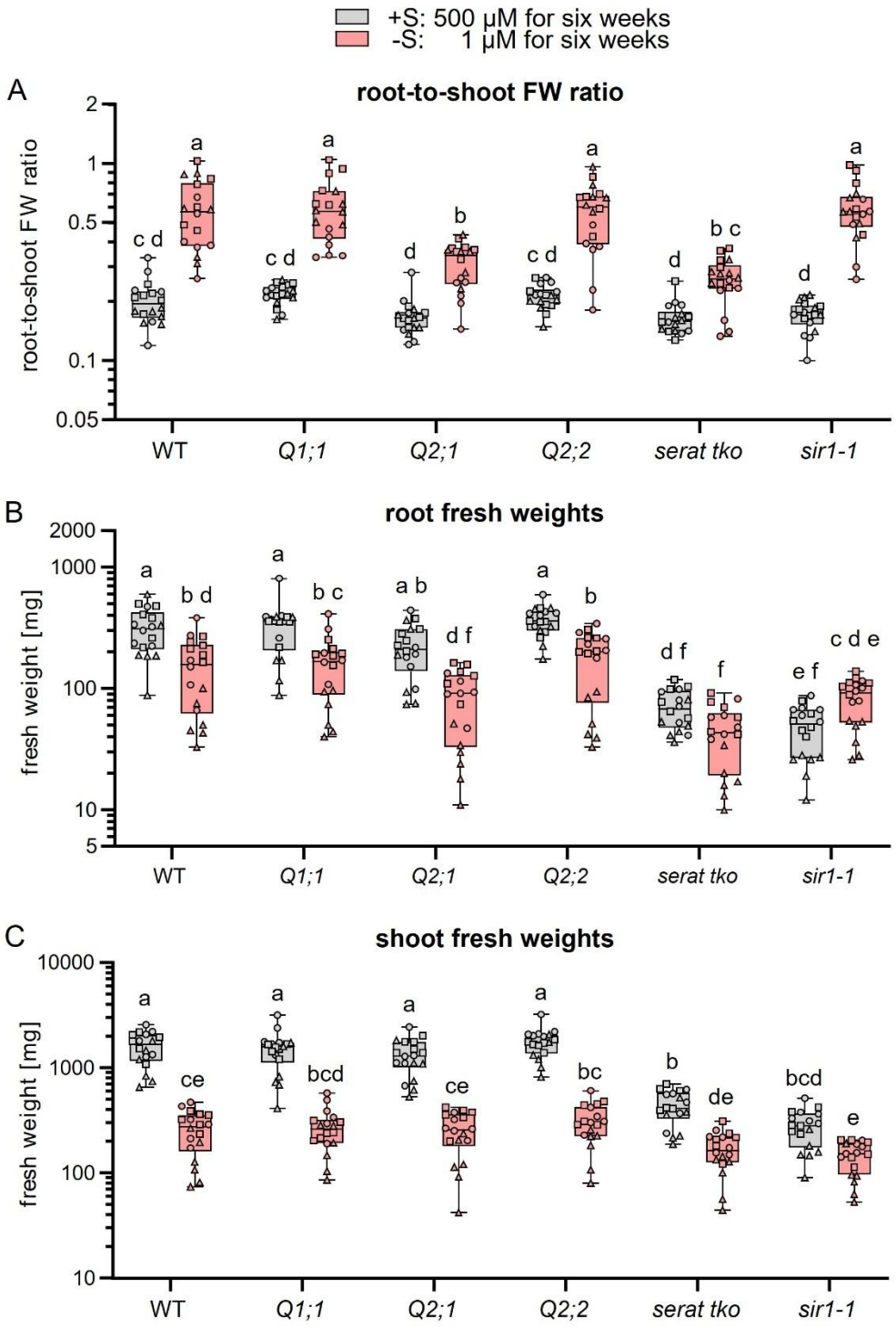

Figure 44: FW phenotype quantification of *Q1;1*, *Q2;1*, *Q2;2*, *serat tko* and *sir1-1* after a shift from two weeks control to six weeks sulfur deficiency condition. *Q1;1*, *Q2;1*, *Q2;2*, *serat tko* and *sir1-1* (2.3.1) were grown next to WT for two weeks in ½ Hoagland medium (500 µM sulfate, +S) (2.3.7). Half of the plants were transferred to ½ Hoagland medium supplemented with 1 µM sulfate (sulfur deficiency, -S), the other half remained in +S medium. After additional six weeks, the plants were harvested and the FWs quantified (2.3.7). **A:** root-to-shoot FW ratio. **B:** root FWs. **C:** shoot FWs. Shapes of data points indicate independent replicates with total n=18. ANOVA two-way with $p < 0.05$ was used for statistical analysis after proper data transformation.

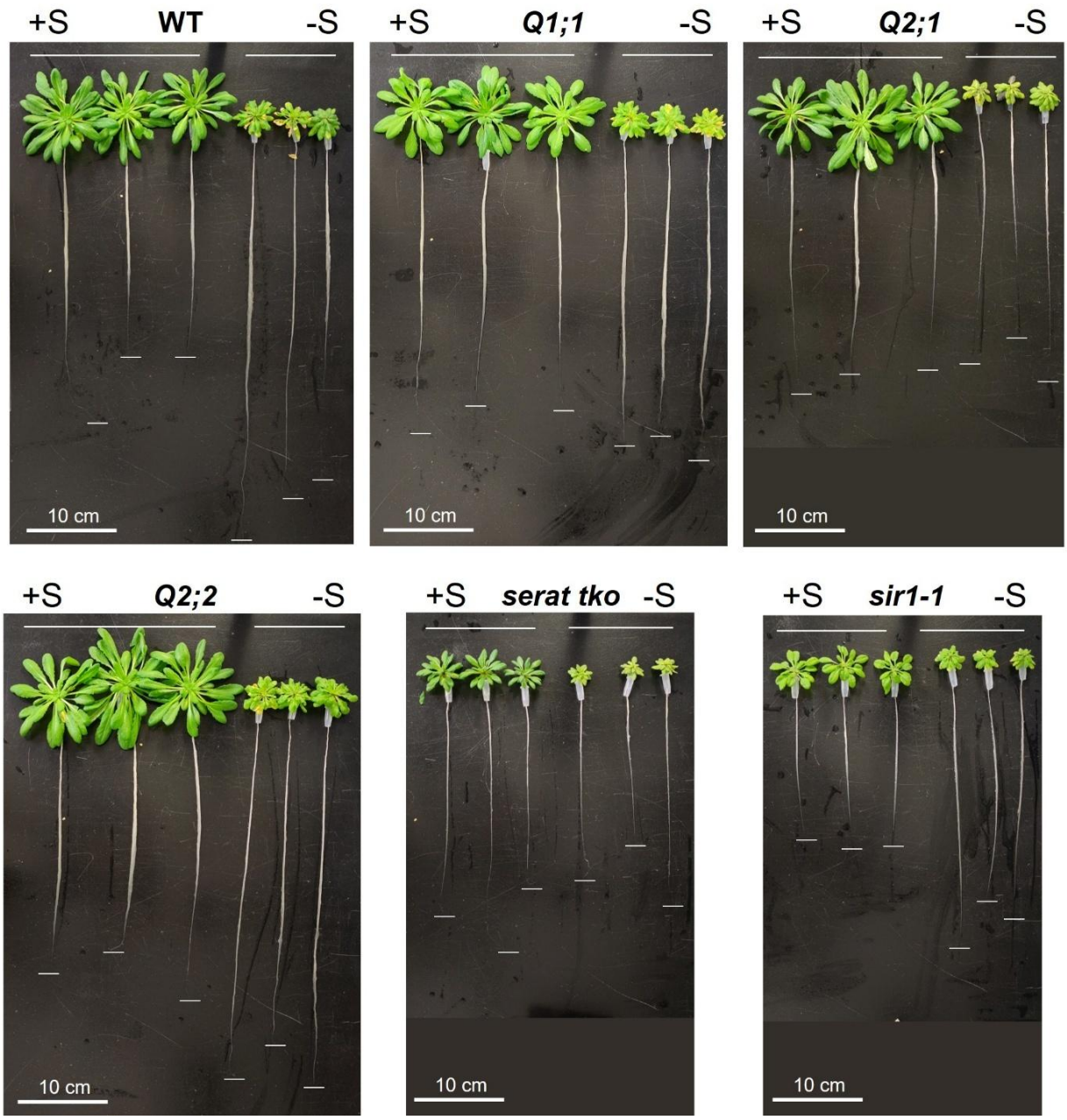

Figure 45: Phenotype of *Q1;1*, *Q2;1*, *Q2;2*, *serat tko* and *sir1-1* after a shift from two weeks control to six weeks sulfur deficiency condition. *Q1;1*, *Q2;1*, *Q2;2*, *serat tko* and *sir1-1* (2.3.1) were grown next to WT for two weeks in ½ Hoagland medium (500 µM sulfate, +S) (2.3.7). Half of the plants were transferred to ½ Hoagland medium supplemented with 1 µM sulfate (sulfur deficiency, -S), the other half remained in +S medium. After an additional six weeks, three individuals per genotype and growth conditions were photographed to visualize the phenotypes. The white lines indicate the end of the primary roots, and the scale bar indicates 10 cm.

To investigate a possible link between the metabolite steady-state levels and the root-to-shoot FW increases of the mutants grown in the hydroponic system, the harvested shoot and root material were used to extract metabolites (2.6.1). OAS (2.6.2) and thiols (2.6.3) were specifically labeled and quantified by UPLC (2.6.4).

Genotypes *Q1;1*, *Q2;2*, and *sir1;1*, which exhibited a WT-like increase in root-to-shoot FW ratio under sulfur deficiency, also demonstrated WT-like OAS accumulation in roots and shoots (Figure 46A, B). In contrast, *Q2;1* and *serat tko*, which failed to increase their root-to-shoot FW ratio, exhibited OAS levels that did not exceed those of the WT control. In sulfur deficiency, serat tko exhibited an even further reduction in shoot OAS of 50% compared to the control. The Pearson

correlation analysis revealed a significant positive relationship between OAS steady-state levels and the root-to-shoot FW ratio for both roots ($p = 0.0001$) and shoots ($p = 0.0015$) (Figure 46 C and D).

In control conditions, *serat tko* and *Q2;1* exhibited a 10% reduction in cysteine steady-state levels in roots, but under sulfur deficiency, cysteine levels were similar across all genotypes in both roots and shoots (Figure 47 A, B). No significant correlation was identified between cysteine levels and the root-to-shoot FW ratio in either roots ($p = 0.1924$) or shoots ($p = 0.6473$) (Figure 47C, D).

In a similar manner, *serat tko* and *Q2;1* demonstrated reduced glutathione levels in roots under control conditions (Figure 48 A). Conversely, WT, *Q1;1*, *Q2;2*, and *sir1;1* exhibited a decline in glutathione levels in response to sulfur deficiency, while the glutathione levels of *serat tko* and *Q2;1* remained unaltered. In shoots, WT, *Q2;2*, and *sir1;1* demonstrated a one-third reduction in glutathione under sulfur deficiency, while *Q1;1* exhibited lower initial levels that remained constant. *Q2;1* and *serat tko* exhibited glutathione levels that were half of those observed in WT under control conditions, with a further decline of two-thirds observed in the presence of sulfur deficiency (Figure 48A, B). However, the steady-state levels of glutathione did not demonstrate a significant correlation with the root-to-shoot FW ratio in either roots ($p = 0.4906$) or shoots ($p = 0.9404$) (Figure 48C, D).

Although cysteine and glutathione steady state levels were also affected in *serat tko* and *Q2;1*, a significant correlation of the root-to-shoot FW ratio was only found with OAS steady-state levels. The altered cysteine and glutathione levels could result from limited precursor availability, as they are downstream metabolites of OAS.

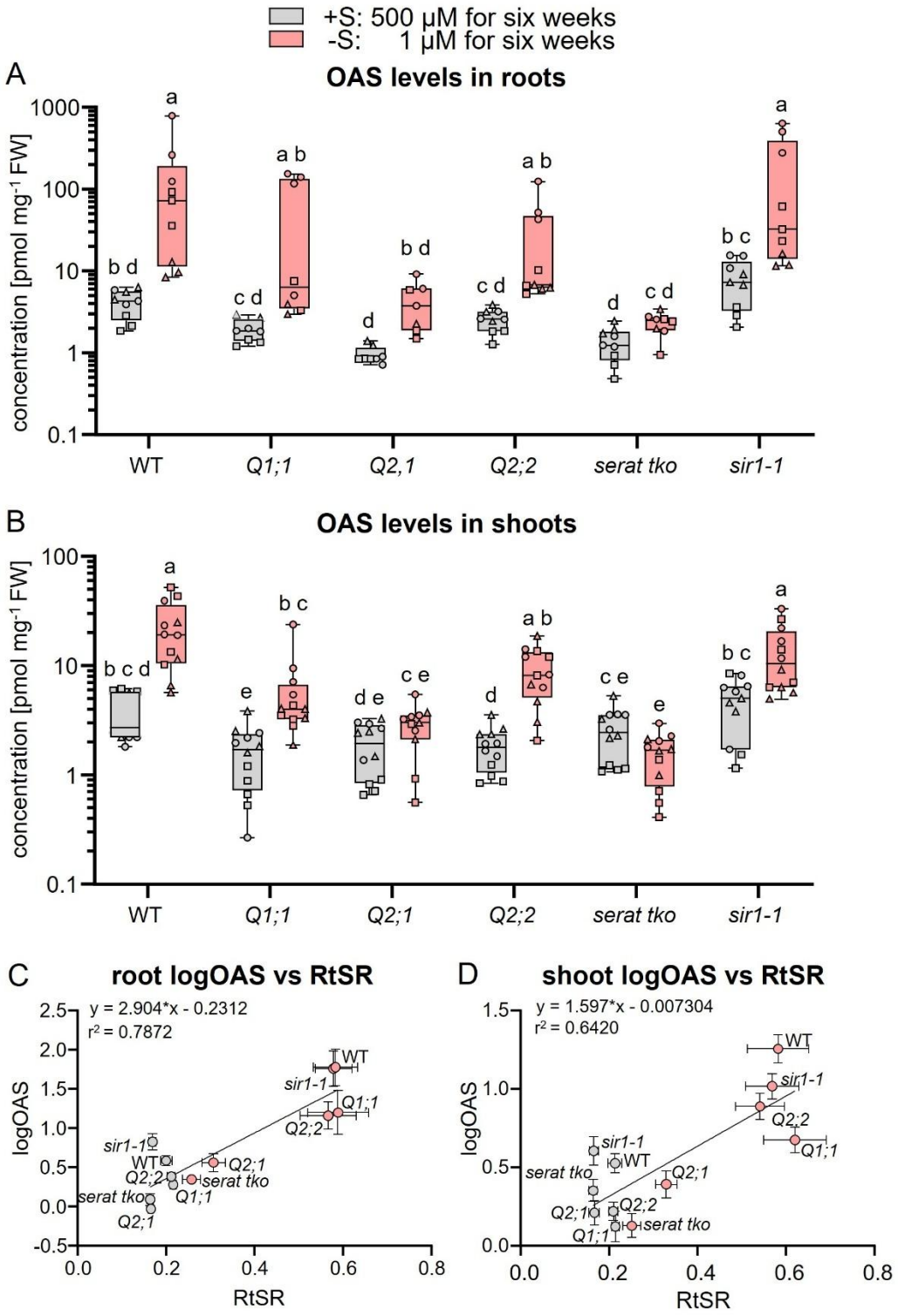

Figure 46: OAS steady-state levels of *Q1;1*, *Q2;1*, *Q2;2*, *serat tko* and *sir1-1* after a shift from two weeks control to six weeks sulfur deficiency condition. *Q1;1*, *Q2;1*, *Q2;2*, *serat tko* and *sir1-1* (2.3.1) were grown next to WT for two weeks in ½ Hoagland medium (500 µM sulfate, +S) (2.3.7). Half of the plants were transferred to ½ Hoagland medium supplemented with 1 µM sulfate (sulfur deficiency, -S), the other half remained in +S medium. After additional six weeks, the plants were harvested and used to extract (2.6.1) and label OAS (2.6.2) for UPLC quantification (2.6.5) **A:** OAS level in roots **B:** OAS level in shoots. Shapes of data points indicate independent experimental repetition. ANOVA two-way with $p < 0.05$ was used for statistical analysis after proper data transformation. **C:** Correlation between roots OAS levels (logOAS) and the root-to-shoot FW ratio (RtSR). **D:** Correlation between shoots OAS levels (logOAS) and the root-to-shoot FW ratio (RtSR). The means of the logOAS data from each genotype were used with the means of the root-to-shoot FW ratio for a Pearson correlation ($p < 0.05$) with standard errors and r^2 displayed.

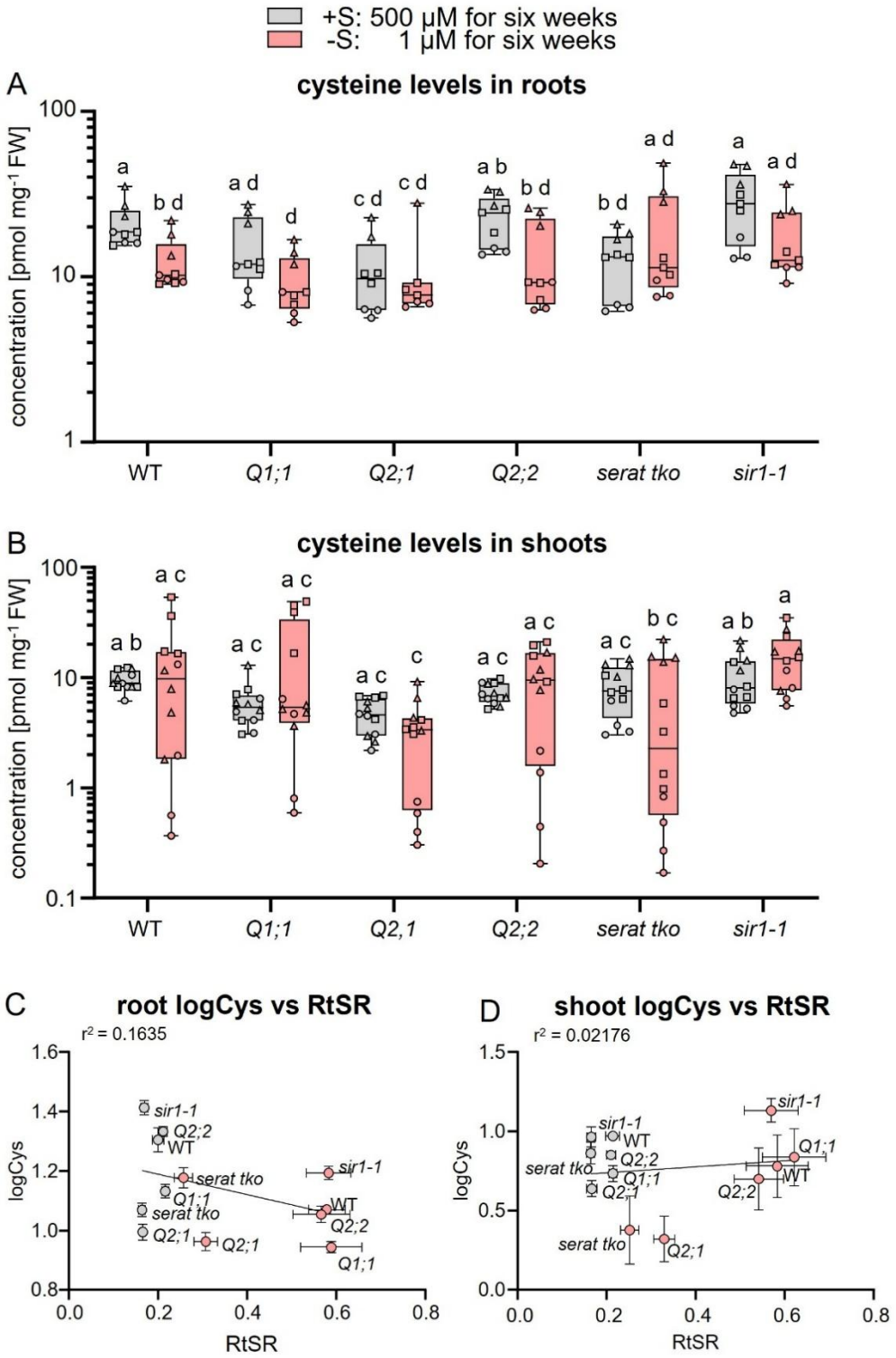

Figure 47: Cysteine steady-state levels of *Q1;1*, *Q2;1*, *Q2;2*, *serat tko* and *sir1-1* after a shift from two weeks control to six weeks sulfur deficiency condition. *Q1;1*, *Q2;1*, *Q2;2*, *serat tko* and *sir1-1* (2.3.1) were grown next to WT for two weeks in ½ Hoagland medium (500 µM sulfate, +S) (2.3.7). Half of the plants were transferred to ½ Hoagland medium supplemented with 1 µM sulfate (sulfur deficiency, -S), and the other half remained in +S medium. After additional six weeks, the plants were harvested and used to extract (2.6.1) and label cysteine (2.6.3) for UPLC quantification (2.6.5) **A:** cysteine level in roots **B:** cysteine level in shoots. Shapes of data points indicate independent experimental repetition. ANOVA two-way with $p < 0.05$ was used for statistical analysis after proper data transformation.**C:** Correlation between root cysteine levels (Cys) and the root-to-shoot FW ratio (RtSR). **D:** Correlation between shoots cysteine levels and the root-to-shoot FW ratio. The means of the cysteine data from each genotype were used with the means of the root-to-shoot FW ratio for a Pearson correlation ($p < 0.05$) with standard errors and r^2 displayed.

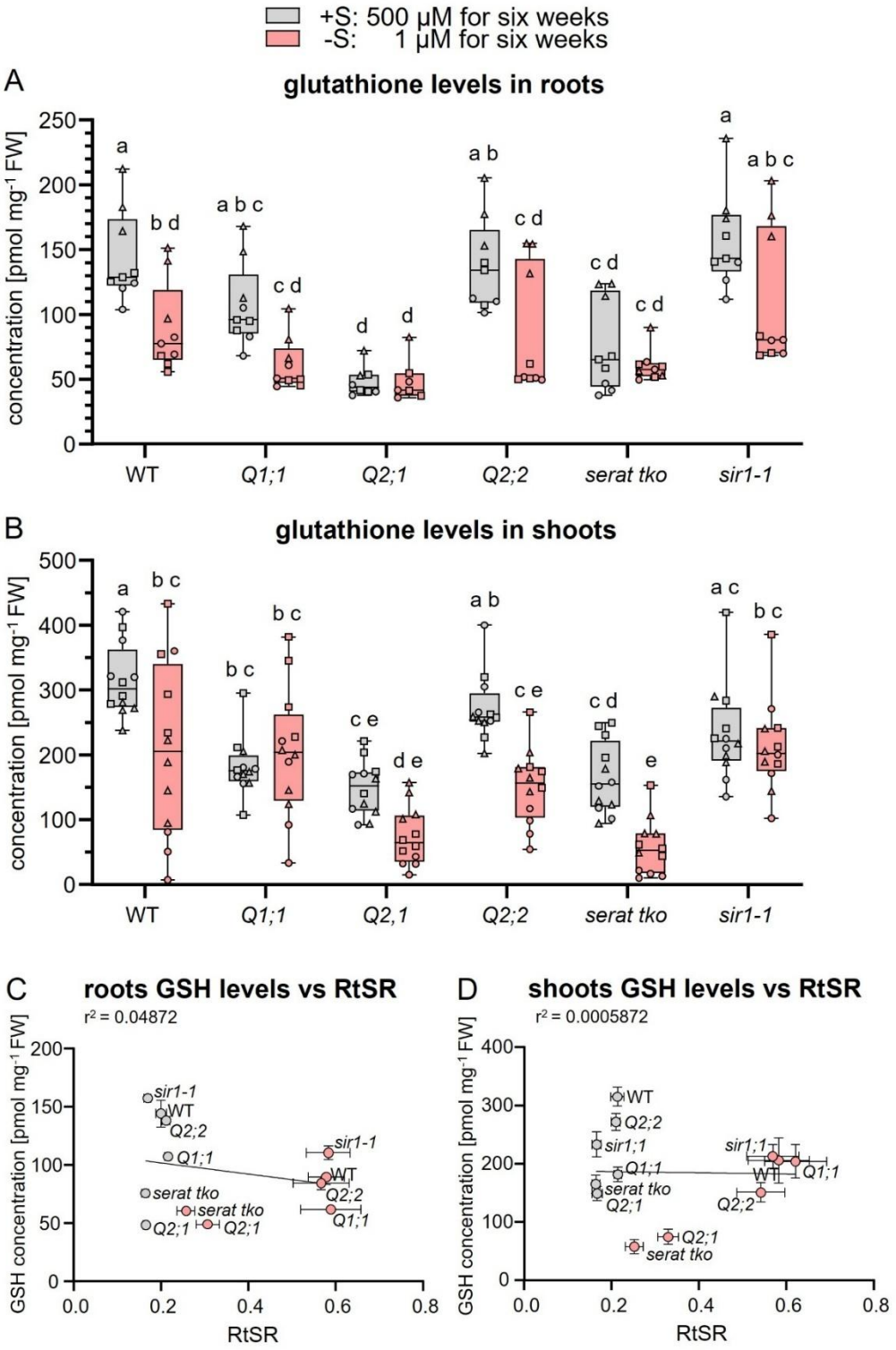

Figure 48: Glutathione steady-state levels of *Q1;1*, *Q2;1*, *Q2;2*, *serat tko* and *sir1-1* after a shift from two weeks control to six weeks sulfur deficiency condition. *Q1;1*, *Q2;1*, *Q2;2*, *serat tko* and *sir1-1* (2.3.1) were grown next to WT for two weeks in ½ Hoagland medium (500 µM sulfate, +S) (2.3.7). Half of the plants were transferred to ½ Hoagland medium supplemented with 1 µM sulfate (sulfur deficiency, -S), and the other half remained in +S medium. After additional six weeks, the plants were harvested and used to extract (2.6.1) and label glutathione (2.6.3) for UPLC quantification (2.6.5) **A:** glutathione level in roots **B:** glutathione level in shoots. Shapes of data points indicate independent experimental repetition. ANOVA two-way with $p < 0.05$ was used for statistical analysis after proper data transformation. **C:** Correlation between *root* cysteine levels (Cys) and the root-to-shoot FW ratio (RtSR). **D:** Correlation between shoots cysteine levels and the root-to-shoot FW ratio. The means of the cysteine data from each genotypes were used with the means of the root-to-shoot FW ratio for a Pearson correlation ($p < 0.05$) with standard errors and r^2 displayed.

3.3.5 External OAS application increased the root-to-shoot FW ratio in *serat tko* in sulfur deficiency condition

The *serat tko* mutant exhibits a limitation in cysteine biosynthesis due to the absence of the three primary isoforms responsible for synthesizing the cysteine precursor, *O*-acetylserine (OAS). In sulfur deficiency conditions, the mutant exhibited an affected root-to-shoot FW ratio increase (3.3.2, 3.3.3, 3.3.4). Preliminary experiments found a correlation between the root-to-shoot FW ratio and the steady-state levels of internal OAS (3.3.4). To test this correlation, *serat tko* was treated with an external OAS supply and investigated regarding restoration of the root-to-shoot FW increase. Given that OAS is a non-proteinogenic amino acid, the isomer *N*-acetylserine (NAS) was also included in the experimental design to control for potential effects of additional carbon and nitrogen supply. Therefore, WT and *serat tko* (2.3.1) seeds were surface sterilized (2.3.3) and cultivated on solid media plates containing either 500 µM sulfate (+S) or 1 µM sulfate (-S)(2.3.4). OAS, NAS, or buffer mock treatments were applied three times per week (2.3.5). After 21 days, the average primary root length was measured (2.3.11), and the root-to-shoot FW ratio was calculated (2.3.10).

In the control condition, WT and *serat tko* exhibited root-to-shoot FW ratios of 0.4 and 0.3 (Figure 49 A), respectively, matching previous observations and indicating no influence of the mock treatment (3.3.2). In sulfur deficiency control condition, WT significantly increased the root-to-shoot FW ratio to 0.7, while *serat tko* exhibited no significant ratio change, indicating the mock treatment also had no effect in this condition (Figure 49 A). OAS supplementation restored the root-to-shoot FW ratio of *serat tko* to WT-like levels, while NAS had no effect indicating specific for OAS in this response. The root FW decreased by 20% in *serat tko* under sulfur deficiency in mock and NAS treatments, but OAS treatment promoted root FW maintenance (Figure 49 B). The shoot FW decreased by 75% in both genotypes under sulfur deficiency, unaffected by OAS or NAS treatment (Figure 49 C). The WT maintained a constant primary root length of 5 cm, disregarding of the growth condition (Figure 49 D). *serat tko* exhibited again a reduced primary root length of 3.5 cm in control conditions, which further decreased to 2.5 cm in sulfur deficiency. Only OAS treatment restored the root length to 3.5 cm, while NAS or mock treatment had no effect.

Taken together, the external application of OAS was sufficient to increase the root-to-shoot FW ratio in *serat tko* in response to sulfur deficiency by improving root FW and maintaining average primary root length.

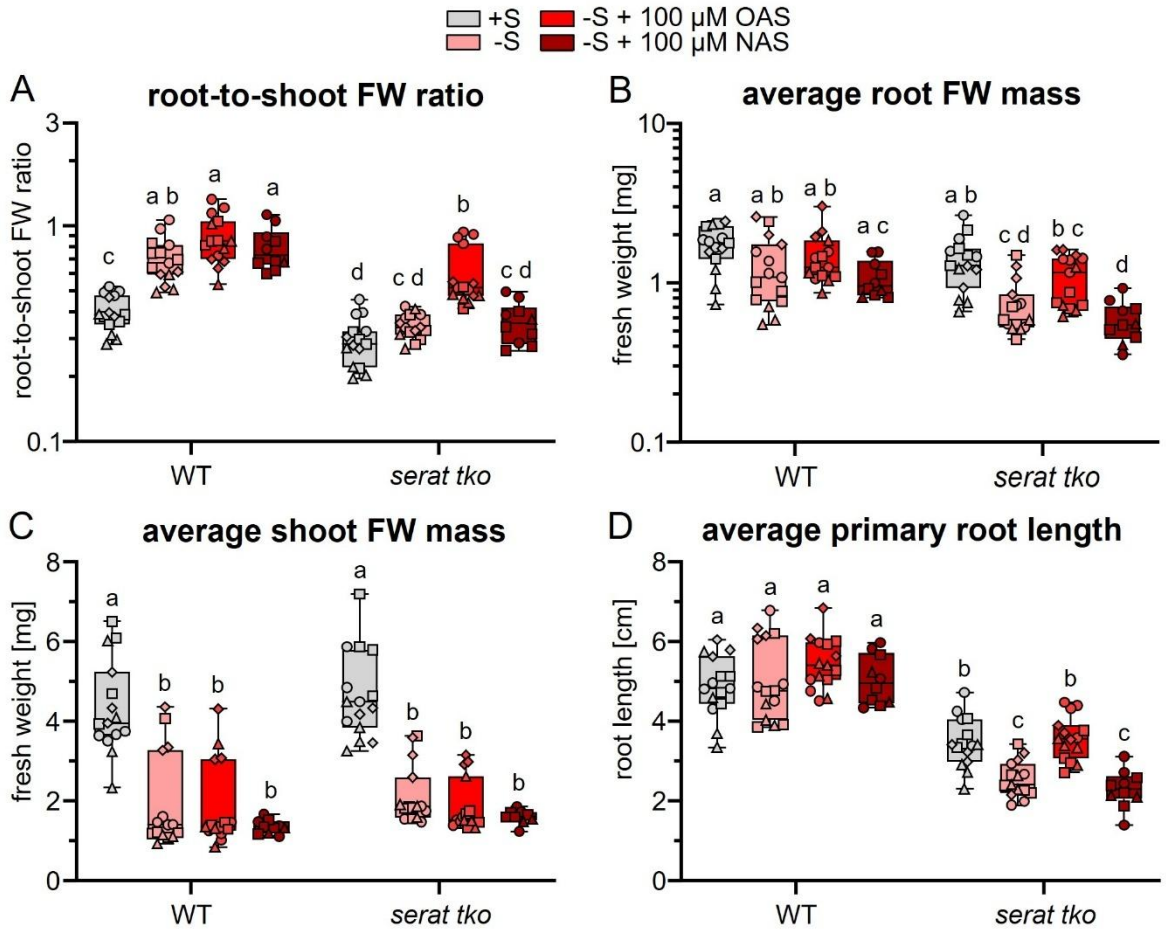

Figure 49: OAS feeding to *serat tko* improved the root-to-shoot FW ratio and maintenance of average primary root length in sulfur deficiency condition. WT and *serat tko* seeds (2.3.1) were surface sterilized (2.3.3) and grown on ½ Hoagland solid media plates supplemented with either 500 µM sulfate (+S) or 1 µM sulfate (-S) (2.3.7). Five days after germinating, OAS, NAS, or mock treatment was performed (2.3.5). After a total of 21 days, the seedlings were harvested, the primary root length measured (2.3.11), root and shoot FW quantified, and the root-to-shoot FW ratio calculated (2.3.10). **A:** root-to-shoot FW ratio. **B:** root FW. **C:** shoot FW. **D:** average primary root length. Shapes of data points indicate independent repetitions. ANOVA two-way with $p < 0.05$ ($n = 9$ of three independent replicates) was used for statistical analysis after proper data transformation.

In the context of sulfur-deficient conditions, the external application of OAS is not expected to yield general growth advantages, as the growth-limiting factor is sulfide. Nonetheless, we cannot exclude that OAS is at least partially used to generate more cysteine in *serat tko*. To investigate if an external supply of cysteine in sulfur deficiency conditions is sufficient to increase the root-to-shoot FW ratio of *serat tko*, seeds were surface sterilized (2.3.3) and sown next to WT on ½ Hoagland solid media plates supplemented with varying concentrations of cysteine but no sulfate (2.3.4). After four weeks, the root-to-shoot FW ratio was determined (2.3.10), and the average primary root length was measured (2.3.11).

WT grown on 500 µM cysteine exhibited a root-to-shoot FW ratio of 0.45, which significantly increased to 0.8 when grown on 50 µM cysteine, and reached a maximum of 1 when grown on 1 µM cysteine (Figure 50A). The root FW was maintained at 3 mg in 50 µM cysteine, similar to the 500 µM condition, but decreased to one-third of this value in the 1 µM cysteine condition (Figure 50B). Shoot FW, initially 6 mg at 500 µM cysteine, decreased to one-sixth of this value at 1 µM cysteine (Figure 50C). Further reduction of cysteine supply to 100 nM or 10 nM did not significantly increase the root-to-shoot FW ratio in WT, nor did it significantly affect root and shoot FW,

suggesting the limit of the adaptational response had been reached (Figure 50A). The similar growth patterns observed for WT at 500 µM cysteine and 500 µM sulfate, along with the response of the root-to-shoot FW ratio to decreasing cysteine concentration, suggest that cysteine is as effective a sulfur source as sulfate.

Interestingly, the *serat tko* mutant exhibited a root-to-shoot FW ratio of 0.45 similar to WT when grown on 500 µM cysteine (Figure 50 A). Furthermore, *serat tko* exhibited a WT-like average primary root length of 8 cm and demonstrated even higher root FW (3.5 mg) and shoot FW (7 mg) than WT (Figure 50). This indicates that 500 µM supply of cysteine restored *serat tko*'s growth retarded phenotype observed when grown on 500 µM sulfate. However, unlike WT, *serat tko* was unable to increase the root-to-shoot FW ratio with decreasing cysteine supply and failed to maintain root FW in 50 µM cysteine (Figure 50). While shoot FW of *serat tko* decreased similar to WT in sulfur deficiency, the mutant was unable to maintain average primary root length (Figure 50D). These findings indicate that external cysteine supply is insufficient to signal the root-to-shoot FW increase and primary root length maintenance in *serat tko* upon sulfur deficiency.

Next to reduced decreased steady-state levels, *serat tko* also exhibited affected glutathione steady-state levels in control and sulfur-deficient conditions (3.3.4). To investigate the possibility that *serat tko*'s deficiency in the root-to-shoot FW ratio increase is at least partially caused by depleted glutathione steady-state levels, *serat tko* was supplemented externally with glutathione as the only source of sulfur. Therefore, *serat tko* and WT seeds (2.3.1) were surface sterilized (2.3.3) and sown on ½ Hoagland plants supplemented with 0 µM sulfate and either 500 µM (+S) or 1 µM glutathione (-S) for four weeks (2.3.4). Afterward, the average primary root length was determined (2.3.10), and the root-to-shoot FW ratio was measured (2.3.11).

When grown on 500 µM glutathione, the WT exhibited a root-to-shoot FW ratio of 0.8, which increased further to 1 when grown on 1 µM glutathione (Figure 51 A). In contrast, the *serat tko* exhibited a reduced root-to-shoot FW ratio of 0.6 at 500 µM glutathione, which did not alter in 1 µM glutathione growth condition. While WT exhibited a root FW of 2 mg and shoot FW of 2.5 mg at 500 µm glutathione, *serat tko* exhibited trends for lower root FW and higher shoot FW explaining the ratio differences (Figure 51 B and C). In sulfur deficiency, both genotypes did not maintain the root FW, which reduced to a third of the control condition. While WT reduced the shoot FW by half in sulfur deficiency to 1.25 mg, *serat tko* exhibited a more maintained shoot FW of 1.7 mg in sulfur deficiency. Interestingly, the average primary root length of WT was maintained at 7 cm in both conditions and was not significantly different from *serat tko* with 6.5 cm (Figure 51 D).

Since WT exhibited a higher root-to-shoot FW ratio at 500 µM glutathione and lower average FWs than observed before with 500 µM sulfate or cysteine, this suggests a pre-induced sulfur deficiency response and indicates that glutathione is a less suitable sulfur source for plants than cysteine or sulfate. The reason for this could be impairments in glutathione uptake or toxicity due to its influence on redox homeostasis. Furthermore, glutathione feeding was insufficient to increase the root-to-shoot FW ratio in *serat tko* in response to sulfur deficiency but promoted maintenance of primary root length. Altogether, the root-to-shoot FW ratio of *serat tko* in response to sulfur deficiency was only improved by the external application of OAS but not by cysteine or glutathione.

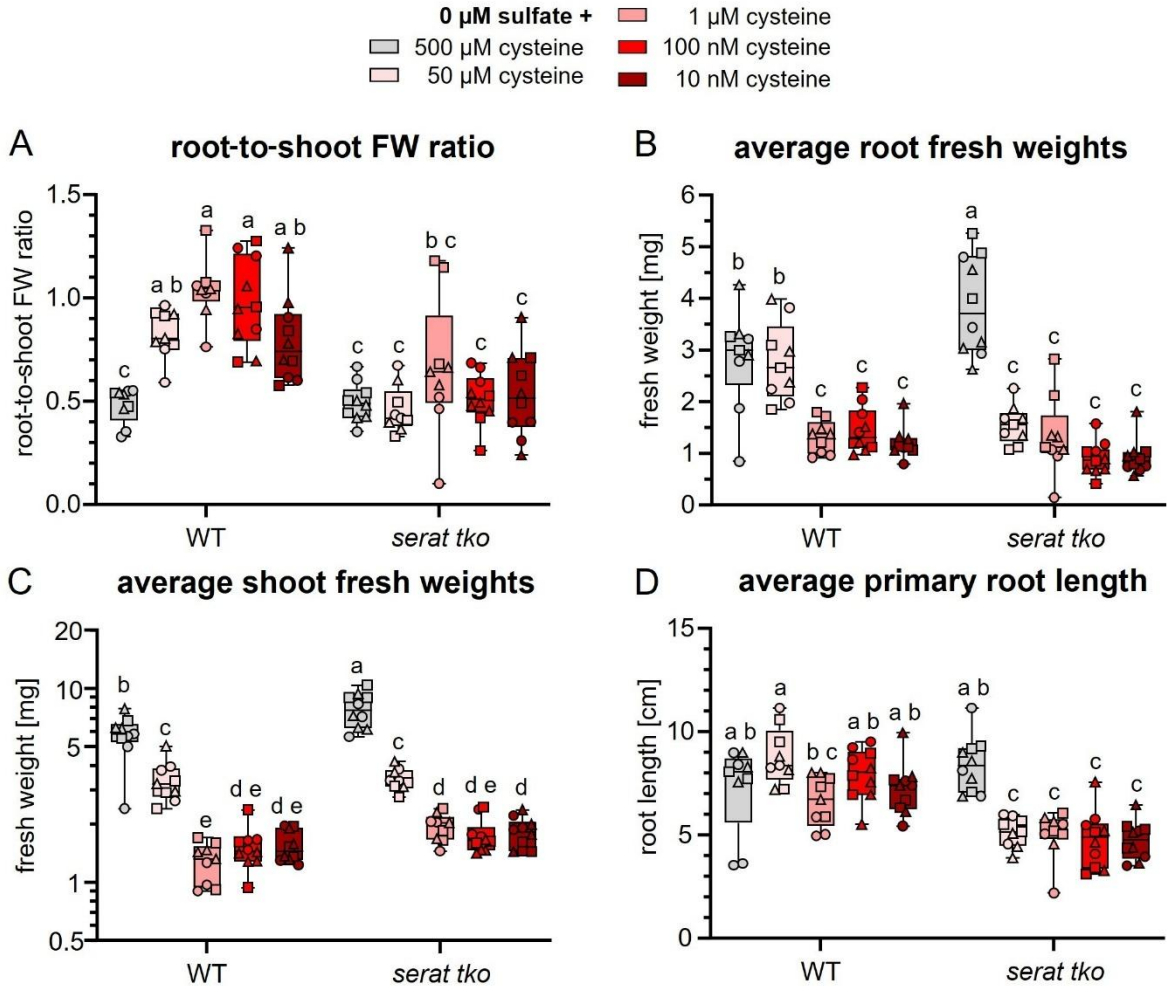

Figure 50: Cysteine feeding to *serat tko* did not improve the root-to-shoot FW ratio in the sulfur deficiency condition. *serat tko* and WT seeds (2.3.1) were surface sterilized (2.3.3) and grown on solid ½ Hoagland media plates supplemented with 0 µM sulfate and either 500 µM, 50 µM, 1 µM, 100 nM, or 1 nM cysteine, as indicated. After four weeks, the plants were harvested, primary root length measured (2.3.11), root and shoot FW quantified and the root-to-shoot FW ratio calculated (2.3.10). Shapes of data points indicate different experimental repetitions. ANOVA two-way with $p < 0.05$ ($n = 9$ of three independent replicates) was used for statistical analysis after proper data transformation. Data was obtained with the help of Daniel Szabo within his Bachelor thesis under my supervision.

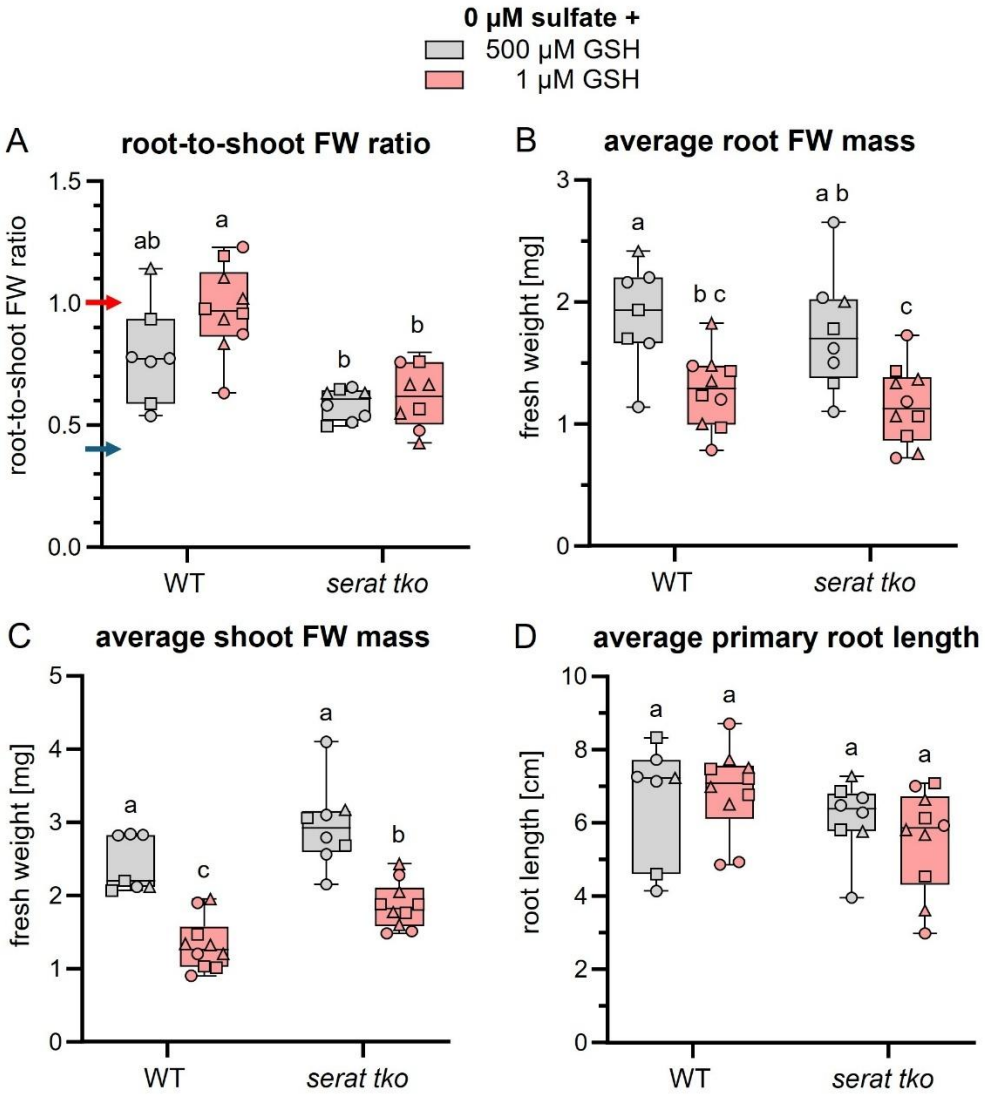

Figure 51: Glutathione feeding to *serat tko* did not improve the root-to-shoot FW ratio in the sulfur deficiency condition. *serat tko* and WT seeds (2.3.1) were surface sterilized (2.3.3) and grown on solid ½ Hoagland media plates supplemented with 0 µM sulfate and either 500 µM, or 1 µM glutathione. After four weeks, the plants were harvested, primary root length measured (2.3.11), root and shoot FW quantified, and the root-to-shoot FW ratio calculated (2.3.10). The blue and red arrows indicate the root-to-shoot FW ratios of WT when grown on 500 µM or 1 µM sulfate, respectively. Shapes of data points indicate independent experimental repetitions. ANOVA two-way with $p < 0.05$ ($n = 9$ of three independent replicates) was used for statistical analysis after proper data transformation. Data was obtained with the help of Daniel Szabo within his Bachelor thesis under my supervision.

3.3.6 The ability to increase the root-to-shoot FW ratio is independent of the location of OAS production in either root or shoot organ

An increase in the root-to-shoot FW ratio is a critical adaptive strategy for coping with sulfur deficiency stress, which is both driven by a strong reduction in shoot FW and a comparatively smaller reduction or maintenance of root FW. Both parts of the response are absent in *serat tko*, which shows higher shoot FW and reduced root FW in sulfur deficiency compared to WT (3.3.2). Previous experiments demonstrated that OAS accumulation is necessary for driving this differential growth pattern (3.3.4, 3.3.5). Nonetheless, it remains unclear whether OAS accumulation is required in a specific organ to trigger the response. To determine which organ perceives sulfur deficiency and regulates the root-to-shoot FW ratio, grafting experiments were performed using WT and *serat tko* plants. Therefore, WT and *serat tko* seeds (2.3.1) were surface sterilized (3.3.3) and grown for nine days in sulfur-sufficient conditions on ½ Hoagland solid media plates (3.3.4). Seedlings were cut at the hypocotyl and reciprocally grafted to generate chimeric plants of WT and *serat tko* (2.3.6). After one week of recovery on ½ Hoagland solid media plates supplemented with 1.4% agarose, 1% sucrose, and 500 µM sulfate, the grafts were transferred to ½ Hoagland plates containing 1 µM sulfate (2.3.4, 2.3.6). After four additional weeks, root and shoot FWs were measured to quantify the root-to-shoot FW ratio (2.3.10).

WT shoots grafted onto WT roots (WT control) exhibited a root-to-shoot FW ratio of 0.45 in control condition, consistent with previously observed values for ungrafted WT. This indicates that the grafting technique does not interfere with the adaptation to long-term sulfur deficiency. The *serat tko* shoots grafted on *serat tko* roots (*serat tko* control) exhibited the previously observed trend for a smaller root-to-shoot FW ratio of 0.3, although this was not statistically significant in this experiment (Figure 52 A). While the WT control grafts exhibited a strong increase in the root-to-shoot FW ratio in sulfur deficiency to 1.3, the *serat tko* also showed a significant increase in the root-to-shoot FW ratio to 0.6. Unexpectedly, the hetero-grafts of WT shoot/*serat tko* root and *serat tko* shoot/WT root showed both an intermediate root-to-shoot FW ratio increase in sulfur deficiency compared to WT and *serat tko* control grafts. This indicates that restoring WT-like OAS production in either organ was sufficient to increase the overall root-to-shoot FW ratio. However, OAS production in both organs seem to be necessary for the complete WT-like response. Matching previous observations, the root-to-shoot FW ratio increase in WT was driven by a decrease in shoot FW and maintenance of root FW (Figure 52 B and C). In contrast, the intermediate phenotype of the chimera plant is mainly driven by a tendency for stronger maintained root FW compared to *serat tko* roots, although not statistically significant.

The induction of the root-to-shoot FW ratio increase in response to sulfur deficiency could not been attributed to either the root or shoot alone suggesting overall OAS production capacity is more critical for the response than its specific site of synthesis. Alternatively, this may indicate that OAS production is required in both organs, with each contributing similarly to regulating the adaptive response.

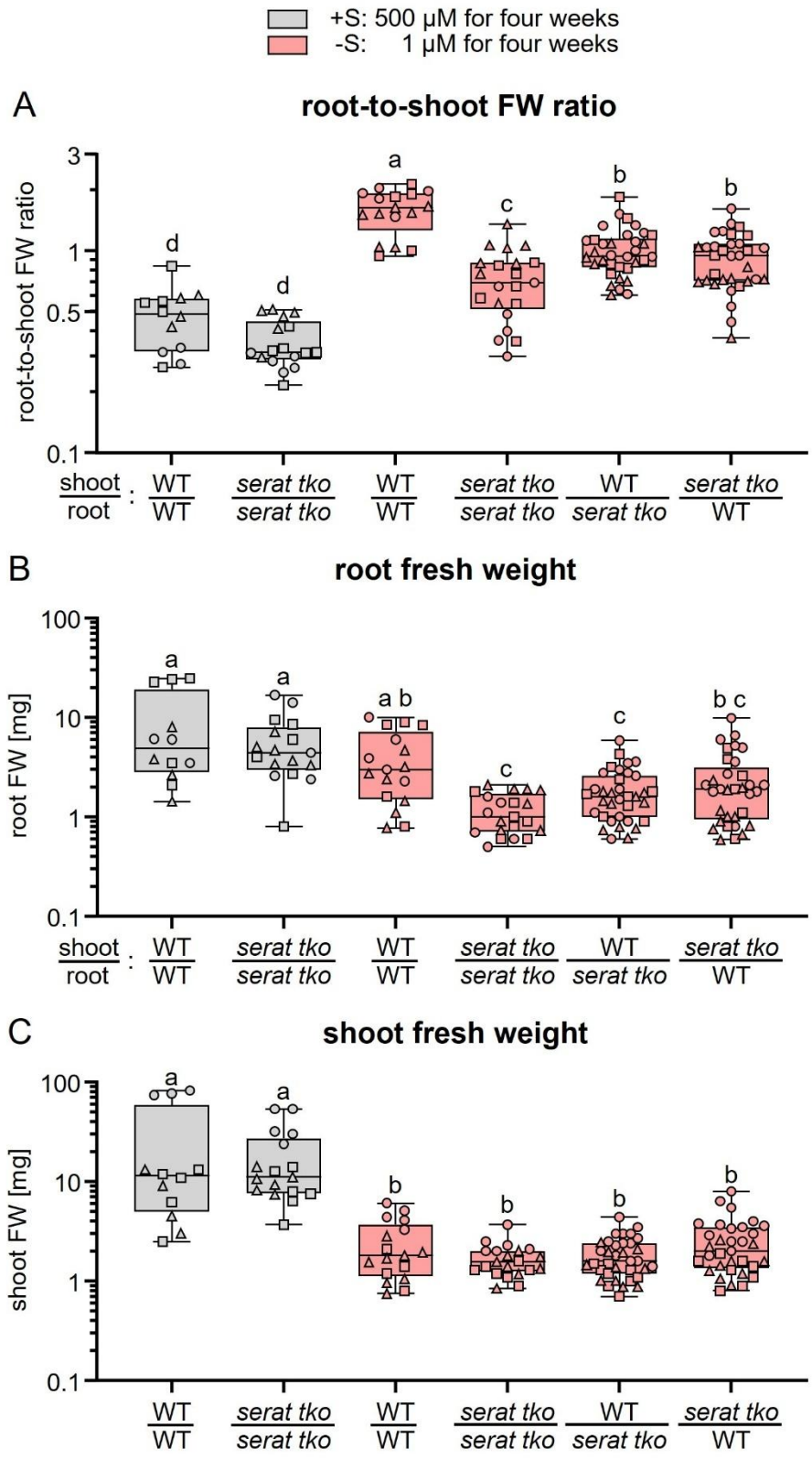

Figure 52: The root-to-shoot FW increase in sulfur deficiency is both driven by shoot and root OAS production. WT and *serat tko* seeds (2.3.1) were surface sterilized (2.3.3) and grown for nine days on sulfur-sufficient ½ Hoagland plates (2.3.4), before seedlings were cut and grafts of both genotypes generated (2.3.6). After one week of recovery on ½ Hoagland medium containing 1% sucrose, 1.4% agarose, and 500 µM sulfate, the seedlings were transferred to ½ Hoagland plates without sucrose containing either 500 µM sulfate (+S) or 1 µM sulfate (-S) (2.3.4, 2.3.6). After four additional weeks, the seedlings were investigated regarding their root and shoot FWs. ANOVA one-way with $p < 0.05$ (n = as indicated of three independent replicates) was used for statistical analysis after proper data transformation.

3.3.7 *SLIM1* is involved in the root-to-shoot FW ratio increase in response to sulfur deficiency

The previous experiments have shown that accumulation of OAS during sulfur deficiency is necessary and sufficient to increase the root-to-shoot FW ratio as a physiological adaptation to this stress (3.3.3, 3.3.4, 3.3.5). OAS accumulation triggers a set of sulfur deficiency-related marker genes called the OAS cluster genes (Hubberten *et al*., 2012a). Part of this set of genes is under control of the transcription factor *SLIM1* (Apodiakou and Hoefgen, 2023; Maruyama-Nakashita *et al*., 2006). Although a connection between OAS and *SLIM1* has not been established yet, OAS could influence transcription via the activation of *SLIM1*. To investigate if the transcription factor participates in the long-term adaptation to sulfur deficiency, the mutant *slim1-1* was tested regarding its phenotype in sulfur deficiency. Therefore, *slim1-1* and WT seeds (2.3.1) were surface sterilized (2.3.3) and sown on solid media plates supplemented with either 500 µM sulfate (+S) or 1 µM sulfate (-S) (2.3.4). After four weeks, the average primary root length was measured (2.3.11). and the root-to-shoot FW ratio quantified (2.3.10).

When growing in sulfur-sufficient control conditions, the WT and *slim1-1* showed a similar root-to-shoot FW ratio of 0.45 (Figure 53 A). In sulfur deficiency, the *slim1-1* mutant increased its root-to-shoot FW ratio significantly to 0.7 but reached only 50% of the WT-like increase (0.9). In general, *slim1-1* showed a growth retardation phenotype in sulfur sufficient control condition when compared to WT control. The root FW of 1.5 mg was a third compared to WT with 4.5 mg (Figure 53 B). *slim1-1* also exhibited with 3 mg only 30% of WT shoot FW (10 mg) in the control condition (Figure 53 C). While WT kept its root FW in sulfur deficiency at 56% of the control condition, *slim1-1* kept it at 66%. The differences in the genotypes' shoot FWs in sulfur deficiency were more pronounced, as WT reduced shoot FW to 30% of the control condition and *slim1-1* to 50% of the control condition (Figure 53 C), explaining the root-to-shoot FW ratio differences observed in Figure 53 A. The average primary root length was maintained in WT at 9.5 cm in both control and sulfur deficiency conditions (Figure 53 D). *slim1-1* exhibited a reduced average primary root length of 7.5 cm in the control condition compared to WT consistent with previous descriptions (Maruyama-Nakashita *et al*., 2006). In sulfur deficiency, *slim1-1* exhibited a trend for a further reduced average primary root length of 6.5 cm, although not statistically significant (Figure 53 D).

Since *slim1-1* exhibited only 50% of the WT root-to-shoot FW increase in sulfur deficiency, I hypothesize that *SLIM1* is at least partially involved in the physiological adaptation to long-term sulfur deficiency.

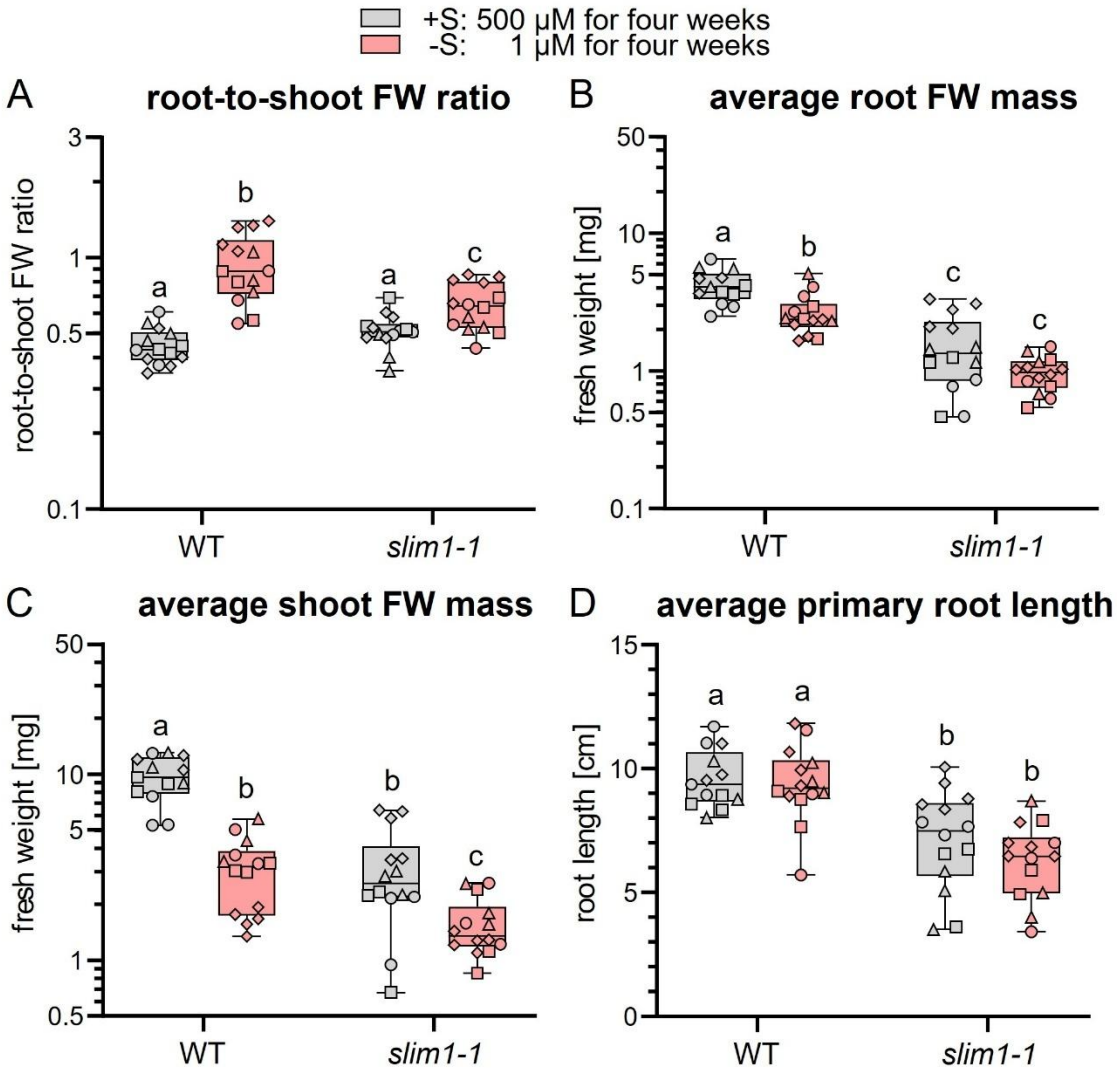

Figure 53: Root-to-shoot FW ratio phenotype of *slim1-1* on solid media plates. Seeds of WT and *slim1-1* (2.3.1) were surface sterilized (2.3.3) and grown on ½ Hoagland plates supplemented with either 500 µM sulfate (+S control) or 1 µM sulfate (-S sulfur deficiency) for four weeks (2.3.4). The root-to-shoot FW ratio (2.3.10) and the average primary root length were measured (2.3.11). **A:** root-to-shoot FW ratio. **B:** root FW. **C:** shoot FW. **D:** average primary root length. Shapes of data points define independent experimental repetitions. ANOVA two-way with $p < 0.05$ ($n = 9$ of three independent replicates) was used for statistical analysis after proper data transformation.

3.3.8 The deficiency in root-to-shoot FW ratio increase in *slim1-1* is independent of OAS steady-state levels

So far, *slim1-1* showed a 50% deficiency in root-to-shoot FW increase when growing on solid media plates with insufficient sulfate supply (3.3.7). Since previous experiments showed that weak phenotypes observed on sulfur deficiency solid media plates could be restored by using a liquid culture system (3.3.3, 3.3.4), the *slim1-1* mutant was grown next to WT in the hydroponic system and investigated regarding its phenotype. Therefore, *slim1-1* and WT seeds (2.3.1) were surface sterilized (3.3.3) and grown in the hydroponic culture in sulfur-sufficient condition for four weeks (2.3.7). Half of the plants were transferred to sulfur deficiency medium (1 µM sulfate), the rest remained in the control condition (2.3.7). Pictures of the phenotypes were taken on the day of harvest, and the root-to-shoot ratio was quantified (2.3.10).

After four weeks of growth in a liquid sulfur-sufficient control medium followed by four weeks of sulfur deficiency, the *slim1-1* mutant showed a significantly smaller root-to-shoot FW increase compared to WT (Figure 54 A), verifying the findings from the solid plate experiments (3.3.7). While the shoot FW remained similar between the genotypes in both conditions, the root FW of *slim1-1* was lower in sulfur deficiency than WT in the same condition, explaining the lower root-to-shoot FW ratio increase (Figure 54 C and D). Overall, the hydroponic culture enhanced the growth retardation phenotype of *slim1-1* observed with the solid media plate culture (Figure 54 B).

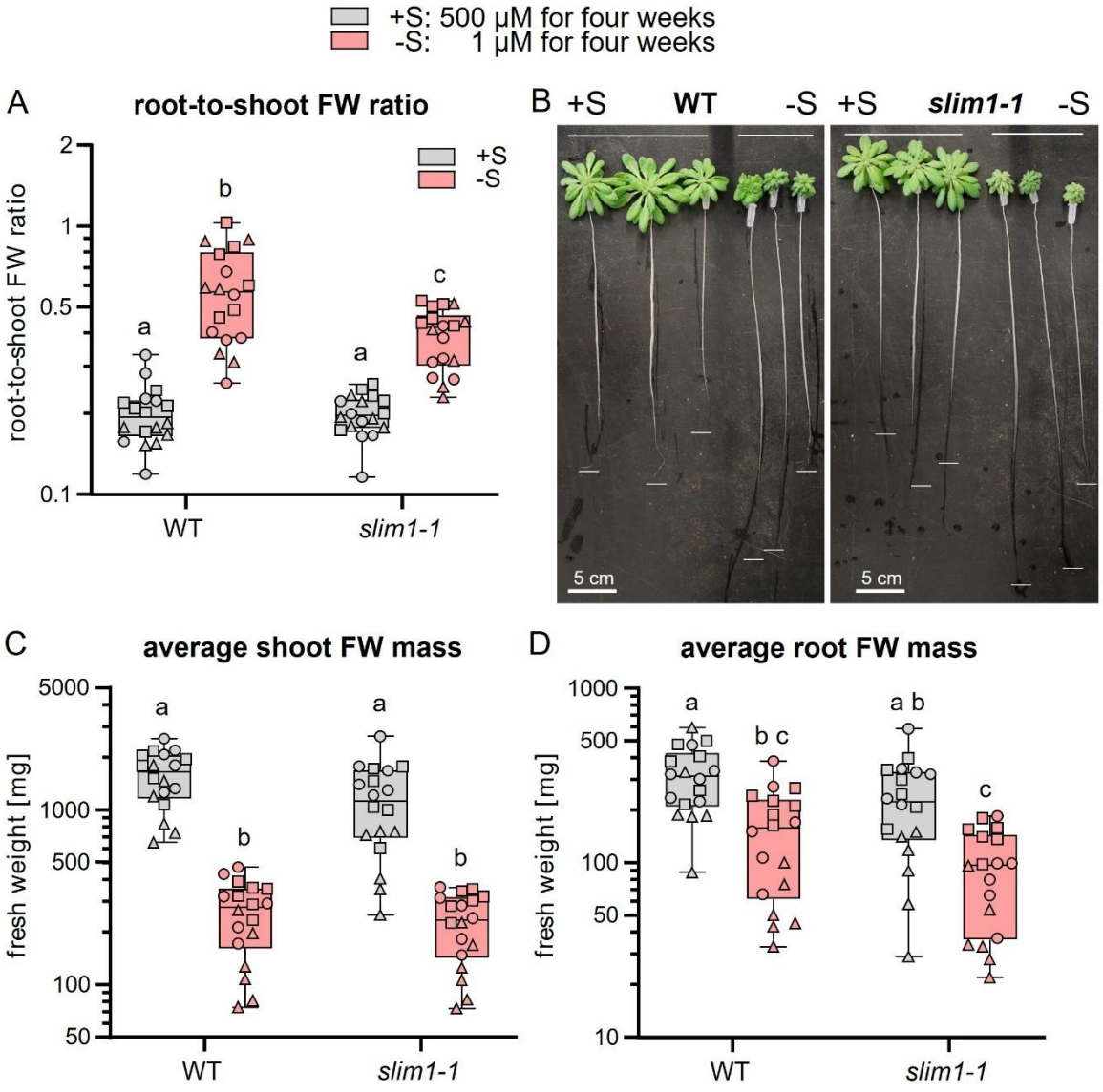

Figure 54: Phenotype of *slim1-1* after a shift from four weeks control to four weeks sulfur deficiency condition. *slim1-1* (2.3.1) were grown next to WT in ½ Hoagland medium containing 500 µM sulfate (+S) (2.3.7). Half of the plants were subjected to ½ Hoagland medium containing 1 µM sulfate for four additional weeks (-S), the other half remained in the control medium (2.3.7). Pictures were taken on the day of harvest, and the root-to-shoot FW ratio was determined (2.3.7). **A:** root-to-shoot FW ratio. **B:** photographs of representative individuals **C:** root FWs. **D:** shoot FWs. Shapes of data points indicate independent replicates. ANOVA two-way with $p < 0.05$ was used for statistical analysis after proper data transformation.

Previously, mutants affected in the root-to-shoot FW ratio increase in sulfur deficiency were correlated with an impaired accumulation of OAS steady-state levels (3.3.4). Since I hypothesize *SLIM1* to work downstream of OAS accumulation in transferring the sulfur deficiency signal, I hypothesize WT-like OAS-steady-state levels in this mutant. To investigate the metabolite steady-state levels of *slim1-1*, the harvested shoot and root material from the hydroponic experiment were ground, and metabolites were extracted (2.6.1), OAS and thiols labeled (2.6.2, 2.6.3) and quantified with UPLC (2.6.5).

Matching to the hypothesis, *slim1-1* exhibited WT-like OAS steady-state levels in shoots and roots, which increased WT-like in sulfur deficiency (Figure 55 A and B). The cysteine steady-state levels of *slim1-1* were also WT-like in control and sulfur deficiency conditions in shoots and roots (Figure 55 C). The same was observed in the glutathione levels in the roots, while in the shoots, *slim1-1* exhibited a significantly 50% lower glutathione steady-state level than WT (Figure 55 F).

Taken together, the WT-like metabolite levels in *slim1-1* could not explain the deficient root-to-shoot FW ratio increase in sulfur deficiency. The fact that the lack of a transcription factor influences the physiological change in growth pattern suggests that *slim1-1* is involved in the signaling chain between sensing and translating the stress response. The WT-like OAS levels in *slim1-1* support the hypothesis that *SLIM1* acts downstream of OAS accumulation as a response to sulfur deficiency.

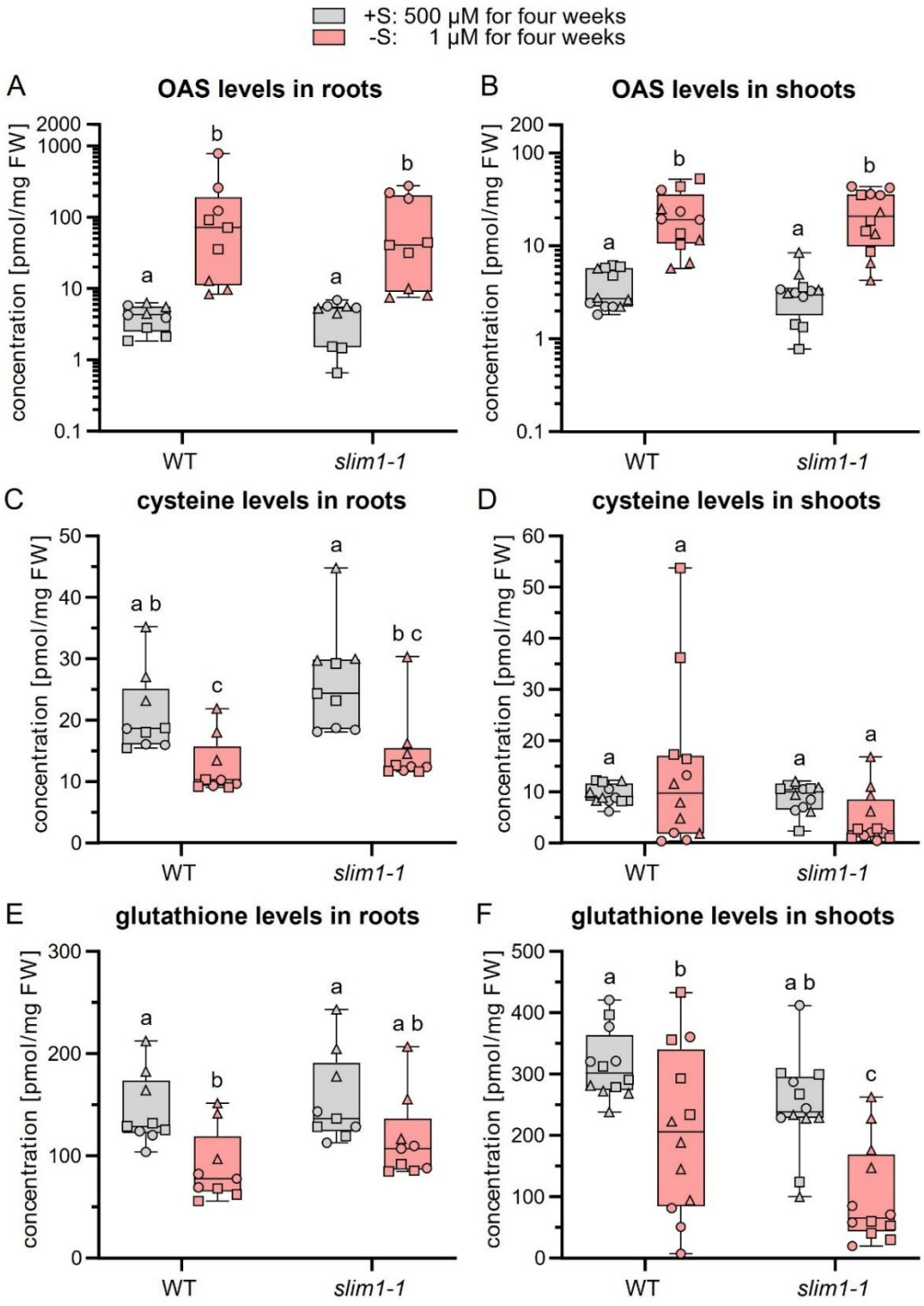

Figure 55: Metabolite steady-state levels of *slim1*-1 after a shift from four weeks control to four weeks sulfur deficiency condition. *slim1-1* was grown next to WT for four weeks in ½ Hoagland medium (500 µM sulfate, +S) (2.3.7). Half of the plants were transferred to ½ Hoagland medium supplemented with 1 µM sulfate (sulfur deficiency, -S), the other half remained in +S medium. After additional four weeks, the plants were harvested and used to extract (2.6.1) and label OAS (2.6.2) and thiols (2.6.3) for UPLC quantification (2.6.5). **A:** OAS level in roots **B:** OAS level in shoots. **C:** cysteine level in roots. **D:** cysteine level in shoots. **E:** glutathione level in roots. **F:** glutathione level in shoots. Shapes of data points indicate independent experimental repetition. ANOVA two-way with $p < 0.05$ was used for statistical analysis after proper data transformation.

3.3.9 OAS feeding to *slim1-1* showed a slight improvement of the root-to-shoot FW ratio in sulfur deficiency

slim1-1 showed a defect in the root-to-shoot FW ratio on solid media plates (3.3.7) and in hydroponic culture, which could not be explained by reduced OAS steady-state levels (3.3.8). According to the hypothesis of *SLIM1* acting downstream in translating the OAS signal to induce the root-to-shoot FW ratio changes, external feeding of OAS should not increase the root-to-shoot FW ratio of *slim1-1* in sulfur deficiency. To test this hypothesis, an OAS feeding experiment was performed with *slim1-1* in sulfur deficiency. Therefore, WT and *slim1-1* (2.3.1) seeds were surface sterilized (2.3.3) and sown on solid media plates supplemented with either 500 µM (+S) or 1 µM sulfate (-S) (2.3.4). OAS treatment was applied three times a week together with the negative controls of NAS and mock treatment for a total of 21 days (2.3.5). Afterward, the average primary root length was quantified (2.3.11), and the root-to-shoot FW ratio was determined (2.3.10).

WT showed the expected increase in root-to-shoot FW ratio from 0.5 in the control condition to 1.2 in sulfur deficiency, which was not further increased by OAS or NAS feeding (Figure 56 A). *slim1-1* showed a WT-like root-to-shoot FW ratio in the control condition, which increased significantly to 50% of the WT increase in sulfur deficiency (Figure 56 A). Interestingly, the OAS feeding improved the root-to-shoot FW ratio increase of *slim1-1* from 0.9 to 1, while NAS feeding showed no effect (Figure 56 A). The root FWs of WT and *slim1-1* were similar in control condition, but in sulfur deficiency, *slim1-1* exhibited one-third lower root FWs than WT (Figure 56 B). While OAS or NAS treatment did not affect the root FW in WT, the OAS treatment but not NAS treatment led to a trend of improved root FW of 0.6 to 0.7 in sulfur deficiency for *slim1-1* mutant (Figure 56 B). In the control condition, *slim1-1* exhibited the significantly lower shoot FWs of 2 mg compared to 3 mg of WT. In sulfur deficiency, the shoot FWs were similar between the genotypes regardless of OAS or NAS feeding (Figure 56 B). While WT maintained the average primary root length of 4.4 cm in sulfur deficiency regardless of additional OAS and NAS, the *slim1-1* showed a significantly lower root length of 3.6 in sulfur deficiency. While the OAS feeding slightly improved the root length to 3.8 cm, although not statistically significant, the NAS treatment had no effect on root length (Figure 56 D).

Taken together, feeding OAS to *slim1-1* resulted in a trend for an increased root-to-shoot FW ratio in sulfur deficiency mainly driven by a trend for improved root FW maintenance. The same positive effect of OAS on *slim1-1* was observed in maintaining the average primary root length in sulfur deficiency. Although all improvements were non-significant trends, the combination and pattern are consistent with the positive effects observed by OAS feeding on *serat tko*. This indicates that *slim1-1* is at least still partially perceptive to OAS treatment. Nonetheless, the OAS feeding was insufficient to trigger the complete WT-like response.

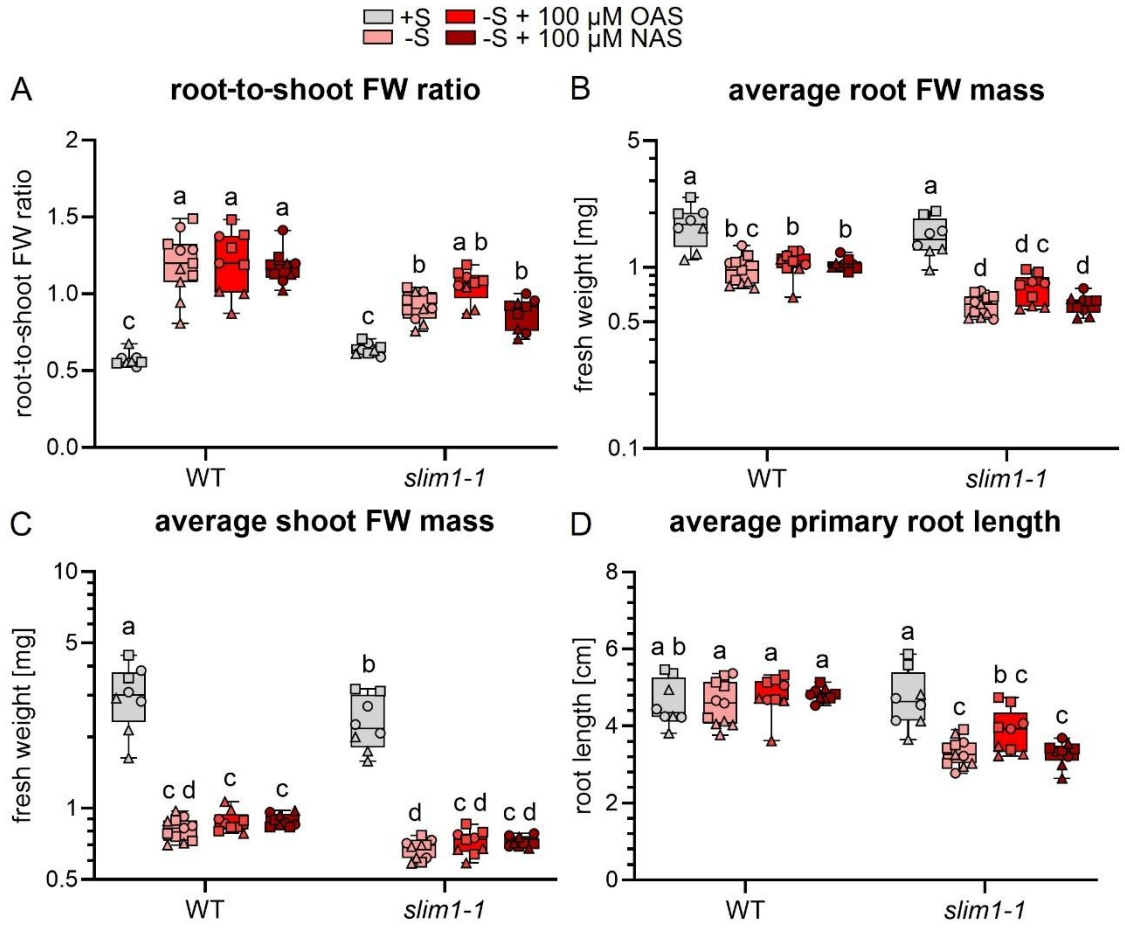

Figure 56: OAS feeding to *slim1-1* resulted in a positive trend for increased root-to-shoot FW ratio in sulfur deficiency. *slim1-1* WT and *serat tko* seeds (2.3.1) were surface sterilized (2.3.3) and grown on ½ Hoagland solid media plates supplemented with either 500 µM sulfate (+S) or 1 µM sulfate (-S) (2.3.7). Five days after germinating, OAS, NAS, or mock treatment was performed (2.3.5). After a total of 21 days, the seedlings were harvested, the primary root length measured (2.3.11), root and shoot FW quantified, and the root-to-shoot FW ratio calculated (2.3.10). **A:** root-to-shoot FW ratio. **B:** root FW. **C:** shoot FW. **D:** average primary root length. Shapes of data points indicate independent repetitions. ANOVA two-way with $p < 0.05$ ($n = 9$ of three independent replicates) was used for statistical analysis after proper data transformation.

3.3.10 The affected root-to-shoot FW ratio in *cad2* indicates further factors influencing the adaptation to sulfur deficiency response

So far, the root-to-shoot FW ratio increase in response to sulfur deficiency was linked to the OAS steady-state levels (3.3.4). Although the most affected mutants in the phenotype, namely *serat tko* and *Q2;1*, also showed depleted cysteine and glutathione steady-state levels, external feeding of either did not improve the root-to-shoot ratio in *serat tko* (3.3.5). In contrast to cysteine feeding, glutathione feeding to *serat tko* resulted in the maintenance of the average primary root length in sulfur deficiency. To further investigate glutathione's role in the adaptation to long-term sulfur deficiency, the mutant *cad2* was investigated regarding its root-to-shoot FW ratio increase in sulfur deficiency. The activity of *GSH1* in *cad2* seedlings is reduced to only 40%, leading to 55 - 70% lower glutathione steady-states levels (Howden *et al.*, 1995). Therefore, *cad2* and WT seeds (2.3.1) were surface sterilized (2.3.3) and grown on solid media plate in sulfur sufficient (500 µM sulfate) or sulfur deficient condition (1 µM sulfate) (2.3.4) for four weeks. Afterward, the average primary root length (2.3.11) and the root-to-shoot FW ratio were measured (2.3.10).

cad2 exhibited a WT-like root-to-shoot FW ratio of 0.35 in the control condition. While WT increased its root-to-shoot FW ratio to 1 in sulfur deficiency, the *cad2* showed an increase to 0.8, resulting in 70% of the WT response (Figure 57 A). This difference was mainly driven by the impaired maintenance of root FW in *cad2* in sulfur deficiency, which was 10% lower than WT. The shoot FWs were similar between the genotypes and the growth conditions (Figure 57 B and C). In control condition, both genotypes exhibited primary root lengths of 9.5 cm. While WT was able to maintain the root length at 8.5 cm, the *cad2* exhibited a reduced average primary root length of 6 cm in sulfur deficiency (Figure 57 D). These findings indicate that glutathione is essential for the root-to-shoot FW ratio increase in sulfur deficiency by maintaining average primary root length and average root FW.

The *sir1-1* mutant previously investigated on sulfur deficiency media plates also showed an affected root-to-shoot FW ratio, which was mainly driven by an insufficient reduction of shoot FW (2.3.2 Figure 39). To investigate whether the inability to reduce shoot FW in *sir1-1* and the inability to maintain root FW in *cad2* are acting in the same molecular pathway, the cross of both mutants *sir1cad2* was investigated (Speiser *et al*., 2018).

In the control condition, all mutants *cad2*, *sir1-1*, and *sir1cad2* showed a WT-like root-to-shoot FW ratio. Compared to its parents, *sir1cad2* showed with 30% of WT an even stronger defect in root-to-shoot FW ratio increase in response to sulfur deficiency (Figure 57 A). Since the phenotype worsens in the double mutant, both mutations must affect the phenotype independently. The root FW of *sir1cad2* was similar to *cad2* in the control condition but was even further reduced in the double mutant in the sulfur-deficient condition (Figure 57 B). While *cad2* exhibited a nonsignificant trend for reduced shoot FW in sulfur deficiency compared to WT, the double mutant exhibited 5% less shoot FW in sulfur deficiency compared to WT (Figure 57 C). The most striking difference was observed in the average primary root length. Although both *cad2* and *sir1-1* showed WT-like average primary root lengths in the control condition, the double mutant exhibited a root length of only 60% WT (Figure 57 D). The root length of *sir1cad2* was even further significantly decreased to 45% WT in sulfur deficiency, showing the inability of root length maintenance observed in *cad2*.

Taken together, the cross with *sir1-1* worsens the *cad2* phenotype in the double mutant regarding both root and shoot FW maintenance and average primary root length in sulfur deficiency. I hypothesize that the small defect in the root-to-shoot FW ratio increase of 90% WT for *sir1-1* when grown in sulfur deficiency on solid media plates is caused by the overall reduced cysteine flux, thereby limiting its growth rate necessary to implement the differences in the growth patterns. This affects the root-to-shoot FW ratio independently of the mutation in glutathione biosynthesis as observed for *cad2*, explaining the worsened phenotype of *sir1cad2*. Nonetheless, the experiments must be repeated in the hydroponic culture, and metabolite steady-state levels must be measured to draw final conclusions.

Overall, these findings suggest that the root-to-shoot FW ratio increase in sulfur deficiency is dependent not only on OAS accumulation but also on glutathione biosynthesis and general translation rate.

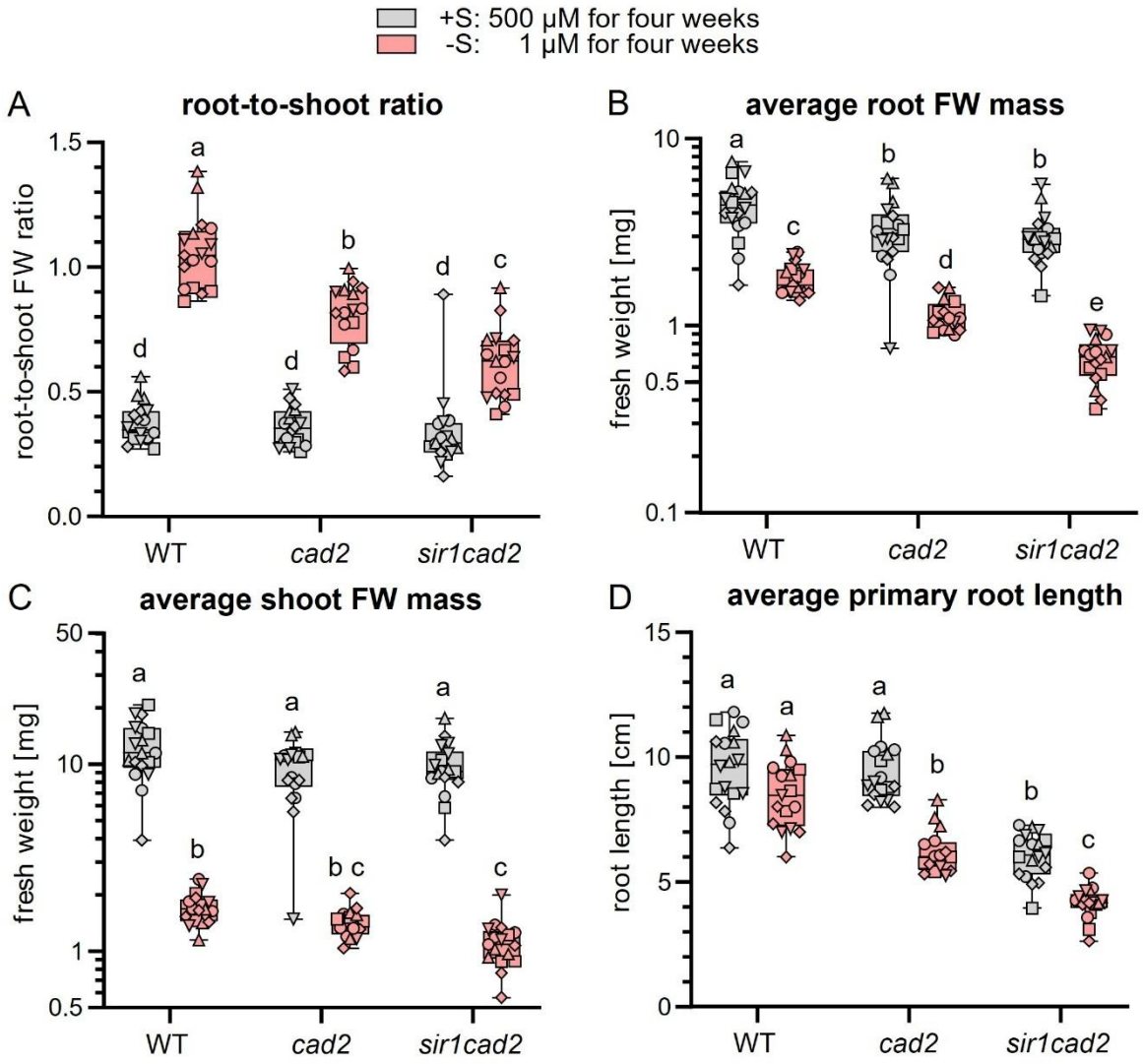

Figure 57: Root-to-shoot FW ratio phenotype of *cad2* and *sir1cad2* on solid media plates. Seeds of *cad2* and *sir1cad2* (2.3.1) were surface sterilized (2.3.3) and grown on ½ Hoagland plates supplemented with either 500 µM sulfate (+S control) or 1 µM sulfate (-S sulfur deficiency) for four weeks (2.3.4). The root-to-shoot FW ratio (2.3.10) and the average primary root length were measured (2.3.11). **A:** root-to-shoot FW ratio. **B:** root FW. **C:** shoot FW. **D:** average primary root length. Shapes of data points define independent experimental repetitions. ANOVA two-way with $p < 0.05$ (n = 9 of three independent replicates) was used for statistical analysis after proper data transformation.

4. Discussion

4.1 Understanding the impact of the cCSC on transcription

The cCSC is composed of SERAT1;1 and OAS-TL A. Its strategical position in the cytosol makes it a modulator of cysteine biosynthesis by integrating the two molecular signals sulfide and OAS (Haas *et al*., 2008), which are primarily produced in the plastids and mitochondria, respectively (Wirtz and Hell, 2006). Furthermore, the cCSC is unique in its close proximity to the nucleus, where OAS-TL A can enter independently of the sulfur status (Haberland, 2017). Since both, the *oastlA* and *serat1;1,* mutant showed a delayed upregulation of the sulfate uptake rate increase after six hours of sulfur deficiency, the cCSC was hypothesized to have sensory and signaling functions in the early onset of sulfur deficiency (Haas, 2010). The delayed sulfate uptake rate of the cCSC mutants was further linked to the delayed transcript induction of *SULTR1;1* (Speiser, 2014), the sulfur starvation-induced sulfate transporter (Takahashi *et al*., 2000). Transcriptome analysis of *oastlA* and *serat1;1* had further corroborated this hypothesis since similar delayed transcript responses were identified for other sulfate deficiency marker genes like *SDI1* or *GGCT2;1* (Speiser, 2014).

In this work, these transcript effects have not been reproduced, as the *oastlA* and *serat1;1* mutant exhibited WT-like upregulation of *SDI1*, *GGCT2;1*, and *SULTR1;1* transcript upon six hours of sulfur deficiency (3.1.1 Figure 3, 3.1.2). After having secured the molecular identity of the T-DNA insertions and absence of SERAT1;1 and OAS-TL A proteins in the respective mutants (Supplemental Figure 1), key experimental variables, such as the timing and severity of sulfur deficiency stress, were ruled out to potentially cause the conflicting observations (3.1.2 Figure 4 and Figure 5). Furthermore, *oastlA* and *serat1;1* exhibited WT-like transcript levels in seven genes (3.1.3 Figure 6), which had previously been reported to be the most strongly up- or downregulated in the mutants under sulfur-sufficient conditions (Speiser, 2014). Epigenetic adaptation of the mutants over the time period since Speiser's experiments was ruled out as a contributing factor, as newly generated cCSC mutants using CRISPR/Cas9 editing also exhibited WT-like upregulation of *SDI1* and *GGCT2;1* in response to six hours sulfur deficiency (3.1.4). At this point, the reason for the differing observations remains unresolved. A potential contributing factor could be the climate chamber change, which included a switch from neon tubes to LED illumination, and which was completed shortly before the start of my experiments. Although technically key growth parameters such as temperature, humidity, light duration and intensity were the same, it cannot be ruled out that an unknown factor was altered or lost in the new growth chambers.

4.1.2 Transcriptome analysis suggests the cCSC balances metabolism with immunity in control condition

Previous transcriptome analysis had identified 841 differentially expressed genes in *oastlA* and 320 in *serat1;1* in sulfur sufficient control condition in root tissue (Speiser, 2014). Constitutive upregulation of a senescence-related gene cluster was also verified for the shoot (Schiel, 2020). To verify known transcript effects or find new transcriptional responses using an untargeted approach, mRNAseq was performed on the newly with CRISPR/Cas9 generated mutants *oastlA_cr#2* and *serat1;1_cr#2* shoot material cultured in control condition (3.1.5). Therefore, the mutants exhibited similar transcriptomes to the WT, as indicated by the correlation heat map and principal component analysis, which revealed no clear clustering of the genotypes (Figure 14). Consistent with this, only four genes were found to be differentially regulated in *oastlA_cr#2*

compared to WT (Figure 15, Table 13), while *serat1;1_cr#2* exhibited no significant changes in transcript level (Figure 16). Since the absence of OAS-TL A and SERAT1;1 protein was verified in *oastlA_cr#2* and *serat1;1_cr#2* (Figure 13), this indicates a minor influence on transcription only for *OAS-TL A* in the control condition, which might be explained by its additional nuclear localization (Haberland, 2017).

Consistent with the absence of OAS-TL A protein, the *OAS-TL A* transcript was downregulated to only 4.8%, representing the most significant change in *oastlA_cr#2* (Table 13). The second most significant change was the upregulation of *ACTIN-RELATED PROTEIN 9 (ARP9)* by 2.87-fold (Table 13). Its specific function remains unresolved, but the ARP family is highly conserved among higher eukaryotes with functions in chromatin remodeling and modification, transcription, and DNA repair. This makes them essential for the epigenetic control of the cell cycle and cell proliferation (Meagher *et al*., 2009). So far, *ARP7* and *ARP4* are the best-characterized members of the ARP family in Arabidopsis. *ARP7* was shown to be essential for embryogenesis, plant architecture, and floral organ abscission (Kandasamy *et al*., 2005), whereas *ARP4* as part of the SWR1 chromatin-remodeling complex was found to regulate gene expression of especially defense-related gene loci (Nie and Wang, 2021). Studying *arp9* mutants could reveal whether it shares functional similarities with ARP4 or ARP7.

The disease resistance-related *RPP13* was the third most significantly differentially regulated gene with a downregulation to 16.8% in *oastlA_cr#2* (Table 13). The gene confers resistance to different isolates of the downy mildew pathogen *Hyaloperonospora arabidopsidis* due to its highly polymorphic leucine-rich repeat (LRR) (Bittner-Eddy and Beynon, 2001; Bittner-Eddy *et al*., 2000; Hall *et al*., 2009). In wheat, the *TaRPP13-3* gene was shown to confer resistance to powdery mildew (Liu *et al*., 2020) and in potatoes, *RPP13-11* was found to participate in disease defense by regulating photosynthesis-related genes and the dynamic balance of reactive oxygen species within the chloroplast (Yuan *et al*., 2024). *RPP13* might function similarly to the *RPP1-like* gene present in the *Landsberg erecta* ecotype, which was shown to recognize the mutated OAS-TL A protein known as old3-1 (Shirzadian-Khorramabad *et al*., 2010; Tahir *et al*., 2013). The RPP1 resistance protein recognizes the ATR1 effector from *Hyaloperonospora arabidopsidis* through its LRR domain, triggering immune responses (Krasileva *et al*., 2010). In *old3-1*, RPP1-like causes auto-necrosis, possibly by mistaking the mutation in OAS-TL A protein for the result of a pathogen attack (Tahir *et al*., 2013). Alvarez *et al*. (2012) found *oastlA* T-DNA mutants *oas-a1.1* (SALK_072213) *and oas-a1.2* (SAIL_94_E12) to be sensitive to biotrophic and necrotrophic pathogens, corroborating a possible function for OAS-TLA in an immune response.

The *MRDI* (*mto1 RESPONDING DOWN*) was the most upregulated transcript in *oastlA_cr#2*, with 187.5 times the WT level (Table 13). *MRDI* is predicted to have a dual subcellular location, mainly cytosolic but weakly nuclear. It was first identified as being strongly downregulated in the *mto1-1* mutant that over-accumulates soluble methionine (Inaba *et al*., 1994). *MRD1* is a cystathionine γ-synthase catalyzing the first step of methionine biosynthesis, and mutation in *MRD1* results in the loss of the negative feedback regulation of the pathway (Chiba *et al*., 1999; Suzuki *et al*., 2001). Its strong overexpression might indicate an inhibitory function of *OAS-TL A* on this gene, indicating a possible mechanism of co-regulating methionine biosynthesis by cysteine biosynthesis. After verification of the differentially regulated transcript level with qRT-PCR, it remains to be tested if altered methionine steady-state levels in *oastlA_cr#2* accompany *MRD1* overexpression. So far, methionine levels have not been investigated in the *oastlA* T-DNA mutant (Heeg *et al*., 2008). As a

direct target of the OZF1 transcription factor in promoting salicylic acid-mediated defense, *MRD1* might also be involved in immune responses (Singh *et al*., 2022).

A possible involvement of OAS-TL A in cell cycle control and immune response was also reflected in the KEGG pathway and GO analyses (Table 14, Figure 17). Notably, *serat1;1_cr#2* and *oastlA_cr#2* exhibited similar KEGG and GO profiles (Table 15, Figure 18). Both mutants share seven out of the ten most affected GO categories, such as upregulated 'cell cycle', 'photosynthesis', 'photosynthesis light reaction', and 'microtubule-based processes' and the downregulated 'response to salicylic acid', 'response to fungus', and 'defense response to bacterium'. This suggests an inhibitory role of primary energy metabolism while promoting defense metabolism in control conditions for both OAS-TL A and SERAT1;1. Given the distinct enzymatic functions of both proteins, the high degree of shared GO alterations could indicate the cCSC as the factor important for balancing primary energy metabolism with defense responses in control conditions. To test this hypothesis, pathogen susceptibility assays should be performed, particularly with *Hyaloperonospora arabidopsidis* as *RPP13* was found downregulated in *oastlA_cr#2*. If *serat1;1_cr#2* also exhibits susceptibility, this would support a role for cCSC in conferring pathogen immunity. Further investigations, including mRNA sequencing under sulfur deficiency and root-specific transcriptomic analysis, could refine the understanding of the transcriptional impact of the cCSC. Additionally, incorporating the *oastlA_cr#1*, *serat1;1_cr#1*, as well as the T-DNA mutants in the experiments, would enhance result robustness. As a closing remark, one could speculate that the presence of a pathogen in the old climate chamber might have influenced the transcriptional responses of the cCSC mutants found by Speiser (2014).

4.2 Function of SERAT group three isoforms in sulfur deficiency

The SERAT family has three major isoforms, SERAT1;1, SERAT2;1, and SERAT2;2, all with redundant functions in OAS production (Watanabe *et al*., 2008b). In comparison, the catalytic activity of SERAT three is negligible, and their sulfur deficiency induced transcriptional upregulation suggests a regulatory function rather than metabolic (Kawashima *et al*., 2005; Watanabe *et al*., 2008b). Haberland (2017) found both SERAT3;1 and SERAT3;2 proteins as potential interaction partners of SERAT1;1 and hypothesized possible functions in regulating the cCSC.

4.2.1 Evolutionary conservation and unique features of SERAT group three isoforms

Next to Arabidopsis, the presence of SERAT3 was reported in *V. vinifera* and *S. lycopersicum* (Liu *et al*., 2022; Tavares *et al*., 2015). Using the web-based tool phylogene (1.4.6) I found the SERAT three isoforms present across the whole plant kingdom (3.2.1), as at least one isoform was identified in single-cell green algae, early land plants and major crop plants (Figure 19). This widespread distribution suggests an evolutionarily conserved and functionally significant role. The emergence of SERAT3 paralogs, for example, in Arabidopsis, cotton, wheat, and soybean, might indicate further functional specialization among isoforms (Figure 19). By comparing SERAT3 of *Arabidopsis thaliana*, *Vitis vinifera* and *Solanum lycopersicum*, SERAT3 proteins were consistently localized in the cytosol (Kawashima *et al*., 2005; Liu *et al*., 2022; Tavares *et al*., 2015). While *SlSERAT3;1* was also highly induced upon sulfur deficiency, the *VvSERAT2;1* was identified as the stress-induced isoform in *V. vinifera* instead *of VvSERAT3;1* (Liu *et al*., 2022; Tavares *et al*., 2015). Interestingly *SlSERAT3;1* exhibited high OAS productivity and CSC formation indicating

major species-specific differences in specialization of SERAT isoforms (Liu *et al*., 2022). The strong sulfur deficiency response in Arabidopsis was confirmed (3.2.2 Figure 24) with seedlings exhibiting a 60-fold induction of *AtSERAT3;2* expression after 96 hours, consistent with previous reports (Kawashima *et al*., 2005). Additionally, the significantly lower expression under control conditions compared to *SERAT1;1* was confirmed using the eFP browser and Arabidopsis root and shoot single-cell atlas (3.2.2, Figure 21, Figure 22, Figure 23) (Kawashima *et al*., 2005). Thereby, *SERAT3;1* always exhibited at least twice as much expression than *SERAT3;2*, whose expression was even more restricted to vasculature tissue than *SERAT3;1* (3.2.2, Figure 21, Figure 22, Figure 23), indicating specializations of SERAT3 isoforms in Arabidopsis.

4.2.2 SERAT3;2 exhibits both cytosolic and nuclear localization *in vivo*

Previously, Kawashima *et al*. (2005) localized SERAT3;1 and SERAT3;2 to the cytosol using only the first 100 amino acids fused to GFP. The subcellular localization of SERAT3;2 to the cytosol was verified using a fusion construct of full-length SERAT3;2 coupled C-terminally with mCherry under the control of the *Ubiquitin10* promoter (Figure 25). Interestingly, in addition to the cytosolic signal, the mCherry signal was also found in the nucleus, which was verified by a co-localized DAPI signal (Figure 25). Interestingly, the images used by Kawashima *et al*. (2005) to determine subcellular localization indicated an additional nuclear presence of SERAT3;1, SERAT3;2, and SERAT1;1. However, back then this was attributed to the use of truncated protein versions. This interpretation appears valid, as full-length SERAT1;1 fused to CFP is exclusively localized in the cytosol (Haberland, 2017). To corroborate the here-found nuclear localization of the full-length SERAT3;2, protoplasts from the stably transformed prUbi::SERAT3;2-mCherry line could be analyzed to achieve a clearer subcellular visualization of SERAT3;2 localization. Additionally, Western blot analysis using an anti-mCherry antibody could be employed to confirm the presence of full-length SERAT3;2-mCherry in the cytosolic and nuclear cell extract fractions. Testing full-length SERAT3;1 for nuclear localization using the same techniques could establish nuclear localization as a defining feature of the SERAT group three isoforms in Arabidopsis and support the hypothesis of a regulatory rather than a solely metabolic function.

4.2.3 Minimal promoter drives *SERAT3;2* sulfur deficiency and cell-type specific

To verify the native localization of SERAT3;2 *in vivo*, the 460 bps upstream of the *SERAT3;2* start codon was used as the minimal native promoter. The promoter was sufficient to drive SERAT3;2-mCherry expression exclusively for sulfur deficiency condition and cell-type specific in the stele cells of *A. thaliana* roots (Figure 25). This is consistent with the single-cell localization of SERTA3;2 transcript in the single-cell root atlas (Figure 23)(Shahan *et al*., 2022). This stable transformed plant line could serve as a tool to investigate the induction kinetics of *SERAT3;2* expression *in vivo* in a concentration and cell type-specific manner. It remains to be tested if the sulfur deficiency induction depends on the SURE core motif GAGAC found 227 bp upstream of the start codon as part of the 5' UTR in the minimal promoter as marked in the vector map (Supplemental Figure 13). Other sulfur starvation marker genes like *MSA1* or *SULTR2;1* were previously reported to rely only on the core SURE motive in their promoter for sulfur deficiency-specific expression (Maruyama-Nakashita *et al*., 2005), but *SERAT3;2* would be the first gene displaying this element as part of the mRNA (Supplemental Figure 13). In this regard, it is more likely that this element influences translation than transcription and could thereby reveal a novel post-transcriptional regulatory mechanism for sulfur deficiency. Expression analysis of a *SERAT3;2* minimal promoter variant containing a mutation in the SURE site could verify the functional significance of this element.

Furthermore, repeating these experiments in the *slim1* mutant background would determine whether the expression depends on SLIM1.

4.2.4 Functional and structural insights into SERAT3 isoforms indicate modulation of the cCSC *in vitro*

A commonly shared characteristic of SERAT3 is the elongated C-terminus, which lacks the conserved motif required for interaction with OAS-TLs (Francois *et al*., 2006; Liu *et al*., 2022; Tavares *et al*., 2015). Tertiary structure prediction of *Arabidopsis* SERAT3;2 using AlphaFold (1.4.6) revealed an α-helix within this C-terminal extension, which was consistently found across plant species (Figure 20). The structural feature might pose a unique characteristic of SERAT group three, although its biological function and significance remain to be elucidated. So far, the C-terminal extension was shown to be not required for interaction of SERAT3;2 with SERAT1;1 *in vitro*, as both full-length STREP-SERAT3;2 and C-terminally truncated version of the last 44 amino acids STREP-SERAT3;2ΔC were consistently Co-purified with HIS-SERAT1;1 (3.2.4, Figure 26, Figure 29). They probably interact via the beta-sheet containing domain responsible for trimerization or the N-terminal oligomerization domain conserved among the Arabidopsis *SERAT* family (Bogdanova and Hell, 1997). Co-expression of STREP-SERAT3;2 and HIS-SERAT1;1 in *E. coli* resulted in the formation of hetero-hexamers (Figure 27), which exhibited less OAS-TL A binding capacity the more SERAT3;2 proteins were present in the multimeric complex (Figure 28). Steric hindrance of the elongated C-terminus of SERAT3;2 as the reason for this was dismissed, as heterocomplexes of HIS-SERAT1;1/STREP-SERAT3;2ΔC exhibited similarly reduced OAS-TL A binding capacities (Figure 29). An alternative explanation could involve electrostatic potential shifts in SERAT1;1 upon SERAT3 interaction, since this mechanism has been hypothesized to restrict OAS-TL binding to only one dimer per opposing side of the SERAT hexamer, despite the theoretical availability of six C-terminal regions as potential docking sites (Feldman-Salit *et al*., 2009). Since Gabler (2023) demonstrated heterohexamer formation between HIS-SERAT3;1 and STREP-SERAT3;2 *in vitro*, I further hypothesize that SERAT3;1 can also form hexamers with SERAT1;1. It remains to be tested, if SERAT3;1 interaction also leads to reduced binding capacity of SERAT1;1 to OAS-TL A or if this represents a specialized function of SERAT3;2. Since SERAT3;1 is generally more broadly and strongly expressed than SERAT3;2 under regular sulfate supply (3.2.2, Figure 21, Figure 22, Figure 23), I propose that SERAT3;1 might be the housekeeping SERAT3 isoform. Consistent with that, SERAT1;1/SERAT3;1 interaction was more pronounced than SERAT1;1/SERAT3;2 in the control condition and only increased two-fold after 72 h of sulfur deficiency (Haberland, 2017), indicating that SERAT3;1 might primarily function in control condition. In contrast, the strong transcriptional induction of SERAT3;2 upon sulfur deficiency (Figure 24, Kawashima 2005) and 40-fold increase in protein interaction to SERAT1;1 after 72 h of sulfur deficiency (Haberland, 2017) indicates that SERAT3;2 might get upregulated to support SERAT3;1 in times of stress condition. This would imply that in sulfur deficiency, the cCSC consists of SERAT1;1/SERAT3;1/SERAT3;2 complexes. *In vitro* studies could be performed to investigate how both SERAT3 influence the oligomeric structure of SERAT1;1/SERAT3;1/SERAT3;2, the binding capacity of OAS-TLA and the catalytic activity. A dissociating function of SERAT3;2 on the cCSC in times of sulfur deficiency is unlikely, as OAS is sufficient to facilitate CSC dissociation (Berkowitz *et al*., 2002; Kredich *et al*., 1969). Nonetheless, SERAT3;2 could promote stabilization of the dissociated form, especially during long-term sulfur deficiency. Alternatively, SERAT3;2 integration into the dissociated SERAT1;1 hexamer could also serve as a signaling platform forming new interaction sites with sulfur deficiency-specific interaction partners. The alpha-

helical domain in the C-terminus could thereby be crucial. Pulldown experiments using tagged SERAT3;2 or SERAT3;2ΔC followed by mass spectrometry could identify possible interaction partners.

4.2.4 The cytosolic SERAT isoforms are unnecessary for adaptation of development or metabolite levels in response to long-term sulfur deficiency

To investigate the function of SERAT3 in dependence of SERAT1;1 presence *in vivo*, the double mutant *serat3;1s3;2* was crossed with *serat1;1* to generate a mutant lacking all cytosolic SERAT isoforms, *serat1;1s3;1s3;2* (3.2.5). Interestingly, both *serat3;1s3;2* and *serat1;1s3;1s3;2* exhibited a WT-like phenotype regarding root-to-shoot FW increase and average primary root length maintenance when cultured on solid media plates in control or long-term sulfur deficiency (Figure 30, 3.2.5). Also, a shift from four weeks of sufficient sulfur supply to four weeks of sulfur deficiency did not lead to a deviation from WT phenotype(Figure 31, Figure 32), indicating that these isoforms are unnecessary for inducing long-term adaptation to sulfur deficiency. Consistent with the finding, key metabolites of the primary sulfur metabolism, e.g., sulfide, OAS, cysteine, and glutathione were unaffected in the mutants. The mutants exhibited only tendencies for reduced OAS steady-state levels in the roots and increased levels in the shoots, which were only significant for *serat1;1s3;1s3;2* or *serat3;1s3;2,* respectively (Figure 33). This could indicate a small organ-specific modulating function on OAS steady-state levels rather than driving them. Interestingly, the loss of *SERAT1;1*, one of the primary OAS-producing isoforms, did not result in a more pronounced reduction in OAS steady-state levels than the loss of the two SERAT group 3 isoforms, which exhibit negligible activity. This suggests that SERAT2;1 and SERAT2;2 have an adaptable compensatory mechanism in maintaining OAS homeostasis. The WT-like metabolite steady-state levels might explain the WT-like phenotypes of *serat3;1s3;2* and *serat1;1s3;1s3;2* and further corroborate the hypothesis that SERAT3s have a function beyond metabolism.

4.2.5 Transcriptome analysis of *serat3;1s3;2* reveal a general repressor function of SERAT3 on sulfur deficiency transcriptional response

To investigate possible transcriptional functions of SERAT3, the shoot material of *serat3;1s3;2* and WT, used for phenotyping and metabolite extraction, was also used for mRNA sequencing (3.2.6). In contrast to the WT-like phenotype and metabolite levels, *serat3;1s3;2* exhibited transcriptome-wide adjustments in both control and sulfur deficiency conditions with 2817 and 2664 differentially expressed genes, respectively (Figure 35). The PCA and Heatmap revealed significant genotype clustering, which seems to be oppositely affected by sulfur deficiency treatment (Figure 34).

Among the genes which are most significantly and highly overexpressed in *serat3;1s3;2* compared to WT in the control condition are the five OAS cluster genes according to (Hubberten *et al*., 2012a): *SDI1* (22-fold), *APR3* (13-fold), *LSU1* (10-fold), *MSA1* (10-fold), *GGCT2;1* (9-fold) (Table 17). Interestingly, the sixth member of this cluster, *BGLU28*, was not differentially expressed. In sulfur deficiency, these genes are less strongly overexpressed in *serat3;1s3;2* ranging between 1.8 and 3.5-fold. This indicates a repressor function of SERAT group three isoforms on OAS-responsive genes in control conditions but also in sulfur deficiency. Apodiakou and Hoefgen (2023) proposed an extended OAS cluster gene network, incorporating genes functionally associated with the OAS core cluster, including SERAT3;2. Seven genes of the extended network showed a similar strong overexpression in the control condition: *SDI2* (16-fold), *APR1* (11-fold), *APR2* (9-fold), *LSU2* (15-

fold), *LSU3* (15-fold), *BBE18* (6-fold) and *AtAvt6C* (3.2-fold) (Table 18). In sulfur deficiency, the overexpression of these genes stayed in the range of 1.9 and 4.6-fold, with an exception for *APR1* whose expression was unchanged in sulfur deficiency suggesting a generally stronger repressor function of SERAT group three is control conditions than in sulfur deficiency. The *LSU4* is also part of the associated OAS cluster network and was the only gene higher overexpressed in sulfur deficiency (3.7-fold) than in the control condition (3-fold), indicating additional regulatory function for this gene. Interestingly, six more OAS cluster-associated genes (*SULTR4;2, SULTR1;2, PYD4, AT5G40670*, *AT1G77670*, and *NmrA-like*) were found only in sulfur deficiency overexpressed but not in the control condition (Table 18), which could suggest that the repressor function of SERAT3 depends on different conditions for different genes. Two members of the extended OAS cluster network, hypothetical protein of *AT2G32487* and *SIP1;2 (AT5G18290)*, were not found to be affected in *serat3;1s3;2* in the control or sulfur deficiency condition, indicating that *serat3;1s3;2* are not repressing the whole OAS cluster extended network. The effect on the OAS cluster gene might result only partially from internal OAS-levels, as they were not strongly affected in *sera3;1s3;2* (Figure 33 B). Additionally, the missing co-regulation of *BGLU28* indicates a different regulatory mechanism than just OAS steady-state levels. The upregulated OAS cluster genes could be part of a general pre-induced sulfur starvation response in *serat3;1s3;2*. This hypothesis is further supported by the differential regulation of 12 out of the 14 most interconnected genes in the sulfate co-expression network (Henriquez-Valencia *et al*., 2018). The affected members were *DIN10, SEN1, AtRZPF34*, *BAM9, AT5G24490*, *TPS8*, *KFB20*, *NSP4*, *DUF179-3* alongside the previously identified *MSA1*, *SULTR4;2*, and *AtAvt6C*, which overlap with OAS-associated genes (Table 19). The gene exhibiting the strongest over-repression in *serat3;1 s3;2* compared to WT under control conditions was *DIN10*, showing a 50-fold decrease. Notably, *DIN10* is typically downregulated in response to sulfur deficiency in WT (Henriquez-Valencia et al., 2018). Under sulfur deficiency, its over-repression in *serat3;1s3;2* was reduced to 3.5-fold, supporting the hypothesis of a pre-induced and exaggerated sulfur starvation response in this mutant.

The list of associated transcription factors of the OAS-associated gene cluster and sulfate co-expression network were investigated for differentially regulated candidates. Matching to the upregulated OAS-associate gene cluster, transcription factors *CCA1*, *LHY*, *LCL5*, *NFYB2*, and *HAP5B* were also upregulated in both control and sulfur deficiency (Table 20) (Apodiakou and Hoefgen, 2023). Additionally, *HB7*, *PAP3*, *HY5*, and *PIF4* were found exclusively upregulated in the control condition, and *EIN3* and *EIL1* were exclusively downregulated in the sulfur deficiency condition. Ten other transcription factors associated with the OAS cluster genes were not found differentially regulated in *serat3;1s3;2* compared to WT, which could explain the specific upregulation of the subset of OAS cluster genes. Additionally, six transcription factors associated with the regulation of sulfur deficiency response (Fernandez *et al*., 2024) were found in the control condition upregulated in *serat3;1s3;2*, namely *MYB75*, *HYH*, *BBX16*, *MYB29*, *MYC2*, and *MYB28* (Table 21). Among those, *MYB75* was the only one found upregulated in sulfur deficiency, highlighting the differential response to control and sulfur deficiency. The transcription factor analysis corroborates the hypothesis that *serat3;1s3;2* has a pre-induced sulfur deficiency response in the control condition and an exaggerated response than WT in sulfur deficiency.

The KEGG and GO analysis supports the hypothesis of the repressor function of SERAT3s since more pathways are upregulated than downregulated (Figure 37, Table 22, Table 23). Matching to

the hypothesis of an over-induced sulfur deficiency response in *serat3;1s3;2*, this mutant shows upregulated pathways of sulfur metabolism and glutathione biosynthesis in both conditions. The GO analysis of control condition indicated repressor function for SERAT3 in other abiotic stress responses like heat or water-stress. In sulfur deficiency, the GO analysis points to a function of SERAT3 in flavonoid and pigment biosynthesis. This could be caused by the upregulated *MYB75* transcription factor responsible for inducing anthocyanin biosynthesis in response to abiotic stresses (Teng *et al*., 2005). After verification of the transcriptional changes, the *serat3;1s3;2* could be investigated regarding pigment phenotypes.

Interestingly, OAS cluster-associated sulfur starvation marker genes like *SDI1*, *LSU1*, *LSU2*, *LSU3*, *GGCT2;1* were also found to accumulate in a control condition in the shoots of *slim1* mutant and even stronger in the *slim1eil1* double mutant (Dietzen *et al*., 2020). Furthermore *APR3*, *APR1* and *SULTR4;2* were only found upregulated in the control condition in the *slim1eil1* double mutant, indicating a possible co-down regulation of *SLIM1* and *EIL1* in the control condition. Furthermore, *BGL28* was neither upregulated in *slim1* or *serat3;1s3;2* mutant, also corroborating the hypothesis that the effects in *serat3;1s3;2* are not dependent on OAS level. Consistent to this, *EIL1* was indeed downregulated in *serat3;1s3;2* although only in sulfur deficiency, while *SLIM1* transcript were not altered in *serat3;1s3;2*. This might not be surprising as SLIM1 transcriptional levels remain unaffected in sulfur deficiency (Maruyama-Nakashita *et al*., 2006) or OAS treatment (Hubberten *et al*., 2012a), and SLIM1's activity is proposed to be post-transcriptionally and/or post-translationally regulated (Wawrzyńska and Sirko, 2020). In contrast, *serat3;1s3;2* exhibited increased MYB75 transcription factors level and upregulated pathways of pigment biosynthesis, which was previously observed in SLIM1 overexpression lines (Apodiakou *et al*., 2024). As SLIM1 was shown to bind the promoter of *MYB75* (Wawrzynska *et al*., 2022) it remains unclear how SLIM1 is affected in *serat3;1s3;2*. Measuring SLIM1 protein steady state levels or turnover could clarify the involvement of *SLIM1* in the observed effects. Different to the *serat3;1s3;2* mutant the *slim1* did not accumulate *MSA1* or *SDI2* transcripts, indicating that the effects in *serat3;1s3;2* not solely depend on a possible *SLIM1 EIL1* connection.

A similar set of OAS-responsive genes was shown to be up-regulation in WT by cytokinin application independent of *SLIM1* presence (Pavlu *et al*., 2022). *APR1*, *APR3*, *GGCT2;1* and *SERAT3;2* were only upregulated in the shoots, while *SDI1*, *MSA1*, and *LSU1* were upregulated to a higher degree in the shoot compared with the root (Pavlu *et al*., 2022). Only *SULTR4;2* upregulation in response to cytokinin was dependent on *SLIM1,* possibly indicating some kind of interplay between cytokinin and SLIM1 (Pavlu *et al*., 2022). While the cytokinin transcription factor ARR10 was not found to be transcriptionally increased in *slim1* (Dietzen *et al*., 2020), it was 1.4 times upregulated in the shoots of *serat3;1s3;2*. Two further cytokinin response transcription factors, *ARR1* and *ARR2,* were downregulated to 70% and 60% in *serat3;1s3;2* grown under regular sulfur supply, respectively, linking SERAT3 function to cytokinin signaling. *BGLU28* and *BGL30* were highly cytokinin responsive, while the sulfate transporter *SULTR1;1* and *SULTR1;2* were repressed upon cytokinin application (Pavlu *et al*., 2022), highlighting some contrasting regulatory effects compared to *serat3;1s3;2*.

Altogether, I propose a repressor function of SERAT group three on the transcription of members of the OAS-associated gene cluster, which might be linked to SLIM1 activity and/or cytokinin signaling. This function becomes very striking in control condition, while in sulfur deficiency, the influence becomes less pronounced as sulfur deficiency marker genes are naturally upregulated.

Since SERAT3;2 is itself part of the extended OAS cluster and strongly upregulated under sulfur deficiency (Apodiakou and Hoefgen, 2023), it may play a role in compensating or fine-tuning the expression levels of other cluster members. It could also be the case that upregulation of SERAT3s in sulfur deficiency functions to downregulate OAS cluster gene expression cell type-specific, especially in the vasculature, as similar functions were shown for miR395 (Kawashima *et al*., 2009). The stable prSERAT3;2::SERAT3;2-mCherry line could be used to verify the cell type-specific expression of SERAT3;2 in the shoots. The single *serat3;1* and *serat3;2* could be investigated for pre-induced and exaggerated sulfur deficiency response in control and sulfur-deficient conditions, to elucidate possible isoform-specific contributions. To investigate if the repressor function of SERAT3 is dependent on the presence of the cytosolic CSC, the triple mutant *serat1;13;1s3;2* and *serat1;1* could be subjected to mRNAseq or tested regarding overexpression of OAS cluster genes in control condition using qRT-PCR. The unaffected phenotypes and metabolite levels in *serat3;1s3;2* might correlate with unaffected transcript levels of genes involved in the sulfate assimilation like *SULTR1;1*, which is consistent with the hypothesis of SERAT3s function in fine-tuning the OAS-cluster gene or indicate the presence of other counteracting elements preventing the implementation of sulfur deficiency signaling.

4.3 Deciphering the molecular signal for the physiological adaptation to long-term sulfur deficiency

4.3.1 The root-to-shoot FW ratio and the average primary root length are quantifiable read-outs for sulfur deficiency phenotypes in Arabidopsis

As sessile organisms, plants must cope with various abiotic stresses on-site, often leading to morphological adaptation of the overall plant body architecture in long-term exposure. In case of nutrient starvation, the root system adapts accordingly to the type of nutrient and depends on the concentration or severity of the deficiency (Gruber *et al*., 2013). So far, Kutz *et al*. (2002) observed lateral root initiation to be increased by sulfur deficiency, especially closer to the root tip, while Dan *et al*. (2007) and Gruber *et al*. (2013) could show inhibited lateral root formation and elongation in sulfur deficiency. Compared to other nutrient deficiencies, the overall root architecture in sulfur deficiency was similar to the control except for a slightly increased primary root length (Gruber *et al*., 2013). The phenotypic documentation of WT growing in 1 µM sulfate deficiency in this work (3.2.5 Figure 30, 3.3.2 Figure 39) matches the observation of Dan *et al*. (2007) and Gruber *et al*. (2013), and the difference to Kutz *et al*. (2002) could be explained by their use of the *Arabidopsis thaliana* C24 ecotype instead Col-0. The characteristic favoring of root growth over shoot growth in sulfur deficiency (Ericsson, 1995) was also observed by Gruber *et al*. (2013). The root-to-shoot FW ratio in the control condition reported by Gruber *et al*. (2013) (0.5) aligns with the 0.45–0.5 observed in this study under similar growth conditions (3.2.5 Figure 30, 3.3.1 Figure 38, 3.3.2 Figure 39, 3.3.7 Figure 53). The stepwise reduction of external sulfate supply from 20 µM to 10 µM to 1 µM significantly increased the root-to-shoot FW ratio from 0.6 to 0.8 to 1 (3.3.1 Figure 38), suggesting a fine-tunable mechanism in plants for sensing sulfate availability and adjusting physiology accordingly. In six independent repetitions, I found the root-to-shoot ratio of WT grown on solid media plates containing 1 µM sulfate stably in the range between 0.9 and 1.2 (Figure 31, Figure 39, Figure 40, Figure 41, Figure 53, Figure 57), indicating a robust read-out. Growing Arabidopsis WT in the hydroponic culture with the same sulfate concentration used in the solid media culture resulted in a root-to-shoot FW ratio of 0.2-0.3 for 500 µM sulfate and 0.4-0.6 for 1 µM sulfate. The substantially lowered root-to-shoot FW ratios could indicate that

sulfate is better absorbed by roots submerged in liquid than roots grown on top of a solidified medium that limits nutrient accessibility by diffusion. Interestingly, WT maintained the primary root length when grown on solid media plates over a range of 500 µM to 20 µM, 10 µM, and 1 µM. In contrast, the root length of hydroponically grown plants always exceeded those of control plants. These findings support the claim of Gruber *et al*. (2013) that the use and kind of gelling agents drastically influence the nutrient availability to the plants and their phenotype. The maintenance of primary root length or even the exceeding of the root length in milder stress conditions was previously not observed for any other nutrient stress (Gruber *et al*., 2013) and might pose a unique adaptation strategy for sulfate. Altogether, the root-to-shot FW ratio and the average primary root length are reliable read-outs to quantify and investigate sulfur deficiency.

4.3.2 SERAT mutants exhibit impaired root-to-shoot FW increases in response to sulfur deficiency

An increase in the root-to-shoot FW ratio is the result of long-term adaptation to sulfur deficiency (Ericsson, 1995; Gruber *et al*., 2013). Mutants impaired in primary sulfur metabolites like OAS and sulfide and deficient in CSC formation were used to elucidate the molecular signal triggering this response (3.3.2). Thereby, the growth retarded triple knock-out mutant *serat tko* (*serat1;1s2;1s2;2*) with only 5 ± 2% SERAT activity (Dong *et al*., 2017) exhibited the most substantial deficit in root-to-shoot FW ratio increase in sulfur deficiency (3.3.2, 3.3.3, 3.3.4). Growing *serat tko* on solid media plates, the root-to-shoot FW ratio was already reduced in the control condition compared to WT and remained at the WT control level upon sulfur deficiency (Figure 39). Because *serat tko* exhibited a WT-like root-to-shoot ratio of 0.2 when grown in liquid control medium (Figure 42), I hypothesize that this ratio of 0.2 reflects the minimal root-to-shoot ratio in the absence of sulfur deficiency stress. Measuring the root-to-shoot FW ratio of WT at higher sulfate concentrations (e.g., 1 mM or 1.5 mM) could verify this claim. After six weeks of sulfur deficiency treatment in the hydroponic culture, the *serat tko* significantly increased its root-to-shoot FW ratio from 0.2 to 0.3 (25% of the WT increase)(Figure 44), suggesting that some adaptive capacity is left in *serat tko* although significantly impaired. The ratio differences were primarily due to its inability to maintain root FW and reduce shoot FW under sulfur deficiency (Figure 39, Figure 42, Figure 44). Very strikingly, the *serat tko* was also unable to maintain the average primary root length in sulfur deficiency (Figure 39, Figure 49), indicating a link between the root-to-shoot FW ratio increase and the maintenance of average primary root length in sulfur deficiency.

The growth retardation was dismissed as a possible cause for the defects in the physiological adaptation in *serat tko* by investigating the *sir1-1* mutant, which retains only 8 ± 4% *SiR* transcript resulting in a similar growth retarded phenotype to *serat tko* (Dong *et al*., 2017) (Figure 42, Figure 43, Figure 44, Figure 45). Despite its smaller size, the *sir1-1* exhibited a WT-like root-to-shoot FW increase in the hydroponic cultures (Figure 42, Figure 44). The *sir1-1* showed a small but significant difference in the root-to-shoot FW ratio only when grown on solid media plates under sulfur deficiency, reaching 90% of the WT increase (Figure 39). This finding corroborated the hypothesis that sulfur deficiency stress on solid media plates affects the plants more strongly than in liquid culture. Unlike WT, which strongly reduced shoot FW and maintained root FW in sulfur deficiency, the *sir1-1* only slightly reduced shoot FW but increased root FW significantly compared to the control condition (Figure 42, Figure 44, Figure 45). This could indicate that plants can

independently adjust shoot and root organ growth to optimize the overall physiological adaptation to environmental clues.

The loss of a specific CSC complex was dismissed as a reason for the adaptational defect in *serat tko*, as all three single mutants *serat1;1*, *serat2;1*, and *serat2;2* exhibited a WT-like root-to-shoot FW increase in sulfur deficiency (Figure 40).

On the other hand, the quadruple *SERAT* mutants left with only one CSC in either cytosol, mitochondria, or plastids were all affected in the root-to-shoot FW ratio increase in response to sulfur deficiency. *Q1;1* mutant with the cytosolic CSC performed closest to WT with an 86% WT increase, *Q2;2* with the mitochondrial CSC exhibited a 38% WT increase, and *Q2;1* with the plastid CSC showed the least root-to-shoot FW ratio increase of 31% WT (Figure 41). This indicates that neither of the CSCs is sufficient for the complete WT-like response and suggests that total SERAT activity instead of specific *SERAT* isoforms is crucial for this phenotype. In the hydroponic culture, *Q1;1* and *Q2;2* showed a WT-like root-to-shoot FW ratio increase in response to sulfur deficiency, as previously observed for *sir1-1* (3.3.4, Figure 44). This underscores the importance of choosing the right growth medium since weak phenotypes observed in the solid media culture are restored using the liquid medium. Only *Q2;1* still exhibited an affected root-to-shoot FW ratio phenotype in the hydroponic system, which was mainly driven by the inability to maintain root FW similar to *serat tko* (Figure 44, Figure 45) corroborating the hypothesis that the root-to-shoot FW ratio increase is independent of plant size.

4.3.2 The root-to-shoot FW ratio increase is dependent on OAS steady-state levels

Since CSC dissociation was dismissed as a possible signal triggering the sulfur deficiency response, metabolite analysis was performed to investigate a possible involvement of primary sulfur metabolites in this response. Consistent with their described growth retarded phenotypes (Dong *et al.*, 2017), *serat tko* and *sir1;1* exhibited in the control condition compared to WT significantly reduced OAS and sulfide steady-state levels, respectively (Figure 43).

Since *sir1-1* exhibited a WT-like root-to-shoot FW ratio increase upon sulfur deficiency in the hydroponic culture, sulfide was excluded as a potential candidate for triggering the response. This was further corroborated by the WT-like sulfide levels measured in *serat tko* in control and sulfur deficiency (Figure 43). However, the results from measuring sulfide steady-state levels should be interpreted with caution, as the detected levels of approximately 500 pmol/mg FW exceed previously reported sulfide concentrations in Col-0 shoots (10 pmol/mg FW) by 50-fold when measured using a micro sulfide ion electrode (Álvarez *et al.*, 2012). The measured sulfide concentration here should not be physiological, as the mitochondrial cytochrome c oxidase with an $IC_{50} \leq 10$ pmol/ml would be fully inhibited (Birke *et al.*, 2012). A reason for the relatively high steady-state levels could be broken persulfide bridges, releasing otherwise bound sulfide during the extraction and labeling procedure (Moseler *et al.*, 2024). Despite the relatively high concentration, the measured sulfide steady-state levels in sulfur deficiency were significantly lower than in control condition (Figure 43). Furthermore, the substantially higher sulfide levels in WT shoots than roots align with the primary site of sulfide production in the shoots (Figure 43), verifying the applied technique for measuring at least qualitative changes in sulfide concentrations.

Consistent with the strong impairment in the root-to-shoot FW increase, OAS steady-state levels were the most affected metabolite levels in *serat tko* (Figure 43, Figure 46). Nonetheless, the

downstream metabolite steady-state levels of cysteine (Figure 43, Figure 47) and glutathione (Figure 43, Figure 48) were also affected in *serat tko* (Figure 42, Figure 43, Figure 44, Figure 45). By including *Q1;1*, *Q2;1*, *Q2;2* in the analysis, the root-to-shoot FW ratios were correlated against internal steady-state levels of OAS, cysteine, and glutathione. The Pearson correlation showed a positive correlation of the root-to-shoot FW ratio with the OAS steady-state levels of $r^2 = 0.79$ for the roots ($p = 0.0001$) and $r^2 = 0.64$ for the shoots ($p = 0.0015$) (Figure 46). In contrast, the cysteine and glutathione steady-state levels did not correlate with the root-to-shoot FW ratio (Figure 47, Figure 48).

The causation of the correlation was tested by applying external OAS to *serat tko* in sulfur deficiency condition (3.3.5). While OAS feeding did not further increase the root-to-shoot FW ratio increase of WT in sulfur deficiency, it significantly increased the root-to-shoot FW ratio of *serat tko* to almost the full WT-like extent (Figure 49). OAS treatment also improved the root FW of *serat tko* and fully restored the maintenance of the average primary root length in sulfur deficiency compared to the control condition (Figure 49). The isomer *N*-Acetylserine (NAS) served as the negative control to exclude possible effects by the additional carbon or nitrogen source. Since NAS application did not affect *serat tko* or WT (Figure 49), the observed improvements in the adaptation to long-term sulfur deficiency in *serat tko* were specific for the molecule OAS.

To fully exclude the possibility that OAS treatment worked via incorporation into downstream metabolites like cysteine or glutathione, the *serat tko* was grown on solid media plates supplemented with decreasing concentrations of cysteine or glutathione as the sole sulfur source. Interestingly, the WT grew similarly well on 500 µM cysteine compared to 500 µM sulfate regarding root and shoot FWs and the root-to-shoot FW ratio, demonstrating the ability of WT to use cysteine as an equal sulfur source to sulfate (Figure 50). The root-to-shoot FW ratio increased was also consistent with previous observations using sulfate as sulfur source (Figure 50). When *serat tko* was grown on 500 µM cysteine, the growth retardation phenotype was rescued, as primary root length was restored and shoot and root FWs exceeded WT (Figure 50). Unlike WT, decreasing cysteine supply did not result in increasing root-to-shoot FW ratios in *serat tko* (Figure 50), eliminating cysteine as the potential driver for the adaptation to sulfur deficiency.

Furthermore, *serat tko* did also not increase its root-to-shoot FW ratio when grown on 1 µM glutathione as the only sulfur source compared to 500 µM glutathione control (Figure 51). Interestingly, *serat tko* was able to maintain its average primary root length when cultured with 1 µM glutathione, while 1 µM sulfate or cysteine led to a root length reduction of 50%, indicating a specific function of glutathione on average primary root length maintenance in sulfur deficiency. Interestingly, the WT showed general growth defects like smaller root and shoot FWs and already pre-induced root-to-shoot FW ratio when grown on 500 µM glutathione control condition compared to 500 µM sulfate (Figure 51). Since these growth defects match the phenotype of mild sulfur deficiency, glutathione might be not an equally usable sulfur source for plants than sulfate. Previously, root growth defects were also observed for plants growing in 500 µM glutathione (Wójcik and Tukiendorf, 2011) and might be toxic through disturbance of plant's redox homeostasis. Further experiments with glutathione concentration curves could clarify the influence of glutathione feeding on WT growth. Nonetheless, neither glutathione nor cysteine feeding is involved in signaling the root-to-shoot FW ratio increase in *serat tko*. This strengthens the hypothesis that OAS is the signal molecule for long-term adaptation to sulfur deficiency.

Interestingly, *serat tko* and WT grafting experiments revealed that the ability to increase the root-to-shoot FW ratio does not depend solely on OAS production in a specific organ (3.3.6, Figure 52). Neither exclusive OAS production in the root nor in the shoot was sufficient to induce the full WT-like root-to-shoot FW ratio increase in sulfur deficiency. As the chimeric grafts exhibited an intermediate root-to-shoot FW ratio between *serat tko* and WT control grafts, this suggests overall OAS production capacity is more important than organ-specific production or that OAS synthesis in both organs is essential for an efficient adaptive response. Nonetheless, this suggests a bidirectional systemic coordination of sulfur deficiency signaling between root and shoot organs.

4.3.3 SLIM1 is involved in the transduction of sulfur deficiency signaling

So far, OAS accumulation has shown to be necessary and sufficient to drive the long-term adaptation to sulfur deficiency in *serat tko* (4.3.2). OAS has a known transcriptional influence (Hubberten *et al*., 2012a), which partially overlaps with functions of the transcription factor SLIM1 in the sulfur deficiency, but a connection between OAS and SLIM1 has not been proven so far (Apodiakou and Hoefgen, 2023). Therefore, *slim1-1* was tested regarding the root-to-shoot FW ratio increase and average root length maintenance in long-term sulfur deficiency (3.3.7). Indeed, the mutant exhibited only of 50% WT root-to-shoot FW increase (Figure 53). Also, the average primary root length of *slim1-1* was reduced compared to WT in the control condition, as previously reported (Maruyama-Nakashita *et al*., 2006). Interestingly, *slim1-1* maintained this root length in sulfur deficiency in contrast to *serat tko,* which exhibited further reduced root length in sulfur deficiency, highlighting phenotypic differences between the mutants (Figure 53). In the hydroponic culture, the *slim1-1* mutant still exhibited the 50% WT response root-to-shoot ratio increase (Figure 54), verifying SLIM1's involvement in this response. Since *slim1-1* exhibited WT-like OAS levels (Figure 55), this suggests that SLIM1 functions downstream of OAS in transducing the sulfur starvation signal. Challenging this hypothesis, OAS feeding to the *slim1-1* mutant resulted in trends for improved root-to-shoot FW ratio increase, root FW maintenance, and average primary root length (Figure 56). This could indicate that SLIM1 is not the only factor necessary for transducing the OAS signal. A candidate for this might be EIL1, which was shown to at least partially exhibit overlapping functions to SLIM1 (Dietzen *et al*., 2020). The *slim1eil1* (Dietzen *et al*., 2020) mutant could be tested regarding a more severe impairment in the root-to-shoot FW ratio increase in sulfur deficiency. If *SLIM1* and *EIL1* work downstream of OAS, the external feeding of OAS to *slim1eil1* should not rescue the lack in the root-to-shoot FW ratio increase. On the other hand, the here used *slim1-1* mutant has a point mutation, leading to a missense mutation but not a complete knock-out of *SLIM1* (Maruyama-Nakashita *et al*., 2006). If the missense mutation in *SLIM1* results in a significantly reduced but not completely abolished function, high levels of externally applied OAS may enhance signaling strength sufficiently to rescue the *slim1-1* mutant phenotype partially. This hypothesis could be tested using verified *SLIM1* knockout mutants generated by CRISPR/Cas9 editing, which generally exhibit stronger phenotypes than *slim1-1* missense mutant (Wawrzynska *et al*., 2022). Testing these mutants could verify SLIM1's involvement in the long-term adaptation to sulfur deficiency. Nonetheless, unknown factors with redundant functions to *SLIM1* might also be involved in OAS-signal transduction for a complete response to sulfur deficiency.

4.3.4 Glutathione is essential for primary root length and root FW maintenance in sulfur deficiency

Next to the defect in increasing its root-to-shoot FW ratio in response to sulfur deficiency, the *serat tko* also exhibited a deficiency in maintaining average primary root length (4.3.2). While only external OAS feeding restored the root-to-shoot FW ratio increase, external feeding of 500 µM cysteine and 500 µM glutathione did rescue the average primary root length phenotype of *serat tko* (Figure 50, Figure 51). Interestingly, in sulfur deficiency, the average primary root length was only maintained with 1 µM glutathione, while 1 µM cysteine was insufficient (Figure 50, Figure 51). Since cysteine is the precursor for glutathione, the 500 µM cysteine could partially be used for glutathione biosynthesis enough to maintain WT-like average primary root length. With only 1 µM cysteine and no sensing of sulfur limitation, the *serat tko* probably fails to generate enough glutathione to maintain average primary root length. Supporting this hypothesis, the *cad2* mutant, which is impaired in glutathione biosynthesis (Cobbett *et al*., 1998), also exhibited a defect in maintaining the average primary root length in 1 µM sulfate compared to the 500 µM sulfate control condition (Figure 57). This was accompanied by significantly reduced root FW in control and sulfur deficiency condition compared to WT, resulting in 70% of the WT root-to-shoot FW increase. This indicates that glutathione is necessary for the root-to-shoot FW ratio increase in sulfur deficiency by maintaining root length but also root FW. The cross of the *cad2* mutant with *sir1-1* (*sir1cad2*) exhibited a stronger deficiency in the root-to-shoot FW ratio increase resulting in 30% WT (Figure 57). Also, the root and shoot FW maintenance and average primary root length in sulfur deficiency were strongly affected in the double mutant compared to the parents, indicating that the mutations *cad2* and *sir1-1* independently affect the root-to-shoot FW ratio. The relatively small defect of 90% WT root-to-shoot FW ratio increase observed for *sir1-1* on solid media (Figure 39) may result from an overall reduced cysteine flux, which could constrain the growth rate required to establish the differential growth pattern (Dong *et al*., 2017). This worsens the phenotype of *cad2* as it affects the root-to-shoot FW ratio independently of the mutation in glutathione biosynthesis. It could also be possible that the reduced flux into cysteine results in even lower glutathione biosynthesis in the double mutant. Verification of the phenotype in the hydroponic culture and measuring steady-state levels of glutathione, but also cysteine and OAS, could verify the hypothesis for this mutant. Then, feeding experiments to *cad2* and *sir1cad2* could prove the influence of the metabolites on the root-to-shoot FW phenotype. So far, these results indicate that next to OAS as the signal for sulfur deficiency, the translation rate and glutathione biosynthesis are important for implementing the increased root-to-shoot FW as the long-term sulfur deficiency adaptation.

4.3.4 OAS is the sulfur deficiency-specific signal for inducing the root-to-shoot FW ratio increase

The root-to-shoot FW ratio increase is a common adaptation strategy to nitrate, phosphate, and sulfate deficiency (Ericsson, 1995). However, plants must sense each nutrient individually. The nitrogen starvation signal is initiated through the perception of nitrate by the NRT1.1 transceptor (Ho *et al*., 2009). This triggers calcium waves leading to the translocation of group III CALCIUM-DEPENDENT PKs (CPKs) CPK10/30/32 into the nucleus, where they phosphorylate NLP7, which then activates nitrate target genes (Liu *et al*., 2017; Maghiaoui *et al*., 2020). In phosphate deficiency, the dephosphorylation of PHOSPHATE TRANSPORTER 1 (PHT1) protein leads to increased accumulation of the transporter at the plasma membrane, which is promoted by TRANSPORTER TRAFFIC FACILITATOR1 (PHF1) (Chen *et al*., 2015). At the transcription level, PHOSPHATE STARVATION RESPONSE 1 (PHR1) and its closest paralog PHR1-LIKE1 (PHL1)

regulate the expression of the phosphate starvation-induced genes, leading to downstream developmental and metabolic modifications (Bustos *et al*., 2010; Rubio *et al*., 2001). Although a transceptor function for SULT1;2 is proposed (Zheng *et al*., 2014), the present data propose OAS accumulation as the signal to trigger physiological adaptation resulting in an increased root-to-shoot ratio in sulfur deficiency. Therefore, all CSCs in roots and shoots contribute. Similar to NLP7 and PHF1, SLIM1 probably participates in the signal transduction downstream of OAS in inducing sulfur starvation marker genes. While cysteine exhibited only a minor influence on the adaptational response, glutathione was critical for maintaining primary root length and root FW under sulfur deficiency. Interestingly, glutathione also plays a crucial role in phosphate starvation, as glutathione-deficient mutants exhibit hypersensitivity to phosphate starvation and altered phosphate accumulation patterns (Shee *et al*., 2023). Glutathione was shown to support root system adaptation to phosphate deprivation through the indole butyric acid pathway (Trujillo-Hernandez *et al*., 2020), which might also be important for maintaining root growth in sulfur deficiency. The complete downstream cascade leading to differential growth patterns in all three nutrient deficiency stresses remains fragmented. In sulfur deficiency, antagonistic activation of the Target of Rapamycin (TOR) kinase in roots and shoots was shown to be essential for the root-to-shoot ratio increase (Dong *et al*., 2022). As a central regulatory hub connecting nutrient availability to metabolic processes in plants (Artins *et al*., 2024; Dobrenel *et al*., 2016), TOR may also play a crucial role in implementing the differential growth pattern in response to long-term nitrate and phosphate starvation. So far, the root-to-shoot FW ratio phenotype has proven to be a solid readout for investigating the sulfur deficiency signaling chain, but further investigation of the interactions between OAS and SLIM1 and other regulatory elements are necessary to fully elucidate the sulfur deficiency signal chain.

5. References

Aarabi, F., Kusajima, M., Tohge, T., Konishi, T., Gigolashvili, T., Takamune, M., Sasazaki, Y., Watanabe, M., Nakashita, H., Fernie, A.R., Saito, K., Takahashi, H., Hubberten, H.M., Hoefgen, R., Maruyama-Nakashita, A. (2016). Sulfur deficiency–induced repressor proteins optimize glucosinolate biosynthesis in plants. Sci Adv. **2**, e1601087.

Aarabi, F., Rakpenthai, A., Barahimipour, R., Gorka, M., Alseekh, S., Zhang, Y., Salem, M.A., Bruckner, F., Omranian, N., Watanabe, M., Nikoloski, Z., Giavalisco, P., Tohge, T., Graf, A., Fernie, A.R., Hoefgen, R. (2021). Sulfur deficiency-induced genes affect seed protein accumulation and composition under sulfate deprivation. Plant Physiol **187**, 2419-2434.

Alvarez, C., Angeles Bermudez, M., Romero, L.C., Gotor, C., Garcia, I. (2012). Cysteine homeostasis plays an essential role in plant immunity. New Phytol **193**, 165-177.

Alvarez, C., Calo, L., Romero, L.C., Garcia, I., Gotor, C. (2010). An *O*-acetylserine(thiol)lyase homolog with l-cysteine desulfhydrase activity regulates cysteine homeostasis in Arabidopsis. Plant Physiol **152**, 656-669.

Álvarez, C., García, I., Moreno, I., Pérez-Pérez, M.E., Crespo, J.L., Romero, L.C., Gotor, C. (2012). Cysteine-generated sulfide in the cytosol negatively regulates autophagy and modulates the transcriptional profile in Arabidopsis. Plant C **24**, 4621-4634.

Alway, F.J. (1940). A nutrient element slighted in agricultural research. J Agron **32**, 913-921.

Apodiakou, A., Alseekh, S., Hoefgen, R., Whitcomb, S.J. (2024). Overexpression of *SLIM1* transcription factor accelerates vegetative development in *Arabidopsis thaliana*. Front Plant Sci **15**, 1327152.

Apodiakou, A., and Hoefgen, R. (2023). New insights into the regulation of plant metabolism by *O*-acetylserine: Sulfate and beyond. J Exp Bot **74**, 3361-3378.

Artins, A., Martins, M.C.M., Meyer, C., Fernie, A.R., Caldana, C. (2024). Sensing and regulation of C and N metabolism - novel features and mechanisms of the TOR and SnRK1 signaling pathways. Plant J **118**, 1268-1280.

Åslund, F., and Beckwith, J. (1999). The thioredoxin superfamily: Redundancy, specificity, and gray-area genomics. J Bacteriol **181**, 1375-1379.

Barroso, C., Vega, J.M., Gotor, C. (1995). A new member of the cytosolic *O-acetylserine(thiol)lyase* gene family in *Arabidopsis thaliana*. FEBS Lett **363**, 1-5.

Bednarek, P. (2012). Sulfur-containing secondary metabolites from *Arabidopsis Thaliana* and other Brassicaceae with function in plant immunity. Chembiochem **13**, 1846-1859.

Berkowitz, O., Wirtz, M., Wolf, A., Kuhlmann, J., Hell, R. (2002). Use of biomolecular interaction analysis to elucidate the regulatory mechanism of the cysteine synthase complex from *Arabidopsis Thaliana*. J Biol Chem **277**, 30629-30634.

Bermudez, M.A., Paez-Ochoa, M.A., Gotor, C., Romero, L.C. (2010). Arabidopsis S-sulfocysteine synthase activity is essential for chloroplast function and long-day light-dependent redox control. Plant C **22**, 403-416.

Bick, J.A., Setterdahl, A.T., Knaff, D.B., Chen, Y., Pitcher, L.H., Zilinskas, B.A., Leustek, T. (2001). Regulation of the plant-type 5'-adenylyl sulfate reductase by oxidative stress. Biochem **40**, 9040-9048.

Birke, H. (2012). Die Bedeutung subzellulärer Kompartimentierung für die Synthese von Cystein in phototrophen Organismen (Heidelberg, Univ., Diss., 2012), pp. VI, 241 Bl.

Birke, H., Haas, F.H., De Kok, L.J., Balk, J., Wirtz, M., Hell, R. (2012). Cysteine biosynthesis, in concert with a novel mechanism, contributes to sulfide detoxification in mitochondria of *Arabidopsis thaliana*. Biochem J **445**, 275-283.

Birke, H., Heeg, C., Wirtz, M., Hell, R. (2013). Successful fertilization requires the presence of at least one major *O-acetylserine(thiol)lyase* for cysteine synthesis in pollen of Arabidopsis. Plant Physiol **163**, 959-972.

Bittner-Eddy, P.D., and Beynon, J.L. (2001). The Arabidopsis Downy Mildew resistance gene, *RPP13-Nd*, functions independently of *NDR1* and *EDS1* and does not require the accumulation of salicylic acid. Mol Plant Microbe Interact **14**, 416-421.

Bittner-Eddy, P.D., Crute, I.R., Holub, E.B., Beynon, J.L. (2000). *RPP13* is a simple locus in *Arabidopsis thaliana* for alleles that specify Downy Mildew resistance to different avirulence determinants in *Peronospora parasitica*. Plant J **21**, 177-188.

Bogdanova, N., and Hell, R. (1997). Cysteine synthesis in plants: Protein-protein interactions of serine acetyltransferase from *Arabidopsis thaliana*. Plant J **11**, 251-262.

Bork, C., Schwenn, J.D., Hell, R. (1998). Isolation and characterization of a gene for assimilatory sulfite reductase from *Arabidopsis thaliana*. Gene **212**, 147-153.

Bray, N.L., Pimentel, H., Melsted, P., Pachter, L. (2016). Near-optimal probabilistic RNA-seq quantification. Nat Biotechnol. **34**, 525-527.

Bustos, R., Castrillo, G., Linhares, F., Puga, M.I., Rubio, V., Perez-Perez, J., Solano, R., Leyva, A., Paz-Ares, J. (2010). A central regulatory system largely controls transcriptional activation and repression responses to phosphate starvation in Arabidopsis. PLoS Genet **6**, e1001102.

Chen, E.Y., Tan, C.M., Kou, Y., Duan, Q., Wang, Z., Meirelles, G.V., Clark, N.R., and Ma'ayan, A. (2013). Enrichr: Interactive and collaborative HTML5 gene list enrichment analysis tool. BMC Bioinformatics **14**, 128.

Chen, J., Wang, Y., Wang, F., Yang, J., Gao, M., Li, C., Liu, Y., Liu, Y., Yamaji, N., Ma, J.F., Paz-Ares, J., Nussaume, L., Zhang, S., Yi, K., Wu, Z., Wu, P. (2015). The rice CK2 kinase regulates trafficking of phosphate transporters in response to phosphate levels. Plant C **27**, 711-723.

Chen, Z., Zhao, P.X., Miao, Z.-Q., Qi, G.-F., Wang, Z., Yuan, Y., Ahmad, N., Cao, M.J., Hell, R., Wirtz, M., Xiang, C. B. (2019). SULTR3s function in chloroplast sulfate uptake and affect ABA biosynthesis and the stress response. Plant Physiol **180**, 593-604.

Chiba, Y., Ishikawa, M., Kijima, F., Tyson, R.H., Kim, J., Yamamoto, A., Nambara, E., Leustek, T., Wallsgrove, R.M., Naito, S. (1999). Evidence for autoregulation of *cystathionine gamma-synthase* mRNA stability in Arabidopsis. Science **286**, 1371-1374.

Cobbett, C., and Goldsbrough, P. (2002). Phytochelatins and metallothioneins: Roles in heavy metal detoxification and homeostasis. Annu Rev Plant Biol. **53**, 159-182.

Cobbett, C.S., May, M.J., Howden, R., Rolls, B. (1998). The glutathione-deficient, cadmium-sensitive mutant, *cad2-1*, of *Arabidopsis thaliana* is deficient in *γ-glutamylcysteine synthetase*. Plant J **16**, 73-78.

Couturier, J., Touraine, B., Briat, J.F., Gaymard, F., Rouhier, N. (2013). The iron-sulfur cluster assembly machineries in plants: Current knowledge and open questions. Front Plant Sci **4**, 259.

Dan, H., Yang, G., Zheng, Z.L. (2007). A negative regulatory role for auxin in sulphate deficiency response in *Arabidopsis thaliana*. Plant Mol Bio **63**, 221-235.

Davidian, J.C., and Kopriva, S. (2010). Regulation of sulfate uptake and assimilation--the same or not the same? Mol Plant **3**, 314-325.

Dietzen, C., Koprivova, A., Whitcomb, S.J., Langen, G., Jobe, T.O., Hoefgen, R., Kopriva, S. (2020). The transcription factor EIL1 participates in the regulation of sulfur-deficiency response. Plant Physiol **184**, 2120-2136.

Dobrenel, T., Caldana, C., Hanson, J., Robaglia, C., Vincentz, M., Veit, B., Meyer, C. (2016). TOR signaling and nutrient sensing. Annu Rev Plant Biol **67**, 261-285.

Dominguez-Solis, J.R., Gutierrez-Alcala, G., Vega, J.M., Romero, L.C., Gotor, C. (2001). The cytosolic *O-acetylserine(thiol)lyase* gene is regulated by heavy metals and can function in cadmium tolerance. J Biol Chem **276**, 9297-9302.

Dominguez-Solis, J.R., Lopez-Martin, M.C., Ager, F.J., Ynsa, M.D., Romero, L.C., Gotor, C. (2004). Increased cysteine availability is essential for cadmium tolerance and accumulation in *Arabidopsis thaliana*. Plant Biotech J **2**, 469-476.

Dong, Y., Aref, R., Forieri, I., Schiel, D., Leemhuis, W., Meyer, C., Hell, R., Wirtz, M. (2022). The plant TOR kinase tunes autophagy and meristem activity for nutrient stress-induced developmental plasticity. The Plant C **34**, 3814-3829.

Dong, Y., Silbermann, M., Speiser, A., Forieri, I., Linster, E., Poschet, G., Allboje Samami, A., Wanatabe, M., Sticht, C., Teleman, A.A., Deragon, J., Saito, K., Hell, R., Wirtz, M. (2017). RETRACTED: Sulfur availability regulates plant growth via glucose-tor signaling. Nat Commun **8**, 1174.

Droux, M., Ruffet, M.L., Douce, R., Job, D. (1998). Interactions between serine acetyltransferase and *O*-acetylserine(thiol)lyase in higher plants-structural and kinetic properties of the free and bound enzymes. Eur J Biochem **255**, 235-245.

Edwards, K., Johnstone, C., Thompson, C. (1991). A simple and rapid method for the preparation of plant genomic DNA for PCR analysis. Nucleic Acids Res **19**, 1349.

Ericsson, T. (1995). Growth and shoot:root ratio of seedlings in relation to nutrient availability. Plant Soil **168-169**, 205-214.

Feinberg, A., Stenke, A., Peter, T., Hinckley, E.L.S., Driscoll, C.T., Winkel, L.H.E. (2021). Reductions in the deposition of sulfur and selenium to agricultural soils pose risk of future nutrient deficiencies. Commun Earth Environ **2**, 101.

Feldman-Salit, A., Wirtz, M., Hell, R., Wade, R.C. (2009). A mechanistic model of the cysteine synthase complex. J Mol Biol **386**, 37-59.

Feldman-Salit, A., Wirtz, M., Lenherr, E.D., Throm, C., Hothorn, M., Scheffzek, K., Hell, R., Wade, R.C. (2012). Allosterically gated enzyme dynamics in the cysteine synthase complex regulate cysteine biosynthesis in *Arabidopsis thaliana*. Structure **20**, 292-302.

Fernandez, J.D., Mino, I., Canales, J., and Vidal, E.A. (2024). Gene regulatory networks underlying sulfate deficiency responses in plants. J Exp Bot **75**, 2781-2798.

Finkelstein, J.D. (1990). Methionine metabolism in mammals. The Journal of nutritional biochemistry **1**, 228-237.

Francois, J.A., Kumaran, S., Jez, J.M. (2006). Structural basis for interaction of *O*-acetylserine sulfhydrylase and serine acetyltransferase in the Arabidopsis cysteine synthase complex. Plant C **18**, 3647-3655.

Gabler, D. (2023). The influence of SERAT3;2 on the cytosolic cysteine synthase complex in *Arabidopsis thaliana*. Faculty of Bioscience (Ruprecht-Karls-Universität Heidelberg).

Geistlinger, L., Csaba, G., Zimmer, R. (2016). Bioconductor's enrichmentbrowser: Seamless navigation through combined results of set- & network-based enrichment analysis. BMC Bioinformatics **17**, 45.

Gotor, C., Garcia, I., Aroca, A., Laureano-Marin, A.M., Arenas-Alfonseca, L., Jurado-Flores, A., Moreno, I., Romero, L.C. (2019). Signaling by hydrogen sulfide and cyanide through post-translational modification. J Exp Bot **70**, 4251-4265.

Gruber, B.D., Giehl, R.F.H., Friedel, S., von Wirén, N. (2013). Plasticity of the Arabidopsis root system under nutrient deficiencies. Plant Physiol **163**, 161-179.

Gu, Z., Eils, R., Schlesner, M. (2016). Complex heatmaps reveal patterns and correlations in multidimensional genomic data. Bioinformatics **32**, 2847-2849.

Guo, H., and Ecker, J.R. (2004). The ethylene signaling pathway: New insights. Curr Opin Plant Biol **7**, 40-49.

Haas, F.H. (2010). Dual function of the cysteine synthase complex in mitochondria from *Arabidopsis thaliana* (Heidelberg, Univ., Diss., 2010), pp. XIV, 178 Bl.

Haas, F.H., Heeg, C., Queiroz, R., Bauer, A., Wirtz, M., Hell, R. (2008). Mitochondrial serine acetyltransferase functions as a pacemaker of cysteine synthesis in plant cells. Plant Physiol **148**, 1055-1067.

Haberland, S. (2017). Die komplexen funktionen des cysteinsynthasekomplexes bei der schwefelmangelantwort in *Arabidopsis thaliana* (Heidelberg, Univ., Diss., 2017), pp. 261.

Hall, S.A., Allen, R.L., Baumber, R.E., Baxter, L.A., Fisher, K., Bittner-Eddy, P.D., Rose, L.E., Holub, E.B., Beynon, J.L. (2009). Maintenance of genetic variation in plants and pathogens involves complex networks of gene-for-gene interactions. Mol Plant Pathol **10**, 449-457.

Hatzfeld, Y., Lee, S., Lee, M., Leustek, T., Saito, K. (2000a). Functional characterization of a gene encoding a fourth *ATP sulfurylase* isoform from *Arabidopsis thaliana*. Gene **248**, 51-58.

Hatzfeld, Y., Maruyama, A., Schmidt, A., Noji, M., Ishizawa, K., and Saito, K. (2000b). β-cyanoalanine synthase is a mitochondrial cysteine synthase-like protein in spinach and Arabidopsis. Plant Physiol **123**, 1163-1172.

Hawkesford, M.J., and De Kok, L.J. (2006). Managing sulphur metabolism in plants. Plant C Environ **29**, 382-395.

Heeg, C., Kruse, C., Jost, R., Gutensohn, M., Ruppert, T., Wirtz, M., Hell, R. (2008). Analysis of the Arabidopsis *O-acetylserine(thiol)lyase* gene family demonstrates compartment-specific differences in the regulation of cysteine synthesis. Plant C **20**, 168-185.

Hell, R., and Hillebrand, H. (2001). Plant concepts for mineral acquisition and allocation. Curr Opin Biotechnol **12**, 161-168.

Hell, R., Jost, R., Berkowitz, O., and Wirtz, M. (2002). Molecular and biochemical analysis of the enzymes of cysteine biosynthesis in the plant *Arabidopsis thaliana*. Amino Acids **22**, 245-257.

Hell, R., and Wirtz, M. (2008). Metabolism of cysteine in plants and phototrophic bacteria. In Sulfur metabolism in phototrophic organisms, **R. Hell, C. Dahl, and T. Leustek,** eds. (Dordrecht, The Netherlands: Springer), pp. 61-94.

Henriquez-Valencia, C., Arenas, M.A., Medina, J., Canales, J. (2018). Integrative transcriptomic analysis uncovers novel gene modules that underlie the sulfate response in *Arabidopsis thaliana*. Front Plant Sci **9**, 470.

Hesse, H., and Hoefgen, R. (1998). Isolation of cDNAs encoding cytosolic (accession no. Af044172) and plastidic (accession no. Af044173) cysteine synthase isoforms from *solanum tuberosum* (pgr98-057). Plant Physiol **116**, 1604.

Hinckley, E.L.S., Crawford, J.T., Fakhraei, H., Driscoll, C.T. (2020). A shift in sulfur-cycle manipulation from atmospheric emissions to agricultural additions. Nat Geosci **13**, 597-604.

Hirai, M., Fujiwara, T., Awazuhara, M., Kimura, T., Noji, M., Saito, K. (2003). Global expression profiling of sulfur-starved Arabidopsis by DNA macroarray reveals the role of *O*-acetyl-l-serine as a general regulator of gene expression in response to sulfur nutrition. Plant J **33**, 651-663.

Hirai, M.Y., Sugiyama, K., Sawada, Y., Tohge, T., Obayashi, T., Suzuki, A., Araki, R., Sakurai, N., Suzuki, H., Aoki, K., Goda, H., Nishizawa, O. I., Shibata, D., Saito, K. (2007). Omics-based identification of Arabidopsis MYB transcription factors regulating aliphatic glucosinolate biosynthesis. PNAS **104**, 6478-6483.

Ho, C.H., Lin, S.H., Hu, H.C., Tsay, Y.F. (2009). CHL1 functions as a nitrate sensor in plants. Cell **138**, 1184-1194.

Hopkins, L., Parmar, S., Blaszczyk, A., Hesse, H., Hoefgen, R., Hawkesford, M.J. (2005). *O*-acetylserine and the regulation of expression of genes encoding components for sulfate uptake and assimilation in potato. Plant Physiol **138**, 433-440.

Howarth, J., Parmar, S., Barraclough, P., Hawkesford, M. (2009). A sulphur deficiency-induced gene, *SDI1*, involved in the utilization of stored sulphate pools under sulphur-limiting conditions has potential as a diagnostic indicator of sulphur nutritional status. Plant Biotechnol J **7**, 200-209.

Howden, R., Andersen, C.R., Goldsbrough, P.B., Cobbett, C.S. (1995) A cadmium-sensitive, glutathione-deficient mutant of *Arabidopsis thaliana*. Plant Physiol **107,** 1067–1073

Huang, B., Vetting, M.W., Roderick, S.L. (2005). The active site of *O*-acetylserine sulfhydrylase is the anchor point for bienzyme complex formation with serine acetyltransferase. J Bacteriol **187**, 3201-3205.

Huang, X.Y., Chao, D.Y., Koprivova, A., Danku, J., Wirtz, M., Muller, S., Sandoval, F.J., Bauwe, H., Roje, S., Dilkes, B., *B.*, Hell, R., Kopriva, S., Salt, D. E.(2016). Nuclear localised MORE SULPHUR ACCUMULATION1 epigenetically regulates sulphur homeostasis in *Arabidopsis thaliana*. PLoS Genet **12**, e1006298.

Hubberten, H., Klie, S., Caldana, C., Degenkolbe, T., Willmitzer, L., Hoefgen, R. (2012a). Additional role of *O*-acetylserine as a sulfur status-independent regulator during plant growth. Plant J **70**, 666-677.

Hubberten, H.M., Drozd, A., Tran, B.V., Hesse, H., and Hoefgen, R. (2012b). Local and systemic regulation of sulphur homeostasis in roots of *Arabidopsis thaliana*. Plant J.**72**, 625–635

Inaba, K., Fujiwara, T., Hayashi, H., Chino, M., Komeda, Y., Naito, S. (1994). Isolation of an *Arabidopsis thaliana* mutant, *mto1*, that overaccumulates soluble methionine. Plant Physiol **104**, 881-887.

Initiative, T.A.G. (2000). Analysis of the genome sequence of the flowering plant *Arabidopsis thaliana*. Nature **408**, 796-815.

Jez, J.M., Cahoon, R.E., and Chen, S. (2004). *Arabidopsis thaliana* glutamate-cysteine ligase: Functional properties, kinetic mechanism, and regulation of activity. J Biol Chem **279**, 33463-33470.

Jez, J.M., Ravilious, G.E., Herrmann, J. (2016). Structural biology and regulation of the plant sulfation pathway. Chem Biol Interact **259**, 31-38.

Jones-Rhoades, M.W., and Bartel, D.P. (2004). Computational identification of plant microRNAs and their targets, including a stress-induced mirna. Molecular Cell **14**, 787-799.

Joshi, N.C., Meyer, A.J., Bangash, S.A.K., Zheng, Z.L., Leustek, T. (2019). Arabidopsis *gamma-glutamylcyclotransferase* affects glutathione content and root system architecture during sulfur starvation. New Phytologist **221**, 1387-1397.

Jost, R., Berkowitz, O., Wirtz, M., Hopkins, L., Hawkesford, M., Hell, R. (2000). Genomic and functional characterization of the OAS gene family encoding *O-acetylserine (thiol) lyases*, enzymes catalyzing the final step in cysteine biosynthesis in *Arabidopsis thaliana*. Gene **253**, 237-247.

Jurado-Flores, A., Romero, L.C., Gotor, C. (2021). Label-free quantitative proteomic analysis of nitrogen starvation in Arabidopsis root reveals new aspects of H_2S signaling by protein persulfidation. Antioxidants (Basel) **10**, 508.

Kandasamy, M.K., McKinney, E.C., Deal, R.B., Meagher, R.B. (2005). Arabidopsis *ARP7* is an essential actin-related protein required for normal embryogenesis, plant architecture, and floral organ abscission. Plant Physiol **138**, 2019-2032.

Kataoka, T., Hayashi, N., Yamaya, T., Takahashi, H. (2004a). Root-to-shoot transport of sulfate in Arabidopsis. Evidence for the role of SULTR3;5 as a component of low-affinity sulfate transport system in the root vasculature. Plant Physiol **136**, 4198-4204.

Kataoka, T., Watanabe-Takahashi, A., Hayashi, N., Ohnishi, M., Mimura, T., Buchner, P., Hawkesford, M.J., Yamaya, T., Takahashi, H. (2004b). Vacuolar sulfate transporters are essential determinants controlling internal distribution of sulfate in Arabidopsis. Plant C **16**, 2693-2704.

Kawashima, C.G., Berkowitz, O., Hell, R., Noji, M., Saito, K. (2005). Characterization and expression analysis of a *serine acetyltransferase* gene family involved in a key step of the sulfur assimilation pathway in Arabidopsis. Plant Physiol **137**, 220-230.

Kawashima, C.G., Yoshimoto N., Maruyama-Nakashita A., Tsuchiya Y.N., Saito K., Takahashi H., Dalmay, T. (2009). Sulphur starvation induces the expression of microRNA-395 and one of its target genes but in different cell types. Plant J **57**, 313-321.

Khan, M.S., Haas, F.H., Allboje Samami, A., Moghaddas Gholami, A., Bauer, A., Fellenberg, K., Reichelt, M., Hansch, R., Mendel, R.R., Meyer, A.J., Wirtz, M., Hell, R. (2010). Sulfite reductase defines a newly discovered bottleneck for assimilatory sulfate reduction and is essential for growth and development in *Arabidopsis thaliana*. Plant Cell **22**, 1216-1231.

Kopriva, S., and Koprivova, A. (2004). Plant adenosine 5'-phosphosulphate reductase: The past, the present, and the future. J Exp Bot **55**, 1775-1783.

Kopriva, S., and Rennenberg, H. (2004). Control of sulphate assimilation and glutathione synthesis: Interaction with N and C metabolism. J Exp Bot **55**, 1831-1842.

Koprivova, A., and Kopriva, S. (2014). Molecular mechanisms of regulation of sulfate assimilation: First steps on a long road. Front Plant Sci **5**, 589.

Koralewska, A., Buchner, P., Stuiver, C.E.E., Posthumus, F.S., Kopriva, S., Hawkesford, M.J., De Kok, L.J. (2009). Expression and activity of sulfate transporters and APS reductase in curly kale in response to sulfate deprivation and re-supply. J Plant Physiol **166**, 168-179.

Korotkevich, G., Sukhov, V., Budin, N., Shpak, B., Artyomov, M.N., Sergushichev, A. (2021) Fast gene set enrichment analysis. bioRxiv, 060012.

Krasileva, K.V., Dahlbeck, D., Staskawicz, B.J. (2010). Activation of an Arabidopsis resistance protein is specified by the *in planta* association of its leucine-rich repeat domain with the cognate oomycete effector. Plant C **22**, 2444-2458.

Kredich, N.M., Becker, M.A., Tomkins, G.M. (1969). Purification and characterization of cysteine synthetase, a bifunctional protein complex, from *salmonella typhimurium*. J Biol Chem **244**, 2428-2439.

Kumar, S., Kaur, A., Chattopadhyay, B., Bachhawat, A.K. (2015). Defining the cytosolic pathway of glutathione degradation in *Arabidopsis thaliana*: Role of the *ChaC/GCG* family of gamma-glutamyl cyclotransferases as glutathione-degrading enzymes and *At*LAP1 as the Cys-Gly peptidase. Biochem J **468**, 73-85.

Kumaran, S., and Jez, J.M. (2007). Thermodynamics of the interaction between *O*-acetylserine sulfhydrylase and the C-terminus of serine acetyltransferase. Biochem **46**, 5586-5594.

Kutz, A., Muller, A., Hennig, P., Kaiser, W.M., Piotrowski, M., and Weiler, E.W. (2002). A role for *nitrilase 3* in the regulation of root morphology in sulphur-starving *Arabidopsis thaliana*. Plant J **30**, 95-106.

Lampropoulos, A., Sutikovic, Z., Wenzl, C., Maegele, I., Lohmann, J.U., Forner, J. (2013). Greengate---a novel, versatile, and efficient cloning system for plant transgenesis. PLoS One **8**, e83043.

Lanctot, A., and Nemhauser, J.L. (2020). It's morphin' time: How multiple signals converge on ARF transcription factors to direct development. Curr Opin Plant Biol **57**, 1-7.

Lappartient, A.G., and Touraine, B. (1996). Demand-driven control of root ATP sulfurylase activity and SO_4^{2-} uptake in intact canola. Plant Physiol **111**, 147-157.

Lappartient, A.G., Vidmar, J.J., Leustek, T., Glass, A.D., Touraine, B. (1999). Inter-organ signaling in plants: Regulation of *ATP sulfurylase* and *sulfate transporter* genes expression in roots mediated by phloem-translocated compound. Plant J **18**, 89-95.

Lee, B.R., Koprivova, A., and Kopriva, S. (2011). The key enzyme of sulfate assimilation, *adenosine 5'-phosphosulfate reductase*, is regulated by HY5 in Arabidopsis. Plant J **67**, 1042-1054.

Lee, L.R., Guillotin, B., Rahni, R., Hutchison, C., Desvoyes, B., Gutierrez, C., Birnbaum, K.D. (2025). Glutathione accelerates the cell cycle and cellular reprogramming in plant regeneration. bioRxiv 2023.11.28.569014.

Lee, S., and Leustek, T. (1998). APS kinase from *Arabidopsis thaliana*: Genomic organization, expression, and kinetic analysis of the recombinant enzyme. Biochem Biophys Res Commun **247**, 171-175.

Lee, S., and Leustek, T. (1999). The affect of cadmium on sulfate assimilation enzymes in *Brassica juncea*. Plant Science **141**, Pages 201-207.

Leustek, T. (2002). Sulfate metabolism. The Arabidopsis Book, 1-16.

Leustek, T., Martin, M.N., Bick, J.A., Davies, J.P. (2000). Pathways and regulation of sulfur metabolism revealed through molecular and genetic studies. Ann Rev Plant Physiol Plant Mol Biol **51**, 141-165.

Leustek, T., Murillo, M., and Cervantes, M. (1994). Cloning of a cDNA encoding ATP sulfurylase from *Arabidopsis thaliana* by functional expression in *Saccharomyces cerevisiae*. Plant Physiol **105**, 897-902.

Leustek, T., and Saito, K. (1999). Sulfate transport and assimilation in plants. Plant Physiol **120**, 637-644.

Lewandowska, M., Wawrzynska, A., Moniuszko, G., Lukomska, J., Zientara, K., Piecho, M., Hodurek, P., Zhukov, I., Liszewska, F., Nikiforova, V.*, et al.* (2010). A contribution to identification of novel regulators of plant response to sulfur deficiency: Characteristics of a tobacco gene *UP9c*, its protein product and the effects of *UP9c* silencing. Mol Plant **3**, 347-360.

Li, Q., Gao, Y., Yang, A. (2020). Sulfur homeostasis in plants. Int J Mol Sci **21**, 8926.

Liang, G., Yang, F., Yu, D. (2010). MicroRNA395 mediates regulation of sulfate accumulation and allocation in *Arabidopsis thaliana*. Plant J, no-no.

Lillig, C.H., Schiffmann, S., Berndt, C., Berken, A., Tischka, R., Schwenn, J.D. (2001). Molecular and catalytic properties of *Arabidopsis thaliana* adenylyl sulfate (APS)-kinase. Arch Biochem Biophys **392**, 303-310.

Liu, D., Li, M., Guo, T., Lu, J., Xie, Y., Hao, Y., Wang, L., Zhao, D., Zhang, L., Liu, Z., *J*in, Z., & Pei, Y. (2022). Functional characterization of the *serine acetyltransferase* family genes uncovers the diversification and conservation of cysteine biosynthesis in tomato. Front Plant Sci **13**, 913856.

Liu, F., Lou, W., Wang, J., Li, Q., Shen, W. (2021). Glutathione produced by gamma-glutamyl cysteine synthetase acts downstream of hydrogen to positively influence lateral root branching. Plant Physiol Biochem **167**, 68-76.

Liu, K.H., Niu, Y., Konishi, M., Wu, Y., Du, H., Sun Chung, H., Li, L., Boudsocq, M., McCormack, M., Maekawa, S., Ishida, T., Zhang, C., Shokat, K., Yanagisawa, S., Sheen, J. (2017). Discovery of nitrate-CPK-NLP signalling in central nutrient-growth networks. Nature **545**, 311-316.

Liu, X., Zhang, C., Zhang, L., Huang, J., Dang, C., Xie, C., Wang, Z. (2020). TaRPP13-3, a CC-NBS-LRR-like gene located on chr 7D, promotes disease resistance to wheat powdery mildew in brock. J Phytopathol **168**, 688-699.

Logan, H.M., Cathala, N., Grignon, C., Davidian, J.C. (1996). Cloning of a cDNA encoded by a member of the *Arabidopsis thaliana ATP sulfurylase* multigene family. Expression studies in yeast and in relation to plant sulfur nutrition. J Biol Chem **271**, 12227-12233.

Loudet, O., Saliba-Colombani, V., Camilleri, C., Calenge, F., Gaudon, V., Koprivova, A., North, K., Kopriva, S., Daniel-Vedele, F. (2007). Natural variation for sulfate content in *Arabidopsis thaliana* is highly controlled by APR2. Nat Genet **39**, 896-900.

Lunn, J.E., Droux, M., Martin, J., Douce, R. (1990). Localization of atp-sulfurylase and *o*-acetylserine(thiol)lyase in spinach leaves. Plant Physiol **94**, 1345-1352.

Maghiaoui, A., Gojon, A., Bach, L. (2020). NRT1.1-centered nitrate signaling in plants. J Exp Bot **71**, 6226-6237.

Malitsky, S., Blum, E., Less, H., Venger, I., Elbaz, M., Morin, S., Eshed, Y., Aharoni, A. (2008). The transcript and metabolite networks affected by the two clades of Arabidopsis glucosinolate biosynthesis regulators. Plant Physiol **148**, 2021-2049.

Maruyama-Nakashita, A., Inoue, E., Watanabe-Takahashi, A., Yamaya, T., Takahashi, H. (2003). Transcriptome profiling of sulfur-responsive genes in Arabidopsis reveals global effects of sulfur nutrition on multiple metabolic pathways. Plant Physiol **132**, 597-605.

Maruyama-Nakashita, A., Nakamura, Y., Tohge, T., Saito, K., Takahashi, H. (2006). Arabidopsis SLIM1 is a central transcriptional regulator of plant sulfur response and metabolism. Plant C **18**, 3235-3251.

Maruyama-Nakashita, A., Nakamura, Y., Watanabe-Takahashi, A., Inoue, E., Yamaya, T., Takahashi, H. (2005). Identification of a novel cis-acting element conferring sulfur deficiency response in Arabidopsis roots. Plant J **42**, 305-314.

Maruyama-Nakashita, A., Nakamura, Y., Watanabe-Takahashi, A., Yamaya, T., Takahashi, H. (2004a). Induction of SULTR1;1 sulfate transporter in Arabidopsis roots involves protein phosphorylation/dephosphorylation circuit for transcriptional regulation. Plant Cell Physiol **45**, 340-345.

Maruyama-Nakashita, A., Nakamura, Y., Yamaya, T., Takahashi, H. (2004b). Regulation of high-affinity sulphate transporters in plants: Towards systematic analysis of sulphur signalling and regulation. J Exp Bot **55**, 1843-1849.

Maruyama-Nakashita, A., Watanabe-Takahashi, A., Inoue, E., Yamaya, T., Saito, K., Takahashi, H. (2015). Sulfur-responsive elements in the 3'-nontranscribed intergenic region are essential for the induction of *SULFATE TRANSPORTER 2;1* gene expression in Arabidopsis roots under sulfur deficiency. Plant C **27**, 1279-1296.

Matsuura, H., Takenami, S., Kubo, Y., Ueda, K., Ueda, A., Yamaguchi, M., Hirata, K., Demura, T., Kanaya, S., Kato, K. (2013). A computational and experimental approach reveals that the 5'-proximal region of the 5'-UTR has a cis-regulatory signature responsible for heat stress-regulated mRNA translation in Arabidopsis. Plant C Physiol **54**, 474-483.

May, M.J., and Leaver, C.J. (1994). *Arabidopsis thaliana* γ-glutamylcysteine synthetase is structurally unrelated to mammalian, yeast, and *Escherichia coli* homologs. Proc Natl Acad Sci U S A **91**, 10059-10063.

Meagher, R.B., Kandasamy, M.K., McKinney, E.C., Roy, E. (2009). Chapter 5 nuclear actin-related proteins in epigenetic control. Int Rev Cell Mol Bio (Academic Press), pp. 157-215.

Meyer, A.J., Dreyer, A., Ugalde, J.M., Feitosa-Araujo, E., Dietz, K.J., Schwarzländer, M. (2020). Shifting paradigms and novel players in cys-based redox regulation and ros signaling in plants - and where to go next. Biol Chem **403**, 399–423.

Meyer, A.J., and Rausch, T. (2008). Biosynthesis, compartmentation and cellular functions of glutathione in plant cells. In Sulfur metabolism in phototrophic organisms, **R. Hell, C. Dahl, D.B. Knaff, and T. Leustek,** eds. (Dordrecht, The Netherlands: Springer), pp. 161-184.

Moseler, A., Wagner, S., Meyer, A.J. (2024). Protein persulfidation in plants: Mechanisms and functions beyond a simple stress response. Biol Chem. doi:10.1515/hsz-2024-0038

Mugford, S.G., Yoshimoto, N., Reichelt, M., Wirtz, M., Hill, L., Mugford, S.T., Nakazato, Y., Noji, M., Takahashi, H., Kramell, R., Gigolashvili, T., Flügge, U. I., Wasternack, C., Gershenzon, J., Hell, R., Saito, K., Kopriva, S. (2009a). Disruption of adenosine-5'-phosphosulfate kinase in Arabidopsis reduces levels of sulfated secondary metabolites. Plant C **21**, 910-927.

Murillo, M., and Leustek, T. (1995). Adenosine-5'-triphosphate-sulfurylase from *Arabidopsis thaliana* and *Escherichia coli* are functionally equivalent but structurally and kinetically divergent: Nucleotide sequence of two adenosine-5'-triphosphate-sulfurylase cDNAs from *Arabidopsis thaliana* and analysis of a recombinant enzyme. Arch Biochem Biophys **323**, 195-204.

Nakai, Y., and Maruyama-Nakashita, A. (2020). Biosynthesis of sulfur-containing small biomolecules in plants. Int J Mol Sci **21**, 3470.

Neuenschwander, U., Suter, M., Brunold, C. (1991). Regulation of sulfate assimilation by light and *O*-acetyl-l-serine in *Lemna minor* l. Plant Physiol **97**, 253-258.

Nie, W.F., and Wang, J. (2021). Actin-related protein 4 interacts with PIE1 and regulates gene expression in Arabidopsis. Genes (Basel) **12**, 520.

Nikiforova, V., Freitag, J., Kempa, S., Adamik, M., Hesse, H., Hoefgen, R. (2003). Transcriptome analysis of sulfur depletion in *Arabidopsis thaliana*: Interlacing of biosynthetic pathways provides response specificity. Plant J **33**, 633-650.

Nikiforova, V.J., Daub, C.O., Hesse, H., Willmitzer, L., Hoefgen, R. (2005). Integrative gene-metabolite network with implemented causality deciphers informational fluxes of sulphur stress response. J Exp Bot **56**, 1887-1896.

Nocito, F.F., Lancilli, C., Crema, B., Fourcroy, P., Davidian, J.C., Sacchi, G.A. (2006). Heavy metal stress and sulfate uptake in maize roots. Plant Physiol **141**, 1138-1148.

Nocito, F.F., Lancilli, C., Giacomini, B., Sacchi, G.A. (2007). Sulfur metabolism and cadmium stress in higher plants. Plant Stress **1**, 142-156.

Noji, M., Inoue, K., Kimura, N., Gouda, A., Saito, K. (1998). Isoform-dependent differences in feedback regulation and subcellular localization of serine acetyltransferase involved in cysteine biosynthesis from *Arabidopsis thaliana*. J Biol Chem **273**, 32739-32745.

Ogawa, K., Hatano-Iwasaki, A., Yanagida, M., Iwabuchi, M. (2004). Level of glutathione is regulated by ATP-dependent ligation of glutamate and cysteine through photosynthesis in *Arabidopsis thaliana*: Mechanism of strong interaction of light intensity with flowering. Plant Cell Physiol **45**, 1-8.

Parisy, V., Poinssot, B., Owsianowski, L., Buchala, A., Glazebrook, J., Mauch, F. (2007). Identification of *PAD2* as a γ-glutamylcysteine synthetase highlights the importance of glutathione in disease resistance of Arabidopsis. Plant J **49**, 159-172.

Paulose, B., Chhikara, S., Coomey, J., Jung, H.I., Vatamaniuk, O., Dhankher, O.P. (2013). A gamma-glutamyl cyclotransferase protects Arabidopsis plants from heavy metal toxicity by recycling glutamate to maintain glutathione homeostasis. Plant C **25**, 4580-4595.

Pavlu, J., Kerchev, P., Cerny, M., Novak, J., Berka, M., Jobe, T.O., Lopez Ramos, J.M., Saiz-Fernandez, I., Rashotte, A.M., Kopriva, S., Brzobohatý, B.(2022). Cytokinin modulates the metabolic network of sulfur and glutathione. J Exp Bot **73**, 7417-7433.

Piotrowska, J., Wawrzynska, A., Olszak, M., Krzyszton, M., Apodiakou, A., Alseekh, S., Ramos, J.M.L., Hoefgen, R., Kopriva, S., Sirko, A. (2024). Analysis of the quadruple *lsu* mutant reveals molecular determinants of the role of LSU proteins in sulfur assimilation in Arabidopsis. Plant J **120**, 2919-2936.

Rabeh, W.M., and Cook, P.F. (2004). Structure and mechanism of *o*-acetylserine sulfhydrylase. J Biol Chem **279**, 26803-26806.

Raipuria, R.K., Kumar, V., Guruprasad, K.N., Bhat, S.R. (2017). Analysis of promoters of *Arabidopsis thaliana* divergent gene pair *SERAT3;2* and *IDH-III* shows *SERAT3;2* promoter is nested within the *IDH-III* promoter. Mol biotechnol **59**, 294-304.

Rakpenthai, A., Apodiakou, A., Whitcomb, S.J., Hoefgen, R. (2022). *In silico* analysis of cis-elements and identification of transcription factors putatively involved in the regulation of the oas cluster genes *SDI1* and *SDI2*. Plant J **110**, 1286-1304.

Rausch, T., Gromes, R., Liedschulte, V., Muller, I., Bogs, J., Galovic, V., Wachter, A. (2007). Novel insight into the regulation of GSH biosynthesis in higher plants. Plant Biol **9**, 565-572.

Rausch, T., and Wachter, A. (2005). Sulfur metabolism: A versatile platform for launching defence operations. Trends Plant Sci **10**, 503-509.

Rawlins, M.R., Leaver, C.J., May, M.J. (1995). Characterisation of an *Arabidopsis thaliana* cDNA encoding glutathione synthetase. FEBS Lett **376**, 81-86.

Ristova, D., and Kopriva, S. (2022). Sulfur signaling and starvation response in Arabidopsis. iScience **25**, 104242-104242.

Ritchie, M.E., Phipson, B., Wu, D., Hu, Y., Law, C.W., Shi, W., Smyth, G.K. (2015). Limma powers differential expression analyses for RNA-sequencing and microarray studies. Nucl Acids Res **43**, e47-e47.

Rotte, C., and Leustek, T. (2000). Differential subcellular localization and expression of ATP sulfurylase and 5'-adenylylsulfate reductase during ontogenesis of Arabidopsis leaves indicates that cytosolic and plastid forms of ATP sulfurylase may have specialized functions. Plant Physiol **124**, 715-724.

Rouached, H., Berthomieu, P., Kassis, E.E., Cathala, N., Catherinot, V., Labesse, G., Davidian, J.C.E., Fourcroy, P. (2005). Structural and functional analysis of the C-terminal STAS (sulfate transporter and anti-sigma antagonist) domain of the *Arabidopsis thaliana* sulfate transporter SULTR1;2. JBC **280**, 15976-15983.

Rouached, H., Wirtz, M., Alary, R., Hell, R., Arpat, A.B., Davidian, J.-C.E., Fourcroy, P., Berthomieu, P. (2008). Differential regulation of the expression of two high-affinity sulfate transporters, *SULTR1.1* and *SULTR1.2* in Arabidopsis. Plant Physiol **147**, 897-911.

Rubio, V., Linhares, F., Solano, R., Martin, A.C., Iglesias, J., Leyva, A., Paz-Ares, J. (2001). A conserved MYB transcription factor involved in phosphate starvation signaling both in vascular plants and in unicellular algae. Genes Dev **15**, 2122-2133.

Ruffet, M.L., Lebrun, M., Droux, M., Douce, R. (1995). Subcellular distribution of serine acetyltransferase from *Pisum sativum* and characterization of an *Arabidopsis thaliana* putative cytosolic isoform. Eur J Biochem **227**, 500-509.

Saito, K. (2000). Regulation of sulfate transport and synthesis of sulfur-containing amino acids. Curr Opin Plant Biol **3**, 188-195.

Sánchez-Fernández, R., Fricker, M., Corben, L.B., White, N.S., Sheard, N., Leaver, C.J., Van Montagu, M., Inze, D., May, M.J. (1997). Cell proliferation and hair tip growth in the Arabidopsis root are under mechanistically different forms of redox control. Proc Natl Acad Sci **94**, 2745-2750.

Scherer, H.W., Pacyna, S., Spoth, K.R., Schulz, M. (2008). Low levels of ferredoxin, ATP and leghemoglobin contribute to limited N_2 fixation of peas (*Pisum sativum L.*) and alfalfa (*Medicago sativa L.*) under S deficiency conditions. Biol Fertil Soils **44**, 909-916.

Schiel, D. (2020). Energy-dependent and subcellular regulation of the SnRK1 signaling network via protein-protein interactions. (Heidelberg, Univ., Diss., 2020).

Shahan, R., Hsu, C.-W., Nolan, T.M., Cole, B.J., Taylor, I.W., Greenstreet, L., Zhang, S., Afanassiev, A., Vlot, A.H.C., Schiebinger, G., Benfey, P. N., Ohler, U. (2022). A single-cell Arabidopsis root atlas reveals developmental trajectories in wild-type and cell identity mutants. Dev Cell **57**, 543-560.

Sharma, R.K., Cox, M.S., Oglesby, C., Dhillon, J.S. (2024). Revisiting the role of sulfur in crop production: A narrative review. J Agric Food Res **15**, 101013.

Shee, R., Shee, D., Sahid, S., Paul, S., and Datta, R. (2023). Glutathione induces Arabidopsis *PHT1;5* gene via WRKY75 transcription factor to regulate phosphate homeostasis. bioRxiv, 2022.2011.2003.515049.

Shibagaki, N., and Grossman, A.R. (2004). Probing the function of STAS domains of the Arabidopsis sulfate transporters. J Biol Chem **279**, 30791-30799.

Shibagaki, N., and Grossman, A.R. (2006). The role of the STAS domain in the function and biogenesis of a sulfate transporter as probed by random mutagenesis. J Biol Chem **281**, 22964-22973.

Shibagaki, N., and Grossman, A.R. (2010). Binding of cysteine synthase to the STAS domain of sulfate transporter and its regulatory consequences. J Biol Chem **285**, 25094-25102.

Shibagaki, N., Rose, A., McDermott, J.P., Fujiwara, T., Hayashi, H., Yoneyama, T., Davies, J.P. (2002). Selenate-resistant mutants of *Arabidopsis thaliana* identify SULTR1;2, a sulfate transporter required for efficient transport of sulfate into roots. Plant J **29**, 475-486.

Shirzadian-Khorramabad, R., Jing, H.C., Everts, G.E., Schippers, J.H., Hille, J., Dijkwel, P.P. (2010). A mutation in the cytosolic *O*-acetylserine(thiol)lyase induces a genome-dependent early leaf death phenotype in Arabidopsis. BMC Plant Biol **10**, 80.

Singh, A., Sharma, A., Singh, N., Nandi, A.K. (2022). *mto1*-responding down 1 (*MRD1*) is a transcriptional target of OZF1 for promoting salicylic acid-mediated defense in Arabidopsis. Plant Cell Rep **41**, 1319-1328.

Sparkes, I.A., Runions, J., Kearns, A., Hawes, C. (2006). Rapid, transient expression of fluorescent fusion proteins in tobacco plants and generation of stably transformed plants. Nat Protoc **1**, 2019-2025.

Speiser, A. (2014). The relevance of cysteine synthase complex formation in different subcellular compartments of plant cells for regulation of sulfur homeostasis. In Combined Faculties for the Natural Sciences and for Mathematics (Heidelberg, Germany: Ruperto-Carola University of Heidelberg), pp. 164.

Speiser, A., Silbermann, M., Dong, Y., Haberland, S., Uslu, V.V., Wang, S., Bangash, S.A.K., Reichelt, M., Meyer, A.J., Wirtz, M., Hell, R. (2018). Sulfur partitioning between glutathione and protein synthesis determines plant growth. Plant Physiol **177**, 927-937.

Stuttmann, J., Barthel, K., Martin, P., Ordon, J., Erickson, J.L., Herr, R., Ferik, F., Kretschmer, C., Berner, T., Keilwagen, J., Marillonnet, S., Bonas, U. (2021). Highly efficient multiplex editing: One-shot generation of 8x *Nicotiana benthamiana* and 12x Arabidopsis mutants. Plant J **106**, 8-22.

Suzuki, A., Shirata, Y., Ishida, H., Chiba, Y., Onouchi, H., Naito, S. (2001). The first exon coding region of *cystathionine gamma-synthase* gene is necessary and sufficient for downregulation of its own mRNA accumulation in transgenic *Arabidopsis thaliana*. Plant Cell Physiol **42**, 1174-1180.

Tahir, J., Watanabe, M., Jing, H.C., Hunter, D.A., Tohge, T., Nunes-Nesi, A., Brotman, Y., Fernie, A.R., Hoefgen, R., and Dijkwel, P.P. (2013). Activation of R-mediated innate immunity and disease susceptibility is affected by mutations in a cytosolic O-acetylserine(thiol)lyase in Arabidopsis. Plant J **73**, 118-130.

Takahashi, H. (2019). Sulfate transport systems in plants: Functional diversity and molecular mechanisms underlying regulatory coordination. J Exp Bot **70**, 4075-4087.

Takahashi, H., Kopriva, S., Giordano, M., Saito, K., Hell, R. (2011). Sulfur assimilation in photosynthetic organisms: Molecular functions and regulations of transporters and assimilatory enzymes. Annu Rev Plant Biol **62**, 157-184.

Takahashi, H., Watanabe-Takahashi, A., Smith, F.W., Blake-Kalff, M., Hawkesford, M.J., and Saito, K. (2000). The roles of three functional sulphate transporters involved in uptake and translocation of sulphate in *Arabidopsis thaliana*. Plant J **23**, 171-182.

Takahashi, H., Yamazaki, M., Sasakura, N., Watanabe, A., Leustek, T., Engler, J.A., Engler, G., Van Montagu, M., Saito, K. (1997). Regulation of sulfur assimilation in higher plants: A sulfate transporter induced in sulfate-starved roots plays a central role in *Arabidopsis thaliana*. Proc Natl Acad Sci **94**, 11102-11107.

Tavares, S., Wirtz, M., Beier, M.P., Bogs, J., Hell, R., Amâncio, S. (2015). Characterization of the *serine acetyltransferase* gene family of *Vitis vinifera* uncovers differences in regulation of OAS synthesis in woody plants. Front Plant Sci **6**.

Teng, S., Keurentjes, J., Bentsink, L., Koornneef, M., Smeekens, S. (2005). Sucrose-specific induction of anthocyanin biosynthesis in Arabidopsis requires the MYB75/PAP1 gene. Plant Physiol **139**, 1840-1852.

Tocquin, P., Corbesier, L., Havelange, A., Pieltain, A., Kurtem, E., Bernier, G., Perilleux, C. (2003). A novel high efficiency, low maintenance, hydroponic system for synchronous growth and flowering of *Arabidopsis thaliana*. BMC Plant Biol **3**, 2.

Trujillo-Hernandez, J.A., Bariat, L., Enders, T.A., Strader, L.C., Reichheld, J.P., Belin, C. (2020). A glutathione-dependent control of the indole butyric acid pathway supports Arabidopsis root system adaptation to phosphate deprivation. J Exp Bot **71**, 4843-4857.

Vauclare, P., Kopriva, S., Fell, D., Suter, M., Sticher, L., von Ballmoos, P., Krahenbuhl, U., den Camp, R.O., Brunold, C. (2002). Flux control of sulphate assimilation in *Arabidopsis thaliana*: Adenosine 5'-phosphosulphate reductase is more susceptible than ATP sulphurylase to negative control by thiols. Plant J **31**, 729-740.

Vidmar, J.J., Tagmount, A., Cathala, N., Touraine, B., Davidian, J.E. (2000). Cloning and characterization of a root specific high-affinity sulfate transporter from *Arabidopsis thaliana*. FEBS Lett **475**, 65-69.

Wachter, A., Wolf, S., Steininger, H., Bogs, J., Rausch, T. (2005). Differential targeting of *GSH1* and *GSH2* is achieved by multiple transcription initiation: Implications for the compartmentation of glutathione biosynthesis in the Brassicaceae. Plant J **41**, 15-30.

Watanabe, M., Kusano, M., Oikawa, A., Fukushima, A., Noji, M., Saito, K. (2008a). Physiological roles of the β-substituted alanine synthase gene family in Arabidopsis. Plant Physiol **146**, 310-320.

Watanabe, M., Mochida, K., Kato, T., Tabata, S., Yoshimoto, N., Noji, M., Saito, K. (2008b). Comparative genomics and reverse genetics analysis reveal indispensable functions of the *serine acetyltransferase* gene family in Arabidopsis. Plant C **20**, 2484-2496.

Wawrzynska, A., Lewandowska, M., Sirko, A. (2010). Nicotiana tabacum EIL2 directly regulates expression of at least one tobacco gene induced by sulphur starvation. J Exp Bot **61**, 889-900.

Wawrzynska, A., Piotrowska, J., Apodiakou, A., Bruckner, F., Hoefgen, R., Sirko, A. (2022). The SLIM1 transcription factor affects sugar signaling during sulfur deficiency in Arabidopsis. J Exp Bot **73**, 7362-7379.

Wawrzyńska, A., and Sirko, A. (2016). EIN3 interferes with the sulfur deficiency signaling in *Arabidopsis thaliana* through direct interaction with the SLIM1 transcription factor. Plant Sci **253**, 50-57.

Wawrzyńska, A., and Sirko, A. (2020). Proteasomal degradation of proteins is important for the proper transcriptional response to sulfur deficiency conditions in plants. PCP **61**, 1548-1564.

Westerman, S., Stulen, I., Suter, M., Brunold, C., De Kok, L.J. (2001). Atmospheric H_2S as sulphur source for *Brassica oleracea*: Consequences for the activity of the enzymes of the assimilatory sulphate reduction pathway. Plant Physiol Biochem **39**, 425-432.

Winter, D., Vinegar, B., Nahal, H., Ammar, R., Wilson, G.V., Provart, N.J. (2007). An "electronic fluorescent pictograph" browser for exploring and analyzing large-scale biological data sets. PLOS ONE **2**, e718.

Wirtz, M., Beard, K.F.M., Lee, C.P., Boltz, A., Schwarzländer, M., Fuchs, C., Meyer, A.J., Heeg, C., Sweetlove, L.J., Ratcliffe, R.G., Hell, R. (2012). Mitochondrial cysteine synthase complex regulates *O*-acetylserine biosynthesis in plants. JBC **287**, 27941-27947.

Wirtz, M., Berkowitz, O., Droux, M., Hell, R. (2001). The cysteine synthase complex from plants. Mitochondrial serine acetyltransferase from *Arabidopsis thaliana* carries a bifunctional domain for catalysis and protein-protein interaction. Eur J Biochem **268**, 686-693.

Wirtz, M., Birke, H., Heeg, C., Mueller, C., Hosp, F., Throm, C., Koenig, S., Feldman-Salit, A., Rippe, K., Petersen, G., Wade, R. C., Rybin, V., Scheffzek, K., Hell, R. (2010a). Structure and function of the hetero-oligomeric cysteine synthase complex in plants. J Biol Chem **285**, 32810-32817.

Wirtz, M., and Droux, M. (2005). Synthesis of the sulfur amino acids: Cysteine and methionine. Photosyn Res **86**, 345-362.

Wirtz, M., Droux, M., Hell, R. (2004). *O*-acetylserine (thiol) lyase: An enigmatic enzyme of plant cysteine biosynthesis revisited in *Arabidopsis thaliana*. J Exp Bot **55**, 1785-1798.

Wirtz, M., Heeg, C., Samami, A.A., Ruppert, T., Hell, R. (2010b). Enzymes of cysteine synthesis show extensive and conserved modifications patterns that include N-alpha-terminal acetylation. Amino Acids **39**, 1077-1086.

Wirtz, M., and Hell, R. (2006). Functional analysis of the cysteine synthase protein complex from plants: Structural, biochemical and regulatory properties. J Plant Physiol **163**, 273-286.

Wójcik, M., and Tukiendorf, A. (2011). Glutathione in adaptation of *Arabidopsis thaliana* to cadmium stress. Biol Plant **55**, 125-132.

Yamaguchi, Y., Nakamura, T., Kusano, T., Sano, H. (2000). Three Arabidopsis genes encoding proteins with differential activities for cysteine synthase and β-cyanoalanine synthase. Plant Cell Physiol **41**, 465-476.

Yatusevich, R., Mugford, S.G., Matthewman, C., Gigolashvili, T., Frerigmann, H., Delaney, S., Koprivova, A., Flugge, U.I., Kopriva, S. (2010). Genes of primary sulfate assimilation are part of the glucosinolate biosynthetic network in *Arabidopsis thaliana*. Plant J **62**, 1-11.

Yoshimoto, N., Inoue, E., Watanabe-Takahashi, A., Saito, K., Takahashi, H. (2007). Posttranscriptional regulation of high-affinity sulfate transporters in Arabidopsis by sulfur nutrition. Plant Physiol **145**, 378-388.

Yoshimoto, N., Takahashi, H., Smith, F.W., Yamaya, T., Saito, K. (2002). Two distinct high-affinity sulfate transporters with different inducibilities mediate uptake of sulfate in Arabidopsis roots. Plant J **29**, 465-473.

Yuan, B., Li, C., Wang, Q., Yao, Q., Guo, X., Zhang, Y., Wang, Z. (2024). Identification and functional characterization of the *RPP13* gene family in potato (*Solanum tuberosum L.*) for disease resistance. Front Plant Sci **15**, 1515060.

Zhang, B., Pasini, R., Dan, H., Joshi, N., Zhao, Y., Leustek, T., Zheng, Z.L. (2014). Aberrant gene expression in the Arabidopsis *sultr1;2* mutants suggests a possible regulatory role for this sulfate transporter in response to sulfur nutrient status. Plant J **77**, 185-197.

Zhang, L., Kawaguchi, R., Enomoto, T., Nishida, S., Burow, M., Maruyama-Nakashita, A. (2023). Glucosinolate catabolism maintains glucosinolate profiles and transport in sulfur-starved Arabidopsis. PCP **64**, 1534-1550.

Zhang, L., Kawaguchi, R., Morikawa-Ichinose, T., Allahham, A., Kim, S.J., Maruyama-Nakashita, A. (2020). Sulfur deficiency-induced glucosinolate catabolism attributed to two β-glucosidases, BGLU28 and BGLU30, is required for plant growth maintenance under sulfur deficiency. PCP **61**, 803-813.

Zhang, T.Q., Chen, Y., Wang, J.W. (2021). A single-cell analysis of the Arabidopsis vegetative shoot apex. Dev Cell **56**, 1056-1074.e1058.

Zheng, Z.L., Zhang, B., and Leustek, T. (2014). Transceptors at the boundary of nutrient transporters and receptors: A new role for Arabidopsis SULTR1;2 in sulfur sensing. Front Plant Sci **5**, 710.

6. Supplemental Figures and Tables

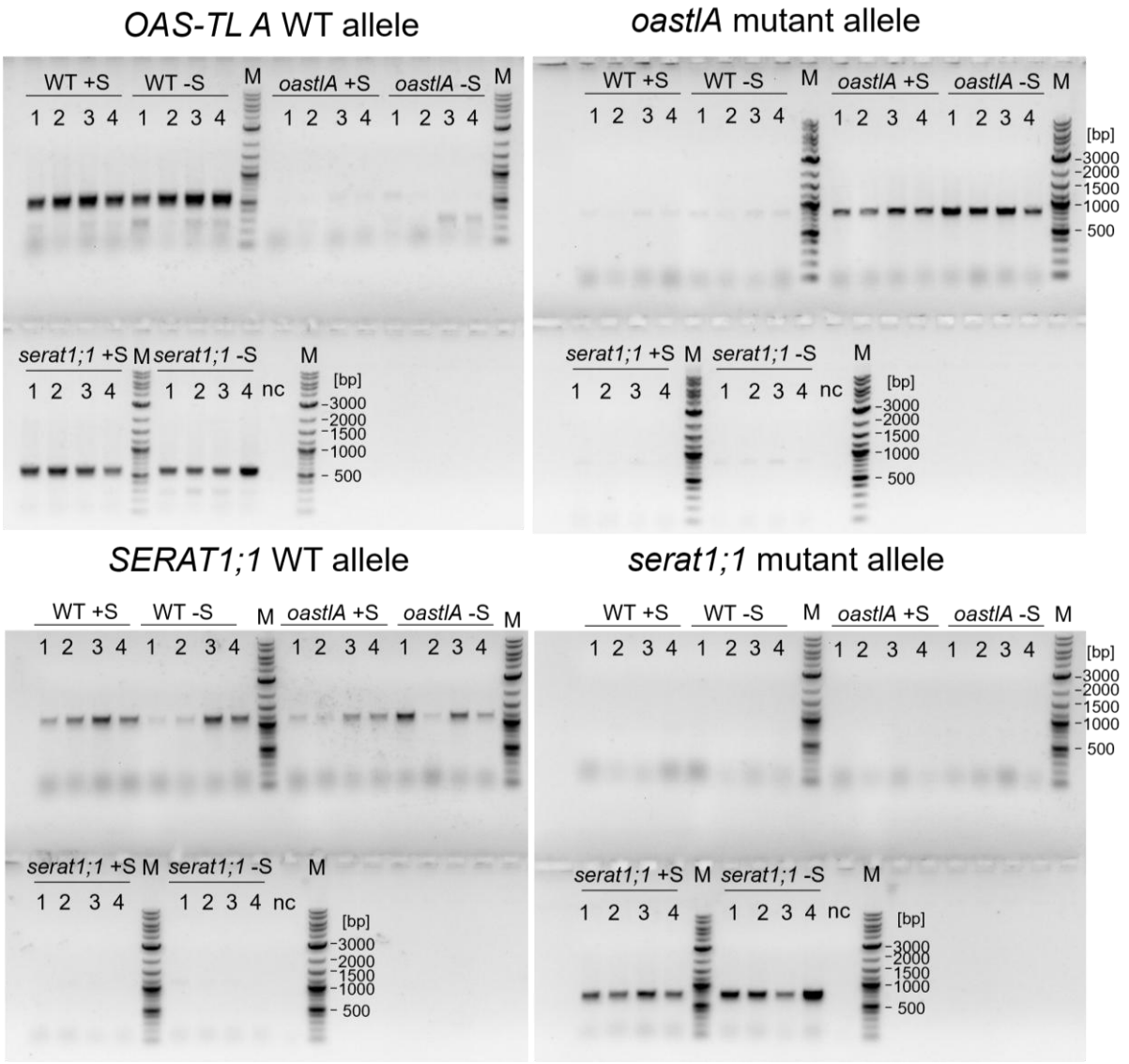

Supplemental Figure 1: Genotyping PCR for *oastlA* and *serat1;1* T-DNA mutants. WT and the T-DNA mutants *oastlA* and *serat1;1* (2.3.1) were grown for seven weeks in liquid +S ½ Hoagland medium (500 µM sulfate) (2.3.7). Before harvest, half of the plants were subjected to sulfur deficiency stress (0 µM sulfate) for 6 h. The root material was snap-frozen, and gDNA extracted (2.4.3) for four individuals of each genotype per treatment. To detect the WT alleles of *SERAT1;1* and *OAS-TL A*, genotyping PCR (2.4.7) was performed with the primers 1639/1640 (1200 bps) and 302/653 (600 bps), respectively (2.4.6). To detect the mutant alleles *serat1;1* and *oastlA,* the genotyping PCR (2.4.7) was performed with primers 1639/1401 (900 bps) and primers 302/1225 (800 bps). The PCR products were size-separated using gel electrophoresis (2.4.9). In nc, the gDNA was replaced by water. The expected genotype was verified for all individuals.

Results of job ID: 202211221ipaxu

Genome: Arabidopsis thaliana (TAIR10), **Position:** 4:8520596-8517960 (2637 bp), **Locus:** AT4G14880

Click Show Restriction Enzyme Sites to show or hide restriction enzyme sites that are present in the candidate targets.

	Bad site warning	Target sequence	Position	Strand	GC (%)	Region	Potential off-target sites(Max score)	Pairing with sgRNA (>=8 nt)
☑		CACATCTTTAGCAATTCTCG AGG	573 - 554	-	40.0	CDS	0.170 (close)	None

Off-target predictor:

Chrom	Position	Sequence	Off-score	Gene	Region
2	16103436	CATATTTATCGCAATTCTCG AGG	0.17	AT2G38460	five_prime_UTR
1	15793405	CAAATCTCTAGCAATTTGCG AGG	0.135		intergenic
3	2764036	GACAGCTTTGCCAATTCTCA AGG	0.13	AT3G09040	CDS
2	5817389	CAAATCTGTAGCAATTTGCG AGG	0.099		intergenic
1	19675599	CAAATCTGTAGCAATTTGCG AGG	0.099		intergenic
3	8650184	TCCATCTTTAGCAATTCTAG AAG	0.087	AT3G23940	CDS
2	13150942	AACGTCTTTAGTATTTCTTG AGG	0.083	AT2G30900	intron
3	2421328	CACATCTTTAGAAAAACTAG AAG	0.042	AT3G07580	CDS
2	16840138	CACATCTTTAGTATTTCTTG AAG	0.034	AT2G40320	five_prime_UTR
3	5827290	CATCTCTTTAACCATTTCG AGG	0.024	AT3G17090	CDS
3	22664840	CACATCTGAAGCAAGTCTTG TGG	0.016	AT3G61230	CDS
1	24578871	CACTTGTTTAGCGATTCTAG ATG	0.003	AT1G66020	CDS
1	17072051	CACTTCTTTAGGTATTCTTG AGA	0.003		intergenic
1	29608330	CACATCTTGAGTAATTATAG ATG	0.003	AT1G78730	CDS
2	425178	CAAATGTTTAGCAATTGTTG AGT	0	AT2G01918	intron
1	18316194	CACATCTTTGGCAGTTCTAG ACT	0	AT1G49480	five_prime_UTR

	Bad site warning	Target sequence	Position	Strand	GC (%)	Region	Potential off-target sites(Max score)	Pairing with sgRNA (>=8 nt)
☑		CAAGTGGAAACACTGGAGTT GGG	1021 - 1040	+	45.0	CDS	0.186 (close)	None

Off-target predictor:

Chrom	Position	Sequence	Off-score	Gene	Region
1	10289367	ATAGTGAAAACAATGGATTT GGG	0.186	AT1G29395	intron
3	879595	CAACCGGAAACACTGGCCTT GGG	0.044	AT3G03630	CDS
5	6316385	CAAGAGTAAATTCTGGAGTT TGG	0.029		intergenic
3	40595	CAAGTTGAAAAACTGGAATT GGA	0.024	AT3G01120	intron
3	2213143	GAAATGGAAGCACTGGAATT GGA	0.022	AT3G07010	CDS
2	3302752	GCAGTGGAAACAGAGGAGTT GAG	0.016		intergenic
5	18934239	CACGTCGAAACACTAGCGAT GGG	0.014		intergenic
3	7964356	CAAGTGGGAACACTGGAGTT GGT	0.012	AT3G22460	CDS
5	4897487	CGAGTGGAAACACTGGAACT GGA	0.011	AT5G15110	CDS
2	8931307	CTTGTGGAAATACTGGATTT GGT	0.002		intergenic
2	3544747	CAAGTGGAGGTAATGGAGTT GGC	0.001		intergenic
3	22074403	CAAGTGGAAACACGGGTATT GGC	0	AT3G59760	CDS
3	1651195	CAAGTGGAAACAATTTCGTT GGA	0	AT3G05660	CDS
3	1545676	CAAGTGGCAACACAGGAGGT GAT	0	AT3G05380	CDS
2	9083905	TAAATGGAAACACGAGAGTT GGT	0	AT2G21195	three_prime_UTR
5	12912324	CAAGTAGAAAGCCTGCATTT GGG	0		intergenic
5	15692867	CAATTGCAAACACTGTGTTT GGG	0	AT5G39190	CDS

Supplemental Figure 2: Predicted off-targets of targets 1 and 2 against *OAS-TL A* by targetDesign.

Results of job ID: 202211221AEulc

Genome: Arabidopsis thaliana (TAIR10), **Position:** 5:22962713-22961229 (1485 bp), **Locus:** AT5G56760

Click Show Restriction Enzyme Sites to show or hide restriction enzyme sites that are present in the candidate targets.

	Bad site warning	Target sequence	Position	Strand	GC (%)	Region	Potential off-target sites(Max score)	Pairing with sgRNA (>=8 nt)
☑		AGCGTCAGCAGCGATATCTG CGG	215 - 234	+	55.0	CDS	0.089 (close)	None

Off-target predictor:

Chrom	Position	Sequence	Off-score	Gene	Region
1	7233757	AGCTTTGGTAGCGATATCTC CGG	0.089	AT1G20816	five_prime_UTR
3	5518629	AGCACGAGCAGCCATATCAG CGG	0.054	AT3G16280	CDS
4	10611116	ATCGCTATCAGCGATAGCTG CGG	0.043	AT4G19460	CDS
4	14840663	CGCGTGAGGAGCCATATCAG CGG	0.032	AT4G30340	CDS
1	2653852	AGCATCAGCAGCGGAAGCTG AGG	0.029	AT1G08420	CDS
4	5230344	AATGGCAGCAGCGATATCAG CGA	0.007	AT4G08280	CDS
3	958624	TGCTTCAGCAGGGATATCAG CGA	0.003	AT3G03780	CDS
1	11473233	AACCTCAGCAGCGATTTCGC CGG	0	AT1G06483	exon
1	9099522	AGCTTCAGCAGCGAATTCTT TGG	0	AT1G26300	CDS

☑		GAACAGATCGTATAAAAGTG TGG	440 - 421	-	35.0	CDS	0.139 (close)	None

Off-target predictor:

Chrom	Position	Sequence	Off-score	Gene	Region
4	7967536	GAACAAAACTAATAAAAGAG TGG	0.139	AT4G13720	intron
3	1850297	AAAAACATCGAATCAAAGTG TGG	0.083	AT3G06125	exon
4	12148731	AAAGAGCTCGTATAAAAATG TAG	0.035	AT4G23210	three_prime_UTR
1	9750309	GAATATATCATATACAAGTG TAC	0.035	AT1G27980	intron
1	29368026	GAACACATCATATTAATGTT TGG	0.032		intergenic
4	13112556	GAACTCATCGAATATAATTG TGG	0.025		intergenic
3	20755308	GAACAGAGCTTATCAGATTG TGG	0.016	AT3G55950	CDS
4	1786051	GAAGAGATAGTATTAGTGTG TGG	0.006	AT4G04765	exon
4	12426995	TTACATATCGTATAAAAGTT TGT	0.005	AT4G23910	intron
2	9816391	GAATATATCGTATGAAAGTG CGT	0.004		intergenic
4	4015476	GAACAAATTGGATATAAGTG TTG	0.003		intergenic
3	17173928	GAAAACATTGTATCAAAGTG TGT	0.002	AT3G46616	intron
1	5602653	GAACATATCTAATAAATGTG TGT	0.001		intergenic
3	10022938	GAACAAGTTGTATAAAAGTG TTT	0		intergenic

Supplemental Figure 3: Predicted off-targets of targets 1 and 2 against *SERAT1;1* by targetDesign.

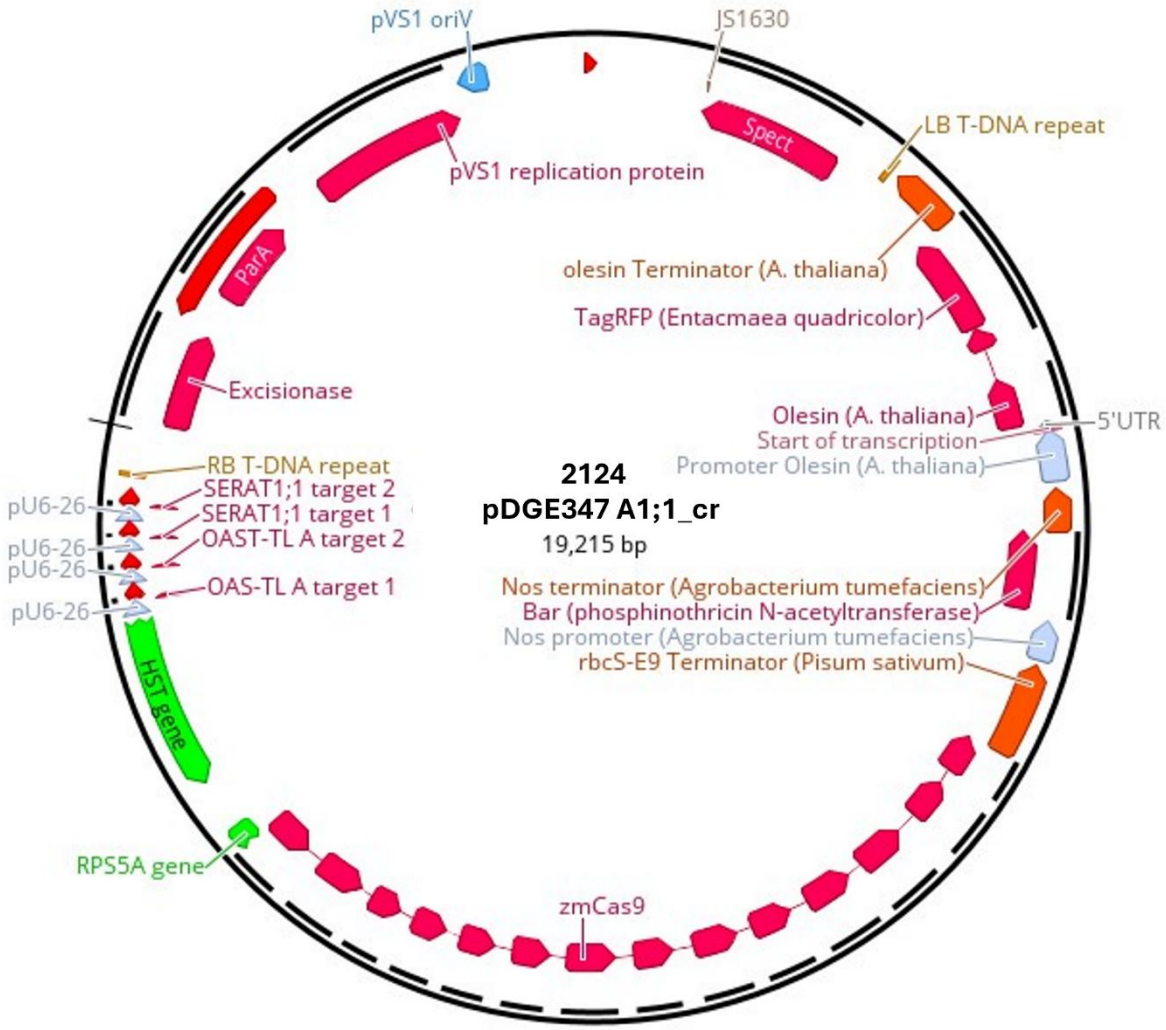

Supplemental Figure 4: Vector card of CRISPR/Cas9 transformation vector pDGE347 A1;1_cr (2124).

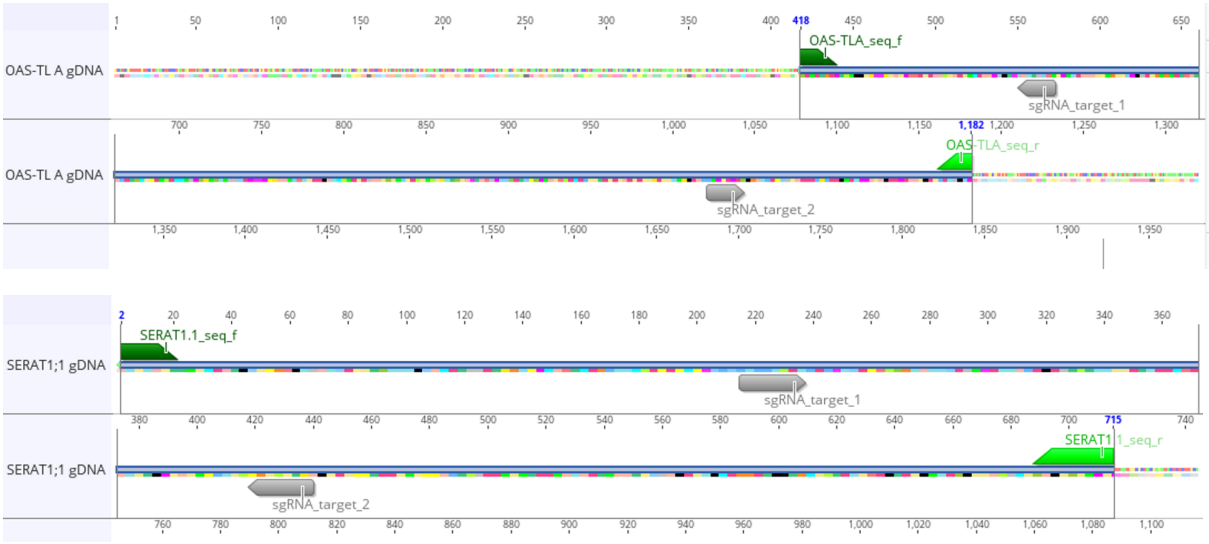

Supplemental Figure 5: Visual representation of the PCR products used to genotype possible CRISPR/Cas9 mutants via sequencing. OAS-TLA (primer: 5728, 5729; product size: 765 bps), SERAT1;1 (primer: 5730, 5731; product size: 714 bps) (2.4.6). This picture was generated with Geneious software application (2.1.6).

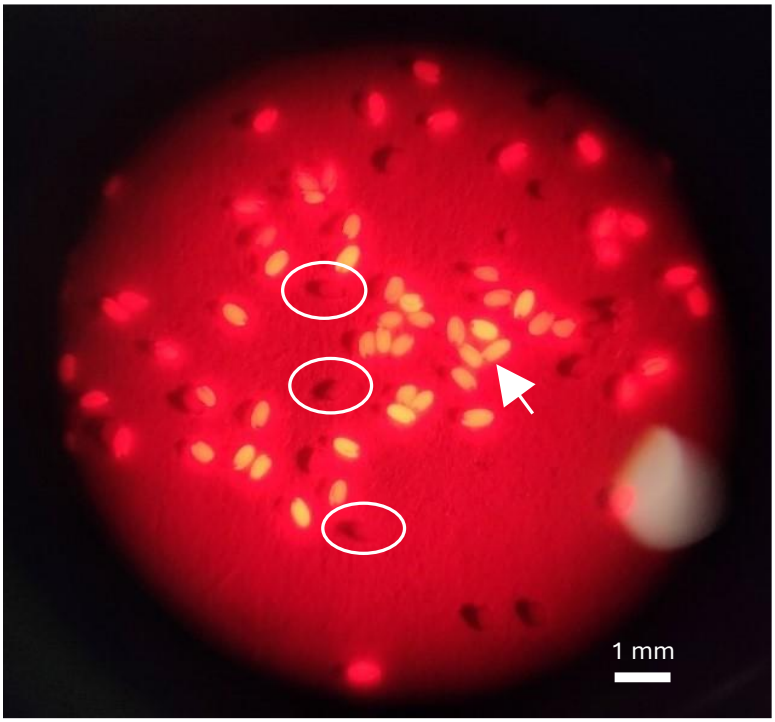

Supplemental Figure 6: *Cas9* screen of seeds using RFP fluorescence the FAST marker. Arabidopsis T2 seeds of CRISPR/Cas9 edited candidate line #2 (2.3.1) were investigated with a binocular (Leica MZFLIII, Wetzler) using 10x magnification, UV excitation at 340 nm, RFP filter with emission wavelength >590 nm, and additional white light. Seeds expressing the RFP marker were *Cas9*-positive and red fluorescent, as indicated with a white arrow. The yellow color of the seeds indicates overexposure of the RFP signal. The white circles indicate *Cas9*-negative seeds.

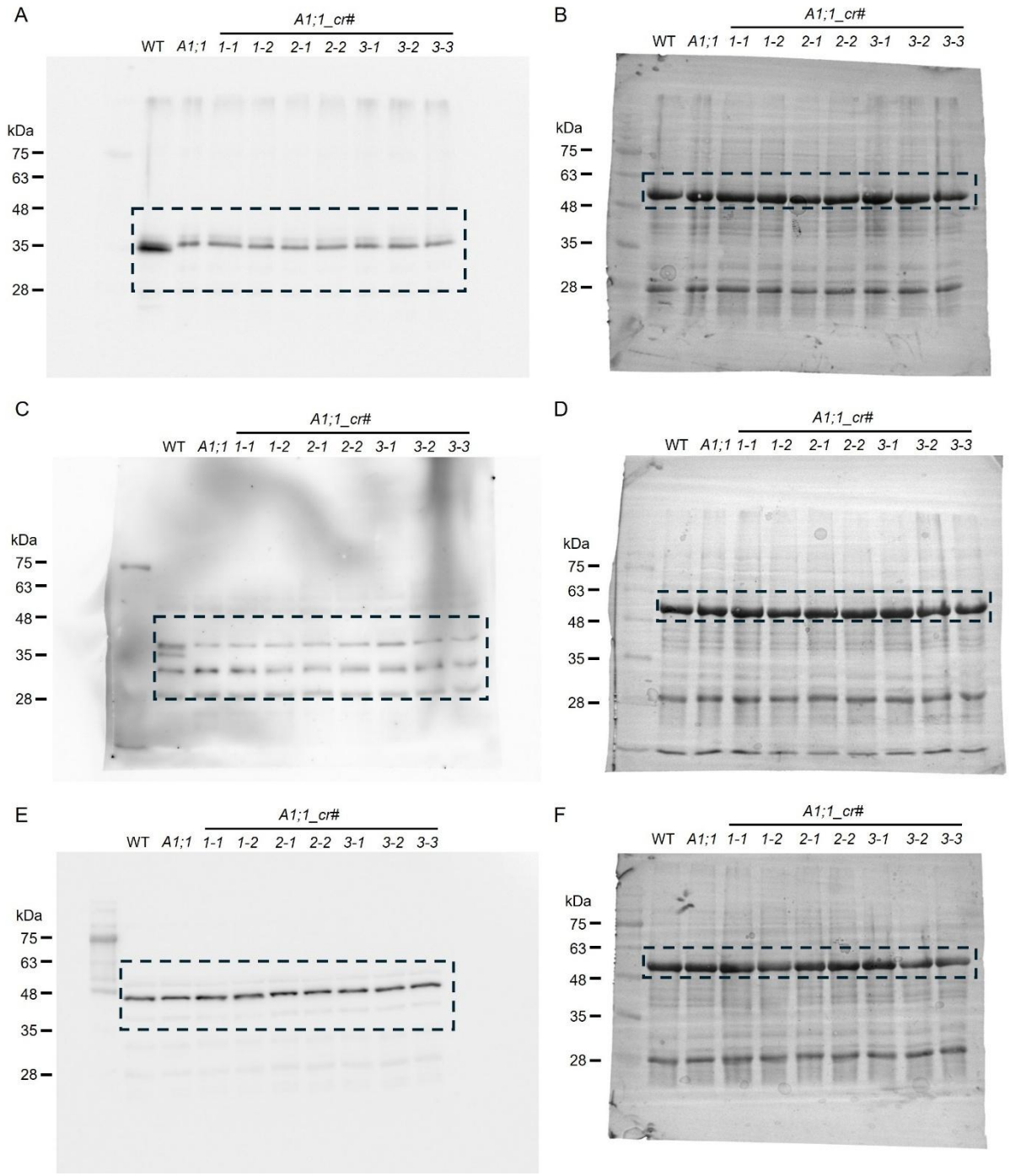

Supplemental Figure 7: Uncropped blots to verify *A1;1_cr#1-3* mutants on protein level in Figure 11: 0.2 g leaf material of seven weeks old soil-grown WT, *A1;1*, *A1;1_cr#1, A1;1_cr#2*, and *A1;1_cr#3* (2.3.2) was used to extract proteins with the NuPAGE buffer (2.5.6). Two individual plants were tested for each *A1;1_cr#1* and *#2*. The *A1;1_cr#3-1* and *3-2* contained the *serat1;1* allele with the 1 bp addition, while the *A1;1_cr#3-3* contained the *serat1;1* allele with the 7 bps gap. WT served as positive control and *A1;1* T-DNA mutant as negative control. The plant extracts were used for SDS-PAGE (2.5.10) and Western blotting (2.5.12) followed by immunological detection (2.5.13) and amido black staining as loading control (2.5.14). **A:** Uncropped blots of OAS-TL A detection. **B:** Amido black staining of A. **C:** Uncropped blots of SERAT1;1 detection. **D:** Amido black staining of C. **E:** Uncropped blots of ACTIN detection. **F:** Amido black staining of **E**.

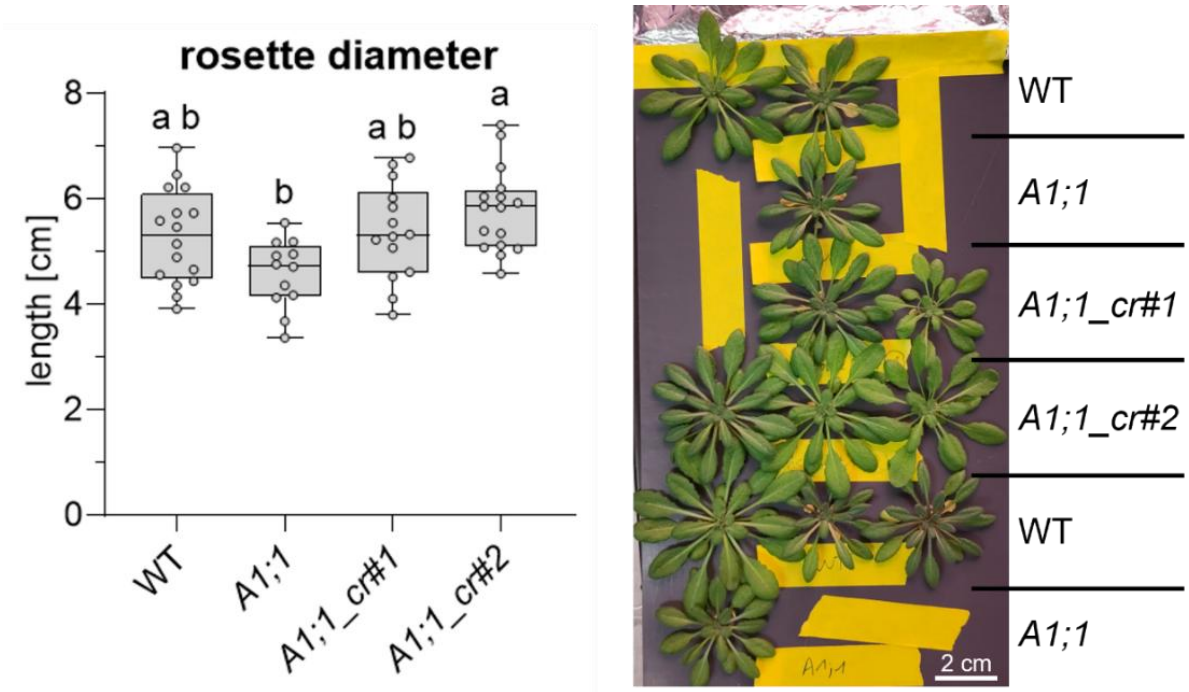

Supplemental Figure 8: Phenotypic assessment of *A1;1_cr#1* and #2. *A1;1_cr#1*, *A1;1_cr#2*, WT and *A1;1* T-DNA mutant were grown in hydroponic culture in sulfur-sufficient ½ Hoagland medium (500 µM sulfate) for seven weeks (2.3.7). The rosette diameters were measured from photographs using FIJI (2.3.12). An example photograph of the hydroponically grown shoots is shown on the right side. The diameters were entered in GraphPad Prism and ANOVA one-way with $p<0.05$ ($n = 12 - 16$) used for statistical analysis (2.7).

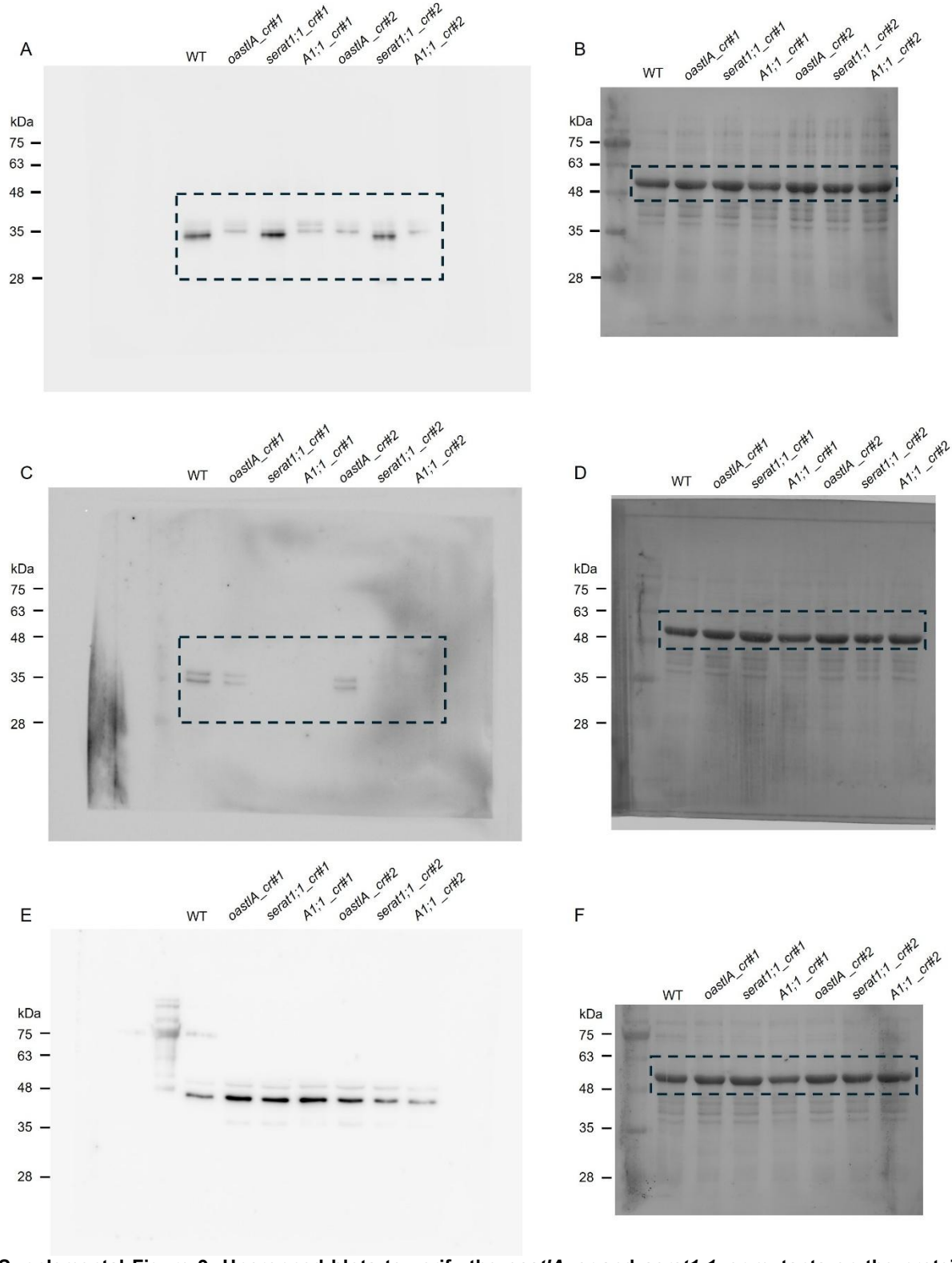

Supplemental Figure 9: Uncropped blots to verify the *oastlA_cr* and *serat1;1_cr* mutants on the protein level in Figure 13: 0.2 g leaf material of seven weeks old soil-grown plants *oastlA_cr#1-#2*, *serat1;1_cr#1-#2* and *A1;1_cr#1-#2* (2.3.2) was used to extract proteins with the NuPage buffer (2.5.6). The plant extracts were used for SDS-Page (2.5.10) and Western blotting (2.5.12) followed by immunological detection (2.5.13). The amido black stainings (2.5.14) were used as loading controls (LC). **A:** Uncropped blot of anti-OAS-TL A antibody detection. **B:** Amido black staining of A. **C:** Uncropped blot of anti-SERAT1;1 antibody detection. **D:** Amido black staining of C. **E:** Uncropped blot of anti-ACTIN antibody detection. **F:** Amido black staining of E.

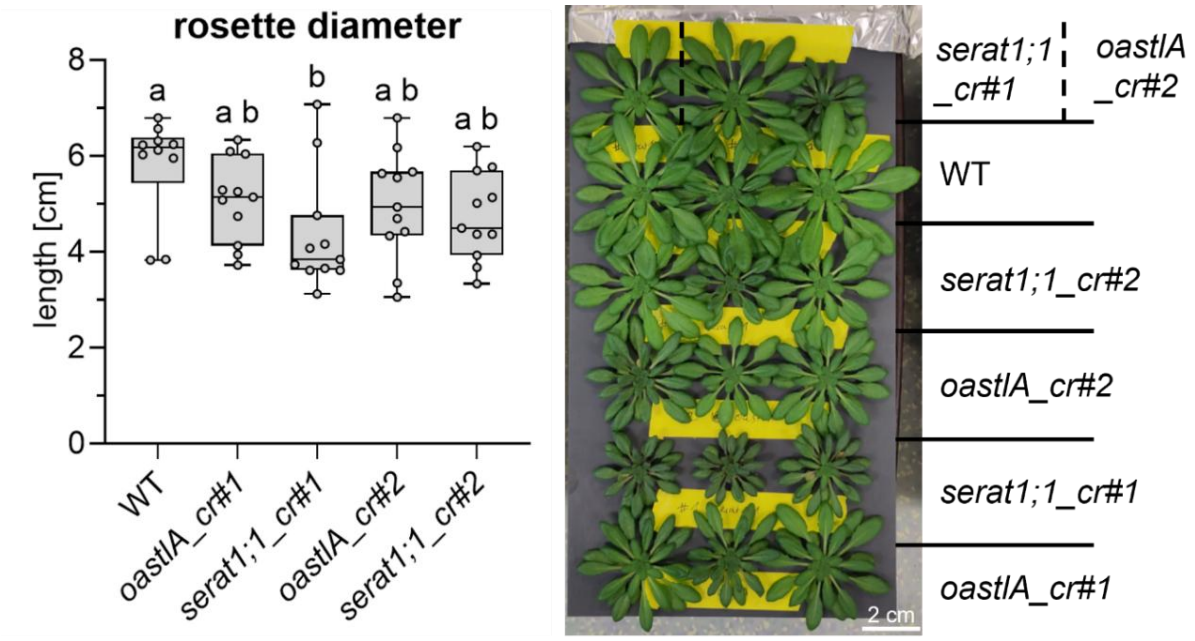

Supplemental Figure 10: Phenotypic assessment of *serat1;1_cr#1* and #2 and *oastlA_cr#1* and #2. *serat1;1_cr#1* and #2, *oastlA_cr#1* and #2, and WT were grown in the hydroponic system in 500 µM sulfate ½ Hoagland medium for seven weeks (2.3.7). The rosette diameters were measured from photographs using FIJI (2.3.12). Therefore, a circle was applied around the leaves of individual plants, the area used to calculate the diameter. An example photograph of the hydroponically grown shoots is shown on the right side. The diameters were entered in GraphPad Prism and ANOVA one-way with $p<0.05$ (n = 10 - 11) used for statistical analysis (2.7).

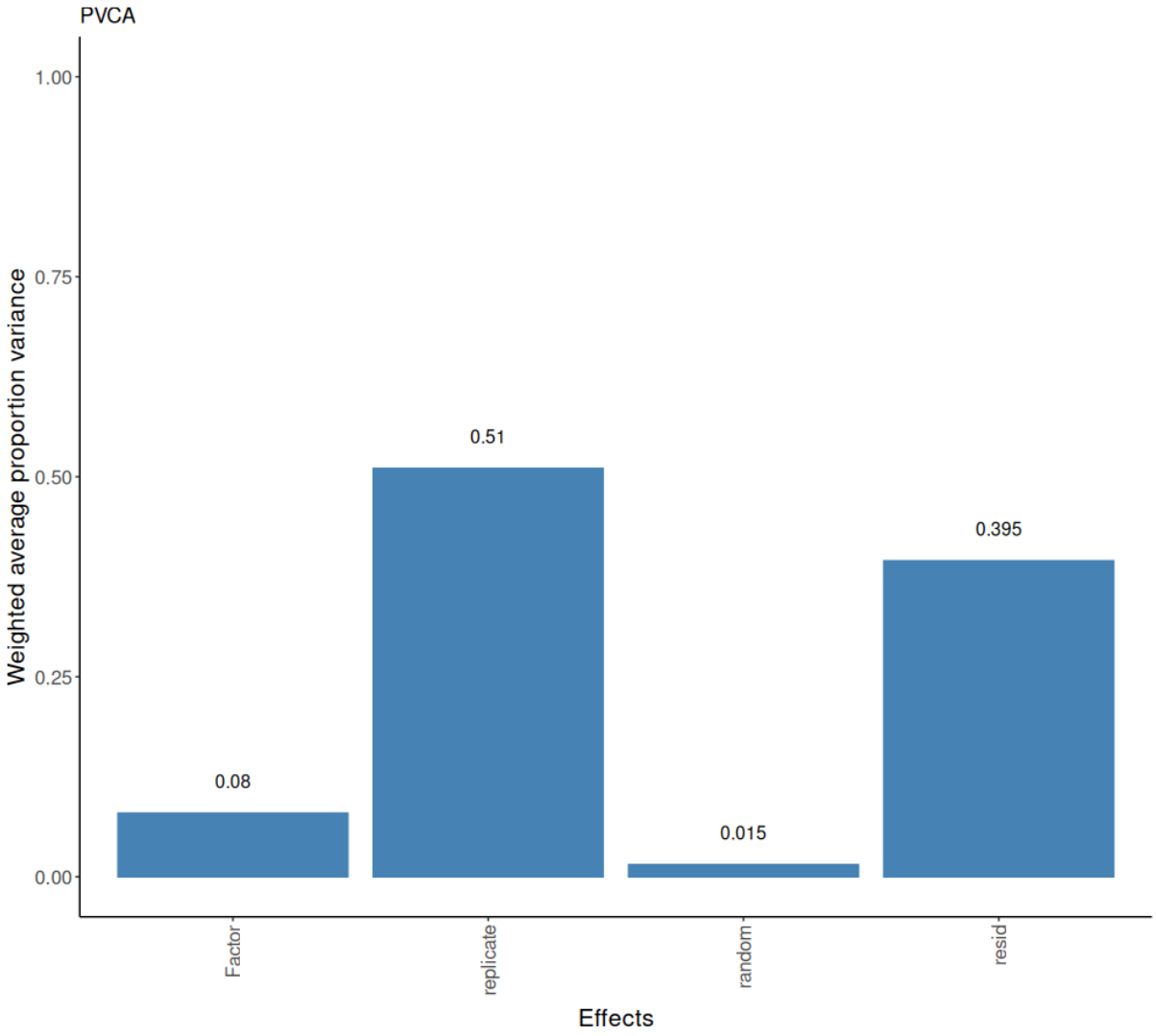

Supplemental Figure 11: Principle variance component analysis for RNAseq analysis of *oastlA_cr#2* and *serat1;1_cr#2*. WT, *serat1;1_cr#2* and *oastlA_cr#2* plants (2.3.1) were grown hydroponically in sulfur-sufficient conditions for seven weeks (2.3.7). Shoot material was harvested, snap-frozen and ground for RNA extraction (2.4.4). Total RNA was sequenced by BGI TECH SOLUTIONS (Hong Kong) (2.4.15), and bioinformatic analysis was conducted in collaboration with Dr. Carolina de la Torre from the NGS Core Facility, University of Mannheim (2.4.15). This figure was generated by Dr. Carolina de la Torre.

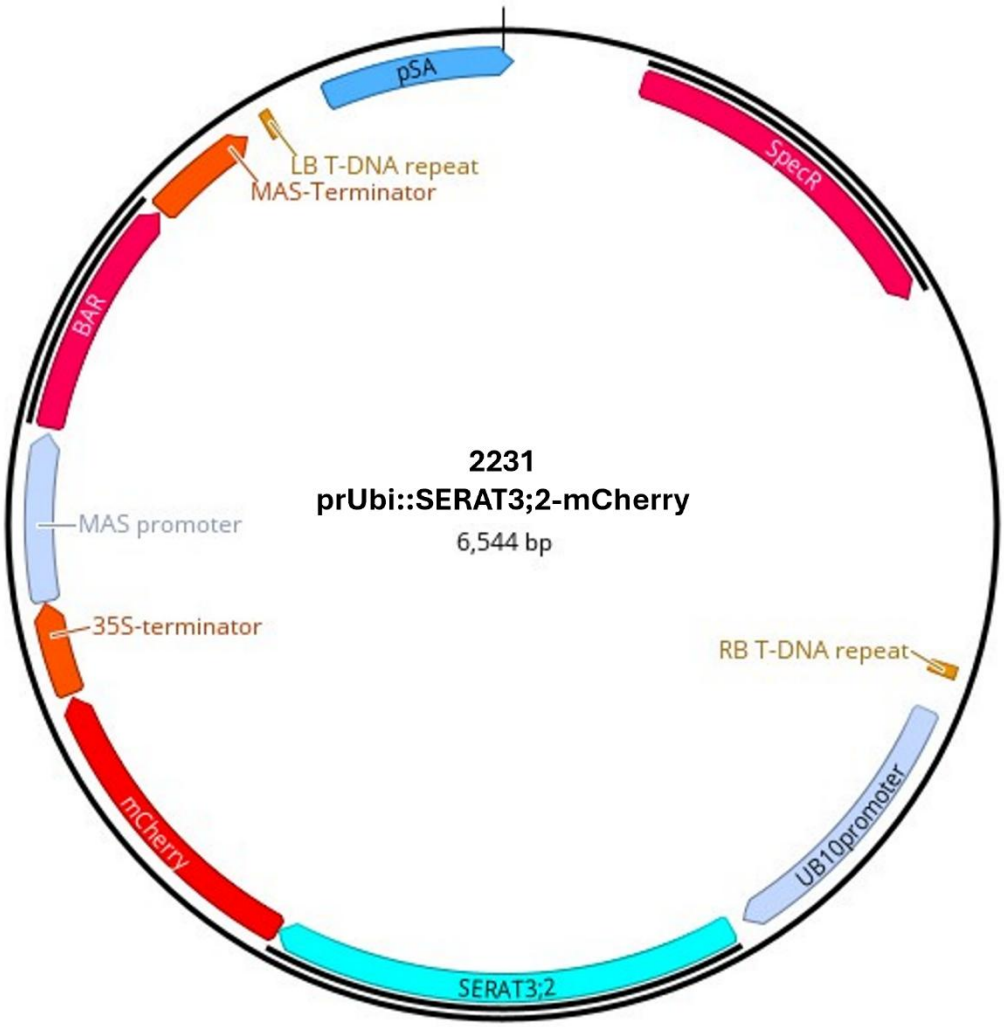

Supplemental Figure 12: Vector map of prUbi::SERAT3;2-mCherry (2231).

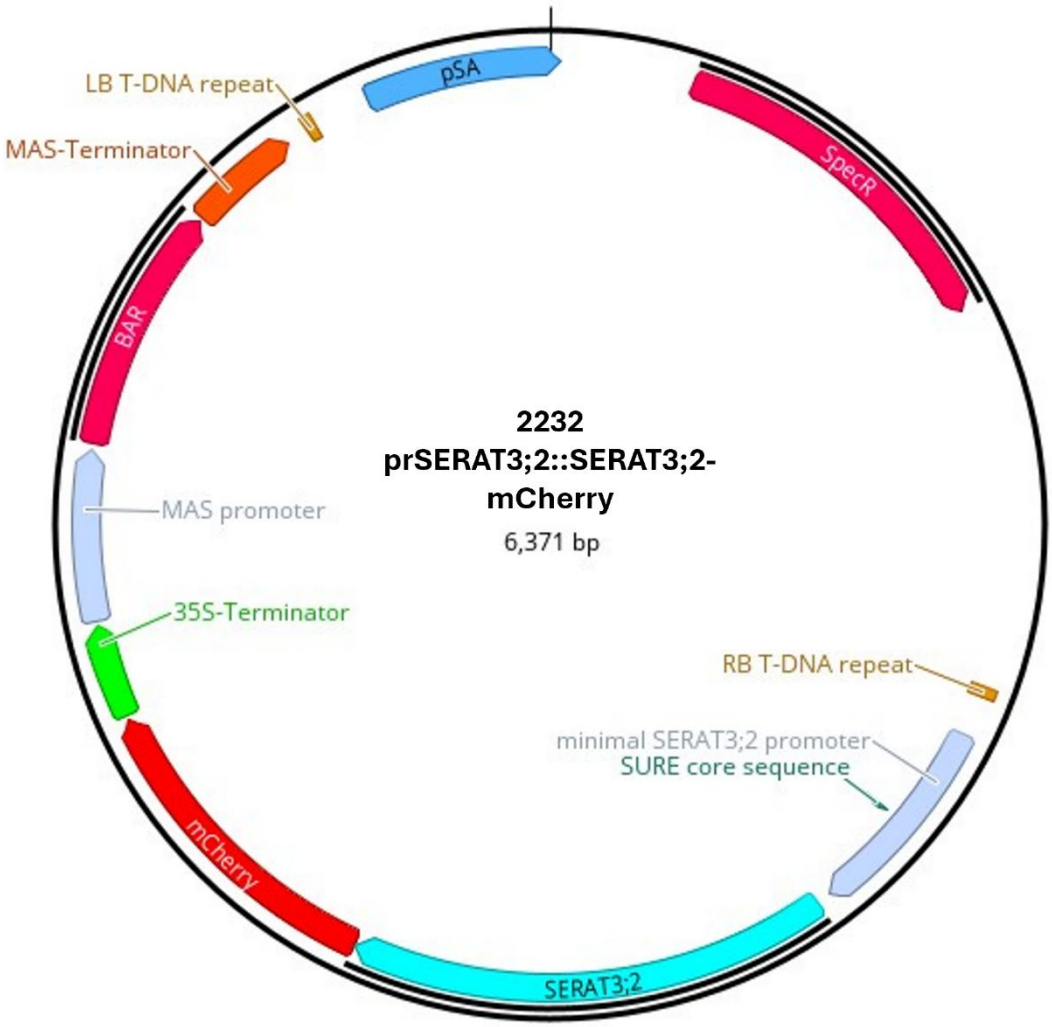

Supplemental Figure 13: Vector map of prSERAT3;2::SERAT3;2-mCherry (2232).

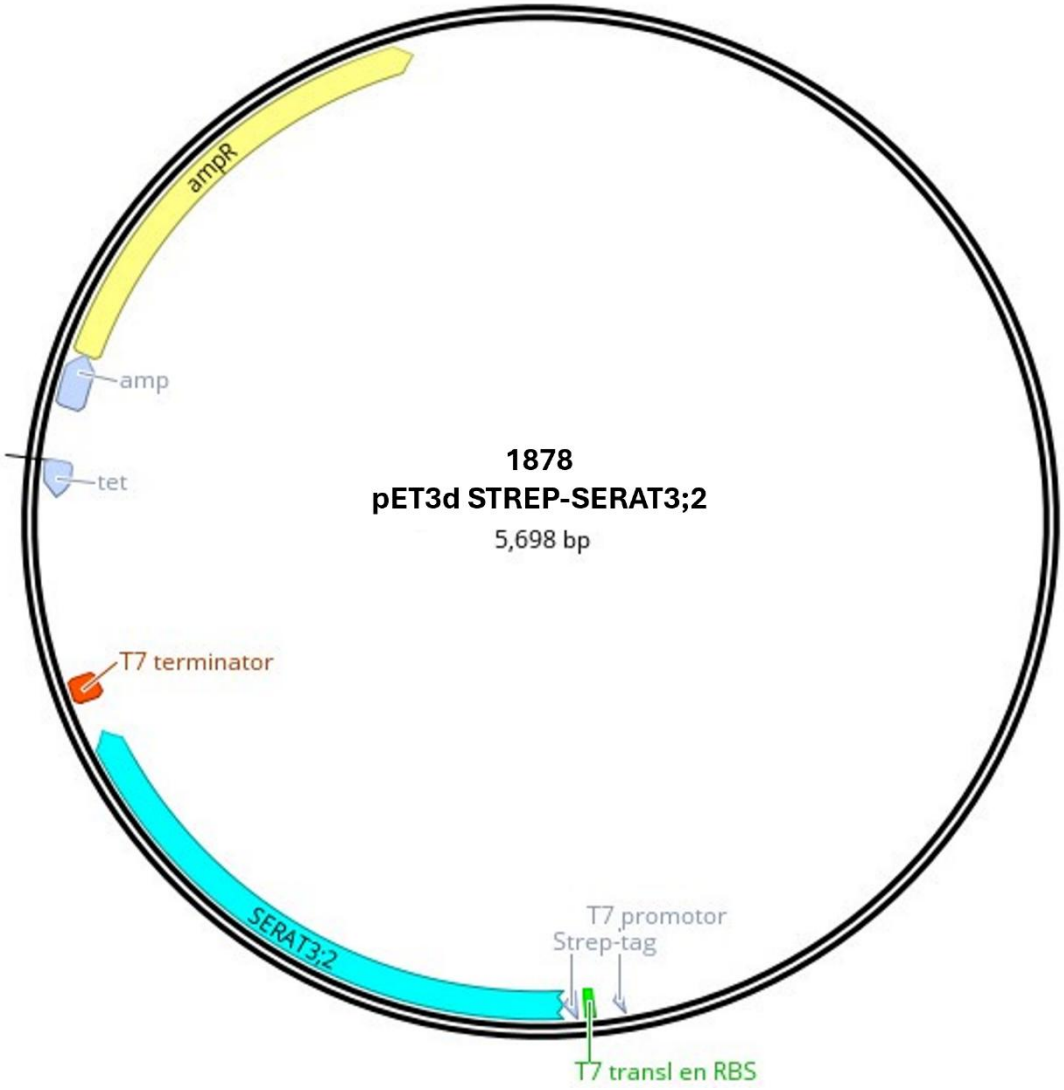

Supplemental Figure 14: Vector map of pET3d STREP-SERAT3;2 (1878).

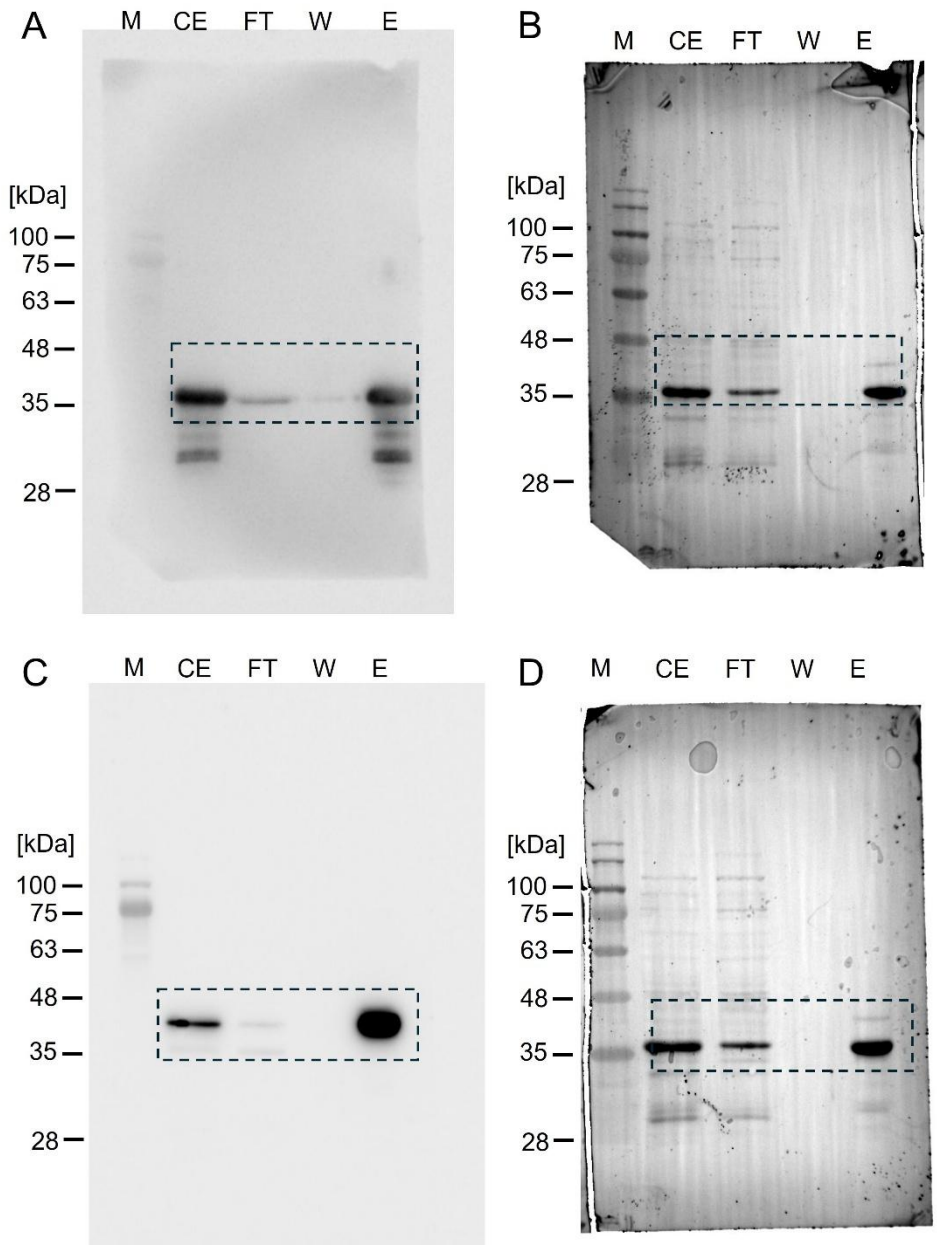

Supplemental Figure 15: Original blots of the interaction study of STREP-SERAT3;2 and HIS-SERAT1;1 using HIS-tag purification of Figure 26. BL21 (DE3) (2.2.1) transformed (2.2.5) with the plasmids pET3d STREP-SERAT3;2 (1878) and pET28a HIS-SERAT1;1 (402) (2.4.1) was cultured to express STREP-SERAT3;2 and HIS-SERAT1;1 (2.5.1) for purification using the HIS-tag proteins (2.5.2).The concentration of the purified proteins was determined (2.5.8). After protein denaturation (2.5.9), SDS-PAGE (2.5.10) and Western blotting were performed (2.5.12). Immunological detection was performed against HIS-SERAT1;1 using anti-HIS antibody and against STREP-SERAT3;2 using anti-STREP antibody (2.5.13). Amido black stainings were performed as loading controls (2.5.14). **A:** Uncropped blot of immunological detection using anti-HIS antibody. **B:** amindo black staining of blot in A. **C:** Uncropped blot of immunological detection using anti-STREP antibody. **D:** amindo black staining of blot in C. M: marker, CE**:** crude extract control, FT: flow-through control, W: washing control, E: elution.

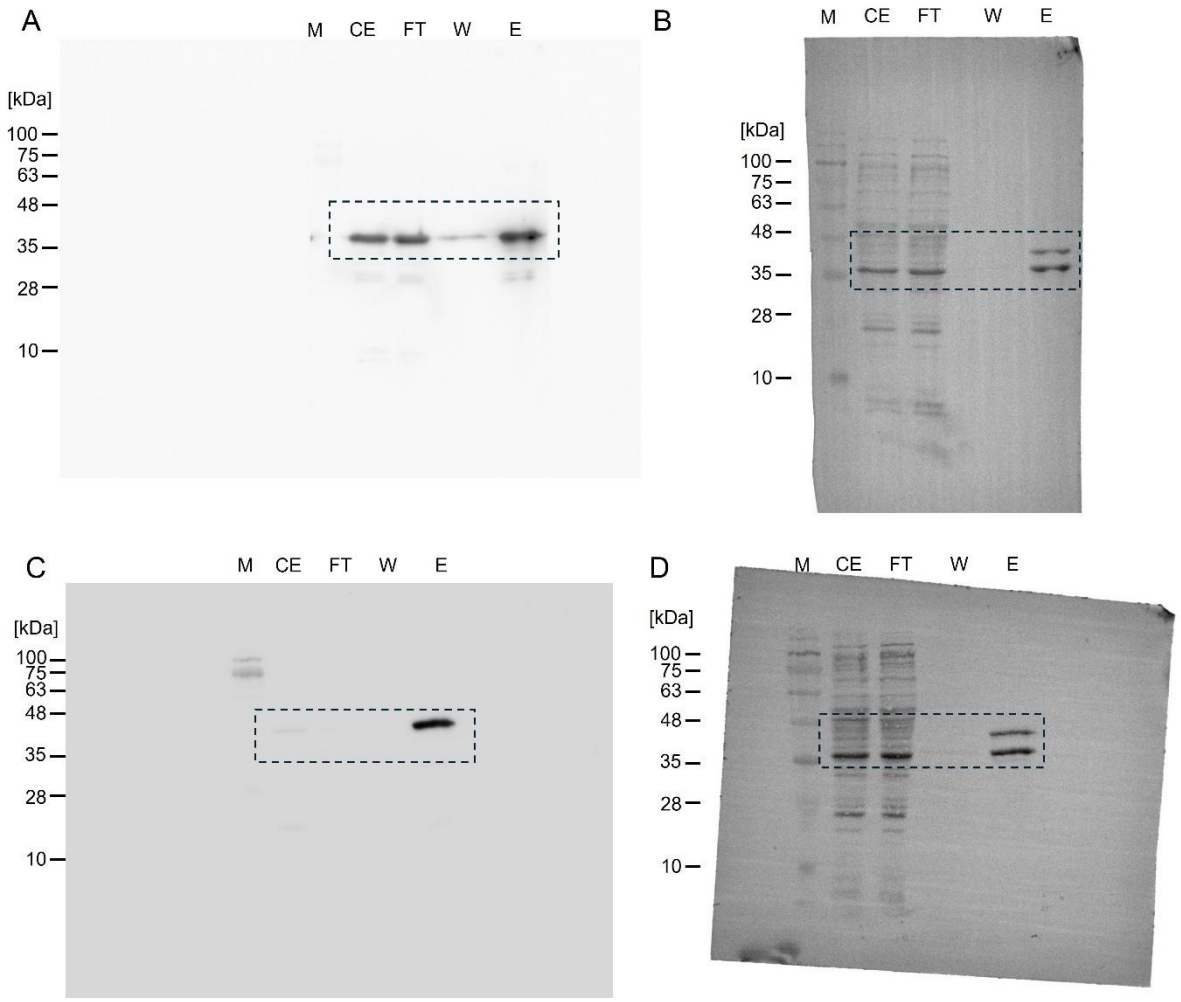

Supplemental Figure 16: Original blots of the interaction study of SERAT3;2 and SERAT1;1 using STREP-tag purification of Figure 26. BL21 (DE3) (2.2.1) transformed (2.2.5) with the plasmids pET3d STREP-SERAT3;2 (1878) and pET28a HIS-SERAT1;1 (402) (2.4.1) was cultured to express STREP-SERAT3;2 and HIS-SERAT1;1 (2.5.1) for purification using the STREP-tag proteins (2.5.3). The concentration of the purified proteins was determined (2.5.8). After protein denaturation (2.5.9), SDS-PAGE (2.5.10) and Western blotting were performed (2.5.12). Immunological detection was performed against HIS-SERAT1;1 using anti-HIS antibody and against STREP-SERAT3;2 using anti-STREP antibody (2.5.13). Amido black stainings were performed as loading controls (2.5.14). **A:** Uncropped blot of immunological detection using anti-HIS antibody. **B:** amido black staining of the blot in A. **C:** Uncropped blot of immunological detection using anti-STREP antibody. **D:** amido black staining of the blot in C. M: marker, CE**:** crude extract control, FT: flow-through control, W: washing control, E: elution.

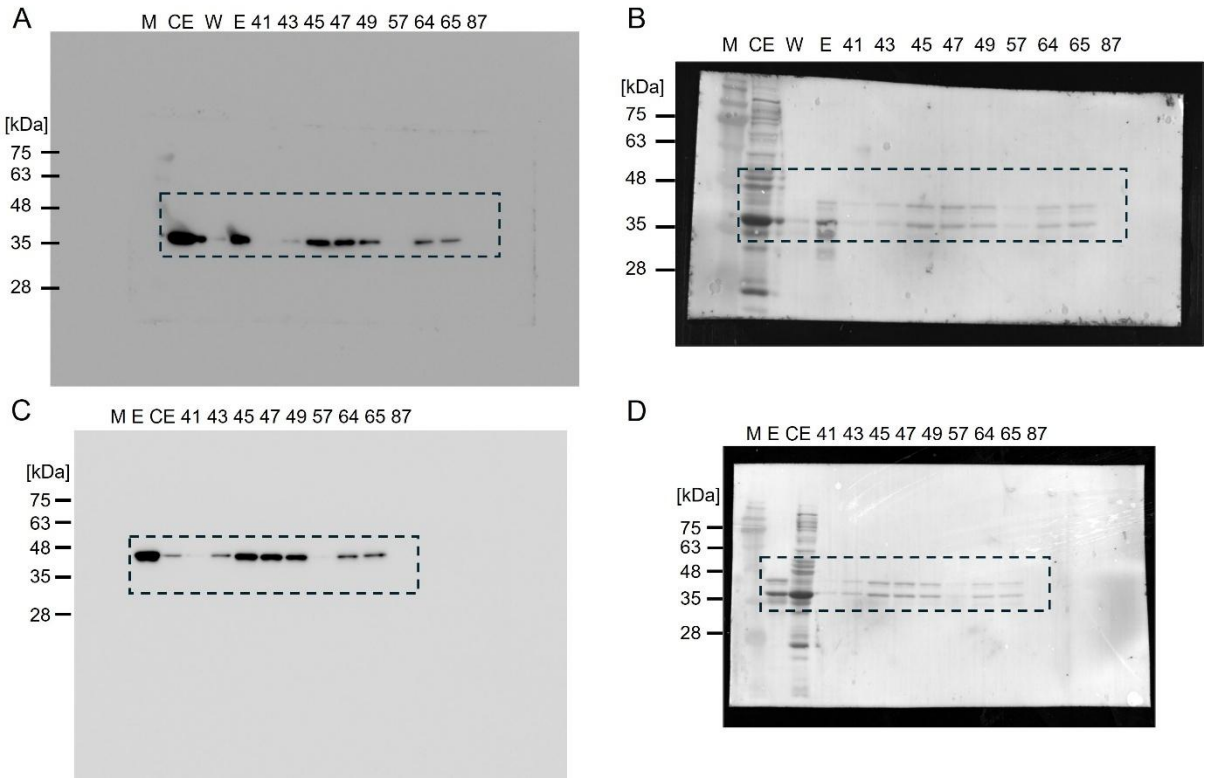

Supplemental Figure 17: Original blots of immunological detection of size exclusion chromatography replicate three of Figure 27: (DE3) (2.2.1) transformed (2.2.5) with the plasmids pET3d STREP-SERAT3;2 (1878) and pET28a HIS-SERAT1;1 (402) (2.4.1) was cultured to express STREP-SERAT3;2 and HIS-SERAT1;1 (2.5.1). The protein crude extract was purified using the STREP-tag (2.5.3). The concentration of the purified proteins was determined (2.5.8), and 2.4 mg in 1 ml buffer was applied to SEC (2.5.5). With the help of Diana Gabler, the crude extract control (CE), the SEC input control (E), a wash control, and the 1 ml fractions collected in SEC after min 41, 43, 45, 47, 49, 57, 64, 65, and 87 of replicate three were denaturated (2.5.9) and used for SDS-PAGE (2.5.10) and Western blotting (2.5.12). Immunological detection was performed using anti-STREP and anti-HIS antibodies (2.5.13). The membranes were stained with amido block as the loading control (LC) (2.5.14). **A:** Uncropped blot of immunological detection using anti-HIS antibody. **B:** amido black staining of the blot in A. **C:** Uncropped blot of immunological detection using anti-STREP antibody. **D:** amido black staining of the blot in C.

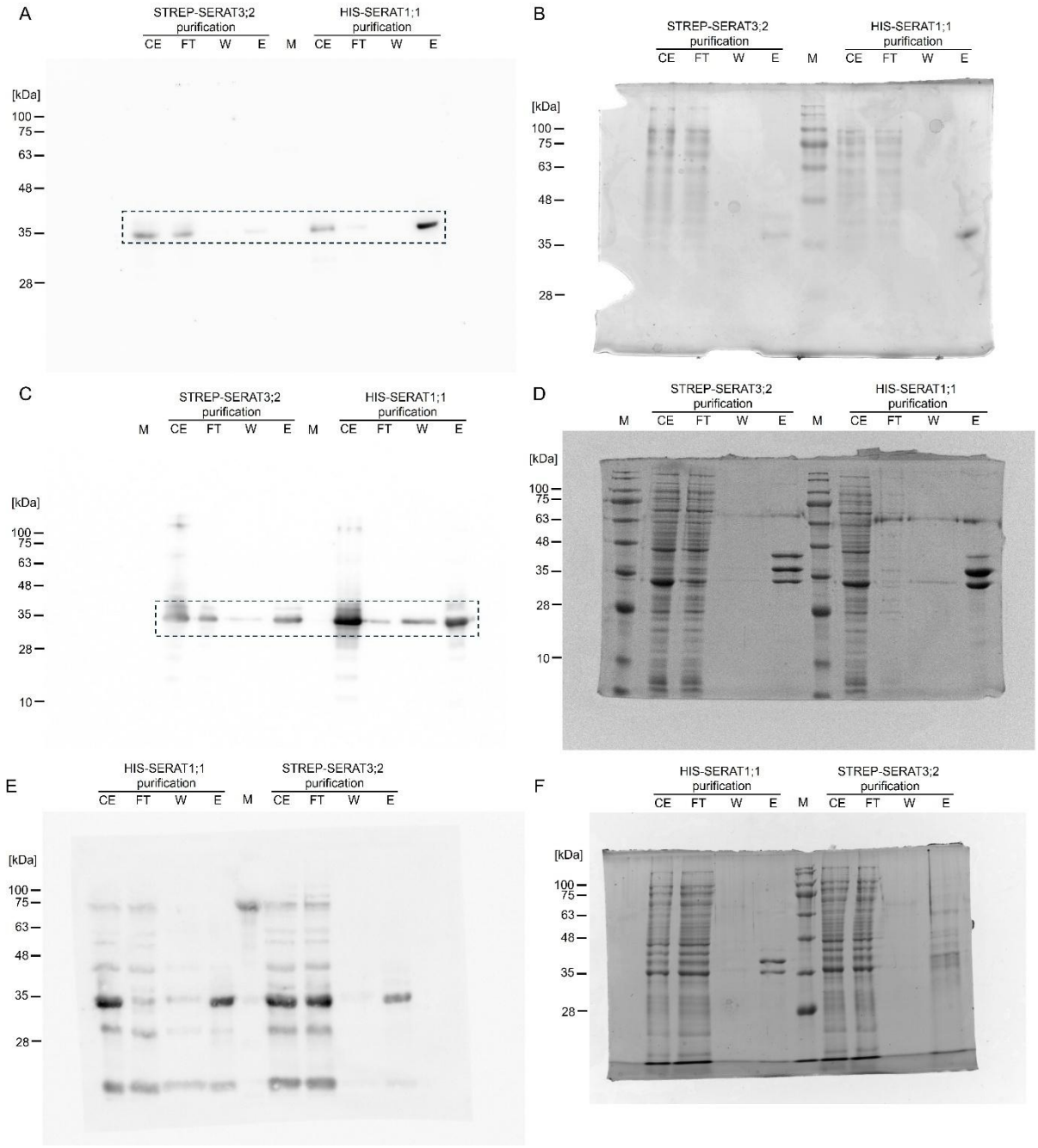

Supplemental Figure 18: Original blots of immunological detection of OAS-TLA in the binding capacity tests of STREP-SERAT3;2/HIS-SERAT1;1 heterocomplexes of Figure 28: BL21 (DE3) (2.2.1) transformed (2.2.5) with the plasmids pET3d STREP-SERAT3;2 (1878) and pET28a HIS-SERAT1;1 (402) (2.4.1) was cultured to express STREP-SERAT3;2 and HIS-SERAT1;1 (2.5.1). Half of the protein extract was used to purify HIS-tagged proteins (2.5.2), and the other half was used to purify STREP-tagged proteins (2.5.3). After applying the crude extracts, BL21 protein crude extract containing OAS-TL A (1894) was loaded on both columns in equal amounts. The elution was performed with HIS or STREP elution buffers. The concentration of the purified proteins was determined (2.5.8). After protein denaturation (2.5.9), SDS-PAGE (2.5.10) and Western blotting were performed (2.5.12). Immunological detection was performed using anti-OAS-TL A antibody (2.5.13). Coomassie staining (2.5.11) was used as the loading control. The experiment was repeated three times. **A:** Uncropped blot of immunological detection of replicate one. **B:** Coomassie staining of the blot in A. **C:** Uncropped blot of immunological detection of replicate two. **D:** Coomassie staining of the blot in C. **E:** Uncropped blot of immunological detection of replicate three. **F:** Coomassie staining of the blot in D. Replicates two and three were performed under my supervision by my Master's student, Diana Gabler, and Bachelor's student, Nicolas Düster, respectively. M: marker, CE: crude extract control, FT: flow-through control, W: washing control, E: elution.

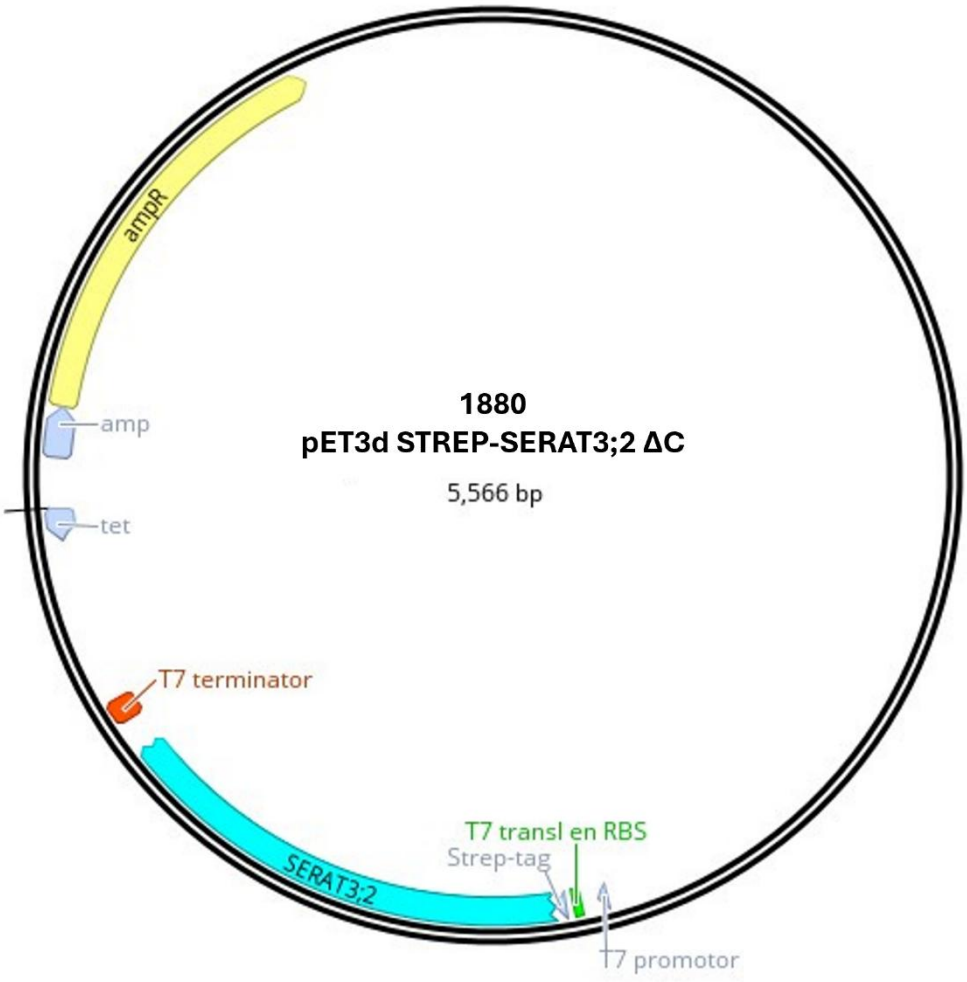

Supplemental Figure 19: Vector map of pET3d STREP-SERAT3;2ΔC (1880).

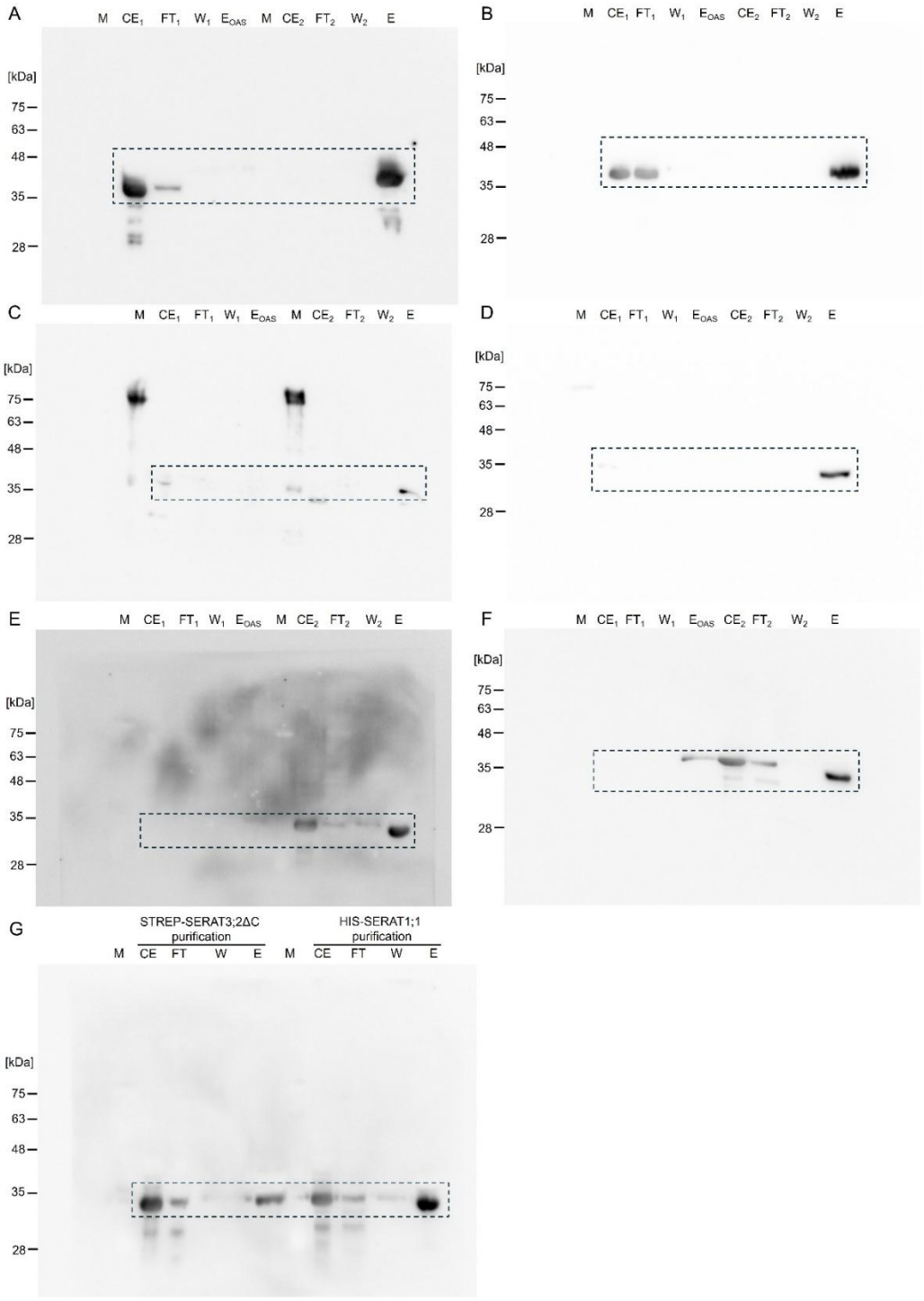

Supplemental Figure 20: Uncropped blots testing OAS-TLA binding capacity of STREP-SERAT3;2ΔC/HIS-SERAT1;1 heterocomplexes in Figure 29: BL21 (DE3) (2.2.1) transformed (2.2.5) with the plasmids pET3d STREP-SERAT3;2ΔC (1880) and pET28a HIS-SERAT1;1 (402) (2.4.1) was cultured to express STREP-SERAT3;2ΔC and HIS-SERAT1;1 (2.5.1). With the help of my Master's student Diana Gabler, half of the protein extract was used to purify HIS-tagged proteins (2.5.2), and the other half was used to purify STREP-tagged proteins (2.5.3). After applying the crude extracts, BL21 (DE3) (1894) protein crude extract containing OAS-TL A was loaded on both columns in equal amounts. The elution was performed with HIS or STREP elution buffers. The concentration of the purified proteins was determined (2.5.8). After protein denaturation (2.5.9), SDS-PAGE (2.5.10) and Western blotting were performed (2.5.12) to detect STREP-SERAT3;2, HIS-SERAT1;1 and OAS-TL A (2.5.13). Immunological detection was performed using anti-OAS-TL A antibody. Uncut blots using anti-HIS antibody in the HIS-tag (**A**) and STREP-tag purification (**B**). Uncut blots using anti-STREP-tag antibody in the HIS-tag (**C**) and STREP-tag purification (**D**). Uncut blots using anti-OAS-TL A antibody in the HIS-tag (**C**), STREP-tag purification (**D**) and in the OAS-TL A binding capacity test (**E**). M: marker, CE_1: crude extract control of 1881, FT_1: flow-through control of 1881, $W_{1\text{-}2}$: washing controls, E_{OAS}: OAS washing elution, CE_2: crude extract control of 1894, FT_2: flow-through control of 1894, W: washing, E: final elution.

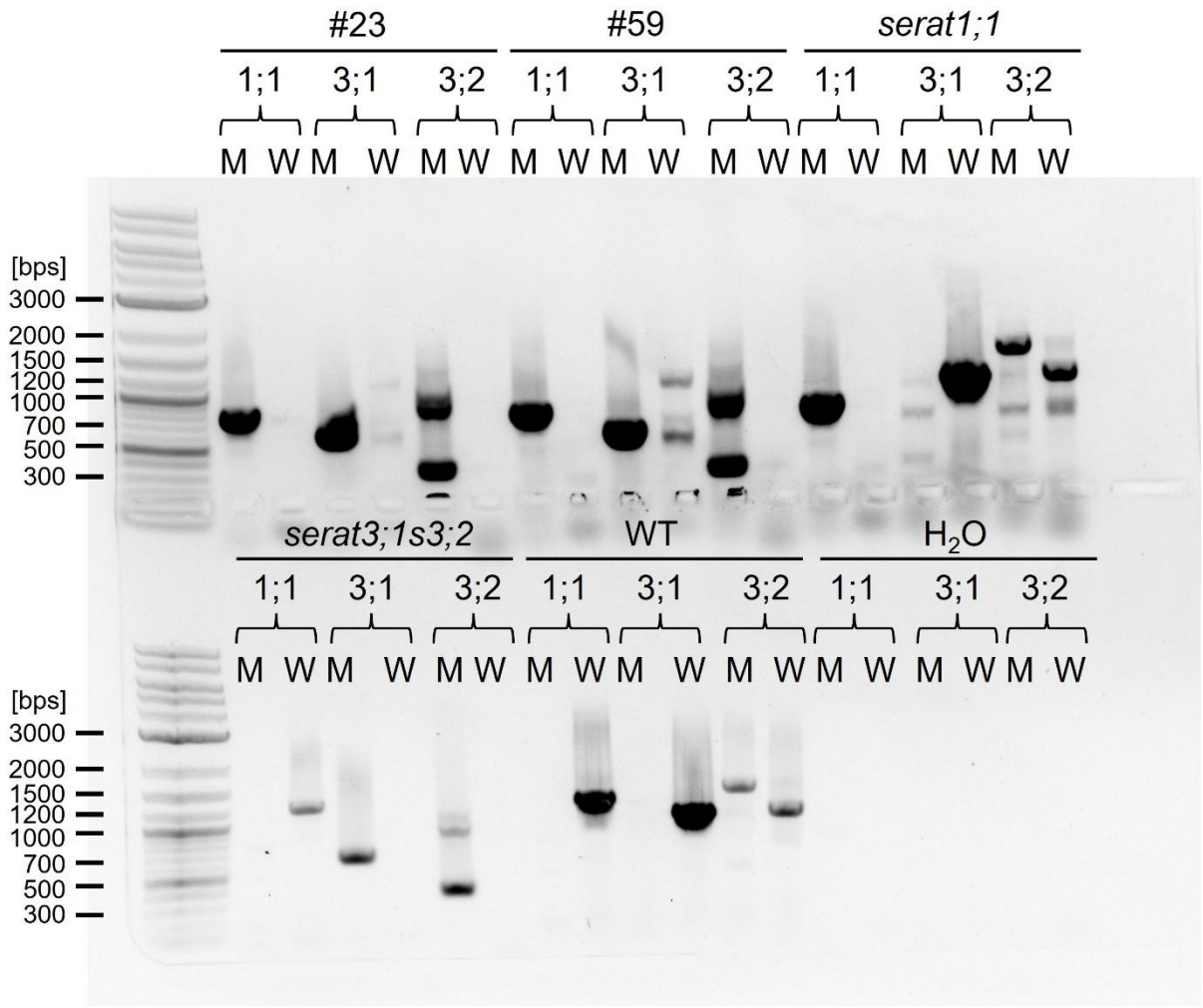

Supplemental Figure 21: Genotyping PCR to identify *serat1;1s3;1s3;2*. Extracted gDNA (2.4.3) of 150 individuals of the T2 generation (2.3.2) of *serat1;1* crossed with *serat3;1s3;2* (2.3.8) were used in genotyping PCR (2.4.7) against the T-DNA insertions (M) in *SERAT1;1* (primer 1639 + 1401, 900 bps), *SERAT3;1* (2218 +1401, 500 bps), and *SERAT3;2* (2219 + 1401, 1000 bps) (2.4.6). To detect the WT alleles (W), the primers 1639 + 1640 (1200 bps) were used for SERAT1;1, 2217 + 2218 (1030 bps) for *SERAT3;1*, and 2219 + 2220 (1060 bps) for *SERAT3;2* (2.4.6). The PCR products were size-separated using gel electrophoresis (2.4.9). WT and the parental mutant lines, *serat1;1* and *serat3;1s3;2* were used as controls. In the H_2O control, the gDNA was replaced by water. Individual #23 and #59 were homozygous for the T-DNA insertion in *SERAT1;1* (1;1), *SERAT3;1* (3;1), *SERAT3;2* (3;2).

Supplemental Table 1: Differentially expressed genes in *serat3;1s3;2* compared to WT found exclusively in control condition. WT and *serat3;1s3;2* (2.3.1) were cultured in liquid ½ Hoagland medium containing 500 µM sulfate (+S) for four weeks (2.3.7). Half of the plants were transferred to a sulfur deficiency medium containing 1 µM sulfate for an additional four weeks (-S). The other half remained in the control medium (2.3.7). Shoot material was harvested, and used for RNA extraction (2.4.4). Total RNA was sequenced by Novogene GmbH (München) (2.4.15), and bioinformatic analysis was conducted in collaboration with Dr. Carolina de la Torre from the NGS Core Facility, University of Mannheim (2.4.15). The table is sorted by the log2 fold change (FC). The p-value is adjusted with the false discovery rate (adj. p-value).

10 most over-expressed genes specifically in +S			
TAIR ID	**Symbol/Description**	**log2FC +S**	**adj. p-value +S**
AT5G11140	protein coding	3.75	3.57E-03
AT1G19210	ERF017	3.73	1.42E-04
AT2G47770	ATTSPO	3.73	5.59E-03
AT1G56600	AtGolS2	3.64	4.10E-05
AT1G01520	ASG4	3.58	7.60E-03
AT5G43840	AT-HSFA6A	3.54	4.98E-03
AT1G60190	AtPUB19	3.53	1.44E-05
AT1G50745	protein coding	3.45	2.08E-04
AT4G04610	APR1	3.41	1.64E-08
AT4G01950	ATGPAT3	3.36	2.23E-07
10 most over-repressed genes specifically in +S			
TAIR ID	**Symbol**	**log2FC +S**	**adj. p-value +S**
AT1G72620	protein coding	-4.58	8.82E-05
AT3G61028	protein coding	-4.36	8.98E-05
AT3G15440	protein coding	-4.04	5.87E-04
AT5G62730	protein coding	-3.85	1.17E-03
AT5G08425	lncRNA	-3.79	2.72E-03
AT3G20340	protein coding	-3.71	3.12E-04
AT4G36820	MCU4	-3.58	9.36E-04
AT1G79330	AMC6	-3.53	4.55E-05
AT2G30615	protein coding	-3.40	2.77E-06
AT5G66110	AtHMP55	-3.26	1.70E-03

Supplemental Table 2: Differentially expressed genes in *serat3;1s3;2* compared to WT found exclusively in sulfur deficiency. WT and *serat3;1s3;2* (2.3.1) were cultured in liquid ½ Hoagland medium containing 500 µM sulfate (+S) for four weeks (2.3.7). Half of the plants were transferred to a sulfur deficiency medium containing 1 µM sulfate for an additional four weeks (-S). The other half remained in the control medium (2.3.7). Shoot material was harvested, and used for RNA extraction (2.4.4). Total RNA was sequenced by Novogene GmbH (München) (2.4.15), and bioinformatic analysis was conducted in collaboration with Dr. Carolina de la Torre from the NGS Core Facility, University of Mannheim (2.4.15). The table is sorted by the log2 fold change (FC). The p-value is adjusted with the false discovery rate (adj. p-value).

10 most over-expressed genes exclusive for sulfur deficiency			
TAIR ID	**Symbol/Description**	**log2FC -S**	**adj. p-value -S**
AT1G48750	protein coding	4.25	6.61E-03
AT4G05815	lncRNA	4.07	3.38E-02
AT2G46670	protein coding	3.64	2.31E-02
AT4G03038	other RNA	3.08	1.44E-02
AT5G14380	AGP6	3.06	3.27E-02
AT5G19470	atnudt24	3.04	3.11E-03
AT2G23000	scpl10	2.81	6.30E-04
AT4G04760	ESL3.03	2.67	6.29E-03
AT5G17220	ATGSTF12	2.66	3.17E-03
AT5G54060	UF3GT	2.54	3.01E-02
10 most over-repressed genes exclusive for sulfur deficiency			
TAIR ID	**Symbol/Description**	**log2FC -S**	**adj. p-value -S**
AT5G01095	lncRNA	-4.54	1.92E-02
AT5G51810	AT2353	-3.72	1.70E-02
AT1G14860	atnudt18	-2.90	6.33E-03
AT1G10770	protein coding	-2.85	1.62E-02
AT2G47520	AtERF71	-2.81	2.93E-02
AT5G39240	protein coding	-2.66	2.34E-02
AT5G27230	protein coding	-2.61	4.77E-03
AT4G25750	ABCG4	-2.53	3.36E-02
AT2G47560	ATL64	-2.44	1.47E-02
AT3G22961	protein coding	-2.44	1.19E-03

Supplemental Table 3: Differentially expressed transcription factors (TF) in *serat3;1s3;2* compared to WT found commonly in +S and -S. WT and *serat3;1s3;2* (2.3.1) were cultured in liquid ½ Hoagland medium containing 500 µM sulfate (+S) for four weeks (2.3.7). Half of the plants were transferred to a sulfur deficiency medium containing 1 µM sulfate for an additional four weeks (-S). The other half remained in the control medium (2.3.7). Shoot material was harvested, and used for RNA extraction (2.4.4). Total RNA was sequenced by Novogene GmbH (München) (2.4.15), and bioinformatic analysis was conducted in collaboration with Dr. Carolina de la Torre from the NGS Core Facility, University of Mannheim (2.4.15). The table is sorted by the difference in the log2 fold change (FC) or significance. The p-value is adjusted with the false discovery rate (adj. p-value). n.a = not annotated.

10 most over-expressed TF in +S compared to -S					
TAIR ID	**Symbol**	**log2FC +S**	**adj. p-value +S**	**log2FC -S**	**adj. p-value -S**
AT5G67450	AZF1	3.77	1.81E-06	1.28	3.07E-02
AT1G18570	AtMYB51	0.85	4.15E-02	-1.28	3.70E-02
AT1G53170	ATERF-8	1.25	3.93E-04	-0.87	4.73E-02
AT2G21320	BBX18	3.23	2.85E-06	1.19	7.61E-03
AT3G46770	REM13	3.52	2.13E-02	1.52	2.46E-03
AT1G01250	n.a.	3.73	1.39E-04	2.27	2.44E-03
AT5G64810	ATWRKY51	2.50	7.33E-03	1.07	1.36E-03
AT5G01900	ATWRKY62	3.06	5.71E-03	1.85	2.15E-03
AT5G48150	PAT1	0.41	1.65E-02	-0.76	4.19E-04
AT2G39250	SNZ	2.54	3.41E-06	1.39	1.73E-04
10 most over-repressed TF in +S compared to -S					
TAIR ID	**Symbol**	**log2FC +S**	**adj. p-value +S**	**log2FC -S**	**adj. p-value -S**
AT4G06746	DEAR5	-3.74	4.30E-03	-1.80	1.91E-02
AT4G39070	BBX20	-4.24	2.50E-04	-2.34	5.67E-03
AT5G15850	ATCOL1	-0.79	5.51E-03	0.86	1.09E-02
AT2G41940	ZFP8	-0.56	1.51E-02	0.98	3.60E-02
AT5G28770	AtbZIP63	-2.43	6.43E-08	-1.04	3.41E-03
AT1G79700	WRI4	-2.61	3.08E-06	-1.39	3.52E-04
AT4G27950	CRF4	-2.27	3.07E-04	-1.07	5.91E-03
AT2G46310	CRF5	-1.85	2.13E-04	-0.66	1.20E-02
AT1G56170	ATHAP5B	1.57	4.34E-05	2.73	2.97E-03
AT5G28300	AtGT2L	-1.61	9.46E-05	-0.61	9.59E-03
10 most significant TF similarly differentially expressed in +S and -S					
TAIR ID	**Symbol**	**log2FC +S**	**adj. p-value +S**	**log2FC -S**	**adj. p-value -S**
AT3G07650	BBX7	-3.22	2.52E-06	-3.26	3.27E-05
AT3G61630	CRF6	-0.92	6.25E-03	-0.92	1.50E-04
AT3G14230	RAP2.2	-0.51	1.98E-03	-0.52	5.81E-04
AT3G59060	A-PUT2	0.57	2.64E-03	0.56	1.10E-03
AT5G25220	KNAT3	0.49	5.45E-03	0.48	4.60E-03
AT5G39760	AtHB23	-0.83	3.75E-03	-0.83	6.77E-03
AT3G51910	AT-HSFA7A	-1.61	1.62E-04	-1.65	8.70E-03
AT1G75710	BRON	0.56	1.62E-02	0.60	1.07E-02
AT2G23290	AtMYB70	0.96	2.38E-03	0.96	1.12E-02
AT2G31380	BBX25	1.05	3.53E-03	1.10	1.56E-02

Supplemental Table 4: Differentially expressed transcription factors (TF) in *serat3;1s3;2* compared to WT found exclusively in +S. WT and *serat3;1s3;2* (2.3.1) were cultured in liquid ½ Hoagland medium containing 500 µM sulfate (+S) for four weeks (2.3.7). Half of the plants were transferred to a sulfur deficiency medium containing 1 µM sulfate for an additional four weeks (-S). The other half remained in the control medium (2.3.7). Shoot material was harvested, and used for RNA extraction (2.4.4). Total RNA was sequenced by Novogene GmbH (München) (2.4.15), and bioinformatic analysis was conducted in collaboration with Dr. Carolina de la Torre from the NGS Core Facility, University of Mannheim (2.4.15). The table is sorted by the difference in the log2 fold change (FC). The p-value is adjusted with the false discovery rate (adj. p-value). n.a = not annotated.

10 most over-expressed TF specifically in +S			
TAIR ID	**Symbol**	**log2FC +S**	**adj. p-value +S**
AT1G19210	ERF017	3.73	1.42E-04
AT1G01520	ASG4	3.58	7.60E-03
AT5G43840	AT-HSFA6A	3.54	4.98E-03
AT1G07900	LBD1	3.30	4.73E-02
AT5G53200	MAU5	3.10	1.91E-03
AT3G44350	anac061	2.94	1.41E-02
AT4G34410	ERF109	2.93	1.38E-04
AT2G40740	ATWRKY55	2.83	1.58E-02
AT1G12610	ATDDF1	2.81	3.36E-04
AT5G04150	BHLH101	2.72	1.01E-02
10 most over-repressed TF specifically in +S			
TAIR ID	**Symbol**	**log2FC +S**	**adj. p-value +S**
AT1G43160	ERF113	-5.96	4.08E-02
AT5G64750	ABR1	-3.52	1.14E-02
AT5G25160	ZFP3	-3.15	1.51E-02
AT5G01380	n.a.	-3.15	5.49E-03
AT2G34140	CDF4	-2.97	1.29E-02
AT4G18170	ATWRKY28	-2.65	5.98E-04
AT4G23550	ATWRKY29	-2.31	5.29E-04
AT5G13790	AGL15	-2.30	1.60E-02
AT1G06160	ERF59	-2.29	7.19E-04
AT1G75520	SRS5	-2.27	4.50E-02

Supplemental Table 5: Differentially expressed transcription factors (TF) in *serat3;1s3;2* compared to WT found exclusively in -S. WT and *serat3;1s3;2* (2.3.1) were cultured in liquid ½ Hoagland medium containing 500 µM sulfate (+S) for four weeks (2.3.7). Half of the plants were transferred to a sulfur deficiency medium containing 1 µM sulfate for an additional four weeks (-S). The other half remained in the control medium (2.3.7). Shoot material was harvested, and used for RNA extraction (2.4.4). Total RNA was sequenced by Novogene GmbH (München) (2.4.15), and bioinformatic analysis was conducted in collaboration with Dr. Carolina de la Torre from the NGS Core Facility, University of Mannheim (2.4.15). The table is sorted by the difference in the log2 fold change (FC). The p-value is adjusted with the false discovery rate (adj. p-value). n.a = not annotated.

10 most over-expressed TF specifically in -S			
TAIR ID	**Symbol**	**log2FC -S**	**adj. p-value -S**
AT2G44910	ATHB-4	1.72	2.93E-03
AT2G36890	ATMYB38	1.37	3.56E-02
AT3G49930	n.a.	1.35	2.21E-02
AT3G07340	CIB3	1.18	5.59E-05
AT1G74650	ATMYB31	1.15	1.63E-02
AT1G77450	anac032	1.07	1.77E-02
AT3G01080	ATWRKY58	1.05	2.15E-04
AT1G46480	WOX4	1.02	3.36E-02
AT1G26960	AtHB23	0.98	2.22E-03
AT2G23340	DEAR3	0.96	4.34E-03
10 most over-repressed TF specifically in -S			
TAIR ID	**Symbol**	**log2FC +S**	**adj. p-value +S**
AT2G47520	AtERF71	-2.81	2.93E-02
AT5G04390	n.a.	-1.85	4.58E-02
AT5G59570	BOA	-1.51	3.43E-02
AT3G11020	DREB2	-1.43	3.60E-02
AT3G01600	anac044	-1.36	4.33E-02
AT1G75490	n.a.	-1.32	7.70E-03
AT3G47640	PYE	-1.30	4.18E-03
AT1G26945	KDR	-1.18	2.25E-03
AT4G36540	BEE2	-1.14	4.89E-03
AT3G04420	anac048	-1.11	3.45E-02

7. List of Abbreviations

A. thaliana	*Arabidopsis thaliana*
A. tumefaciens	*Agrobacterium tumefaciens*
acetyl-CoA	Acetyl coenzym A
Amp^R	ampicillin resistance
BSA	bovine serum albumin
cDNA	complementary DNA
ddH_2O	double distilled water
DNA	deoxyribonucleic acid
DTT	dithiothreitol
E. coli	*Escherichia coli*
FW	fresh weight
gDNA	genomic DNA
GFP	green fluorescent protein
GO	gene ontology
Kan^R	kanamycin resistance
KEGG	Kyoto encyclopedia of genes and genomes
lncRNA	long noncoding RNA
mRNA	messenger RNA
OAS	*O*-acetylserine
OAS-TL	*O*-acetylserine(thiol)lyases
PAGE	polyacrylamide gel electrophoresis
PCR	polymerase chain reaction
qRT-PCR	quantitative real-time polymerase chain reaction
RNA	ribonucleic acid
SERAT	serine acetyltransferase
T-DNA	transfer DNA
v/v	volume/volume
w/v	weight/volume
WT	wild type

8. Acknowledgment

First of all, I would like to thank Prof. Dr. Rüdiger Hell, who has given me the opportunity to work in his research group since my first years at the University. His expertise and kind leadership made me stay for many years and ultimately come back to do my PhD thesis. I thank you for believing in me and for your scientific support; without it, this work would not have been possible. Thank you for the shared meals in the mensa and that your door always felt open, despite your busy schedule.

I especially thank Dr. Markus Wirtz, whose richness of scientific ideas seems to never end. Without his guidance, I would have been lost many times. Thank you for always being eager to discuss results, brainstorm ideas, and plan new experiments, which most often led to whole new projects. Thank you for the lunch break discussion and late-night corrections.

I would like to thank my TAC committee members, Prof. Dr. Thomas Greb and Prof. Dr. Aurelio Teleman, for assessing my research progress and the fresh perspectives and scientific contributions in our meetings.

Special thanks goes to the MCTP (Metabolomics Core Technology Platform), which let me use their equipment for the metabolite measurements and was always helpful in answering questions or fixing technical problems. I also want to thank Dr. Carolina de la Torre from the NGS Core Facility, University of Mannheim, for processing the mRNAseq data and always being willing to video call in case of urgent questions. Furthermore, I would like to thank my various students, especially my Master's student, Diana Gabler, and my Bachelor's students, Nicolas Düster, Daniel Szabo, and David Sauer, whose supervision taught me a great deal and resulted in fruitful and enjoyable cooperation.

I would also like to thank my current and former colleagues from AG Hell, especially Dr. Marlena Pozoga, José Cruz-Cruz, Dr. Shengkai Sun, Dr. Xiaodi Gong, Dr. Laura Armbruster, Dr. Sara Haghani, and Dr. Eric Linster, for their teamwork and supportive atmosphere. I especially will remember all the barbecues and birthday breakfasts.

Many thanks go to Birgit Maresch for assisting with administration, Olga Keberling for autoclaving and preparing stock solutions, Michael Kraft for repairing pipettes and centrifuges, and Michael Schilbach for protecting the plants against pests and lice.

Last but not least, I thank my family, especially my mother and brother, my grandparents, and my friends for their support and unshakable belief in me.